

**Controls on the Geometry and Evolution of Deep-water Fold  
Thrust Belt of the NW Borneo.**

Norasiah Binti Sulaiman

Submitted in accordance with the requirements for the degree of  
Doctor of Philosophy

The University of Leeds  
School of Earth and Environment

May, 2017

The candidate confirms that the work submitted is his/her own and that appropriate credit has been given where reference has been made to the work of others.

This copy has been supplied on the understanding that it is copyright material and that no quotation from the thesis may be published without proper acknowledgement.

The right of Norasiah Binti Sulaiman to be identified as Author of this work has been asserted by her in accordance with the Copyright, Designs and Patents Act 1988.

©2017 The University of Leeds and Norasiah Binti Sulaiman

## **Acknowledgements**

Praise to Allah, the Almighty God, for giving me the ability to complete this thesis.

I would like to express my sincere gratitude to my supervisor, Prof Dr Douglas Paton and Dr Richard Collier, for their help and guidance over the years which is unmeasurable. Without their kind help and support, the past PhD years would be much harder.

The National University of Malaysia and Government of Malaysia are gratefully acknowledged for financially supporting my PhD studies at University of Leeds.

Finally, I wish to thank my family for their loving support throughout my studies, particularly my parents, my husband, Syamsul and my two lovely daughters, Qaiys and Sabriena. Their countless love gives me strength to keep going.

## **Abstract**

The key driving mechanisms for establishing deep-water fold-thrust belt are either lithospheric stress or gravity-driven associated with margin instability or a combination of both. Despite long academic interest, we still lack of detailed understanding of the interaction between the deformation mechanisms (gravity- and tectonic-driven). The results of an evaluation of the interaction between the deformation mechanisms, with focused attention upon the NW Borneo deep-water fold-thrust belt, are reported. A methodology integrating a detailed structural analysis of the deep-water fold-thrust belt from the available subsurface data and equivalent onshore outcrop is utilized in this study.

Detailed structural analysis of 2D seismic profiles is used to present a basin-scale seismic-stratigraphic framework and detailed description of the general appearance of the deformational style along the deltaic system. Sub-seismic scale investigation of well-exposed outcrops onshore NW Sabah is used to extract information on onshore tectonic deformation, making it possible to evaluate the differences of structural architecture related to different deformation mechanisms. The result has led to an improved understanding of the regional-scale structural geometry along the NW Borneo margin.

Regional scale cross-sections are used to demonstrate a regional-scale analysis of the NW Borneo margin that includes structural restoration. The results allow an assessment of the relative timing of deformation, the domain interaction and the possible processes and parameters that control deformation. This has led to an improved insight relating to the kinematic nature of the allochthon and the interaction between the deformation mechanisms. Structural restorations are also used to evaluate of areas of compressionally and extensionally dominated systems, in order to verify the main proses responsible for the margin evolution.

This study illustrates outcrop-scale to seismic-scale analysis and quantitative measurements combined with seismic interpretations, with the aim to identify the interaction between gravity- and tectonic-driven deformation, and their controls on the geometry and evolution of deep-water fold-thrust systems. Additionally, the margin evolution and the implications on NW Borneo are evaluated.



## Table of Contents

<b>Acknowledgements</b> .....	iii
Abstract .....	iv
<b>Table of Contents</b> .....	v
<b>List of Tables</b> .....	viii
List of Figures.....	ix
<b>Chapter 1 Introduction</b> .....	1
1.1 Rationale.....	1
1.2 Thesis Aims and Objectives .....	2
1.3 Location and Data Set.....	3
<b>Chapter 2 Background</b> .....	7
2.1 Deep-Water Fold-Thrust Belts.....	7
2.1.1 Driving Mechanism for Deep-Water Fold-Thrust Belt .....	7
2.1.2 Structural Deformation.....	10
2.1.3 Shale Detachments .....	14
2.2 The NW Borneo Deep-Water Fold-Thrust Belt.....	17
2.2.1 Geological Setting of NW Borneo .....	17
2.2.2 Stratigraphy .....	20
2.2.3 Style of Deformation .....	23
<b>Chapter 3 Deformation Style along the DWFT System and the Allochthonous Wedge of NW Borneo - Integrating Field and Seismic Studies.</b> .....	27
3.1 Introduction .....	27
3.2 Offshore Studies .....	29
3.2.1 Data and Methodology.....	29
3.2.2 Deltaic (Seismic) Stratigraphy .....	32
3.2.3 Observations and Interpretation .....	38
3.5 Outcrop Studies .....	50

3.5.1	Observations .....	50
3.6.	Integrating Field and Seismic Studies .....	60
3.7	Discussion.....	69
3.8	Conclusion .....	71
<b>Chapter 4 Tectonic and Gravity Driven Deformation; their Controls on the Geometry and Evolution of DWFTB. ....</b>		<b>74</b>
4.1	Introduction .....	74
4.2	Data and Methodology .....	75
4.3	Section Restoration: Synthesis of Margin Evolution.....	79
4.3.1	Regional Cross Section Geometry .....	79
4.3.2	Section Restoration .....	80
4.4	Domain Interaction .....	89
4.4.1	Translation magnitudes .....	94
4.5	Stratigraphic Thickness Variation: How does it affect the Critical Wedge Geometry and Deformation Styles of the Area?.....	97
4.6	Discussion: Model of Evolution and How This Fits With Current Understanding of the Area .....	104
4.7	Conclusion .....	108
<b>Chapter 5 Regional restorations of 2D profiles across NW Borneo, quantifying the amount of extension vs compression. ....</b>		<b>110</b>
5.1	Introduction .....	110
5.2	Structural Reconstruction.....	112
5.3	Miocene-Recent Shortening.....	123
5.4	Lengthening Vs Shortening.....	126
5.4.1	Early Pliocene-Recent .....	126
5.4.2	Miocene-Recent .....	131
5.5	Discussion.....	133
5.5.1	Spatial and Lateral Variation in Deep-Water Shortening; How Does This Link with the Formation and Translational event of the allochthon... ..	133
5.5.2	Gravity-Tectonics Imbalance .....	135

5.6	Conclusion .....	137
<b>Chapter 6 Discussion and Conclusion.....</b>		<b>139</b>
6.1	Contrasting Deformation of Different Structural Domains. ....	139
6.2	Succession of Significant Events and Their Implication for NW Borneo Evolution .....	140
6.3	Parameters Controlling Deformation .....	144
6.3.1	Proximal Uplift .....	144
6.3.2	Stratigraphic Thickness .....	144
6.3.3	Pre-existing Compressional Structure .....	145
6.4	Summary and Future Work .....	146
<b>List of Reference .....</b>		<b>148</b>

## List of Tables

<b>Table 3. 1: Sequence boundaries used in this study and their relationships with previous studies.....</b>	<b>33</b>
<b>Table 3. 2: Measurement of geometrical aspects of the fold and thrust in 2D depth converted seismic data: tightness of the fold (fold inter-limb angles), thrust spacing and dips (bold black, measurements of the deep-water fold thrust structures; italic black, measurements of the allochthon internal thrusting). ...</b>	<b>65</b>
<b>Table 4. 1: Total cross-sectional area of allochthon above their regional level and total cross-sectional area of deltaic sediments that sink below their regional level. ....</b>	<b>91</b>
<b>Table 4. 2: Critical taper wedge angle of the deforming wedge measured across the study area. ....</b>	<b>98</b>
<b>Table 5. 1: Incremental deep-water shortening values based on age division (Middle Miocene to Recent), measured by structural restoration of nine NW-SE-trending seismic profiles, across the study area (see Figure 5.2 to Figure 5.10). The location of line profiles is shown in Figure 5.1.....</b>	<b>125</b>
<b>Table 5. 2: The amount of Early Pliocene-Recent shortening and lengthening measured by structural restoration of nine selected seismic profiles across the study area (see Figure 5.2 to Figure 5.10) linked with previous studies of Hesse et al.(2010b) and the references therein (Bold italic letters: Early Pliocene-Recent shortening and lengthening values from Hesse et al.(2010b) and the references therein). ....</b>	<b>127</b>
<b>Table 5. 3: Total and incremental Middle Miocene-Recent shortening and lengthening measured by structural restoration of three selected seismic profiles (BGR86-10, BGR86-06 and BGR86-02). ....</b>	<b>131</b>

## List of Figures

- Figure 1. 1: (A) Regional location map of NW Borneo (red rectangle) in South East Asia. (B) Structural map of NW Borneo (modified from Hesse et al, 2010b) showing the location of the 2D regional seismic data presented in this study (green lines) and the approximate location of outcrop studies (blue rectangle). The location of three major deltas of the NW Borneo margin is from Tingay et al., (2005)..... 4**
- Figure 1. 2: The location of the available 2D seismic surveys from Hess Corporation (blue-green), and the selected regional seismic profiles from the available seismic survey data (bold blue) and the previously published seismic profiles from Hesse et al., (2010b) (bold red). ..... 6**
- Figure 2. 1: Schematic cross section representing an accretionary prism (from Krueger and Gilbert, 2009).....8**
- Figure 2. 2: Gravity-driven deformation: (a) gravity gliding of a rigid body down a slope above a detachment level; (b) gravity spreading of a rock mass under its own weight that's collapse vertically and extending laterally; (c) mixed-mode deformation, in which both components are combined (from Morley et al., 2011)... 10**
- Figure 2. 3: Cross-section through the gravity-driven deep-water fold and thrust belt of the Niger Delta, showing three linked structural domains of the delta top extensional, a translational and the delta toe compressional, formed above a weak basal detachment composed of mobile shales (from Corredor et al., 2005).....12**
- Figure 2. 4: Cross-section through the Hikurangi Subduction zone, showing the main characteristic of active margin fold-and thrust belt (compression throughout the deforming wedge) (from Morley et al., 2011)..... 13**
- Figure 2. 5: Cross-section through the NW Borneo deep-water fold and thrust belt, showing the onshore-inner shelf zone of compression/inversion domain, associated with three linked structural domains: the delta top outer shelf extensional**

domain, a translational domain and the delta toe deep-water compressional domain (this study).....	13
<b>Figure 2. 6: Mohr-Coulomb failure criterion (in term of effective stress) showing the relationship between the shear strength of shale (<math>\tau</math>) with its frictional coefficient (<math>\phi</math>) and cohesion (C).....</b>	<b>14</b>
<b>Figure 2. 7: Diagram showing the range of geometries interpreted to be shale diapirs (from Morley, 2003).....</b>	<b>16</b>
<b>Figure 2. 8: Regional location map of NW Borneo (red box) in South East Asia.....</b>	<b>17</b>
<b>Figure 2. 9: Schematic evolution of the NW Borneo Wedge from subduction of the Proto-SouthChina Sea oceanic crust to collision between Dangerous Grounds-Reed Bank Block with northern Borneo and the Cagayan Arc, and to post-collision event (from Sapin et al., 2013).....</b>	<b>19</b>
<b>Figure 2. 10: The stratigraphic record from subduction to collision, and to post-collision of NW Borneo. Location of three major delta systems is from Tingay et al., (2005).....</b>	<b>20</b>
<b>Figure 2. 11: Simplified stratigraphy of Sabah and Brunei modified from Hall (2013), Balaguru and Nichols (2004), and sources therein. Major unconformities offshore are from Bol and van Hoorn (1980), Levell (1987); Gartrell et al. (2011) and Van Hattum et al. (2006).....</b>	<b>21</b>
<b>Figure 2. 12: Recent analysis of present-day maximum horizontal stress (<math>Sh_{max}</math>) of the NW Borneo divided the margin into five provinces; 1) Deep-water fold and thrust belt; 2) Extensional growth faults in Baram Delta Province; 3) Inverted zone of Baram Delta Province; 4) Mobile shale deformation province; 5) Zone of strong inversion (from Morley et al., 2011).....</b>	<b>24</b>
<b>Figure 3. 1: (A) Regional location map of NW Borneo (red rectangle) in South East Asia. (B) Structural map of NW Borneo (modified from Hesse et al, 2010b) showing the location of the 2D profile presented in this study (green lines) and the approximate location of outcrop studies (blue rectangle).</b>	

Location of the three major delta systems of NW Borneo margin is from Tingay et al. (2005). .....	28
<b>Figure 3. 2:</b> NW-SE-trending TWT seismic profiles (above) and depth converted seismic profiles (below) of offshore Sabah (BGR-10). Note the geometric impact of depth conversion here is minimal; as the depth converted geometry of a fault-related fold is relatively unchanged from its equivalent time section. ....	31
<b>Figure 3. 3:</b> The locations of the selected 2D seismic profiles from the available 2D TWT seismic survey data sets that acquired by Hess Corporation (blue) and previously published depth-migrated seismic profiles from Hesse et al. (2010b) acquired by the Federal Institute for Geosciences and Natural Resources (BGR) in 1986 (red). ....	32
<b>Figure 3. 4:</b> Regional seismic profiles delineate the key features of margin deformation from northern segment (BGR86-02) segment to southern (BGR86-24) segment.....	37
<b>Figure 3. 5:</b> Un-interpreted and interpreted seismic profiles in the extensional domain, showing north to south (BGR86-02 to BGR86-12) lateral variation of the extensional deformation. Regional growth faults dominate deformational style with relatively thin depocentres in the northern segment, compared to more complex deformation with both paired regional and counter-regional growth faults and the largest portion of the sediment thickness in the southern segment.	40
<b>Figure 3. 6:</b> Un-interpreted and interpreted seismic profiles of the allochthon wedge showing north-west-ward and sea-ward progression of the over-thrusted allochthon over the Middle Miocene to Recent deltaic sequence; the allochthon front is best developed and almost cuts the seafloor in the most distal part of the northern wedge (BGR86-02); whereas it dies out and displaces the Late Miocene/Middle Miocene strata in the transitional zone in the southern segment.....	42
<b>Figure 3. 7:</b> The deformed allochthon wedge overlain by a low- to moderate-relief smoothly undulating folded roof of Latest Miocene to Recent deltaic sediment with; asymmetric and	

offshore verging anticlines, compatible with a compaction drape rooted by landward-dipping internal imbricated thrusts (a) , and nearly symmetrical, broad, upright fold geometries of the upper roof units with no visible relationship to contractional faults as there is no sense of movement, no verging direction and no significant stratigraphic throw (b). 44

**Figure 3. 8:** High-relief elongate ridges with seismically chaotic and transparent cores have been elevated above regional stratigraphic level and are overlapped by younger strata in the adjoining mini-basins, indicating an element of contraction and uplift (a), while in section BGR86-10, the extension is interpreted as a younger event superposed on an older high relief contractional detachment fold with a weak, over-pressured mobile shale core (b). ..... 45

**Figure 3. 9:** Interpreted seismic profiles of the compressional domain showing variation of the compressional deformation from a broad, well developed imbricate zone with generally similar sized, uniform-length thrusts associated with significant accommodation space in piggy-back basins, and undeveloped over-thrusted allochthonous wedge in the southern segment ( BGR86-20 to BGR86-16) pass into a region of narrow, considerably more strongly compressed style with different sizes of thrusts separated by narrow piggyback basins, and a chaotic compressive belt where the of the over-thrust allochthonous wedge is involved (BGR86-14 to BGR86-02). ..... 49

**Figure 3. 10:** The distribution of the West Crocker Formation in the study area. The locations of the 7 selected outcrops for detailed study are marked in red..... 52

**Figure 3. 11:** Stereonet presentations of strike measurements for bedding planes (a) and faults (b) in the study area..... 52

**Figure 3. 12:** Equal area projections of fold data collected in the study area. Most of the observed outcrop-scale folds are tight ( $46^{\circ}$ - $66^{\circ}$ ) and moderately plunging ( $34^{\circ}$ - $66^{\circ}$ ) to the SW and NE (c-f) with some open folds ( $146^{\circ}$ ) plunging moderately ( $67^{\circ}$ ) to the



NW (b). The fold axes trend NE-SW and NW-SE with a dominant trend of NE-SW.....	53
Figure 3. 13: Large, tightly folded fold at locality 4 (figure a), 5 (figure b) and 6 (figure c) have been cut by sets of faults with various scales and orientations that offset their respective beds. ....	56
Figure 3. 14: A large, upright, tight fold at locality 3. The rock mass in the core of the tight fold comprises thick, disrupted, sandstone beds.....	57
Figure 3. 15: An open fold at locality 2 has been cut by numerous faults.	58
Figure 3. 16: A NNW-SSE trending fault exhibit drags folding, offsetting the interbedded thick sandstone with thin shale sequence at locality 1.....	59
Figure 3. 17: Interpreted seismic profiles of the compressional domain used for fold analysis (from north to south; BGR86-02 to BGR86-24).....	64
Figure 4. 1: The location of two selected NW-SE-trending regional seismic profiles representing the southern and northern segments that were used for restorations.....	77
Figure 4. 2: Two selected NW-SE-trending regional seismic profiles of the offshore Sabah (BGR86-10) and Brunei margin highlighting the key features of contrasting margin deformation in the northern and southern segments respectively, and illustrating the deformation styles of the different structural domains. The offshore Sabah profile was constructed from seismic survey data acquired by Hess Corporation whereas the Brunei profile was modified from previously published seismic profiles of Gartrell et al., (2011). .....	78
Figure 4. 3: Seismic section from the inboard area of the northern segment (Sabah) showing the shelf edge trajectories through time (illustrated by the red dots). The line profile shown is shown in figure 4.1.....	81
Figure 4. 4 : Structural restoration of the Sabah (northern) margin using Midland Valley 2D Move. The line profile shown was in depth (km) and the location of lines is shown in figure 4.1. ....	82

- Figure 4. 5: Structural restoration of the Brunei margin using Midland Valley 2D Move. The line profile shown was in depth (km) and the location of lines is shown in figure 4.1. .... 83**
- Figure 4. 6: Schematic diagram showing conceptual basis for allochthon above regional calculations (modified from Hudec and Jackson, 2004). (a) In the absence of basement shortening, the cross-sectional area of allochthon displaced upward/seaward above their regional level should be compensated by an equivalent (or lesser) area of deltaic sediments in their piggyback basin that sink below their regional level. (b) If basement is shortened, the cross-sectional area of allochthon displaced upward/seaward above their regional level may exceed the area of deltaic sediments in their piggyback basin that sink below their regional level.91**
- Figure 4. 7: Regional profile across the northern segment of the NW Borneo margin (Sabah) used to measure the present-day total cross-sectional area of allochthon above regional and the deltaic sediments in their piggyback basin that sinks below regional. .... 92**
- Figure 4. 8: Regional profile across the southern segment of the NW Borneo margin (Brunei) used to measure the present-day total cross-sectional area of allochthon above regional and the deltaic sediments in their piggyback basin that sinks below regional. .... 93**
- Figure 4. 9: The wedge surface slope ( $\alpha$  = angle of the wedge surface to the horizontal) and the dip of the basal décollement ( $\beta$  = angle of décollement to the horizontal) measured across the study area. Note that lateral thickness variation from north (a) to south (d) is consistent with variation in the deformational style. .... 99**
- Figure 4. 10: Basic diagram of a critically tapered wedge. Wedge taper is defined as the wedge surface slope ( $\alpha$  = angle of the wedge surface to the horizontal) plus the dip of the basal décollement ( $\beta$  = angle of décollement to the horizontal). The wedge will respond to unstable states by attempting to obtain the critical taper angle, either by deforming internally and**

uplifting the wedge, or by propagating forward and lengthening the wedge. .... 101

**Figure 4. 11: Relationship between pore-fluid pressure ratio ( $\lambda$ ), surface slope ( $\alpha$ ), and basal detachment dip ( $\beta$ ) for a submarine fold-and thrust belt at critical taper, assuming Coulomb material behaviour (Dahlen, 1984; Morley, 2007). Critical wedge geometry and taper angle of offshore NW Sabah are based on seismic reflection data acquired by Hess Corporation (BGR02 and BGR10) and previously published seismic profiles of Hesse et al. (2010; BGR20 and BGR24).  $\mu$  - internal coefficient friction for the wedge;  $\mu_b$  - internal coefficient friction at the base of the wedge;  $\lambda_b$  - ratio of pore fluid pressure to lithostatic pressure at the base of the wedge..... 103**

**Figure 4. 12: (a) Model of structural deformation consisting of a sedimentary wedge which prograded over and grew in thickness above a former fold and thrust front; (b) Initial progradation of the delta caused substantial upper-slope subsidence in the hanging-wall of a regional growth fault (RGF) and/or counter-regional growth faults (CRGF); (c) & (d) The delta-front continues to prograde and initiate a second CRGF on top of the early folds, foreward of the earlier CRGF, while the earlier fault was inverted by tectonic compressional pulse. The up-dip extension linked at depth with the down-dip contraction through a diffuse region of distributed strain within the mobile allochthon, that transmitted down-dip overtime, causing a feedback mechanism that translated the allochthon sporadically basinwards and upwards above its regional stratigraphic level, by reactivating the pre-existing thrusts, then progressing seaward to generate toe thrusting in the deep-water area, without a discrete decollement surface; (e) &(f) Tectonic compressional pulses continue to invert the earlier CRGF up slope whereas the extensional deformation was succeed by outer shelf growth faulting, as the cycle of sedimentary loading and delta front prograding continues. Due to variation in sediment supply and stratigraphic thickness in the study area, RGF dominate the**

southern segment while CRGF dominate the northern segment. Moving down-dip, the translational event of the allochthon slowed down as the deltaic progradation capped and sealed the allochthon, thus restraining the outward advance of the allochthon. In the deepwater, contractional deformation that formed forward of the allochthon continued to develop and expand further seaward, resulting in the formation of a series of seaward-migrating deep-water fold and thrust systems subsequent to the continuous uplift and gravitational loading up-dip, with a considerably more compressed style towards the northern segment. .... 107

Figure 5. 1: The location of the selected seismic profiles from the available seismic survey data acquired by Hess Corporation (blue) and the previously published seismic profiles from Hesse et al. (2010b) (red)..... 111

Figure 5. 10: Structural restoration of BGR86-24 using Midland Valley 2D Move. The location of line profile is shown in Figure 5.1. .... 114

Figure 5. 3: Structural restoration of BGR86-22 using Midland Valley 2D Move. The location of line profile is shown in Figure 5.1. .... 115

Figure 5. 4: Structural restoration of BGR86-20 using Midland Valley 2D Move. The location of line profile is shown in Figure 5.1. .... 116

Figure 5. 5: Structural restoration of BGR86-18 using Midland Valley 2D Move. The location of line profile is shown in Figure 5.1. .... 117

Figure 5. 6: Structural restoration of BGR86-14 using Midland Valley 2D Move. The location of line profile is shown in Figure 5.1. .... 118

Figure 5. 7: Structural restoration of BGR86-12 using Midland Valley 2D Move. The location of line profile is shown in Figure 5.1. .... 119

Figure 5. 8: Structural restoration of BGR86-10 using Midland Valley 2D Move. The location of line profile is shown in Figure 5.1. .... 120

Figure 5. 9: Structural restoration of BGR86-06 using Midland Valley 2D Move. The location of line profile is shown in Figure 5.1. .... 121

Figure 5. 10: Structural restoration of BGR86-02 using Midland Valley 2D Move. The location of line profile is shown in Figure 5.1. .... 122

Figure 5. 11: Incremental value of Middle Miocene-Recent deep-water shortening measured by structural restoration of nine

	selected seismic profiles, across the study area (see Figure 5.2 to Figure 5.10). The location of line profiles is shown in Figure 5.1.....	126
Figure 5. 12:	Early Pliocene-Recent shelfal extension and deep-water compression from Hesse et al. (2010b) and the references therein.....	128
Figure 5. 13:	Early Pliocene-Recent shelfal extension and deep-water compression measured by structural restoration of nine selected seismic profiles across the study area (see Figure 5.2 to Figure 5.10) linked with previous studies of Hesse et al.(2010b) and the references therein (Grey shaded data)...	129
Figure 5. 14:	Early Pliocene-Recent excess of shortening (given by the subtraction of the Early Pliocene-Recent shelfal extension from the Early Pliocene-Recent deep-water shortening) measured by structural restoration of nine selected seismic profiles across the study area (see Figure 5.2 to Figure 5.10) linked with previous studies of Hesse et al.(2010b) and the references therein. High excess of Early Pliocene-Recent shortening between line BGR86-10 and line BGR86-22 can be interpreted as indicating of an increase in basement-driven shortening in the central part of the study area.....	130
Figure 5. 15:	Middle Miocene, Late Miocene and Early Pliocene shelfal extension and deep-water compression measured by structural restoration of three selected seismic profiles (BGR86-10, BGR86-06 and BGR86-02).....	132
Figure 5. 16:	Total Middle Miocene-Recent shelfal extension and deep-water compression measured by structural restoration of three selected seismic profiles (BGR86-10, BGR86-06 and BGR86-02). The location of line profiles is shown in figure 5.1. ....	132

## **Chapter 1 Introduction**

### **1.1 Rationale**

Deep-water fold–thrust belts develop at both active and passive continental margins. Active margins are related to plate convergence involving subduction, while passive margins are driven by gravitational instability of large deltaic sediment wedges: gravity gliding, gravity spreading or a combination of both. Over the past two decades, deep-water fold-thrust belts have become an important setting for hydrocarbon exploration, with thrust hanging-wall anticlines representing the prime trapping structures (e.g., Morgan, 2003; Ingram et al., 2004). Thus, a better understanding of deep-water fold and thrust belts is important in many aspects.

Great efforts have been made to understand the basic geometries of deep-water fold and thrust belts (Schultz-Ela, 2001; Rowan et al., 2004; Bilotti and Shaw, 2005; Krueger and Gilbert, 2009; Morley et al., 2011). However, we still lack a detailed understanding of the interaction between gravity-driven and tectonic-driven deformation and how they affect the style, timing, and location of deformation. One reason for the limited understanding is that linked systems can seldom be studied in other basins since the two mechanisms are commonly considered in isolation in previous studies and models, for example the passive margin gravity-driven tectonics of the Orange Basin (e.g., Paton, et al., 2008) and the Niger Delta (e.g., Morley and Guerin, 1996; Billotti and Shaw, 2005) or the convergence (tectonic-driven) of the Sinu Accretionary prism (e.g., Vinnels et al., 2010).

An exception is the NW Borneo deep-water fold-thrust belt where the Champion-Baram deltaic formation has prograded over the actively deforming region of NW Borneo, resulting in a combined gravity/orogenic system. Therefore, the area is ideal for modelling to investigate the interaction between tectonic-driven and gravity-driven deformation and their controls on the geometry and evolution of deep-water fold and thrust systems by considering the spatial and temporal variations in magnitude of deformation.

The North West Borneo margin hosts a number of proven hydrocarbon accumulations. It is anticipated that the research will provide timely and critical insights into margin evolution in deep-water settings, ranging from crustal-scale deformation to spatial and temporal changes in basin-scale architecture to structural influences on stratigraphy.

## **1.2 Thesis Aims and Objectives**

The objective of this research is to undertake a detailed structural analysis of the NW Borneo deep-water fold-thrust system using both sub-surface data and equivalent onshore outcrops to provide a better understanding of the geometry and evolution of such systems. The key questions that this thesis aims to investigate are:-

- I. How tectonic-driven and gravity-driven deformations interact with each other, and with the structural development?
- II. What is the effect of tectonic compressional structures on the development of later phase gravity-driven structures?
- III. What are the main driving forces for deep-water fold and thrust belt development? How the strain is distributed and what is its influence on the structural development?
- IV. How the margin evolves through time (characterized by the deep-water fold and thrust belts)?

The detailed objectives of the thesis are described as followed:

- I. Identification of the basin-scale seismic-stratigraphic framework including the analysis and structural mapping of 2D regional seismic data.
- II. A detailed description and interpretation of the general appearance of deformational style along the deep-water fold-thrust belt combined with sub-seismic scale investigations of onshore compressive deformation,

which lead to a better understanding of the regional-scale structural geometry along the NW Borneo margin.

- III. A detailed description and interpretation of the allochthon's deformation style and its relative timing of deformation and the influence that such a succession has on deformation styles of the gravity-driven system.
- IV. Development of regional cross-sections, showing the main structural and stratigraphic components and use of this framework to demonstrate a regional-scale structural analysis of the margin to provide several insights into unanswered questions; interaction between gravity-driven and tectonic-driven deformation, how it affects the style, timing, and location of deformation and its relative influence for the formation and evolution of deep-water fold and thrust belt.
- V. A 2D structural restoration to evaluate areas of compressional and extensionally dominated systems, to verify the amount of extension and compression over time, to consider the spatial and temporal variations in magnitude of deformation and to discuss how the strain is accommodated.
- VI. A discussion of the controls on deformation to address the relative influence of compression vs. gravity.

### **1.3 Location and Data Set**

The NW Borneo deep-water fold and thrust belt is ~ 100 km wide (Franke et al., 2008), and is situated adjacent to the NW Borneo Trough in a continental margin considered to be one of the world class oil and gas reserves and production since 1899 (Ingram et al., 2004; Figure 1.1). It is filled with Early-Middle Miocene to Recent sedimentary successions of the Champion-Baram Deltaic System (Hall and Nichols, 2002; see Figure 1.1). The NW Borneo deep-water fold and thrust belt can be divided into two distinct regions: (1) the offshore NW Sabah margin in the NE; and (2) the offshore Brunei margin to the SW (see Figure 1.1). The offshore NW Sabah margin is the key area of interest in this study.



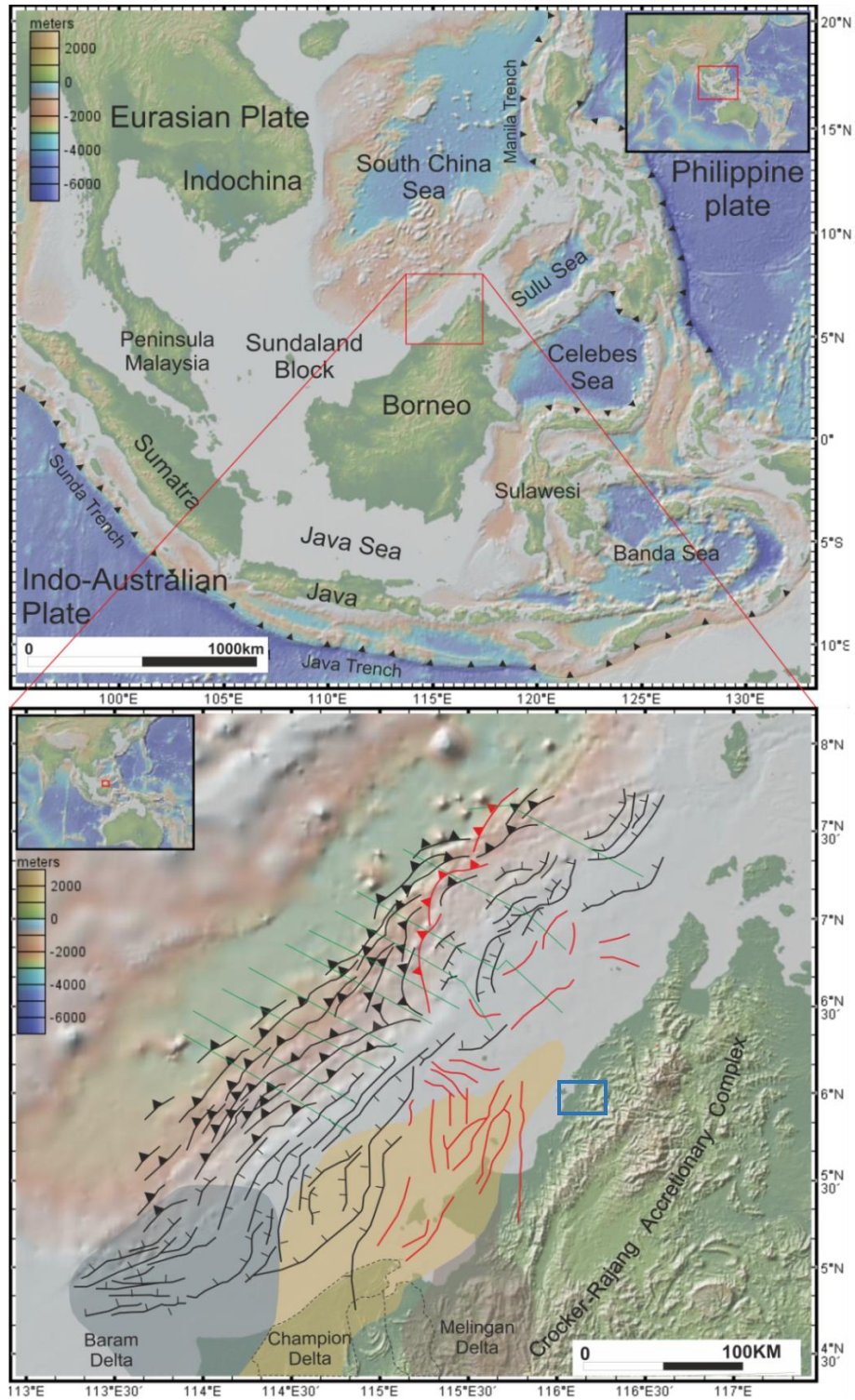


Figure 1. 1: (A) Regional location map of NW Borneo (red rectangle) in South East Asia. (B) Structural map of NW Borneo (modified from Hesse et al, 2010b) showing the location of the 2D regional seismic data presented in this study (green lines) and the approximate location of outcrop studies (blue rectangle). The location of three major deltas of the NW Borneo margin is from Tingay et al., (2005).

The primary sources of data are marine seismic reflection surveys, which have a vertical axis in milliseconds two-way-travel-time (ms TWT). The 2D seismic survey data sets were acquired by Hess Corporation. Geographically, the 2D seismic data lie between 6° to 8° N and 114.5° to 117° E within the South China Sea, with dip lines trending approximately NW-SE across the northern half of the NW Sabah margin (northern NW Borneo). This is approximately perpendicular to the strike of structures in the subsurface. The quality of the seismic resolution of the stratigraphic intervals is generally good, enabling accurate mapping of seismic reflection packages, unconformities and structural features. The seismic signal deteriorates beneath faults and in the forelimb regions of faults. In addition, there is a rapid decrease in vertical resolution with depth, interpreted to be due to fluid overpressures and to the resultant attenuation of propagating seismic waves with increasing depth.

A selection of pre-existing 2D seismic reflection profiles from Hesse et al., (2010b) transecting the southern half of the NW Borneo deep-water fold thrust belt (BGR86-24 to BGR86-12) was combined with the available seismic data across the northern half of the NW Borneo deep-water fold thrust belt (BGR86-10 to BGR86-02) to provide a better overview of margin deformation. The locations of the available 2D seismic profiles and the selected regional seismic profiles (from the available seismic data and previously published seismic profiles) are shown in Figure 1.2. Moreover, since there is no directly available well information for this project, stratigraphic boundaries and other information (velocity and age) have been collected from open-sources (i.e., published papers). The interpretation was based on the patterns of amplitude continuity, strength and internal geometry of the units.

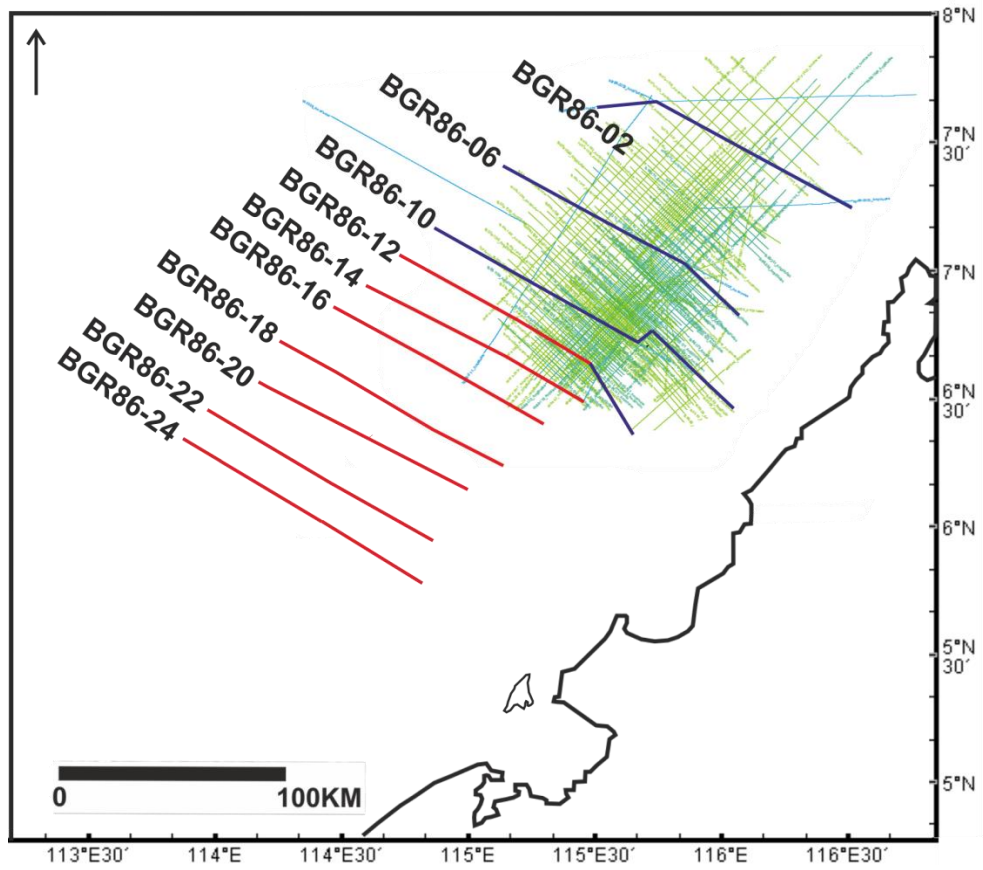


Figure 1. 2: The location of the available 2D seismic surveys from Hess Corporation (blue-green), and the selected regional seismic profiles from the available seismic survey data (bold blue) and the previously published seismic profiles from Hesse et al., (2010b) (bold red).

## **Chapter 2 Background**

The following background review provides a general overview on deep-water fold and thrust belts and the regional geology of NW Borneo.

### **2.1 Deep-Water Fold-Thrust Belts**

Deep-water fold–thrust belts develop at both active and passive continental margins (Rowan et al., 2004; Bilotti and Shaw, 2005; Krueger and Gilbert, 2009; Morley et al., 2011). The key driving mechanisms for establishing deep-water fold and thrust belts are either lithospheric stress/convergence of plate margins or gravity-driven tectonics associated with margin instability or a combination of both (mixed-mode) (Morley et al., 2011).

#### **2.1.1 Driving Mechanism for Deep-Water Fold-Thrust Belt**

##### **2.1.1.1 *Tectonic-Driven***

Active-margin or convergence deep-water fold and thrust belts are created by the shearing of sediments of the collided/subducted plate forming thrust sheets (Krueger and Gilbert, 2009; Figure 2.1). The entire crust is involved in the deformation of this type of deep-water fold and thrust belt, and their ultimate driving mechanism is plate tectonic stress (Krueger and Gilbert, 2009). The active-margin or convergence deep-water fold and thrust belts tend to have relatively long duration and continuous deformation, and rapid offshore propagation of the thrust front (Rowan et al., 2004; Krueger and Gilbert, 2009). Shortening may occur throughout the deforming wedge with large amount of shortening as determined by tectonic plate velocities (Krueger and Gilbert, 2009). Deformation of collisional/accretionary/tectonically driven fold belts can be described in the context of the critical taper theory, where out-of-sequence deformation is necessary to uplift the back of the wedge so that the thrust front can continue to propagate forwards (Platt, 1986).

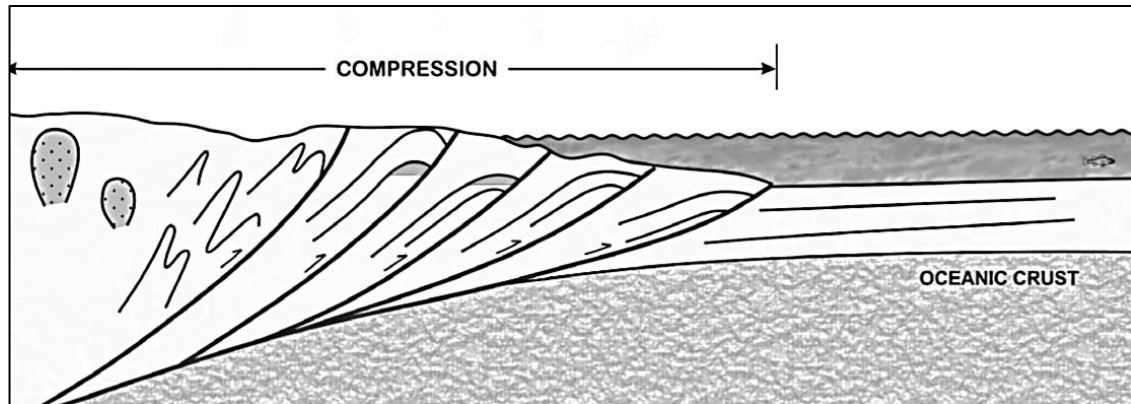


Figure 2. 1: Schematic cross section representing an accretionary prism (from Krueger and Gilbert, 2009).

#### **2.1.1.2 Gravity-Driven (*Gravity Gliding and Gravity Spreading*)**

Deformation of passive margin deep-water fold and thrust belts are driven by an interaction between differential loading and gravitational instability; gravity gliding above a basin-ward dipping detachment and gravity spreading of a sedimentary wedge with a seaward-dipping bathymetric surface, or a combination of both (Schultz-Ela, 2001; Rowan et al., 2004; Krueger and Gilbert, 2009; Figure 2.2). Gravity gliding refers to translation of a rock mass downslope parallel to the underlying basinward dipping detachment plane whereas gravity spreading is the failure of a rock mass under its own weight, by vertical contraction and lateral extension above a horizontal or a landward dipping detachment (Rowan et al., 2004, Schultz-Ela, 2001).

The component of gravity gliding is controlled by the basinward dip of the detachment (see Figure 2.2). Steeper detachment dip will have greater shear stress acting upon the detachment plane; hence it is easier for the weight of the overlying body to overcome the resistance to glide along the detachment plane (Rowan et al., 2004). A slight increase in basinward tilt of the detachment through time, as a response to crustal-scale processes (e.g., different thermal subsidence and uplift) will favour gravity gliding (Rowan et al., 2004; Schultz-Ela, 2001). However, the basinward dip of the detachment alone is insufficient to induce widespread large-scale gravity sliding. Instead the gravity gliding

component develops in areas with high sedimentation rates associated with large deltas (Morley et al., 2011).

Gravity spreading, on the other hand, is controlled by the basinward dip of the bathymetric slope (Rowan et al., 2004; see Figure 2.2). Delta progradation on the outer shelf and upper slope increase the bathymetric slope angle and the sedimentary weight on the slope favour gravity spreading (Rowan et al., 2004). Erosion of the shelf during a major sea level fall that reduces the bathymetric slope angle can decrease the driving forces for gravity spreading (Rowan et al., 2004). The gravity spreading component becomes an effective driving mechanism in the presence of thick overpressured or undercompacted mobile units (Morley and Guerin, 1996). The deformation commonly limited to the mobile zone (either thick shale or salt) underlying the gravity driven system hardly effect the whole sedimentary section (Morley et al., 2011).

Deformation of gravity driven fold belts developed on passive margins can also be described in the context of the critical taper theory (Dahlen et al, 1984), as it involves a wedge shaped geometry that is deforming by brittle processes (Bilotti and Shaw, 2005). Deformation along passive margins can be interpreted as a function of the interaction between 1) the internal strength of material deforming within the wedge, 2) the strength of the detachment surface, 3) the dip of the basal detachment layer, and 4) the surface slope of the deforming wedge. In other words, deformation can only take place when the gravity potential is great enough to overcome the internal strength of the overburden (Rowan et al., 2004). For the deforming wedge to continue to propagate seaward, the shear stress operating through the propagating wedge must be stronger than the shear strength of the basal detachment (Bilotti and Shaw, 2005).

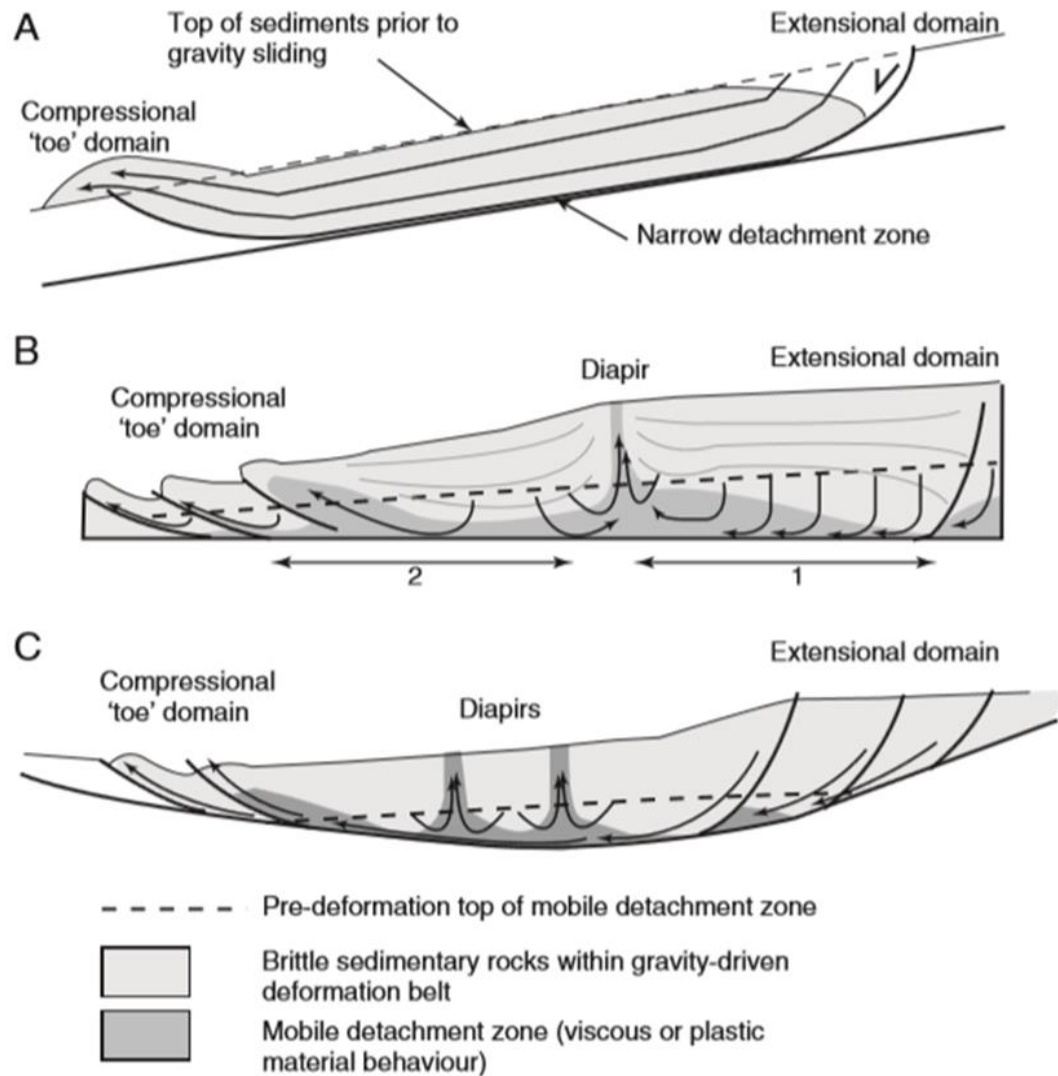


Figure 2. 2: Gravity-driven deformation: (a) gravity gliding of a rigid body down a slope above a detachment level; (b) gravity spreading of a rock mass under its own weight that's collapse vertically and extending laterally; (c) mixed-mode deformation, in which both components are combined (from Morley et al., 2011).

### 2.1.2 Structural Deformation

Deep-water fold and thrust belts driven by gravity tectonics associated with margin instability commonly form three linked structural domains: the delta top extensional domain, a translational domain and the delta toe compressional



domain. All domains are above a weak basal detachment composed of ductile material such as salt or over-pressured shales (Rowan et al., 2004; Billotti and Shaw, 2005; Krueger and Gilbert, 2009; Figure 2.3). Lithospheric stress or tectonic-driven deep-water fold and thrust belts, on the other hand, are characterized by compression throughout the deforming wedge (Krueger and Gilbert, 2009; Morley et al., 2011; Figure 2.4). Gravitational collapse and episodes of major extensional faulting can also develop in accretionary wedges, (e.g. due to the thickening of the wedge by underplating (critical wedge model; Platt, 1986; Morley et al., 2011)). Deep-water fold and thrust belts driven by a combination of gravity-driven and tectonic-driven deformation, usually form an onshore-inner shelf zone of compression/inversion domain, associated with three linked structural domains: the delta top outer shelf extensional domain, a translational domain and the delta toe deep-water compressional domain, but with a narrower zone of active extensional tectonics (Morley et al., 2011; Figure 2.5).

The development of large regional (seaward-dipping) and counter regional (landward-dipping) listric normal fault is a common component of gravitationally-driven detachment systems with prograding delta (e.g. Morley, 2003; Morley et al., 2011). However, different driving mechanisms generate different structural styles in the extensional domain. The extensional structures are subparallel to each other where the component of gravity gliding dominates, whereas they become multidirectional where the component of gravity gliding dominates (Loncke et al., 2006). In the compressional domain, on the other hand, the main difference in structural style is controlled by the nature of the decollement layer, not the driving mechanism (e.g., Rowan et al., 2004; Morley et al., 2011). Shale detachments commonly produce extensive regions of predominantly offshore verging fold and thrust belts (usually fault bend folds and fault propagation folds) whereas salt detachments, conversely, produce regions of fold belts associated with little thrusting and variable vergence directions (Morley et al., 2011). Moreover, fold belts with thick basal shales tend to be associated with break thrusts and thrusted shale diapirs, whereas fold belts with thin shale detachments tend to develop imbricate thrusts, popups and triangle zones (Corredor et al., 2005).



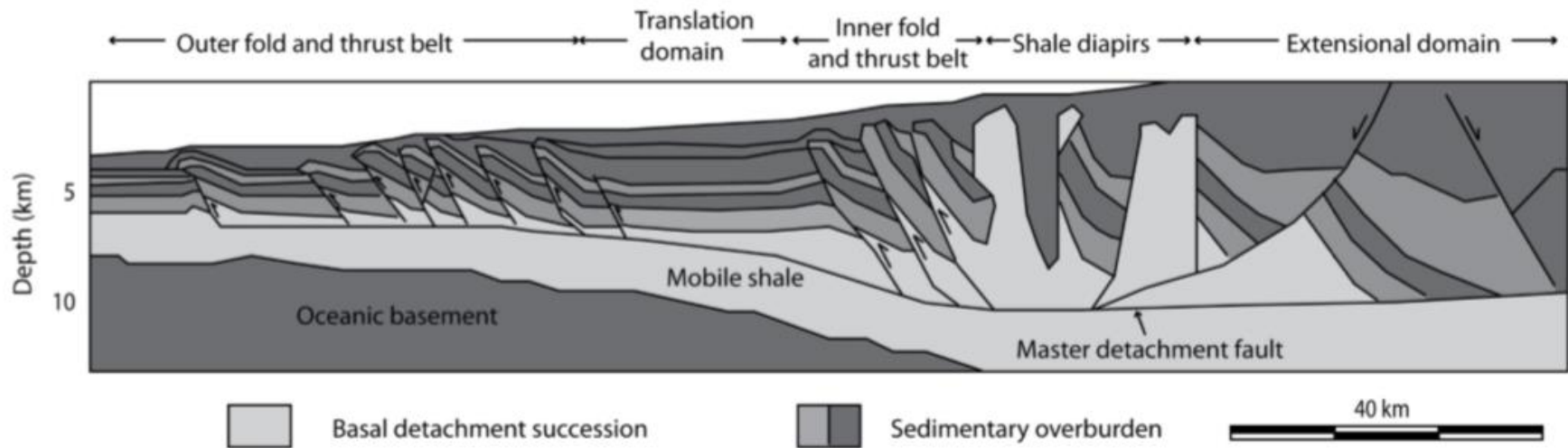


Figure 2. 3: Cross-section through the gravity-driven deep-water fold and thrust belt of the Niger Delta, showing three linked structural domains of the delta top extensional, a translational and the delta toe compressional, formed above a weak basal detachment composed of mobile shales (from Corredor et al., 2005).

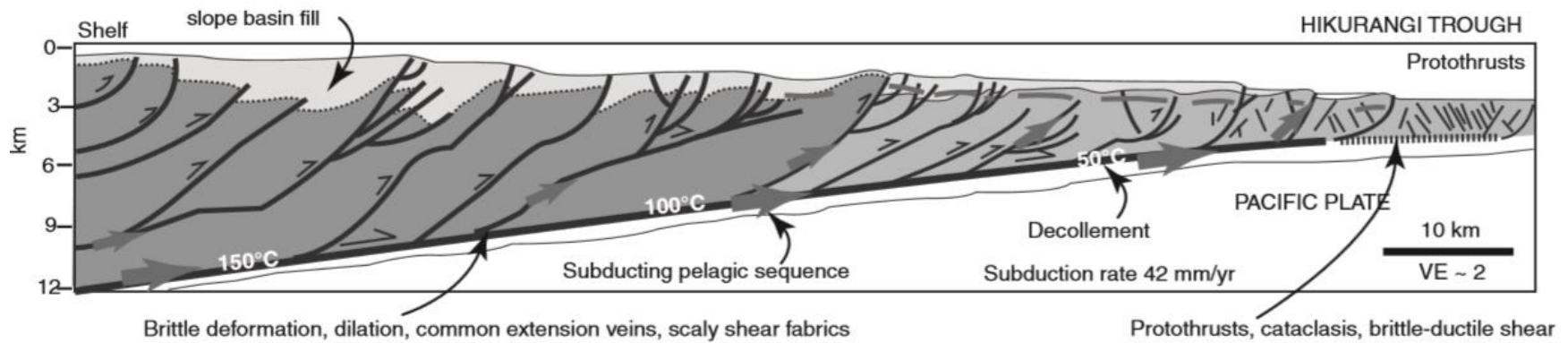


Figure 2. 4: Cross-section through the Hikurangi Subduction zone, showing the main characteristic of active margin fold-and thrust belt (compression throughout the deforming wedge) (from Morley et al., 2011).

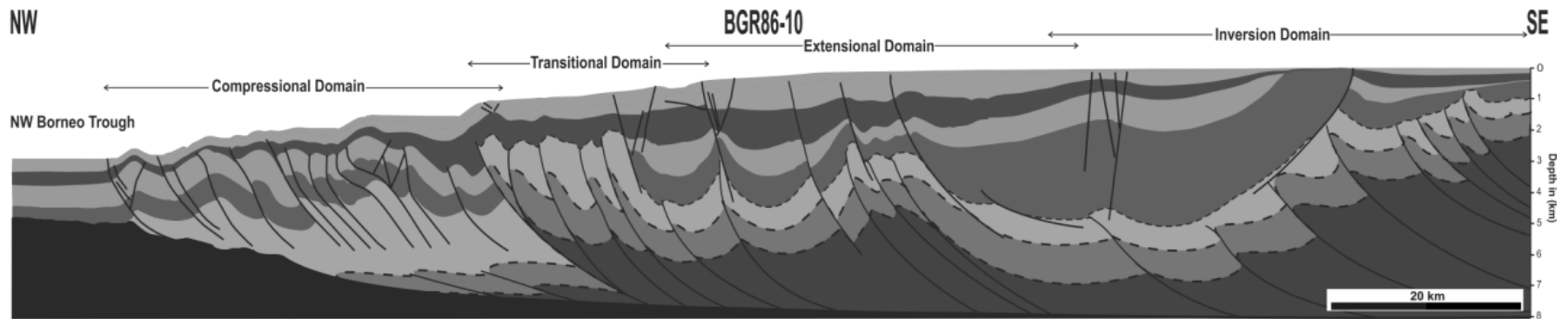


Figure 2. 5: Cross-section through the NW Borneo deep-water fold and thrust belt, showing the onshore-inner shelf zone of compression/inversion domain, associated with three linked structural domains: the delta top outer shelf extensional domain, a translational domain and the delta toe deep-water compressional domain (this study).

### 2.1.3 Shale Detachments

By definition, shale tectonics is a term related to deformation involving over-pressured, under-compacted, fine-grained sediments that deform in either macroscopically ductile or a mixed brittle and ductile manner (Weiner et al., 2010). The mechanism of shale deformation is mainly a result of over-pressuring that reduces the internal shear strength of rock in shale-rich sequences (Weimer and Slatt, 2004). The shear strength of shale is a function of its frictional coefficient and cohesion, and the effective stress (Maltman, 1994). Friction is a resisting force between two surfaces whereas cohesion results from a bonding between the surfaces of particles. The relationship between these parameters can be expressed with the Mohr-Coulomb equation,  $\tau = C + \sigma_n \tan \phi$  (where  $\tau$  is the maximum shear stress sustained at the point of maximum resistance,  $\sigma_n$  is the component of stress acting normal to the plane of failure,  $C$  is the cohesion and  $\phi$  is the angle of internal friction; Figure 2.6). Over-pressuring reduces the internal shear strength of sediment and the effective stress (Weimer and Slatt, 2004) by decreasing the magnitude of cohesion ( $C$ ) and intergrain friction ( $\tan \phi$ ) between grains (Maltman and Bolton, 2003), while the reduction in the effective normal stress causes the sediments to become over-consolidated and weak (Maltman and Bolton, 2003).

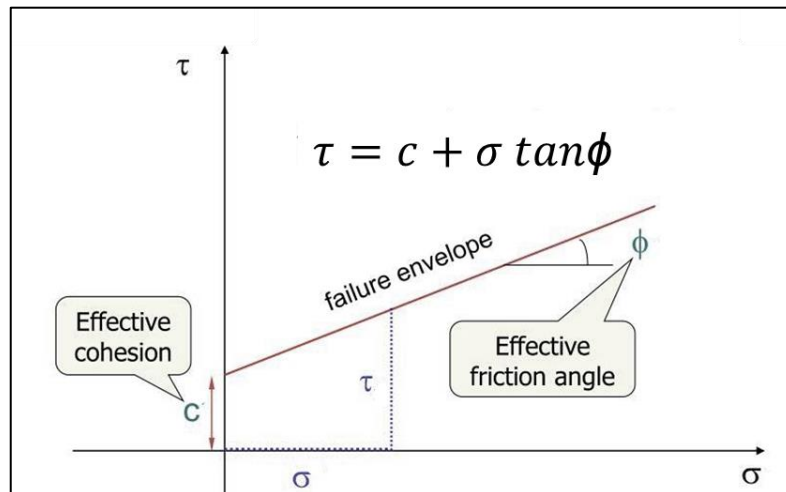


Figure 2. 6: Mohr-Coulomb failure criterion (in term of effective stress) showing the relationship between the shear strength of shale ( $\tau$ ) with its frictional coefficient ( $\phi$ ) and cohesion ( $C$ ).

Disequilibrium compaction and rapid burial of fine-grained sediments is the primarily mechanism advocated to generate overpressures in sediments (Morley and Guerin, 1996; Weiner et al., 2010). The low permeability nature of fine-grained sediments leads to entrapment of pore-fluids and the development of fluid overpressure, during rapid loading (Osborne and Swarbrick, 1997). Thick accumulations of overburden sustained by the sediment's pore-fluids cause the sediments to lose their ability to transmit a shear stress, hence effectively behave as a fluid (Maltman and Bolton, 2003; Rowan et al, 2004). Overpressures develop in sediments secondarily due to hydrocarbon maturation that result in a significant increase in volume and pressure (Morley and Guerin, 1996; Weiner et al., 2010). Secondary overpressure may also develop due to superposed tectonic stresses either by a gravitational movement in a linked system (delta toe compression-delta top extension) and/or superposed plate tectonic stresses in an active margin (Weiner et al., 2010).

Moreover, the weak mechanical behavior of a shale-rich sequence is not confined to a specific stratigraphic unit in either time or space (Morley, 2003; Morley and Guerin, 1996) and can occur at multiple stratigraphic levels depending on the migration of pore fluids pressure (Weiner et al., 2010). The pore fluid pressure of under-compacted mobile shale can migrate and induce overpressure to a degree where the stratified shales within the country rock become mobile (Van Rensbergen et al., 1999; Morley and Guerin, 1996), and lithified blocks are incorporated within the shale mass (Van Rensbergen et al., 1999). Overpressure generation in sediments induce ductile movement of the mobile shale, showing A range of geometries from large listric faults and/or the rise of shale diapirs (Morley and Guerin, 1996) or form the core to imbricated structures (Morley, 2003; Ajakaiye and Bally, 2002; Figure 2.7).

The presence of thick over-pressured mobile shales and thin detachment zones of shale layer that deform in highly ductile manners has long been reported in many over-pressured deltas and deep-water fold thrust belt (e.g. Morley and Guerin, 1996; McClay et al., 1998; Ajakaiye and Bally, 2002). However, the presence of thick, deeply buried mobile shales remains the subject of disagreement and discussion. However, down-building synformal depocentres and strong evidence for pinching and swelling of the mobile shale zone observed in part of the Niger Delta, caused Morley and Guerin (1996) and Ajakaiye and Bally (2002) to conclude that the delta were underlain by a thick

mobile shale. Moreover, a study by Wiener et al. (2009) using seismic reflection geometries, velocities and gravity data, conclude that the seismically transparent 'mobile' zone in the Niger Delta was a thick, low density and low velocity overpressured ductile zone. Furthermore, numerical modelling of delta systems by McClay et al. (1998) has shown that ductile substrates such as over-pressured mobile shales are required to generate deformation features similar to those of the Baram Deltaic Province and Niger Delta.

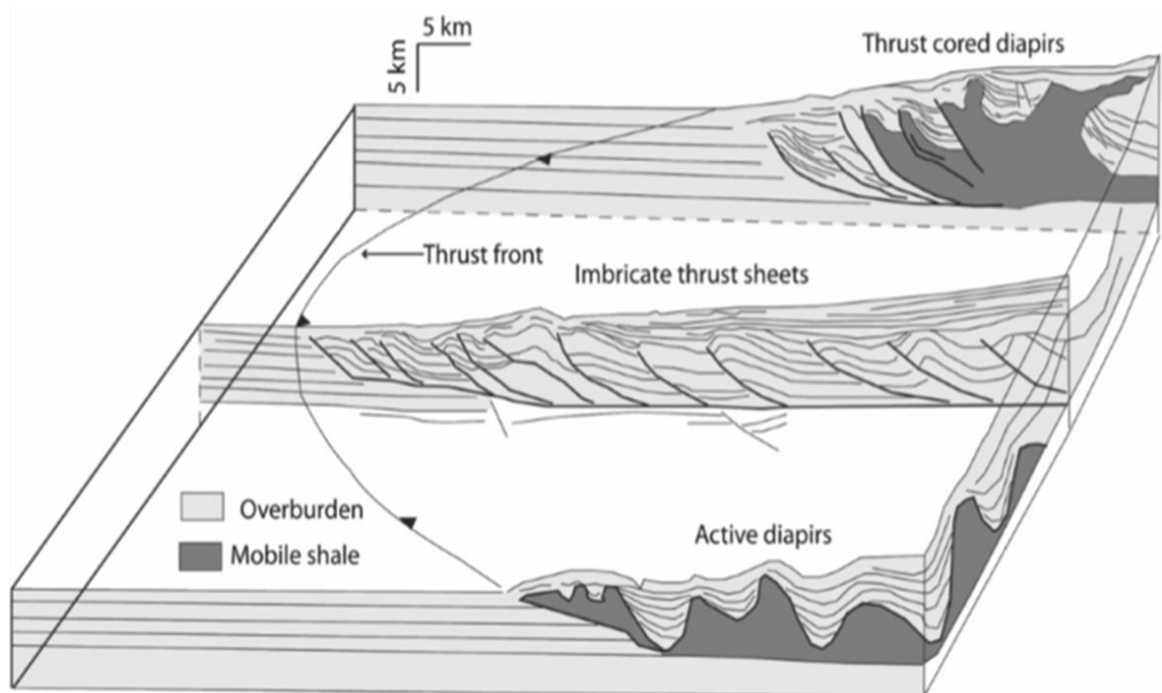


Figure 2. 7: Diagram showing the range of geometries interpreted to be shale diapirs (from Morley, 2003).

## 2.2 The NW Borneo Deep-Water Fold-Thrust Belt

### 2.2.1 Geological Setting of NW Borneo

Significant structural variations across the NW Borneo margin reflect the complex tectonic evolution of this margin as it is surrounded by an actively deforming region. It forms part of Sundaland, which is surrounded by the Philippine subduction zone to the east and the Indonesian subduction zone to the south and west, and the South China Block to the north (Figure 2.8). Opening of the South China Sea during the Oligocene to Early Miocene has strongly controlled the margin history.

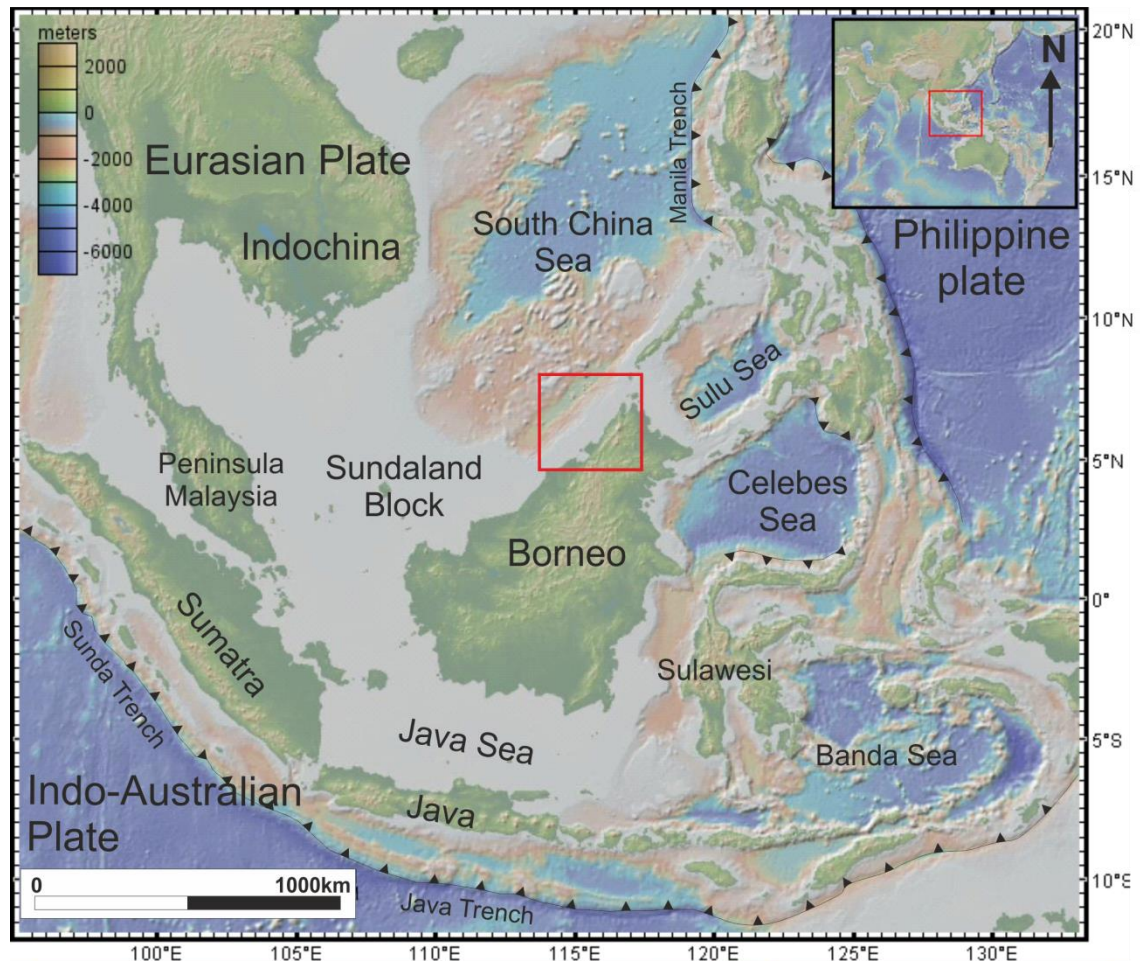


Figure 2. 8: Regional location map of NW Borneo (red box) in South East Asia.

In the subduction model, the NW Borneo collisional margin was formerly a subduction zone of the Proto South China Sea oceanic crust beneath the margin as a result of southward Oligocene-Early Miocene active spreading in the South China Sea Basin due to slab pull (e.g., Hall, 1996, 2002; Hutchison et al., 2000; Morley, 2002; Figure 2.9 (a)). The first convergence occurred in the southwest part of Borneo (Sarawak) in the Eocene, causing the Sarawak Orogeny (Hutchison, 2005). Significant contractional deformation is seen onshore in sedimentary units of Cretaceous-Eocene deep-water clastic deposits that are thrust, folded and locally metamorphosed to phyllite (Crocker and Rajang Groups exposed in the Crocker Mountain Range that extends along the central part of Borneo, from Sabah to central-south Sarawak) (Hutchison 1996).

Following complete subduction of the Proto-South China Sea oceanic crust (Hall, 1996), the attenuated South China continental margin, variously referred to as the North Palawan or Dangerous Grounds-Reed Bank Block, collided with northern Borneo and the Cagayan Arc, switching off the south-south-east dipping subduction zone, and leading to folding and thrusting in northern Borneo (Sabah) in the Early Miocene, (e.g., Levell 1987; Hazebroek & Tan 1993; Hutchison 1996; Hall 1996; Milsom et al. 1997; Rangin et al., 1990; Morley, 2002; Figure 2.9 (b)), an event which Hutchison (1996) named the Sabah Orogeny. Isostasy (due to slab breakoff) then caused emergence of central and northern Borneo during the Middle and late Miocene (Levell, 1987; Hutchison et al., 2000; Figure 2.9 (c)).

Progressive uplift and erosion of the Crocker-Rajang mountainous terrain of inland Borneo, from the latest Early Miocene onwards, resulted in rapid progradation and deposition of thick deltaic sequences onto the over-pressured Setap prodelta shale sequences (Hutchison 2005), with sediments up to 10 km thick in offshore Brunei but less than 6 km thick offshore NW Sabah (e.g., Hall and Nichols, 2002). These sediments were deformed by an external fold-thrust belt and an internal extensional zone (e.g. Hall and Nichols, 2002). Further exhumation of Borneo caused offshore propagation of structures, the progressive uplift and inversion of selected faults, and the erosion of earlier sedimentary sequences, leading to the development of a pronounced unconformity above active structures (e.g. Bol and van Hoorn, 1980; Levell, 1987) that becomes an equivalent conformable succession in the seaward direction (Levell 1987).



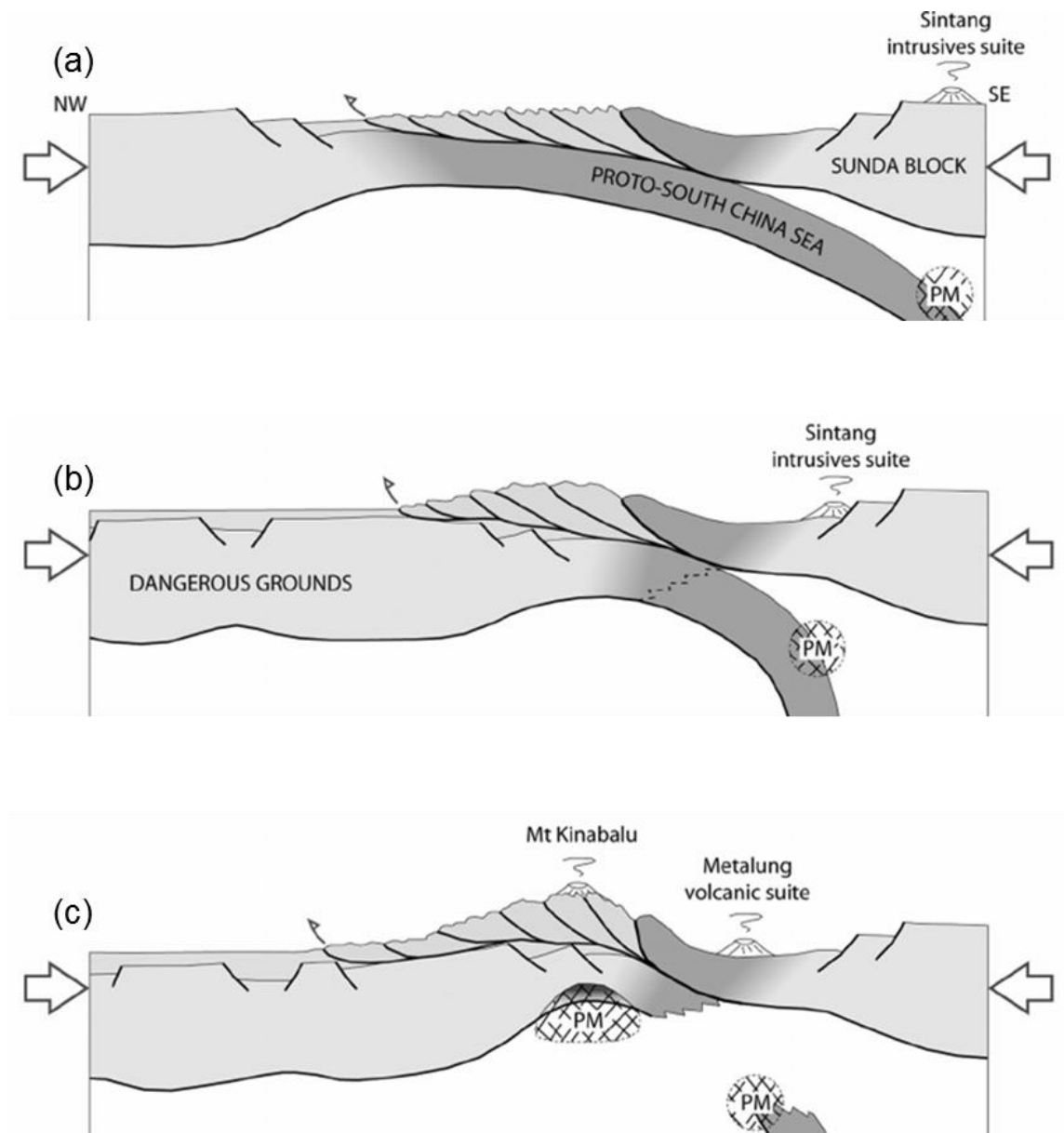


Figure 2. 9: Schematic evolution of the NW Borneo Wedge from subduction of the Proto-SouthChina Sea oceanic crust to collision between Dangerous Grounds-Reed Bank Block with northern Borneo and the Cagayan Arc, and to post-collision event (from Sapin et al., 2013).



## 2.2.2 Stratigraphy

The general tectono-stratigraphic sequences of NW Borneo define a westward, onshore to offshore younging accretionary complex (Hutchison et al., 2000). The stratigraphic record from subduction to collision, and to post-collision can be divided into two principle sedimentary phases; a) Pre-Mid Miocene deposition of highly deformed deep-water turbidite sediments of the Rajang-Crocker accretionary complex, with tectonic imbrications related to south-eastward convergence and overlain by the less deformed Meligan-Temburong Formations, and b) the younger Neogene (Miocene to Recent) deltaic of the Champion/Baram systems that were deposited outboard of the Crocker-Temburong sequences after the cessation of subduction (Figure 2.10). A summary of the stratigraphy of the NW Borneo basin is presented in Figure 2.11.

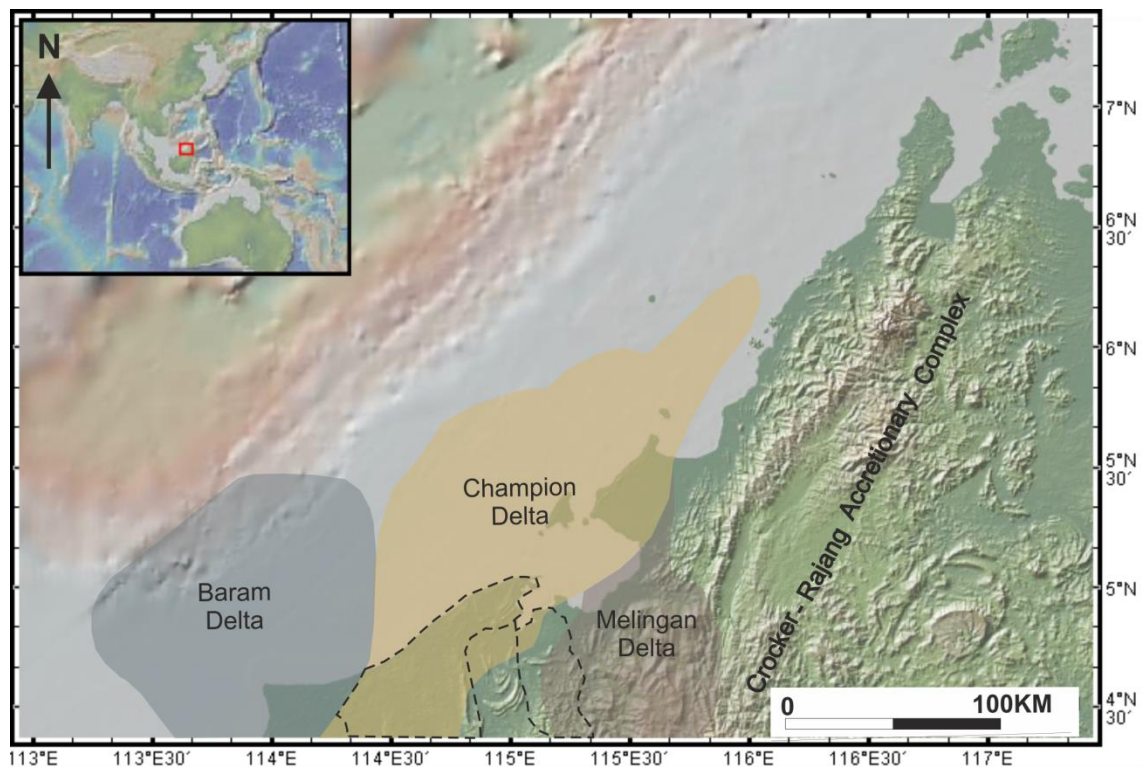


Figure 2. 10: The stratigraphic record from subduction to collision, and to post-collision of NW Borneo. Location of three major delta systems is from Tingay et al., (2005).

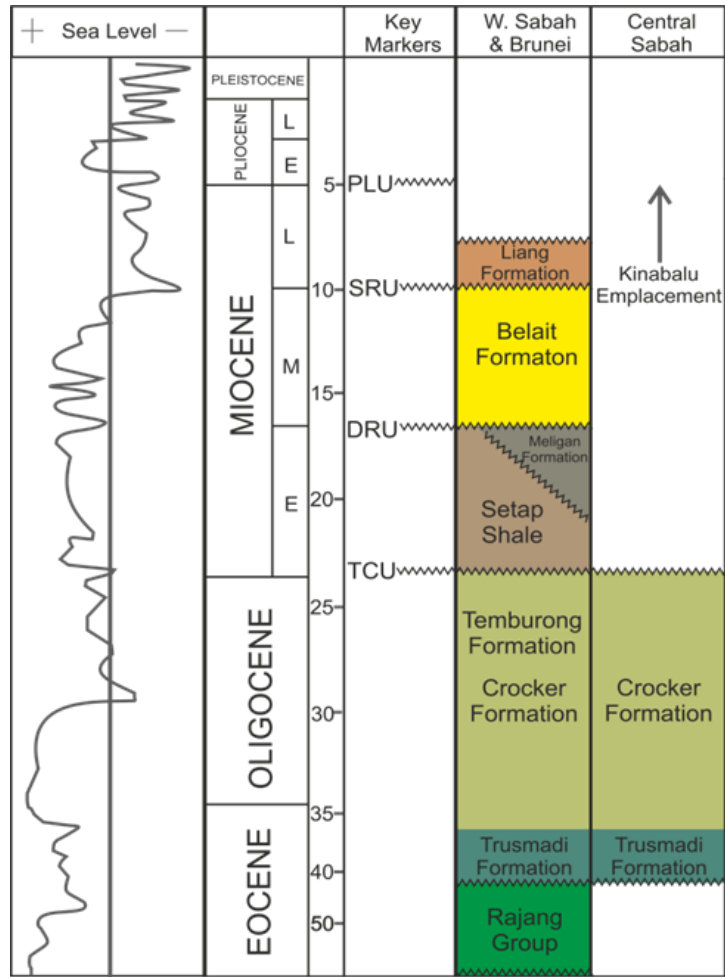


Figure 2. 11: Simplified stratigraphy of Sabah and Brunei modified from Hall (2013), Balaguru and Nichols (2004), and sources therein. Major unconformities offshore are from Bol and van Hoorn (1980), Levell (1987); Gartrell et al. (2011) and Van Hattum et al. (2006).

### 2.2.2.1 Crocker Formation

The folded and thrustured Crocker Range represents an elongate trough of Oligocene-Lower Miocene deep-water sediments that lie outboard of the Paleocene-Eocene Rajang Range, itself originating as an elongate trough which was folded, metamorphosed and uplifted to form a landmass by the Late Eocene (Hutchison, 1996). The Crocker Range is separated from the Rajang Range by a thrust fault and its probable unconformity (Hutchison, 1996), although the field relationship is not well exposed (Crevello, 2001). Continued

accretion of NW Borneo resulted in uplift of the Crocker Formation in the Miocene (Hutchison, 1996b; Hutchison et al., 2000).

The Crocker Formation lies immediately below the Deep Regional Unconformity of Levell (1987), a profound angular unconformity that was generated during an orogenic event which uplifted the Paleogene and older rocks. This unconformity marks the transition from uplift to rapid subsidence that was accompanied by deposition of the thick Neogene, shallow-marine clastic succession (Lambiase et al., 2008). The sedimentary sequence of this formation was folded, faulted and imbricated into a series of thrust slices by a compressive force operating during the Middle Miocene (Rangin et al., 1990) and forms elongated ridges trending N-S and NW-SE in strike directions in Southwest and West Sabah, respectively.

The original thickness of this sedimentary succession is uncertain because of the occurrence of numerous thrusts due to tectonic shortening, making stratigraphic reconstruction between outcrops nearly impossible; Wilson (1964) suggested that at least 6000 m of section is present, Tongkul (1987) argues for ~1000 m, whereas Crevello (2001) proposed that the net accumulation ranged between 1000 to > 10,000 metres. Several depositional elements are recognized in the Crocker turbidite complex: levee channels which are comprise channel axis and marginal facies, proximal levee and distal overbank levee facies, splays and avulsed channels, clay plugged channels, and distributary lobe-sheet splays (Crevello, 2001).

The age of the Crocker Formation is poorly constrained. Based on pelagic foraminifera found by Bowen and Wright (1957), the age of the Crocker Formation ranged from Oligocene to Miocene. Wilson (1964) at the regional scale assigned an Eocene–Early Miocene age for the formation. Tongkul (1987) mentioned that a shale sample in the western part of Sabah which was examined by the Shell group of paleontologists at Seria was fossiliferous and comprised of a few arenaceous foraminifera which have a long age range; ranging from Eocene to Early Miocene. Recent studies suggest that the outcrops around Kota Kinabalu are Late Eocene in age (Lambiase et al., 2008; Cullen, 2010). These data suggest that the age of the clastic Crocker Formation should be estimated to range from Eocene (?) to Late Oligocene – Early Miocene.

### **2.2.2.2 Miocene to Recent Deltaic Systems**

The Neogene (Miocene to Recent) deltaic systems formed a series of seaward prograding shelf/slope sequences that were locally sourced from uplift of the Borneo highlands. Traditionally, the deltaic systems have been divided into three main delta complexes generally younging from east to west (see Figure 2.10); 1) the Meligan Delta formed of the Upper Oligocene to Early Miocene sand-dominant Meligan Formation and the Early Miocene to Middle Miocene shale-dominant Setap Formation; 2) the Champion Delta of Middle to Late Miocene age comprising the onshore outcrop equivalents of the Belait, Miri and Sibuti Formations; and 3) the Baram Delta of mostly Pliocene age (Balaguru and Lukie, 2012). This deltaic succession is bounded by two significant regional erosional unconformities (see Figure 2.11); the Deep Regional Unconformity (MMU/DRU) separates the Champion Delta from the older Meligan Delta; and the Shallow Regional Unconformity (SRU) separates the Baram Delta from underlying the Champion Delta (Levell, 1987).

### **2.2.3 Style of Deformation**

The NW Borneo deep-water fold-thrust belt is a basinward thinning deep-water clastic wedge that is heavily deformed by numerous folds and thrusts. The NW Borneo margin can be divided into two distinct regions:(1) the offshore NW Sabah margin in the NE and (2) the offshore Brunei margin in the SW. Present-day maximum horizontal stress ( $Sh_{max}$ ) analysis across the NW Borneo margin reveals five tectonic provinces (e.g., King et al., 2009, 2010; Tingay et al., 2005, 2009; Morley et al., 2008, 2011; Figure 2.12). Three of these provinces describe the offshore Brunei margin. The extensional delta top province ( $Sh_{max}$  margin-parallel, NE-SW) coupled with the compressional delta toe province ( $Sh_{max}$  margin-normal, NW-SE) is consistent with gravitationally driven deformation observed in a delta system, whereas an inverted province ( $Sh_{max}$  margin-normal, NW-SE) of an older extensional province in the onshore and inner shelf area, reflects the margin's position on an active margin (e.g., King et al., 2009, 2010; Tingay et al., 2005, 2009; Morley et al., 2008, 2011).

The offshore NW Sabah margin is traditionally described by the inboard belt and the outboard belt. The inboard belt is characterized as regions of multiple

deformational phases of a structural style involving extension, inversion and compression, whereas the outboard belt is characterized as regions of gravity-driven delta tectonics (e.g., Hinz et al., 1989; Hiscott, 2001; Ingram et al., 2004). Recent studies by King et al. (2009, 2010) further divided the NW Sabah margin into an inner shelf mini basin province and an outer shelf thickened mobile shale province (see Figure 2.12).

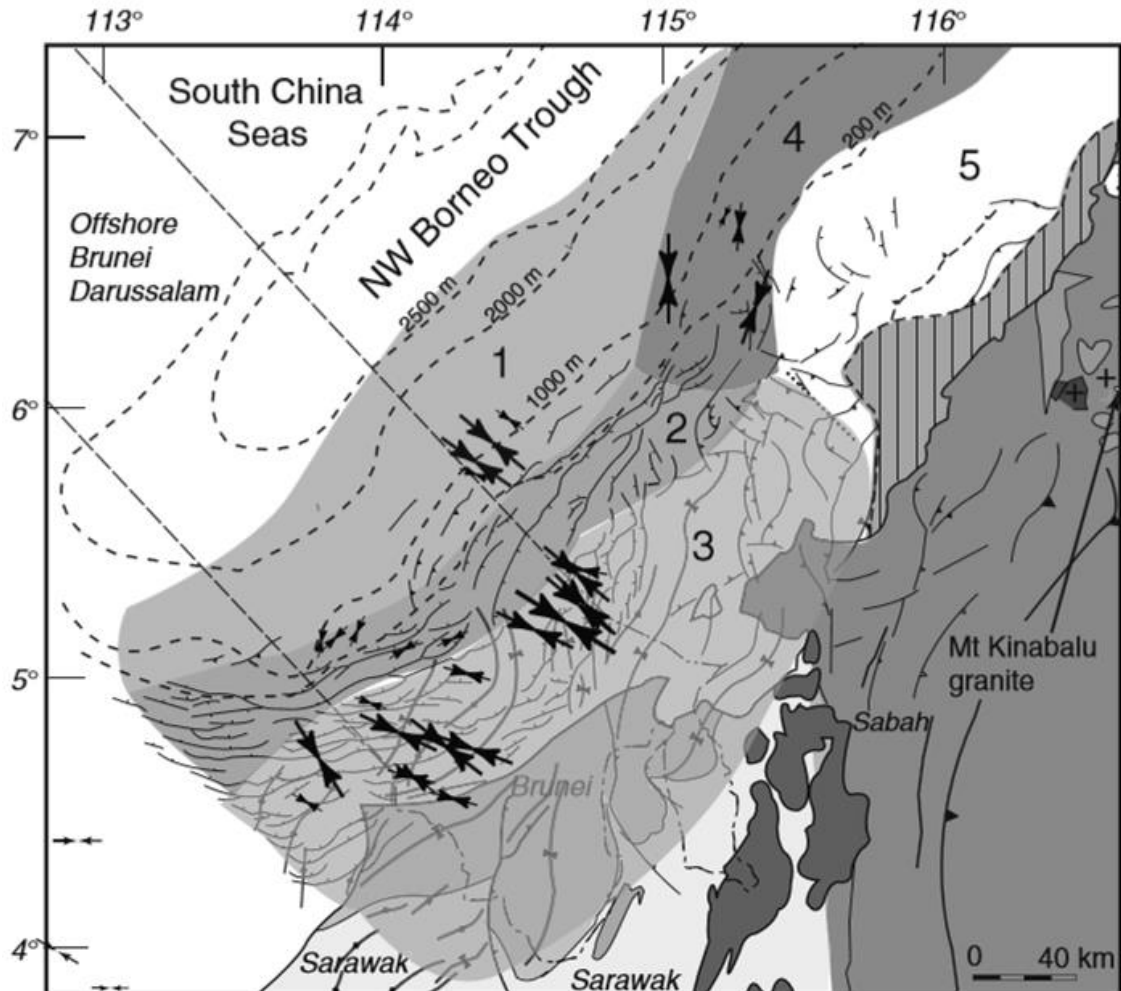


Figure 2. 12: Recent analysis of present-day maximum horizontal stress (Shmax) of the NW Borneo divided the margin into five provinces; 1) Deep-water fold and thrust belt; 2) Extensional growth faults in Baram Delta Province; 3) Inverted zone of Baram Delta Province; 4) Mobile shale deformation province; 5) Zone of strong inversion (from Morley et al., 2011).

The compressional delta toe, or deep-water fold and thrust belt of offshore NW Borneo is composed of a series of landward (southeast) dipping imbricate thrust sheets associated with fault-propagation folds that appear to sole into a common decollement surface, namely, the over-pressured Setap Shale (e.g., Hinz et al., 1989; Ingram et al., 2004, Hesse et al., 2009, 2010a, 2010b, Morley et al., 2011). The degree of deformation of the fold-thrust belt varies significantly along strike; with a general decrease towards the southwest. The southern part of the NW Borneo delta toe exhibits fewer, wider spaced anticlines with less surface expression (e.g., Franke et al., 2008; Hinz et al., 1989; Ingram et al., 2004, Hesse et al., 2009, 2010a, 2010b, Morley et al., 2011). While further northwards, the anticlines are steep, closely spaced with clear sea-floor expression (e.g., Franke et al., 2008; Hinz et al., 1989; Ingram et al., 2004, Hesse et al., 2009, 2010a, 2010b, Morley et al., 2011). The extensional delta top is characterized by seismic-scale normal growth faults striking NE-SW, which appear to detach within the Setap Shale (e.g., King et al., 2009, 2010; Morley et al., 2011). However, many well-developed extensional growth faults observed across the Baram Delta province have been inverted and are inactive. In the northern part of NW Borneo, there is very little active up-dip deltaic extension in the delta top to account for the delta toe compression (e.g., Hesse et al., 2009, 2010a, 2010b, Morley et al., 2011).

The cause of the northern Borneo offshore fold and thrust belt remains the subject of disagreement and discussion. Several key mechanisms have been discussed as the main controlling factors for deep-water compressional deformation. Some authors suggest that subduction has continued until the Late Neogene or until the present-day, and that the NW Borneo deep-water fold-thrust belt and trough represents an accretionary complex and an active subduction trench respectively (Tongkul, 1991, Simons et al., 2007, Sapin et al., 2011). Others interpret that the offshore deformation is the result of regional compressional events with thrusting resulting in a foreland fold and thrust belt (Bol and van Hoorn, 1980; Hinz et al., 1989; Cullen, 2010). Several authors interpret that the offshore deformation is largely gravity-driven but still suggest a contribution of regional compression on the offshore deformation in the northern Borneo (Tan and Lamy, 1990; Morley, 2007; Hesse et al., 2009, 2010b; King et al., 2010; Gartrell et al., 2011), and inferred that the imbalance between lengthening and shortening amount (excess of shortening) (Hesse et al., 2009, 2010b), stress orientations and GPS observations (Simons et al., 2007) to

indicate a role of tectonic stresses. The fold and thrust belt has also been interpreted as primarily developed in response to gravitational delta tectonics (e.g., Hazebroek and Tan, 1993, Hall, 2013) analogous to the deep-water fold and thrust belt of the Niger Delta. Hall (2013) suggests that most Neogene deformation is a result of episodes of extension, not compression as there is no shortage of tectonic events that could cause inversion in the sedimentary basins of northern Borneo during the Miocene–Recent. Extension caused subsidence and elevation in different places, was accompanied by magmatism (Mount Kinabalu), and mobility of the deeper crust and topographically induced stresses can account for the deformation that continues at present (Hall, 2013).

The occurrence of a major feature in the northern half of the margin (offshore NW Sabah) which was termed the “*allochthon unit*” has caused conflicting interpretations and extensive discussion. This unit is characterized by a thick zone of poor seismic data quality. Hinz et al. (1989) interpreted this unit as two “thrust sheet systems” representing an allochthon mass of pre-Middle Miocene rocks that came to its present position by gravity gliding; the “Major Thrust Sheet System” overlying the “Lower Thrust Sheet System”. In contrast, Franke et al. (2008), based on new 2D seismic data and gravity modelling, found no evidence to separate the thrust sheet system. These authors suggested that the unit could be Paleogene sediments surrounded by an ophiolite of the Proto South China Sea or a carbonate body. It is interpreted to have been deformed by a crustal shortening process that then provides an explanation for the observed chaotic seismic facies. However, a recent analysis of present-day maximum horizontal stress ( $Sh_{max}$ ) characterizes the margin as a shale province (e.g., King et al., 2009, 2010). The chaotic internal reflections of this unit are interpreted to represent thickened mobile shales, with N-S directed  $Sh_{max}$  orientations of the shale province that are rotated clockwise compared to the NW-SE  $Sh_{max}$  orientations of the toe thrust belt and aligned parallel or sub-parallel to the boundary of the chaotic internal reflections unit. This could suggest a geo-mechanical property contrast between a soft, thickened mobile shale and surrounding stiffer sediments of the deep-water fold and thrust belt (e.g., King et al., 2009, 2010; Morley et al., 2011; see Figure 2.12).

## **Chapter 3**

### **Deformation Style along the DWFT System and the Allochthonous Wedge of NW Borneo - Integrating Field and Seismic Studies.**

#### **3.1 Introduction**

The offshore NW Borneo has been the focus of several studies through the years. Despite the long-standing academic interest in deep-water fold-and-thrust belts of offshore NW Borneo, the occurrence of the "*allochthon unit*" that is characterized by a thick zone of poor seismic data quality still caused conflicting interpretations and discussion. As a consequence of low seismic resolution, relatively little research has been directed at these units in comparison to overlying, well imaged, sedimentary successions. This has left important, unanswered questions relating to the nature of the NW Borneo allochthonous wedge. This chapter attempts to throw some light on these problems and hopefully will generate further discussions.

The aim of this chapter is to provide a detailed characterization, through description and interpretation of the general appearance of deformational style along the deltaic system and the allochthonous wedge, which can lead to a better understanding of the regional-scale structural geometry along the NW Borneo margin. The main basis of the study presented in this chapter was the structural interpretation and mapping based upon 2D multi-channel seismic profiles across the northern half of the NW Sabah margin (northern NW Borneo), and a selection of published seismic profiles across the southern half of the NW Sabah margin (towards offshore Brunei), transecting the NW Borneo deep-water fold and thrust system (Figure 3.1). This is combined with a sub-seismic scale investigation of onshore outcrops in NW Sabah that illustrate onshore compressive deformation, and which provide insight into the deformation geometries that are likely to be present but which are below seismic resolution in the directly equivalent offshore seismic data (see Figure 3.1).



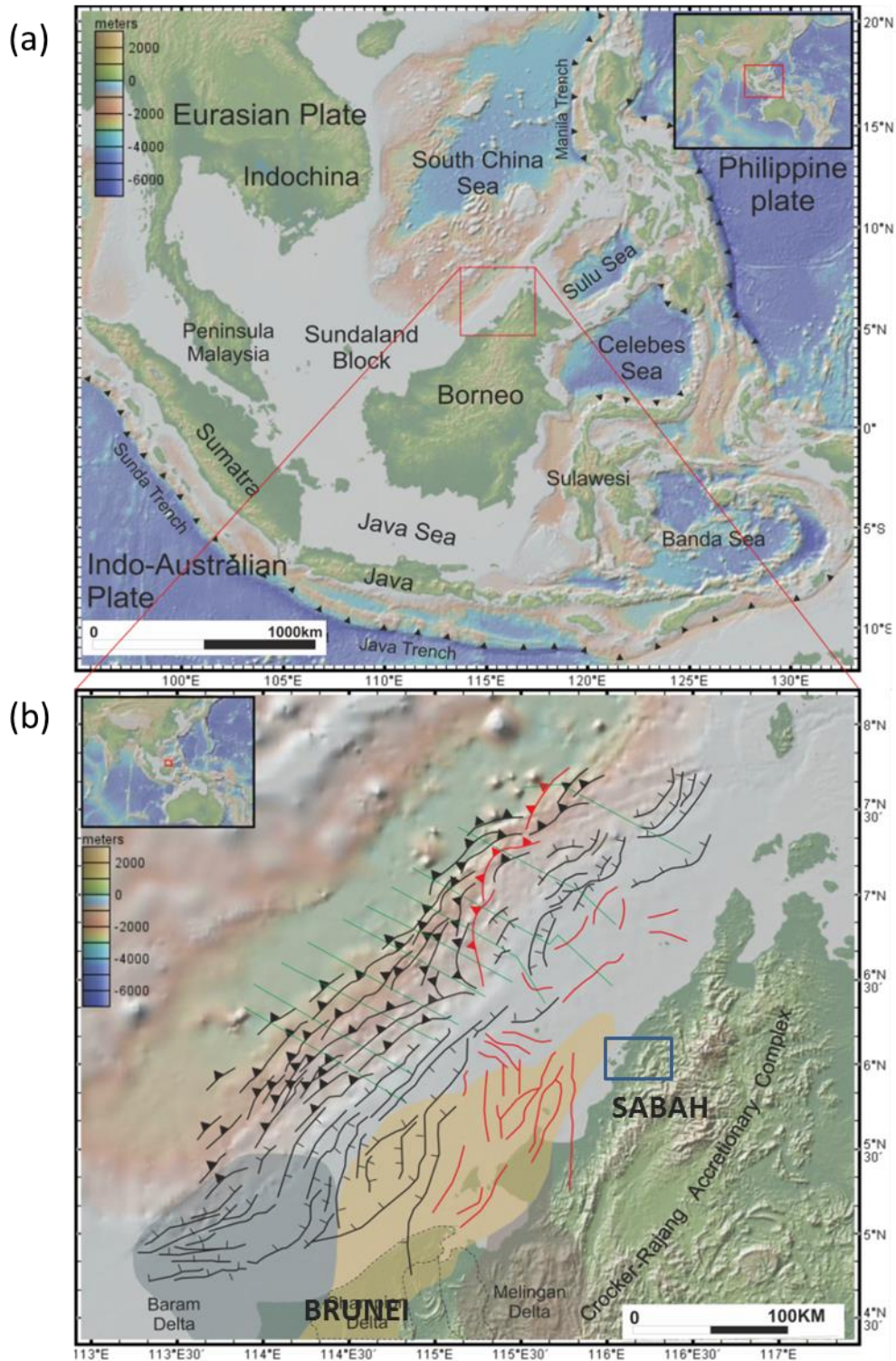


Figure 3. 1: (A) Regional location map of NW Borneo (red rectangle) in South East Asia. (B) Structural map of NW Borneo (modified from Hesse et al, 2010b) showing the location of the 2D profile presented in this study (green lines) and the approximate location of outcrop studies (blue rectangle). Location of the three major delta systems of NW Borneo margin is from Tingay et al. (2005).

## **3.2 Offshore Studies**

### **3.2.1 Data and Methodology**

Selected 2D seismic profiles from the available 2D TWT seismic survey data sets that acquired by Hess Corporation were depth-converted using Petrel software to be used for determining the geometries of faults and folds. Geographically, the 2D seismic data lie between 6° to 8° N and 114.5° to 117° E within the South China Sea, with dip lines trending approximately NW-SE across the northern half of the NW Sabah margin (northern NW Borneo), running generally perpendicular to the shoreline and perpendicular to the strike of structures within the subsurface.

To convert TWT to depth (metres), a simple velocity model with average interval velocities were assigned to each reflection interval. Since there is no well data were available, average interval velocities of the deltaic stratigraphy published by Franke et al. (2008) was used. The velocity values used were 1500 m/ sec for water, 2000 m/ sec for average velocity of Pliocene/Pleistocene sediment, 2350 m/ sec for average velocity of Late Miocene-Pliocene sediment, and 3150 m/ sec for average velocity of Middle-Miocene-Late Miocene sediment. A depth-converted section shows that the geometric effect of converting TWT to depth is minimal. Importantly, fault planes have similar geometries to their corresponding time sections (Figure 3.2).

A selection of previously published depth-migrated seismic profiles from Hesse et al. (2010b) transecting the southern half of the NW Borneo deep-water fold thrust belt (BGR86-24 to BGR86-12) was combined with the selected available seismic data across the northern half of the NW Borneo deep-water fold thrust belt (BGR86-10 to BGR86-02) to provide a better overview of margin deformation. The data were acquired by the Federal Institute for Geosciences and Natural Resources (BGR) in 1986. The data have been reprocessed and depth-migrated by Hesse et al. (2009, 2010a, 2010b). Detail description of the data processing and depth-migration is outlined below.

The pre-stack processing included trace editing, CMP-sort (25 m spacing), predictive deconvolution, amplitude correction for spherical divergence based on stacking velocities, normal move-out correction and muting. Multiple attenuations were performed by a Radon velocity filtering technique that was

combined with an inner trace mute providing sufficient results. Stacking velocities were picked at regular intervals of 1.5 km along every line. The seismic data were stacked after the normal move-out correction. The velocity field for the post-stack depth migration was estimated by a step-by-step approach based on the stacking velocities determined by semblance analysis. The velocity information was converted into interval velocities using a smoothed-gradient algorithm. The final depth migration algorithm used was an implicit finite difference (FD) migration code. FD time-migration was run for quality control of the post-stack depth migration (Hesse et al., 2009, 2010a, 2010b).

There is no directly available well information for this project; stratigraphic boundaries and other information (velocity, age and other) have been collected from open-sources (i.e., published papers and reports). The interpretation was based on the patterns of amplitude continuity, strength and internal geometry of the units. The key focus of interpretation of structures was on dip lines, as the geometry of the structures can be more easily visualized on sections perpendicular to the strike. Strike lines were used for loop-ties with other seismic sections to delineate the features of larger scale geological significance (i.e. structural features and basin geometry). Seismic data interpretation was done using the Petrel software. Faults were interpreted according to the discontinuity of reflections, where seismic reflections with low coherency represent the fault plane. Subsequently, the selection of key horizons and major unconformities was carried out and was crucial for the work that follows.

The locations of the selected 2D seismic profiles from the available 2D TWT seismic survey data sets that acquired by Hess Corporation and previously published depth-migrated seismic profiles from Hesse et al. (2010b) acquired by the Federal Institute for Geosciences and Natural Resources (BGR) in 1986, are shown in figure 3.3.



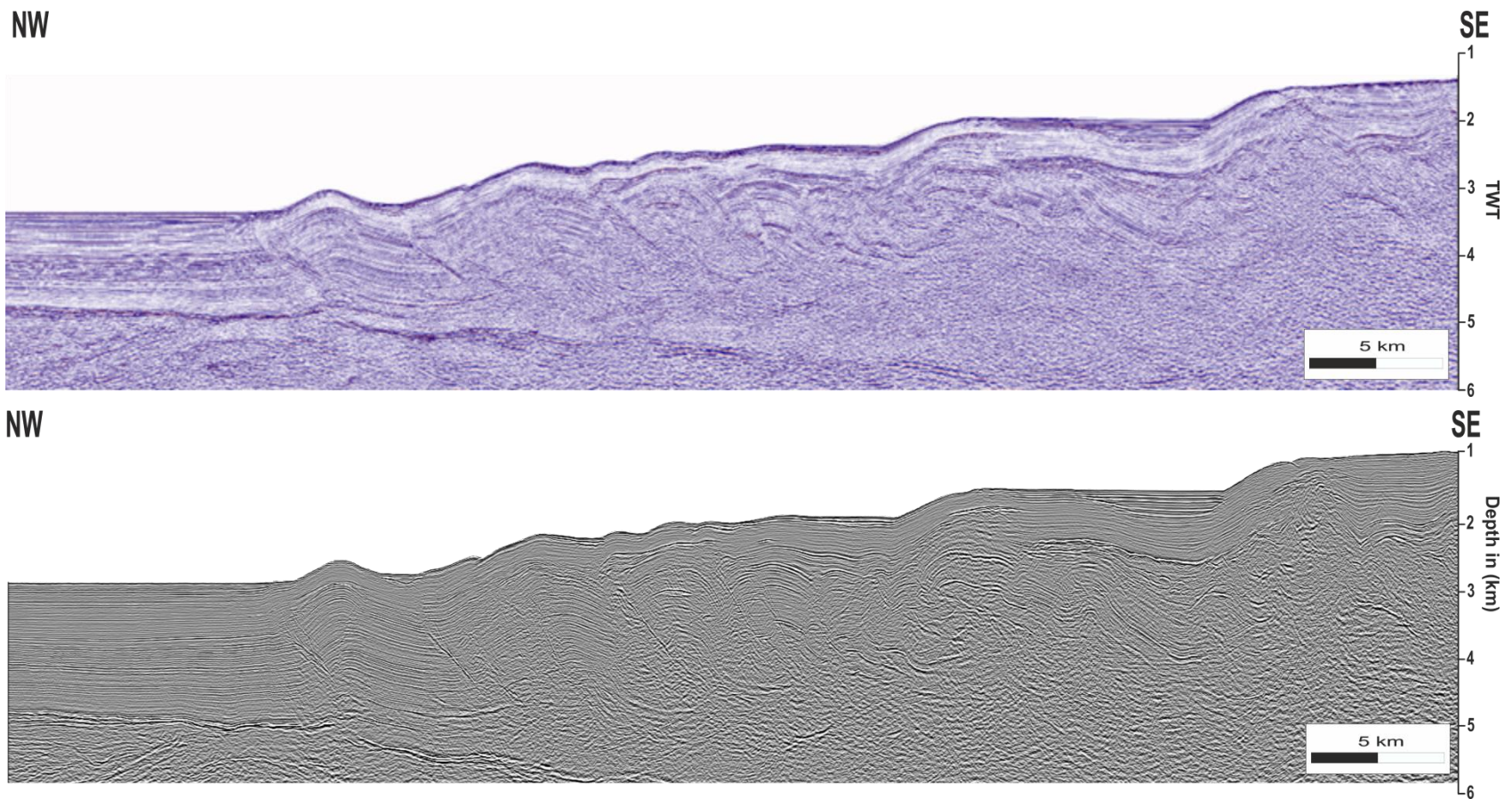


Figure 3. 2: NW-SE-trending TWT seismic profiles (above) and depth converted seismic profiles (below) of offshore Sabah (BGR-10). Note the geometric impact of depth conversion here is minimal; as the depth converted geometry of a fault-related fold is relatively unchanged from its equivalent time section.

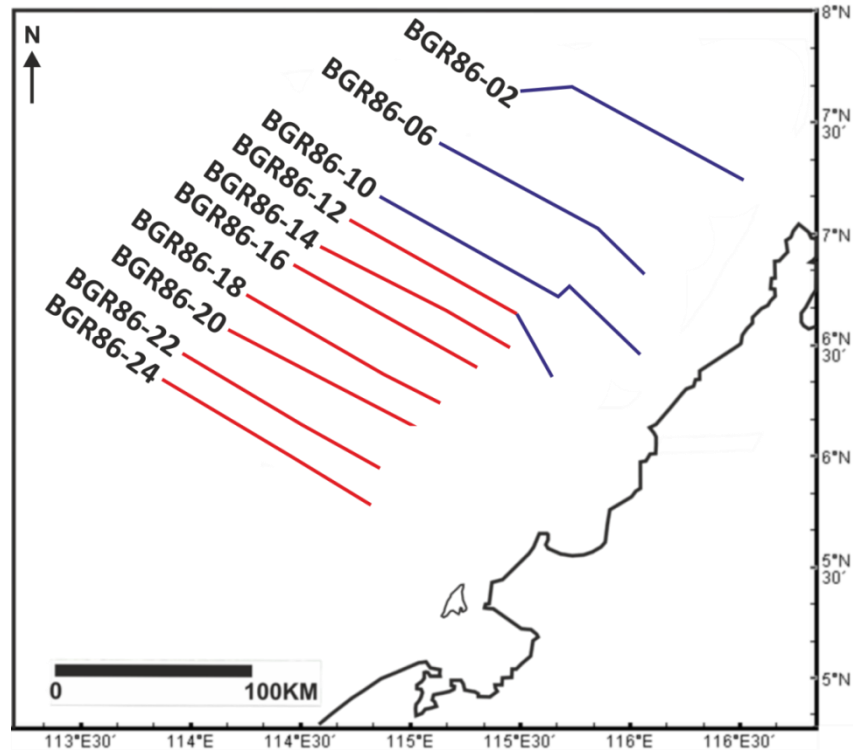
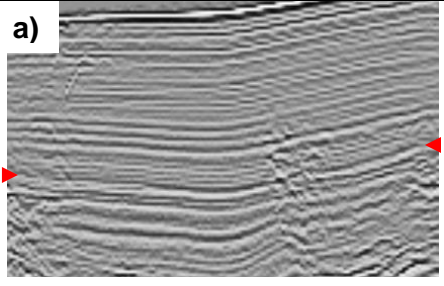
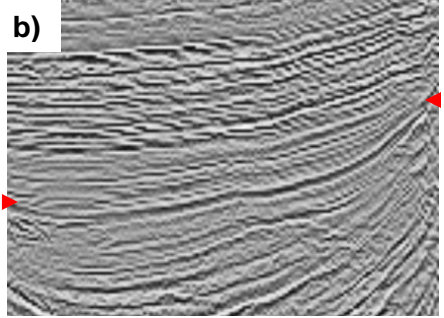
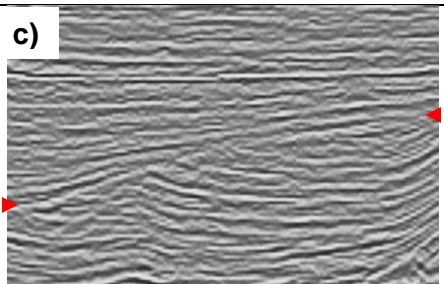


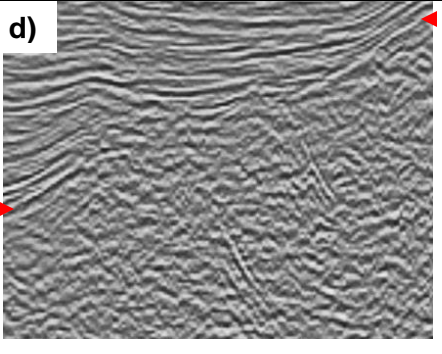
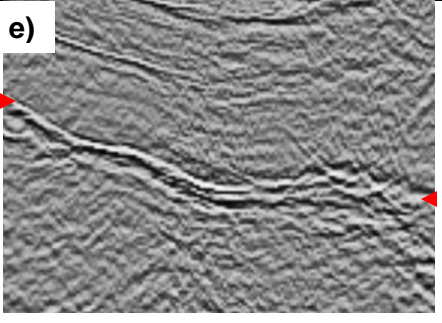
Figure 3. 3: The locations of the selected 2D seismic profiles from the available 2D TWT seismic survey data sets that acquired by Hess Corporation (blue) and previously published depth-migrated seismic profiles from Hesse et al. (2010b) acquired by the Federal Institute for Geosciences and Natural Resources (BGR) in 1986 (red).

### 3.2.2 Deltaic (seismic) Stratigraphy

A widely extensive seismic facies characterised by uninterrupted sub-parallel stratification, observed in the NW Borneo Trough, can be traced towards the NE (up-dip) into time equivalent unconformities. Six seismic units (1, 2, 3, 4, 5 and 6) were interpreted according to their characteristics, featuring particular reflection patterns, geological age and internal structure, and being separated by five sequence boundaries. These sequence boundaries represent horizons/unconformities assigned from youngest to oldest, as Late Pliocene (Late Pliocene Horizon, LPH), Early Pliocene (Pliocene Unconformity, PLU), Late Miocene (Shallow Regional Unconformity, SRU), Early Middle Miocene (Deep Regional Unconformity, DRU) and Oligocene-Late Early Miocene (Top Crocker Unconformity, TCU). Table 3.1 summarizes the seismic characteristics of the key laterally extensive horizons used in this study and their relationships with previous studies.

Table 3. 1: Sequence boundaries used in this study and their relationships with previous studies.

Horizon	Time	Previous Studies	Seismic Characteristics
A (LPH)	Near-top Late Pliocene	Horizon A (Hinz et al., 1989; Franke et al., 2008)	Nearly parallel to seafloor, moderate to strong amplitude, high to moderately continuous reflector. 
B (PLU)	Near-top Early Pliocene	Pliocene Unconformity, PLU (Levell, 1987) Horizon 4 ( Hesse et al., 2009)	Moderate to strong amplitude, high to moderately continuous reflector with subtle onlap. 
C (SRU)	Near-top Late Miocene	Horizon B/5 (Hinz et al., 1989; Franke et al., 2008) Shallow Regional Unconformity, SRU (Levell, 1987) Horizon 3 (Hesse et al., 2009)	Moderate amplitude, moderately continuous reflector with onlap above and truncation below. 

E (DRU)	Early Middle Miocene	Horizon C/6 (Hinz et al., 1989; Franke et al., 2008) Deep Regional Unconformity, DRU (Levell, 1987) Horizon 2 (Hesse et al., 2009)	Moderate amplitude, low to moderately continuous reflector with onlap above and truncation below.	
F (TCU)	Oligocene -Late Early Miocene	Horizon D (Hinz et al., 1989; Franke et al., 2008) Horizon 1 (Hesse et al., 2009) Top Crocker Unconformity, TCU (Van Hattum et al., 2006)	Strong amplitude, strongly continuous reflector with onlap above and truncation below.	



**(1) Seismic Units 1 and 2 (Late Pliocene-Recent and Early Pliocene-Late Pliocene).**

The prominent, high-amplitude seabed reflection is underlain by a package of parallel to sub-parallel, locally divergent, mostly continuous reflectors of low to moderate amplitudes (Late Pliocene-Recent) (Table 3.1 (Figure a); Figure 3.4). This unit is often affected by numerous small tensional normal faults especially at the crests of anticlines (Figure 3.4). Seismic unit 1 is bound at its base by a triplet of moderate to strong amplitude reflections, labelled as Horizon A (LPH). This sequence boundary is nearly parallel to the sea floor and is represented as a highly to moderately continuous reflector (Table 3.1 (Figure a)). The underlying seismic unit 2 (Early Pliocene-Late Pliocene) is characterized by alternating intervals of low, moderate and higher amplitude reflectors showing parallel to sub-parallel, mostly continuous reflections (Table 3.1 (Figure a); Figure 3.4). This seismic unit (seismic unit 2) is bound at its base by an unconformity labelled as Horizon B (PLU). Horizon B (PLU) is defined by the subtle onlap of overlying reflectors above a moderate to strong amplitude of highly to moderately continuous seismic reflection (Table 3.1 (Figure b)).

**(2) Seismic Unit 3 (Late Miocene-Early Pliocene, SRU)**

The seismic character of the unit (seismic unit 3, Late Miocene- Early Pliocene) underlying the Horizon B (PLU) is of parallel to sub-parallel, locally divergent, continuous to sub-continuous reflections with the amplitude of reflectors increasing from low to high upward (Table 3.1 (Figure c); Figure 3.4). This seismic unit (seismic unit 3) is bound at its base by an erosional unconformity labelled as Horizon C (SRU). Horizon C (SRU) is defined by apparent erosional truncation of underlying reflectors below a moderately continuous reflector of moderate amplitude (Table 3.1 (Figure c)). This unconformity correlates with the Shallow Regional Unconformity (SRU) of Levell, (1987). This unconformity is seen as a well-developed Late Miocene erosional unconformity in Sabah and coincides with significant regional uplift and erosion of the margin around that time (Cullen, 2010).



**(3) Seismic Units 4 and 5 (Middle Miocene-Late Miocene and Early Miocene-Middle Miocene)**

Horizon D represents a strong erosional unconformity characterized by a low to moderately continuous reflector of moderate amplitude with onlapping reflectors above and erosional truncation below (Table 3.1 (Figure d)). This surface boundary separates the overlying seismic reflections showing parallel, sub-parallel to divergent, continuous to sub-continuous reflections of low to moderate amplitude (seismic unit 4, Middle Miocene-Late Miocene) from the underlying highly discontinuous, chaotic to nearly transparent seismic reflections (seismic unit 5, Early Miocene- Middle Miocene) (Table 3.1 (Figure d); Figure 3.4). This surface boundary correlates to the Middle Miocene Deep Regional Unconformity (DRU) that has been dated at 16–15 Ma (Hutchison, 2005; Gartrell et al., 2011). It is considered to be related to the end of subduction (Levell, 1987) and represents a sedimentary transition from shallow-water to bathyal depositional environments (Hinz & Schlueter, 1985).

**(4) Seismic Unit 6 (Late Oligocene-Early Miocene, BMU)**

Horizon E at the top of seismic unit 6 represents the most prominent regional unconformity, which correlates to the Late Early Miocene regionally mappable unconformity extending from the Dangerous Grounds to beneath the NW Borneo Trough (Figure 3.4). It is related to the rifting and opening of the South China Sea (Hinz et al., 1989). This unconformity is characterized by strong amplitude of continuous reflector, with truncating reflectors of the Oligocene-Late Early Miocene syn-rift sequence (seismic unit 6) beneath, which displays numerous horst and graben features (Table 3.1 (Figure e); Figure 3.4). This unconformity has been given several names that correspond to the Top Crocker Unconformity of Van Hattum et al. (2006), but is often called the Base Miocene Unconformity (BMU) by oil companies (e.g. Gartrell et al., 2011). Hutchison (2004) refers to this unconformity as the Middle Miocene Unconformity while Hall (2013) and Cullen (2010) have argued that this unconformity is older than the Middle Miocene Unconformity (MMU).



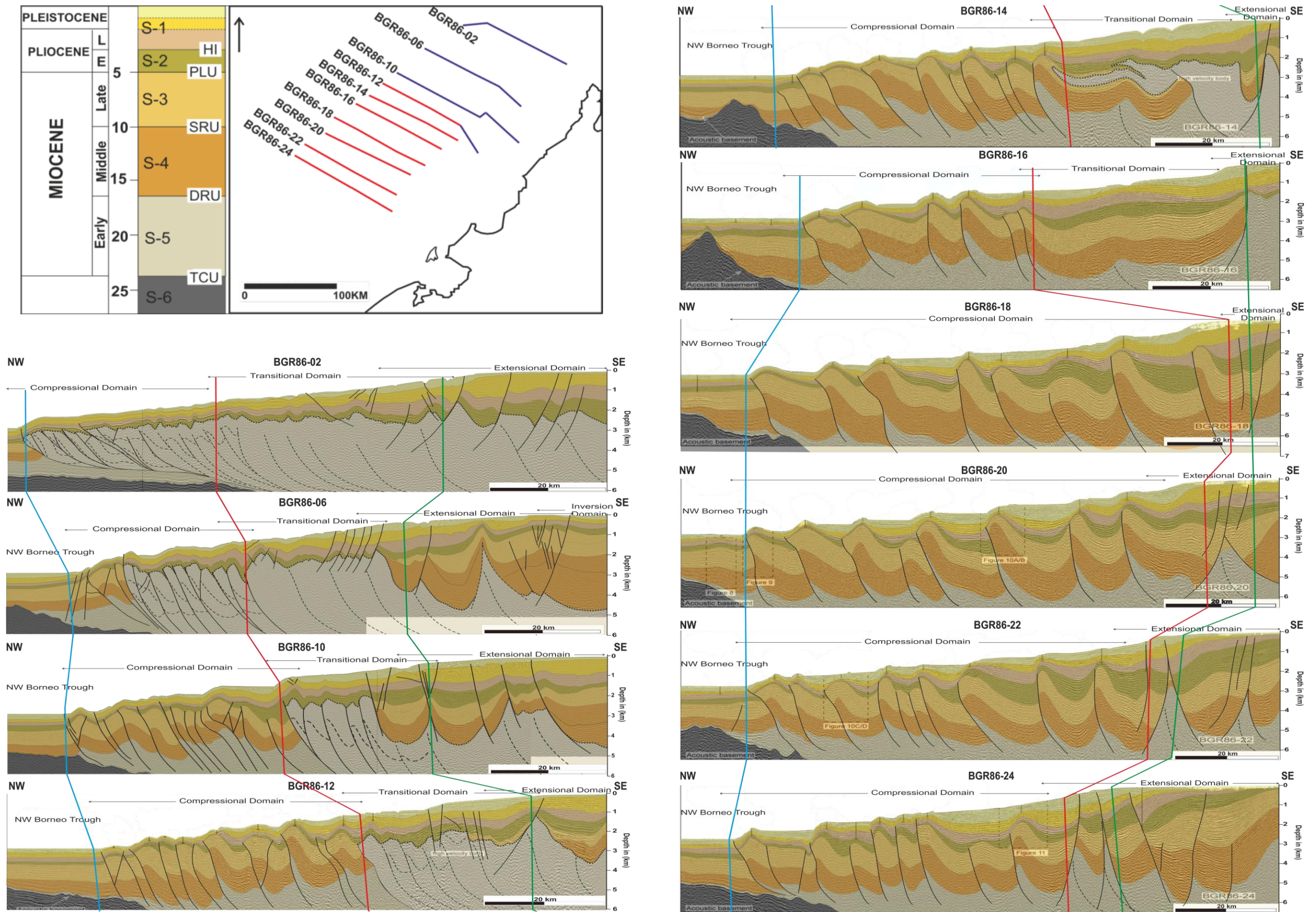


Figure 3. 4: Regional seismic profiles delineate the key features of margin deformation from northern segment (BGR86-02) segment to southern (BGR86-24) segment.



### **3.2.3 Observations and Interpretation**

Structural mapping of the seismic data has allowed further subdivision of the deformation of the deltaic sequence into four structural domains, based on structural styles imaged on the data (as seen in Figure 3.4); 1) an inversion province in the inner shelf and onshore region, 2) a proximal extensional province, 3) a transitional zone situated over the outer continental shelf, and 4) a contractional zone in deep-water down-dip regions.

#### **3.2.3.1 *Inversion and Extensional Domain***

The extensional domain includes both regional (seaward-dipping) and counter-regional (landward-dipping) growth faults. Some of the growth fault geometries indicate that they are formed on top of the fold limbs of earlier compressional structures, which could themselves be from an earlier phase of gravity-induced compressional structure or the pre-existing tectonic compressional structure (Figure 3.5). The southern half of NW Sabah is characterized by relatively more complex deformation that is made up of both paired regional and counter-regional growth faults (see Figure 3.4). These faults have created significant accommodation space, with the largest portion of the sediment thickness. Significant stratal bending with anticlinal or synclinal geometries is seen of adjacent individual hanging wall stratal reflections. In contrast, moving towards the northern end of the margin, the deformational style is dominated by a series of more closely-spaced seaward-dipping regional growth fault-bounded depocentres forming an asymmetric basin that is tilted to the south-east with a relatively thinner depocentre (see Figure 3.4).

Most of the upper tips of major growth faults terminate at either the seabed reflection or within seismic unit 1. Seismic units 2 to 4 display varying degrees of thickening and wedge forms in the hanging walls of individual faults, indicative of accommodation created during fault activity due to sediment loading during delta progradation. The Pliocene to Recent episode of extensional activity is interpreted to reactivate older collapse faults and was associated with additional tensional faulting; a series of antithetic, synthetic, conjugate fault pairs and crestal collapse structures, subordinate to the main deformational structure (Figure 3.5).

The overall structural pattern of the extensional domain have been interpreted to have been interrupted by episodic compressional events which deformed and inverted most of the extensional structures in the eastern part of the study area (in the inner shelf and onshore region) (e.g., Bol and van Hoorn, 1980; Hinz et al., 1989; Hazebroek and Tan, 1993; Morley et al., 2003; Saller & Blake, 2003; Hesse et al., 2009, 2010b; King et al., 2009, 2010). This observation is justified by the thickness difference of the Middle Miocene sequence between the hanging wall and footwall of the SW-directed reverse faults (Figure 3.5 (BGR86-10)) and displacement of the faults that still retain net-normal offset, but which appear to have been structurally inverted above their original regional elevation (Figure 3.5 (BGR86-12)). Thinning of the Early Pliocene sequence above the core of each inversion anticline and the onlapping relationship of the Late Miocene Sequence onto the top of the Middle Miocene Sequence suggests that the first identifiable phase of inversion occurred within the Latest Miocene-Early Pliocene. Inversion appears to have continued over several older structures until the Recent as evidenced by continued thinning of the Pliocene-Recent sequence and subsequent erosion above active structures (see Figure 3.5).

#### ***3.4.3.2 Transitional Domain***

The proximal extensional to distal compressional transition is marked by deformation involving the superimposition of gravity-driven extension and contraction structures. The length of the transitional area in the northern segment is greater, up to 40 km wide and is typically shorter and diminished southward, to the point where the extensional domain is almost adjacent to the contractional domain, and consists of listric extensional faults with associated growth packages at the trailing edge, and thrust faults at the leading front of the domain (as seen in Figure 3.4). This domain is marked by the culmination of the over-thrust allochthonous wedge and reveals contrasting structures and geometries varying from discrete features of internal thrusting to a folded roof. The observed deformational style affecting this domain can be subdivided into several structural elements which include an over-thrust wedge culmination, internal imbricate thrusting, and a folded roof and structural high, as will be described in more detail below.



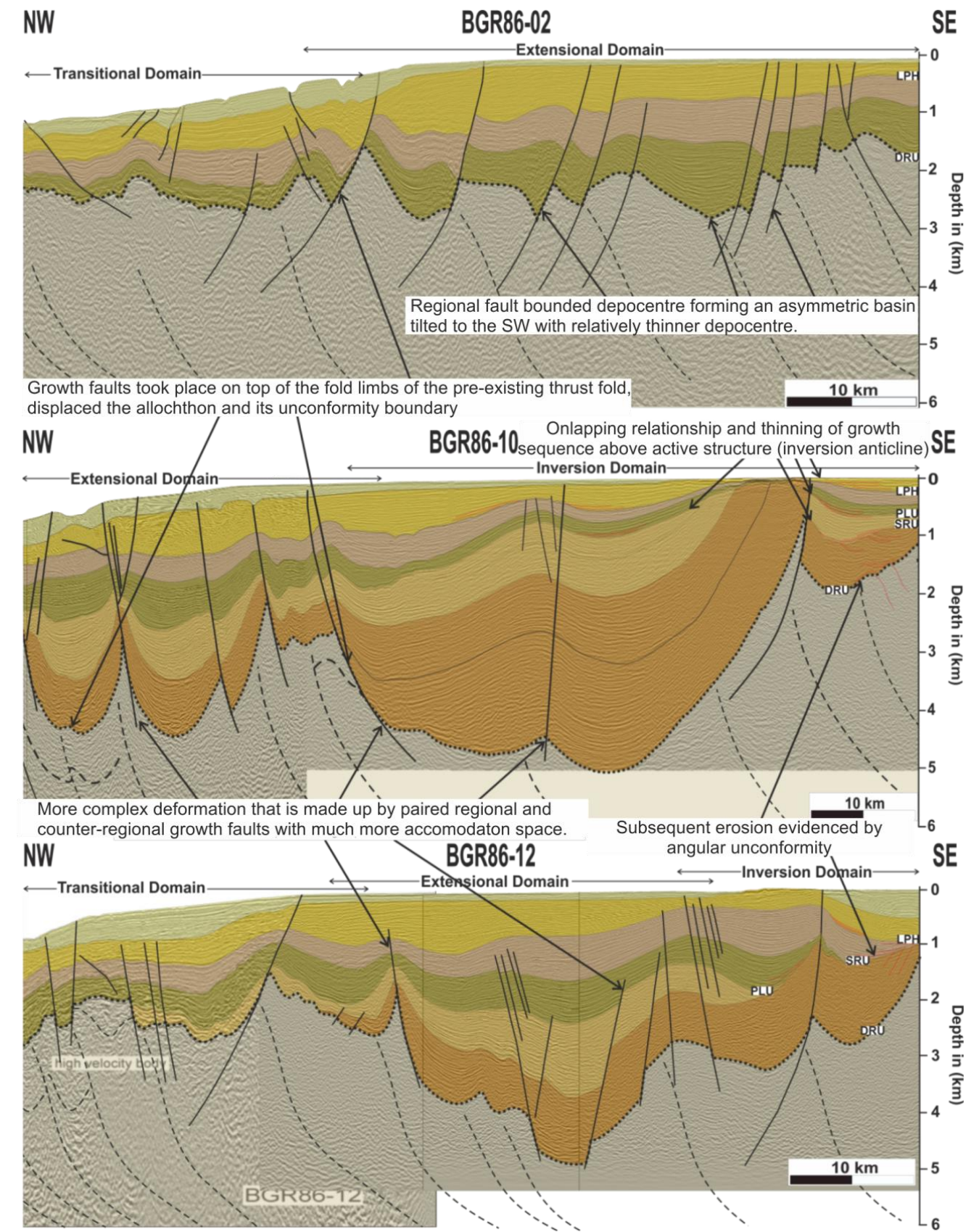
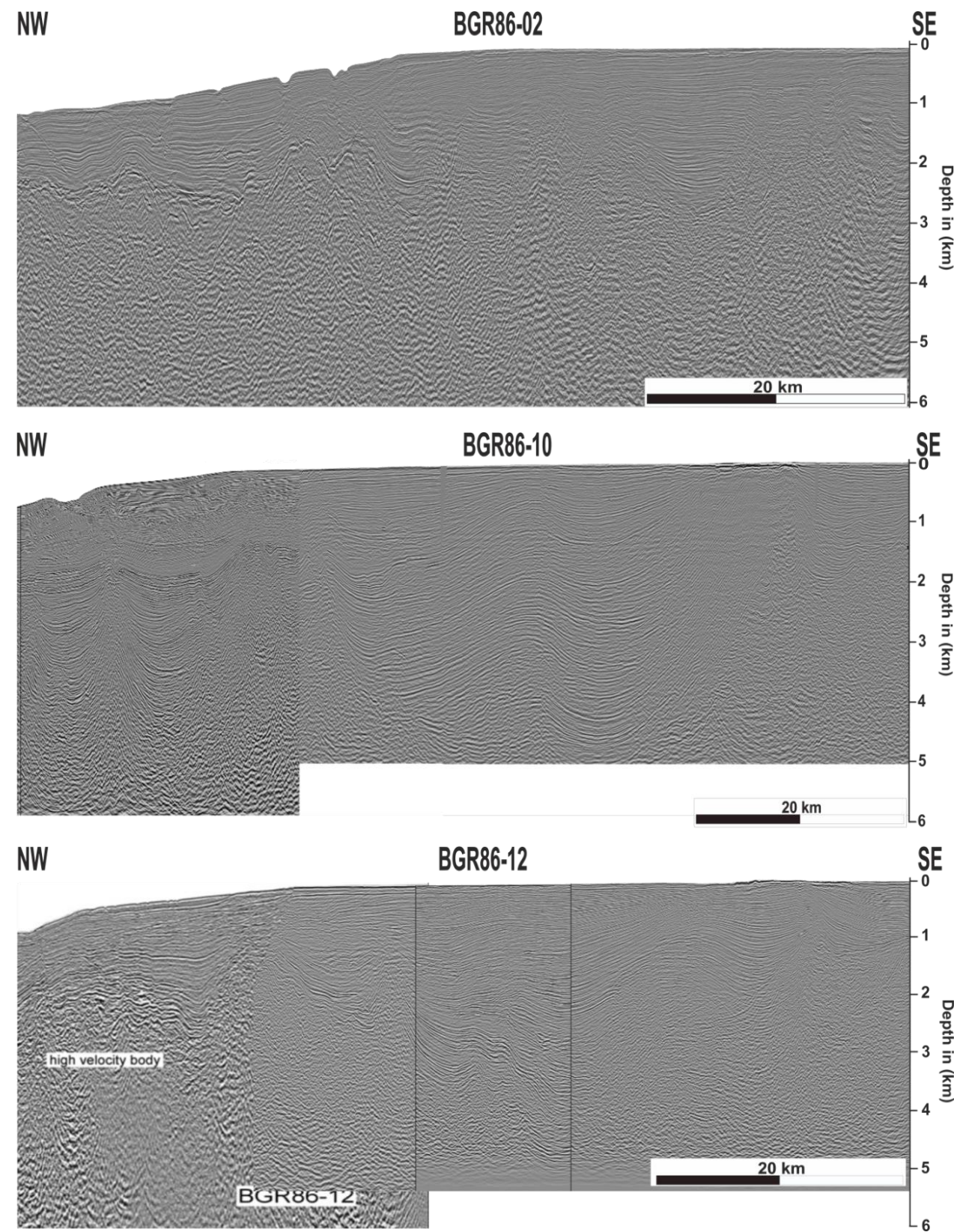


Figure 3. 5: Un-interpreted and interpreted seismic profiles in the extensional domain, showing north to south (BGR86-02 to BGR86-12) lateral variation of the extensional deformation. Regional growth faults dominate deformational style with relatively thin depocentres in the northern segment, compared to more complex deformation with both paired regional and counter-regional growth faults and the largest portion of the sediment thickness in the southern segment.



**i) Wedge Culmination**

The leading edge of the allochthon wedge is characterized by a seaward-tapering wedge with its roof against an over-thrust hanging wall. The over-thrust displacement creates a culmination of an imbricate allochthon wedge thrust over the Middle Miocene to Recent deltaic sequence (Figure 3.6). Seismic reflection character indicates a significant lateral transition from a coherent and stratified seismic facies in the deep-water down-dip deltaic contractional domain to a seismically chaotic and incoherent seismic facies closer towards the leading over-thrust wedge, which suggests that this over-thrust marks the seaward limit of the allochthon advanced (see Figure 3.6). The over-thrusted allochthon is best developed in the northern segment, as seen in BGR-02 to BGR-14, and dies out southward beneath the extensional domain (as seen in Figure 3.4). The leading thrusts with out-of-section movements displaced the Late Miocene/Middle Miocene strata in the extensional/transition domain in the southern segment (Figure 3.6 (BGR86-14)), and almost cuts the seafloor in the most distal part of the northern wedge (Figure 3.6 (BGR86-02)).

**ii) Internal Imbricate Thrusting**

Most internal reflectors of the thick, highly deformed, wedge-shaped allochthon package are seismically chaotic and incoherent. However, some nearby lines show that some high-amplitude events are present (see Figure 3.6). This chaotic sequence of deformed reflectors appears to contain many oblique reflectors suggestive of intense zones of internal deformation. These reflections are unlikely to be seismic artefacts as their geometry, spacing and landward dips resemble an imbricate stack of thrust sheets dipping to the south-east (see Figure 3.6). Seismic profiles across the allochthon illustrate that these internal thrust and fold structures are bounded at the top by an unconformity and capped by seaward-migrating and basin-ward-thinning Middle Miocene-Recent deltaic sediments (see Figure 3.6). The individual internal thrust faults of the allochthon imbricate system are generally truncated beneath this unconformity except in local areas where a recent activation of the reverse faults is implied with faults penetrating through the unconformity, and segmenting the unconformity's reflectors (see Figure 3.6). On some sections, the crest of the internal fault-related fold were evidently eroded and clearly truncated below the unconformity boundary (see Figure 3.6).



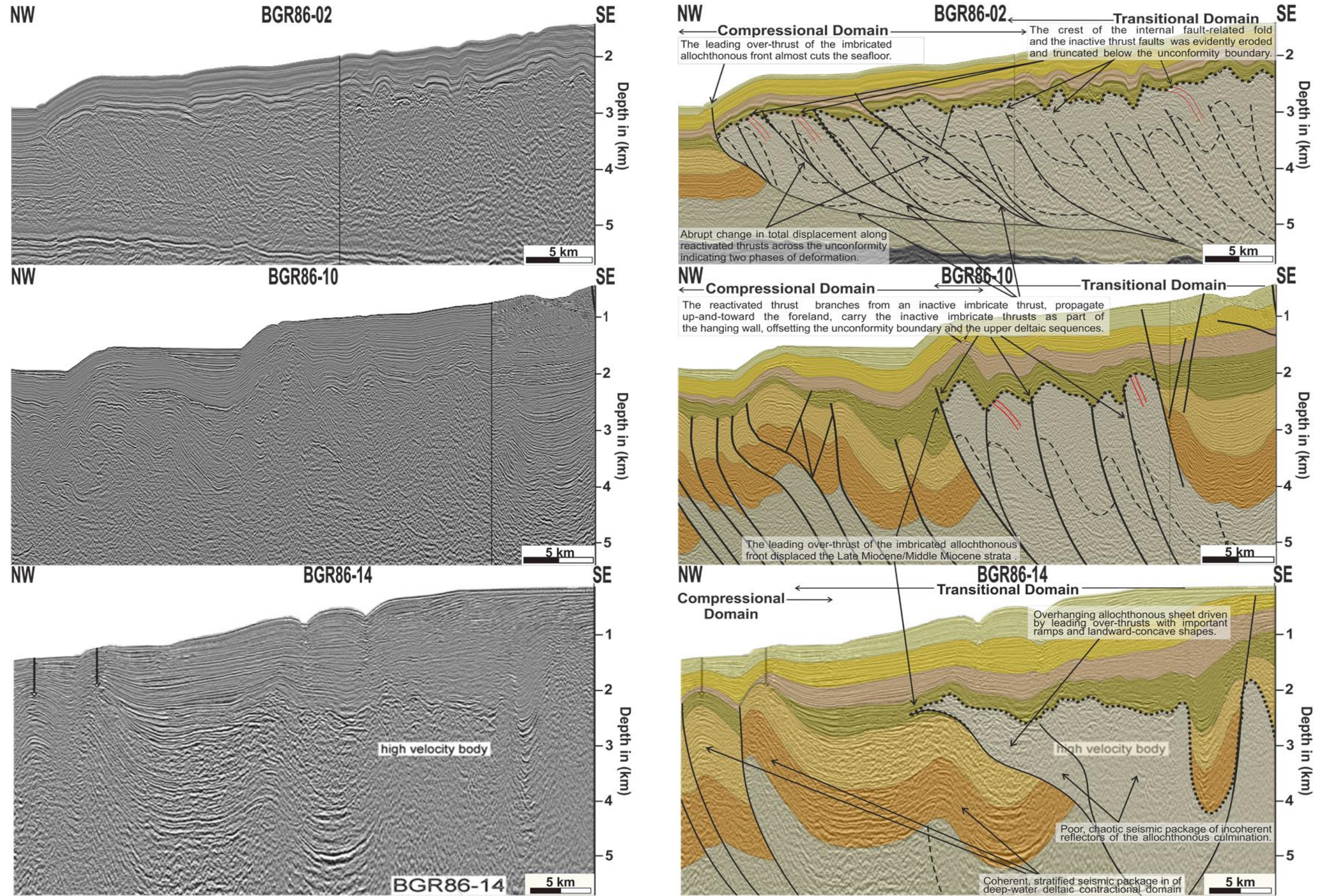


Figure 3. 6: Un-interpreted and interpreted seismic profiles of the allochthon wedge showing north-west-ward and sea-ward progression of the over-thrusted allochthon over the Middle Miocene to Recent deltaic sequence; the allochthon front is best developed and almost cuts the seafloor in the most distal part of the northern wedge (BGR86-02); whereas it dies out and displaces the Late Miocene/Middle Miocene strata in the transitional zone in the southern segment.



### iii) **Folded Roof and Structural High**

The over-thrusted allochthon wedge is overlain by a low- to moderate-relief, smoothly undulating folded roof of Latest Miocene to Recent deltaic sediments. Geometrically, the overlying strata generally show asymmetric and offshore verging anticlines, compatible with a compacted drape rooted in landward dipping imbricated thrusts (Figure 3.7 (a)). Whereas, in some sections, although much less developed, some folds are characterized by nearly symmetrical broad upright fold geometries of the upper roof units and the lower, seismically chaotic, incoherent reflectors of the allochthon units are isoclinally folded (Figure 3.7 (b)).

One question that can be raised about the symmetrically folded roofs is whether they are draping steeply dipping imbricated folds rooted by a near vertical thrust/reverse fault or whether they are mobile bodies piercing the overburden. However, the folded roof shows a symmetrical upright style of folding with no visible relationship to contractional faulting; no verging direction and no significant stratigraphic throw (see Figure 3.7 (b)). A number of secondary minor crestal faults do occur but primarily accommodate variations in strain depending on structural and stratigraphic position (see Figure 3.7 (b)). The combination of observations suggest that this folded roof has a buckling origin, where any shortening is accommodated by folding rather than thrusting as a consequence of competent overburden that probably cored by mobile underlying unit.

In more proximal positions, high-relief elongate ridges with seismically chaotic and transparent cores have also been interpreted. In most places, the roof of these high-relief structures has been elevated above regional stratigraphic level, and has stretched to form a crestal graben that is overlapped by younger strata in the adjoining mini basins (Figure 3.8). The sedimentary sequences show thickening wedges towards the inferred diapir flanks and were uplifted toward the crest of diapirs, suggesting a link between diapir rise and growth faulting (“reactive diapirism” of; Vendeville and Jackson, 1992; Figure 3.8 (a)). In other sections where normal faulting is associated with the structural highs, the extension is interpreted as a younger event superposed on older, high relief contractional detachment folds with a weak, over-pressured mobile shale core, as indicated by the growth packages being older (Figure 3.8 (b)).



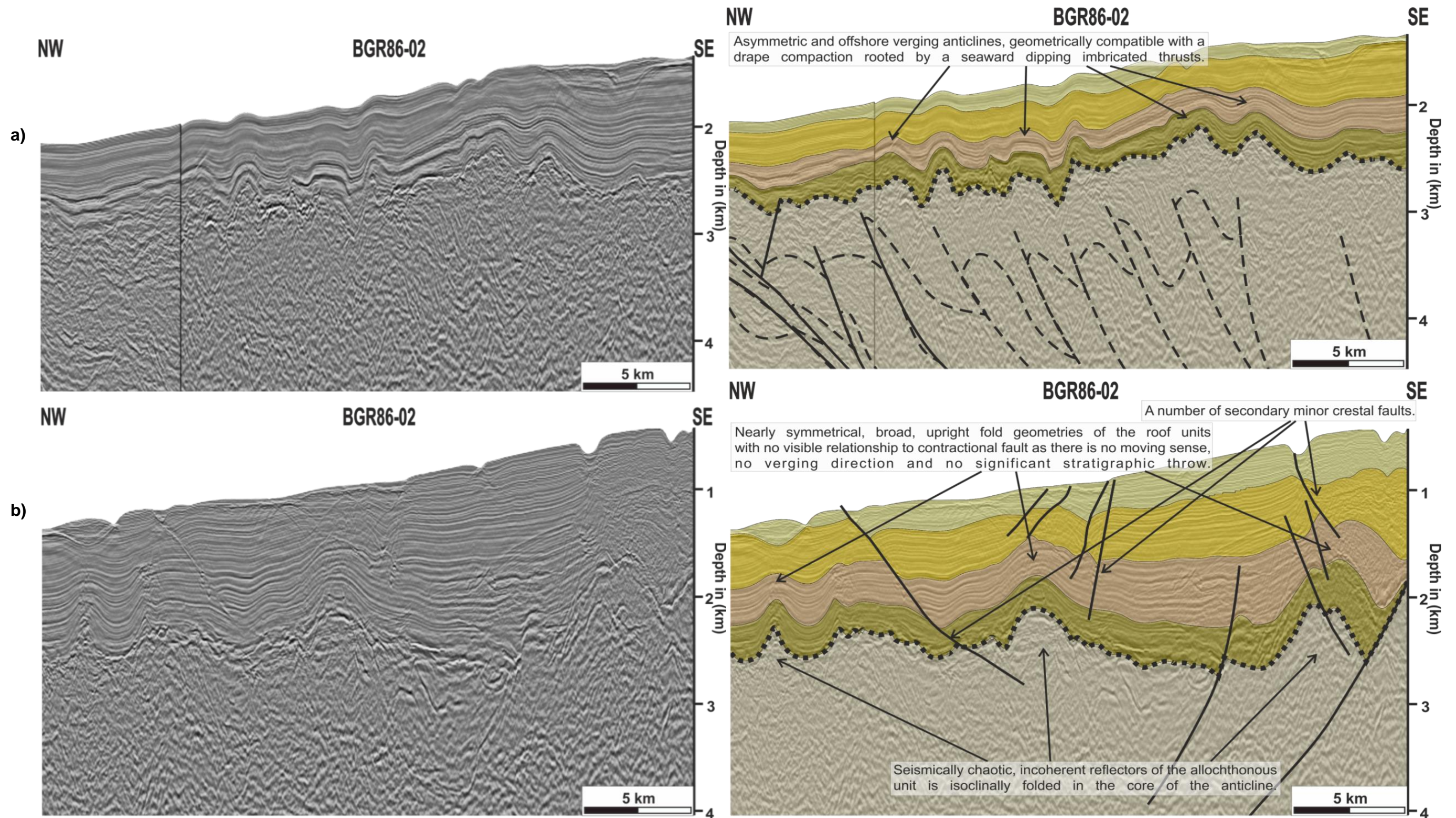


Figure 3. 7: The deformed allochthon wedge overlain by a low- to moderate-relief smoothly undulating folded roof of Latest Miocene to Recent deltaic sediment with; asymmetric and offshore verging anticlines, compatible with a compaction drape rooted by landward-dipping internal imbricated thrusts (a) , and nearly symmetrical, broad, upright fold geometries of the upper roof units with no visible relationship to contractional faults as there is no sense of movement, no verging direction and no significant stratigraphic throw (b).



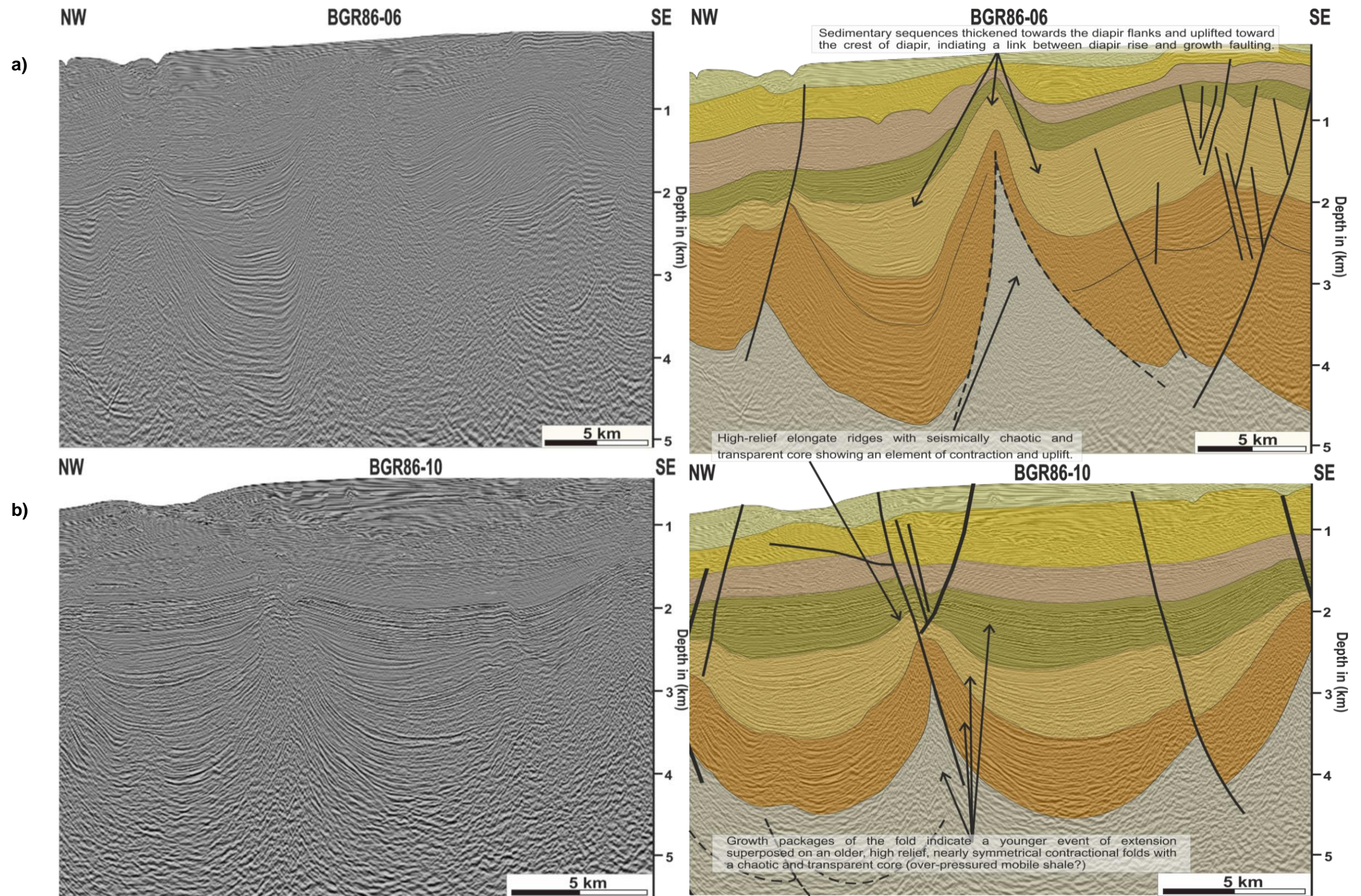


Figure 3. 8: High-relief elongate ridges with seismically chaotic and transparent cores have been elevated above regional stratigraphic level and are onlapped by younger strata in the adjoining mini-basins, indicating an element of contraction and uplift (a), while in section BGR86-10, the extension is interpreted as a younger event superposed on an older high relief contractional detachment fold with a weak, over-pressured mobile shale core (b).



### **3.4.3.3      *Compressional Domain***

The down-slope domain of the gravity driven deformation system corresponds to the gravity-driven compressional fold and thrust belt that has migrated seaward. Fault-propagation folding with asymmetric anticlines, over-steepened forelimbs and long planar back-limbs, is the most common style of deformation found in the outer fold–thrust belt (as seen in Figure 3.4). The individual structures do not generally show long-lived activity as the belt generally propagates basin-ward, but varied patterns of systematic break-forward and systematic break-backward of imbrications exist in local areas (Figure 3.9). Mapping of the thrust faults has led to division of the margin in two segments based on their lateral difference in deformation styles; these geographic divisions are here termed the northern segment and the southern segment thrust-belts. The width of the compressional domain varies from the broad, well developed imbricate zones (~ 100 km wide) of the southern segment NW Sabah deep-water-fold-thrust belt into a region with a narrower imbricate zone (~ 40 km wide) in the northern segment NW Sabah deep-water-fold-thrust belt (see Figure 3.4 & 3.9).

The southern segment deep-water-fold-thrust belt is characterized by generally similar sized, uniform-length thrusts with an average spacing of 3-15 km between them. These are associated with significant accommodation space in piggy-back basins and footwall synclines, and less well-developed out-of-sequence thrusting. The deep-water-fold-thrust belt represents continuous deformation from the Late Miocene to Recent and is independent of any culmination of the over-thrusted allochthon wedge (see Figure 3.4 & 3.9 (BGR86-24 to BGR86-16)). Conversely, moving along strike, the northern segment deep-water-fold-thrust belt is dominated by a narrow and chaotic compressive belt where the thick culmination of the over-thrust allochthon wedge is involved. The deep-water-fold-thrust belt shows a considerably more strongly compressed style with an average spacing of 1-9 km between faults, and different sizes of thrusts separated by narrow piggyback basins. The deep-water-fold-thrust belt in this segment did not form sequentially from the hinterland to the foreland but in a rather irregular sequence, that sometimes over-thrusts (see Figure 3.4 & 3.9 (BGR86-14 to BGR86-02)).

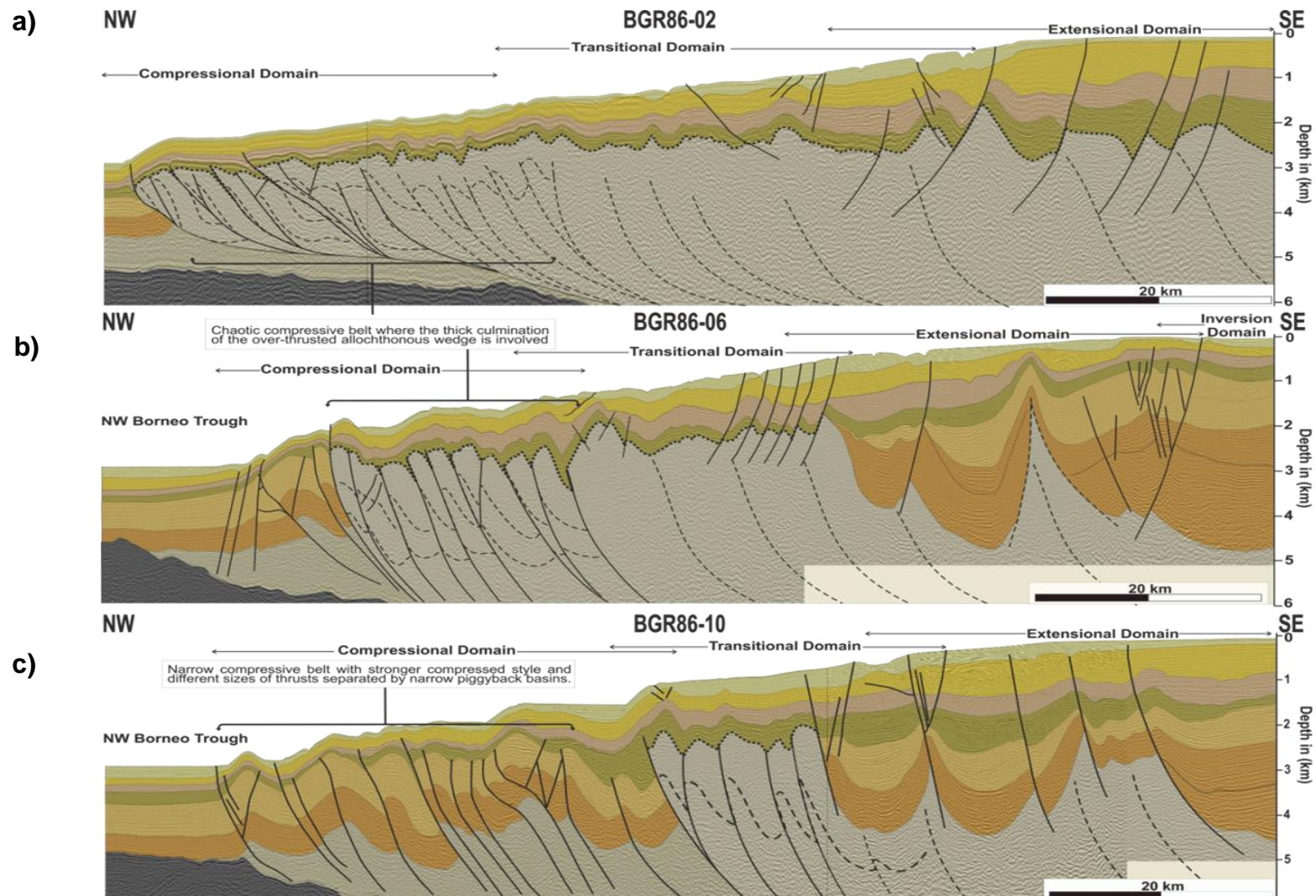


Figure 3. 9. Continued.

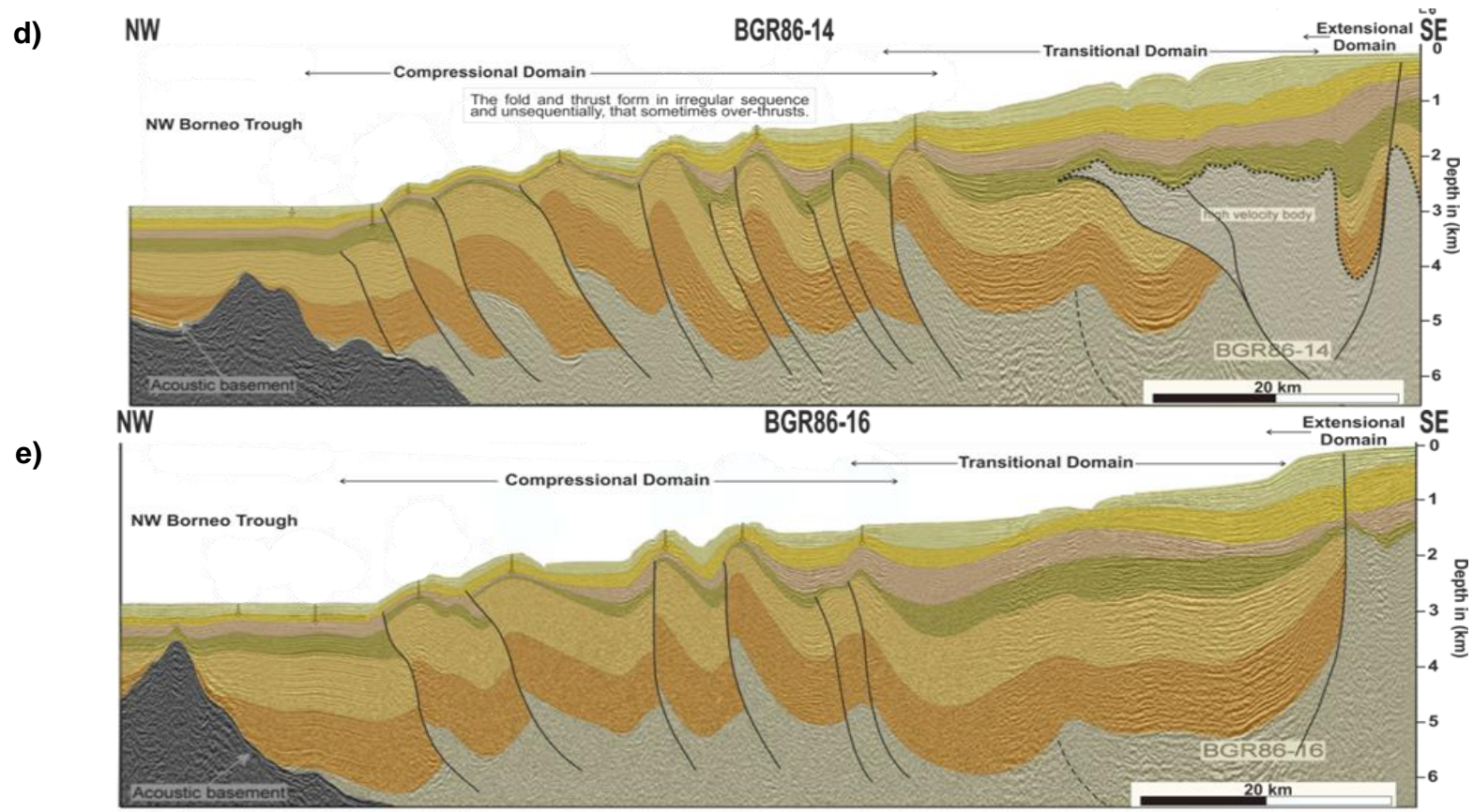
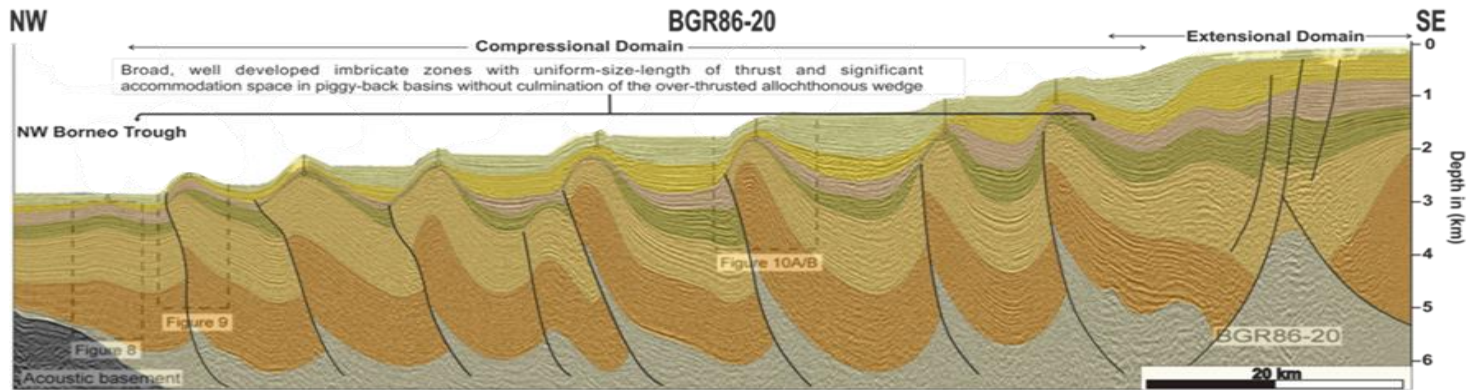


Figure 3. 9. Continued.



f)



g)

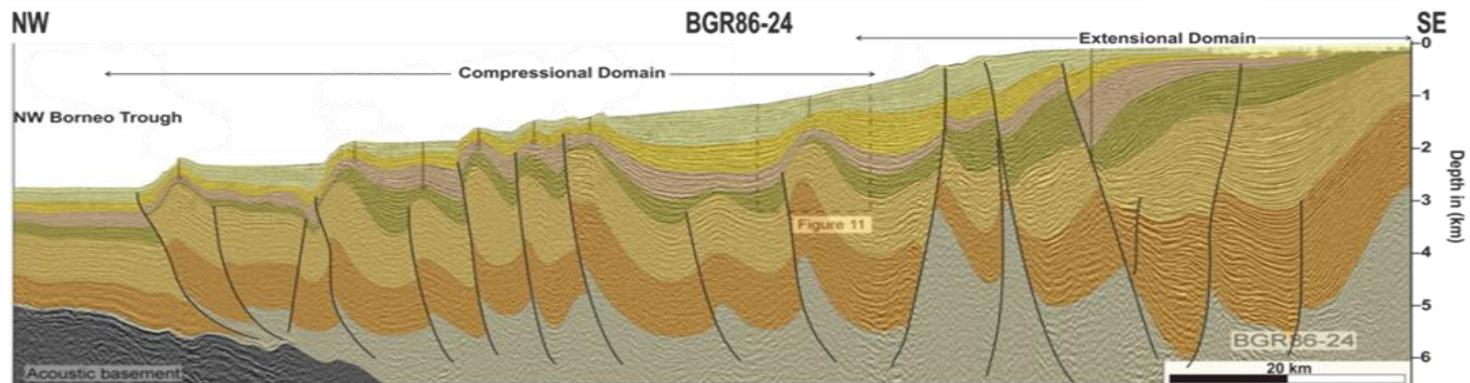


Figure 3. 9: Interpreted seismic profiles of the compressional domain showing variation of the compressional deformation from a broad, well developed imbricate zone with generally similar sized, uniform-length thrusts associated with significant accommodation space in piggy-back basins, and undeveloped over-thrusted allochthonous wedge in the southern segment ( BGR86-20 to BGR86-16) pass into a region of narrow, considerably more strongly compressed style with different sizes of thrusts separated by narrow piggyback basins, and a chaotic compressive belt where the of the over-thrust allochthonous wedge is involved (BGR86-14 to BGR86-02).

### **3.5 Outcrop Studies**

One of the important questions that need to be answered is whether the internal imbricate thrusting of the allochthonous wedge is pre- or syn-kinematic; developed during the first phase of shortening (tectonic) or second phase of shortening (gravity). Therefore, in this situation, a study of the first-order structures in the inner compressive zone exposed onshore was considered useful to provide constraints that could aid interpretation of the behaviour and characteristics of tectonic compressional structures, and to provide evidence of direct equivalence to features seen in offshore seismic data. The results of field observations and seismic data analysis can then be compared, through consideration of scale and comparison of the similarities and differences between the onshore and the offshore.

#### **3.5.1 Observations**

This section is focused on the investigation of sub-seismic scale deformation of an inner compressive zone, localized in onshore NW Sabah. The kinematics of thrusting is expressed in the form of numerous inactive thrust faults best preserved in Pre-Mid Miocene Rajang-Crocker-West Crocker accretionary complex. A simplified stratigraphic correlation of offshore and onshore NW Borneo is shown in Figure 2.11.

Field investigations were carried out during a March 2013 field season that concentrated on the few well-exposed outcrops of the Crocker-West Crocker Formation in the vicinity of Kota Kinabalu, Sabah. Figure 3.10 shows the distribution of the Formation in the study area. The Formation is exposed in a series of thrust sheets in sand-rich 'proximal' fan systems that made up of the sand-rich Crocker-West Crocker Formation and shale-rich 'distal' basinal depositional systems of shaly equivalent, the Temburong Formation (e.g., Hutchison et al., 2000). The Formation is basically classified into 4 major lithological units; the Massive Sandstone Unit, the Interbedded Sandstone and Shale Unit, the Grey Shale Unit and the Red Shale Unit (Tongkul, 2003).

About 7 selected well exposed outcrop-scale folds were observed, photographed, sketched, digitized in Corel-DRAW and analysed to identify the

signatures characteristic of the deformation. Measurements of bed dips and fold axes were measured in the field and then were plotted using a Stereonet 9 Program. The locations of the selected outcrops for detailed study are marked in Figure 3.10. The following are descriptions of the relevant outcrops of the Crocker-West Crocker Formation exposed in road cuts in the area of Kota Kinabalu, Sabah. The rock strata in the study area generally strike NE-SW, based on the strike and dip readings collected in the field (Figure 3.11 (a)).

Folding is a common feature observed in the study area, with several types of folds. The fold axes trend NE-SW and NW-SE with a dominant trend of NE-SW as shown by an equal area projection for the folds (Figure 3.12). In the field, most of the observed outcrop-scale folds are large, asymmetric, tight ( $46^{\circ}$ - $66^{\circ}$ ) and moderately plunging ( $34^{\circ}$ - $66^{\circ}$ ) to the SW and NE (Figure 3.12, 3.13 & 3.14). The rock mass in the core of the tight fold comprises thick, disrupted, sandstone beds (Figure 3.14). Some much less developed, open folds are observed, for example at locality 2, where there is an asymmetrical open fold ( $146^{\circ}$ ) plunging moderately ( $67^{\circ}$ ) to the NW (Figure 3.12 & 3.15). At most outcrops, these folds generally have associated faults. For example, at locality 1, a NNW-SSE trending faults exhibit drags folding, offsetting the interbedded thick sandstone with thin shale sequence (Figure 3.16). Fold at localities 4, 5 and 6 have been cut by sets of reverse faults with dip angles ranges from  $20^{\circ}$ - $80^{\circ}$  that offset beds in a tightly folded zone (as seen in Figure 3.13 & 3.15). These faults can be observed with various scales and orientations; i.e. to the NE-SW and NW-SE, but generally with a dominant trend of NE-SW, parallel to the NE-SW trend of the overall accretionary prism and of the small-scale folds axes (see Figure 3.11 (b)). This shows that both result from a common compressional force from the NW-SE.





Figure 3. 10: The distribution of the West Crocker Formation in the study area. The locations of the 7 selected outcrops for detailed study are marked in red.

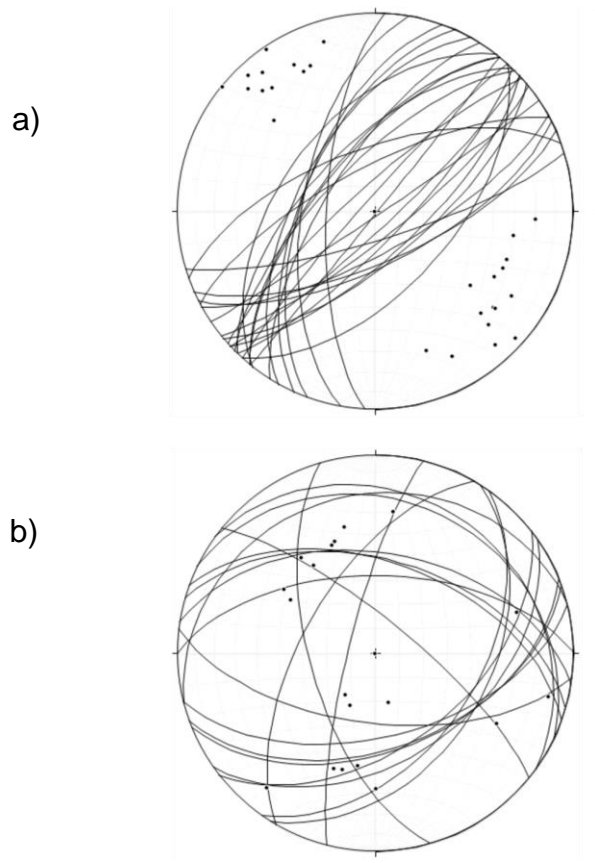


Figure 3. 11: Stereonet presentations of strike measurements for bedding planes (a) and faults (b) in the study area.

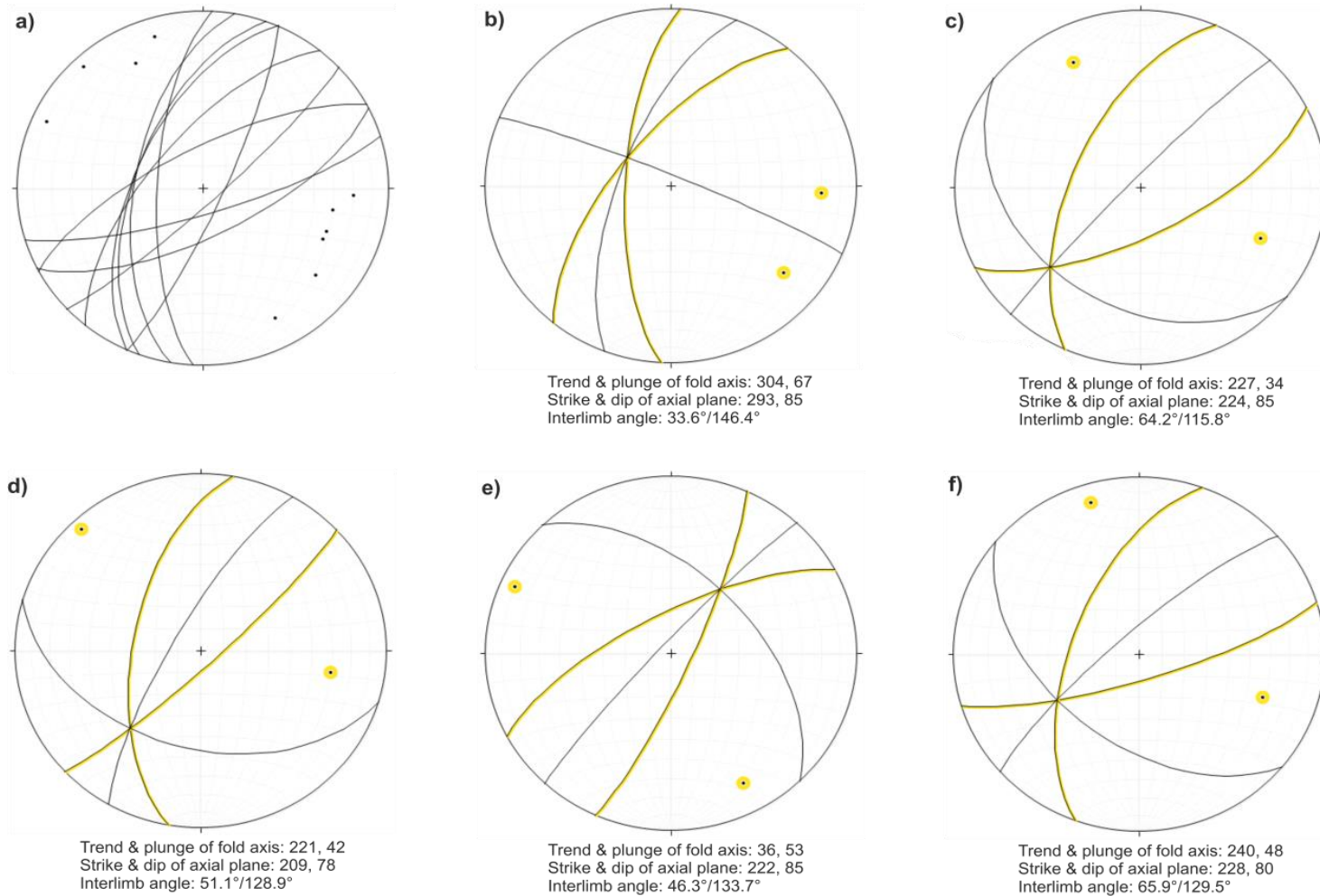


Figure 3. 12: Equal area projections of fold data collected in the study area. Most of the observed outcrop-scale folds are tight (46°-66°) and moderately plunging (34°-66°) to the SW and NE (c-f) with some open folds (146°) plunging moderately (67°) to the NW (b). The fold axes trend NE-SW and NW-SE with a dominant trend of NE-SW.

a)

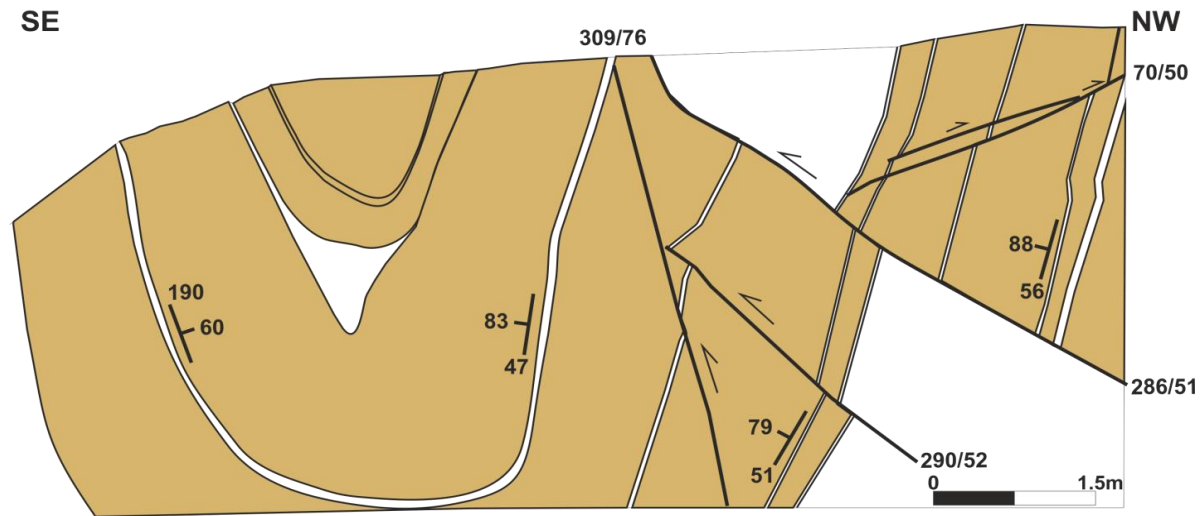


Figure 3.13a. Continued.



b)



Figure 3.13b. Continued.

c)

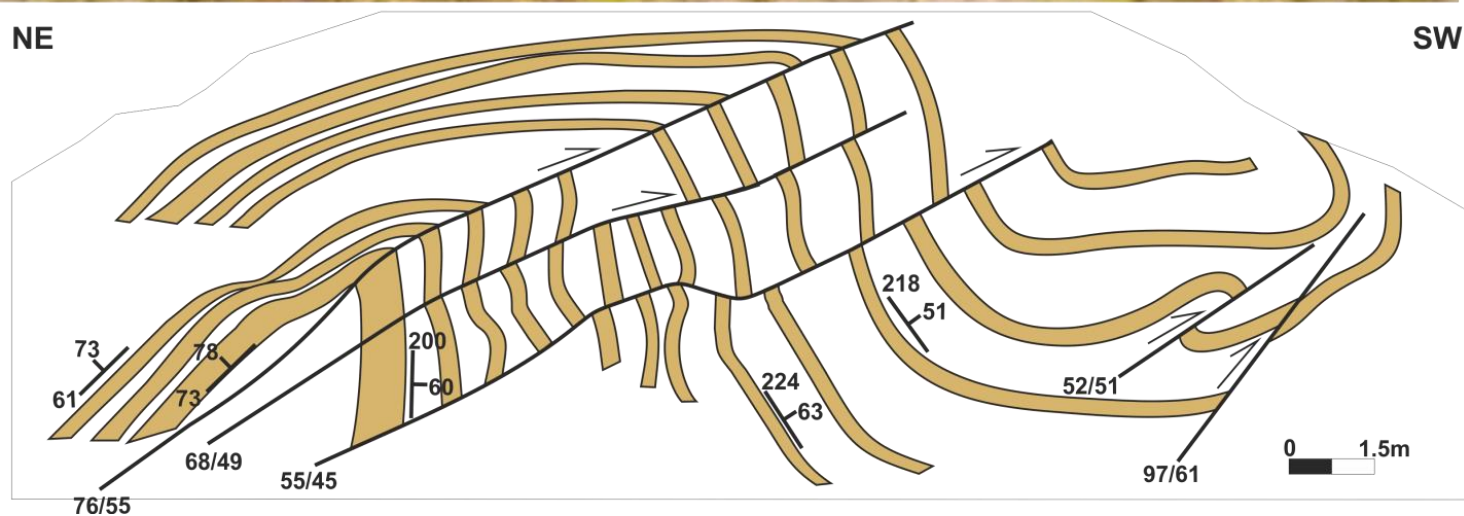


Figure 3. 13: Large, tightly folded fold at locality 4 (figure a), 5 (figure b) and 6 (figure c) have been cut by sets of faults with various scales and orientations that offset their respective beds.



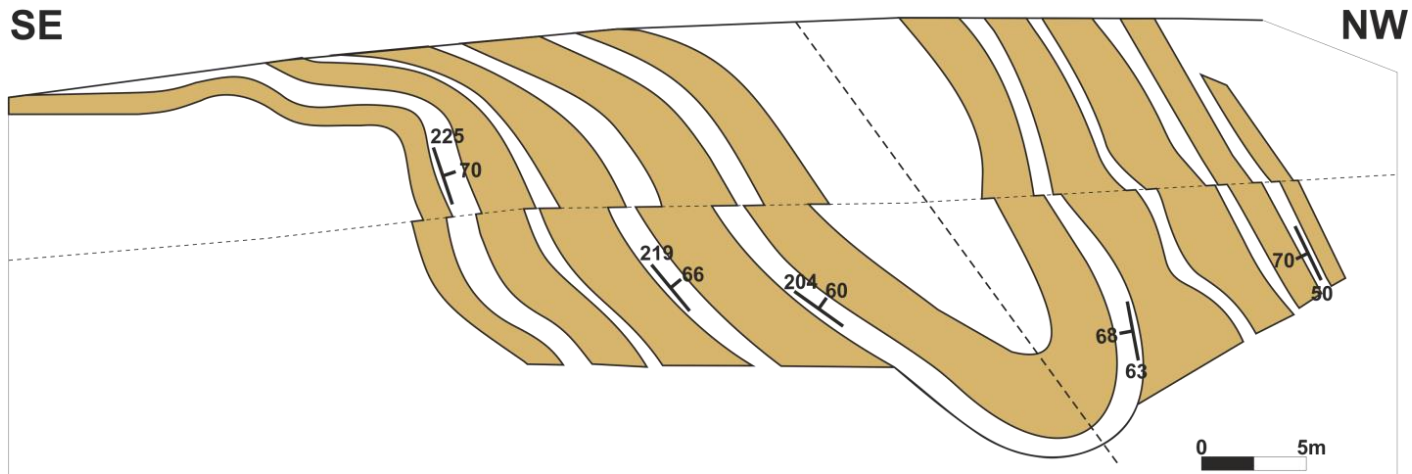


Figure 3. 14: A large, upright, tight fold at locality 3. The rock mass in the core of the tight fold comprises thick, disrupted, sandstone beds.

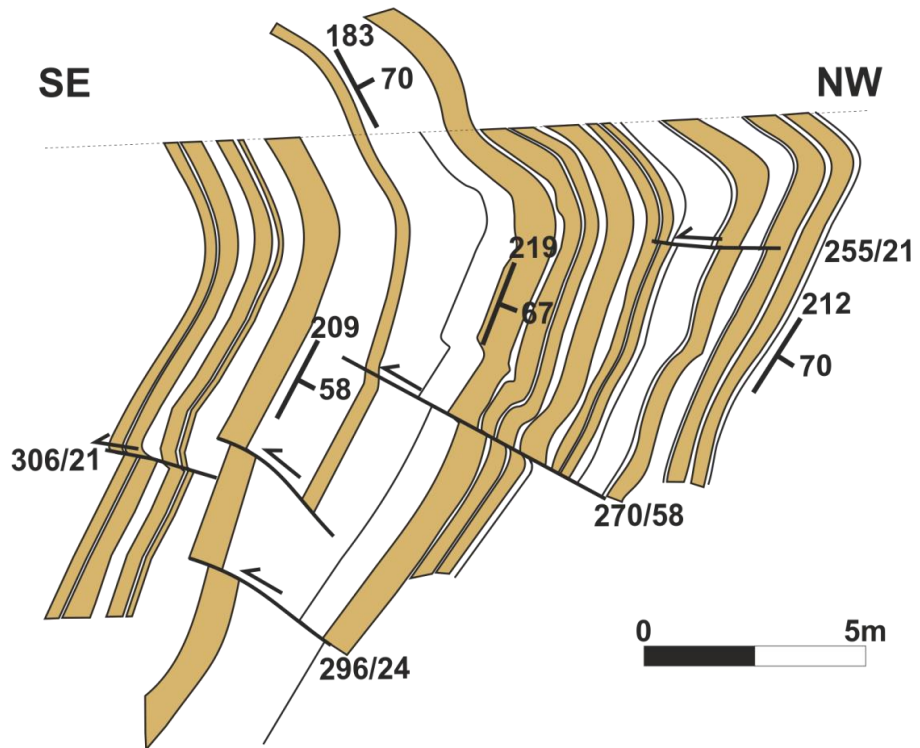


Figure 3. 15: An open fold at locality 2 has been cut by numerous faults.



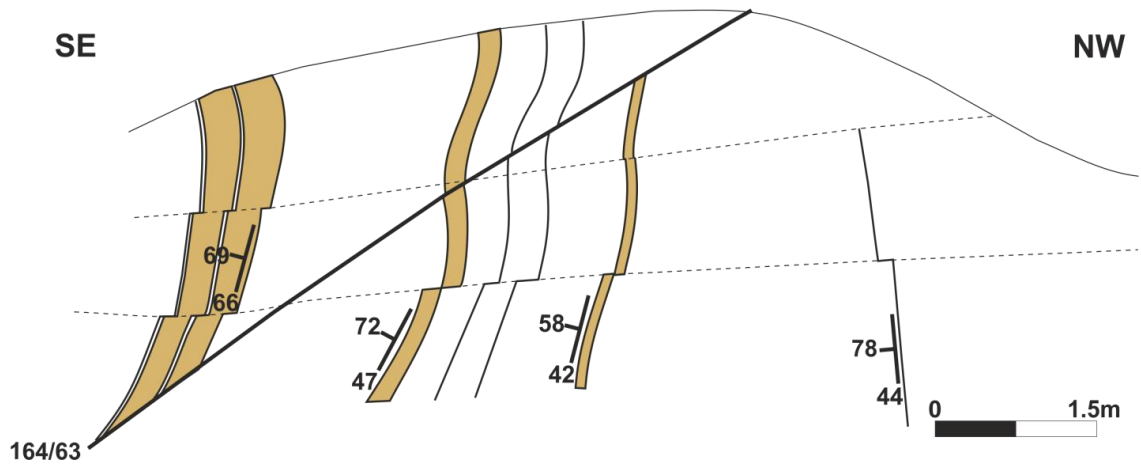


Figure 3. 16: A NNW-SSE trending fault exhibit drags folding, offsetting the interbedded thick sandstone with thin shale sequence at locality 1.



### **3.6. Integrating Field and Seismic Studies**

The potential processes that formed the earlier compressional structures of the allochthon wedge could be either an earlier phase of gravity driven compressional deformation or pre-existing tectonic compressional deformation. Therefore by integrating field and seismic studies, the aim was to use folds and thrust geometrical characteristics as indicators of the structural architectures related to different deformation mechanisms, which may provide insights into how the region evolved. Morley (2007; 2009) and Hesse et al., (2010a) have studied the individual fold types and have discussed some of the geometrical aspects of the folding in the offshore Brunei margin and the southern part of offshore NW Sabah respectively. They focus on the relationship of fold style and inter-limb angles to fold development. Hesse et al., (2010a) document that at least four different types of thrust-hanging wall anticlines characterize the deep-water fold-thrust belt offshore Sabah, NW Borneo. Both Morley (2007; 2009) and Hesse et al., (2010a) document how a general landward decrease of fold-inter-limb-angles relates to lateral changes in the “maturity” of folding, along the offshore Brunei and southern NW Sabah margins respectively.

In this study, descriptions are presented of the geometrical aspects of the folding and thrusting, including tightness of the folds (fold inter-limb angles), and thrust spacing and dips, which may reflect the intensity of compression. The results are listed in table 3.2. Moreover, the regional scale of the seismic data used in this study has allowed the analyses to be extended another 100 km northwards along the northern Sabah fold-thrust belt compared to previous studies. For the fold analysis presented in this study, fold-limb angles were measured on depth migrated (BGR-12 to BGR-24) 2D seismic data from Hesse et al. (2010b) and depth converted (BGR-10 to BGR-02) 2D seismic data acquired by Hess Corporation, with an Early Pliocene horizon being used as the marker horizon (Figure 3.17). The result from integrating the field and seismic studies are discussed below.

In the field examples, several tectonic compressional folds have been investigated. Most of them are large, asymmetric, tight ( $46^{\circ}$ - $66^{\circ}$ ) and moderately plunging ( $34^{\circ}$ - $66^{\circ}$ ), while some are open folds ( $146^{\circ}$ ) with moderate plunges ( $67^{\circ}$ ). These folds are typically associated with sets of reverse faults with variable dip angles ( $20^{\circ}$ - $80^{\circ}$ ) that offset beds in a tightly folded zone. Both

the fold axes and the reverse faults are oriented NE-SW and NW-SE with a dominant trend of NE-SW, parallel to the NE-SW trend of the deep-water fold thrust belt, implying that they resulted from a common NW-SE compressional force.

Moving into the deep-water areas, the allochthonous wedge culminates in the northern half of the margin. Internal structures generally consist of closely spaced tight folds, or locally gentler and wider spaced folds, with no significant changes from landward to seaward (see Figure 3.17). Most of the observed internal structures generally have fold inter-limb angles that range between  $\approx 90^\circ$  and  $150^\circ$ , with more than half being below  $140^\circ$  (Table 3.2). The south-eastwards dipping internal thrust faults of the frontal allochthonous wedge dip between  $\approx 10^\circ$  and  $40^\circ$ , approximately equal to those in more inward positions (which also dip between  $\approx 10^\circ$  and  $40^\circ$ ) (refer Table 3.2). Moreover, their initial structure spacings are also approximately equal to those in more inward positions (average 1-4 km) (refer Table 3.2). In the field examples, even though an average value of thrust spacing could not be measured due to insufficient exposed marker beds, previous studies have documented that the sedimentary rock units have been imbricated into a series of closely spaced thrust slices with approximately 1-2 km spacing (Tongkul, 1990).

In the deep-water fold-thrust belt, the northern segment deep-water fold-thrust-belt structures (BGR-14 to BGR-02) typically exhibit a general landward narrowing and steepening trend respectively (see Figure 3.17). The most distal anticlines exhibit an inter-limb angle between  $\approx 140^\circ$  and  $170^\circ$ , with the underlying south-eastwards dipping thrust faults having dips that range between  $\approx 15^\circ$  and  $50^\circ$  (refer Table 3.2). In contrast, in more landward positions of the fold-thrust belt, the average inter-limb angles were between  $\approx 120^\circ$  and  $140^\circ$ , with the underlying south-eastwards dipping thrust faults having dips that range between  $\approx 20^\circ$  and  $60^\circ$  (refer Table 3.2). Moreover, it is notable that the intensity of deep-water-thrust-fold deformation increases towards the allochthon front (landward), with the average structural spacing of major thrusts decreasing from 3-9 km in the frontal fold-thrust belt (2-4 km stratigraphic thickness), to about 1-5 km in more internal positions (6-8 km stratigraphic thickness), towards the allochthonous wedge culmination (refer Table 3.2; Figure 3.17).

The absence of the allochthon culmination in the southern segment deep-water fold-thrust-belt marks a notable difference in the geometrical characteristics of folding and the deformation structural style (see Figure 3.17). From BGR-24 to BGR-16, the most distal anticlines exhibit an inter-limb angle between  $\approx 140^\circ$  and  $170^\circ$ , with the underlying south-eastwards dipping thrust faults having dips that range between  $\approx 20^\circ$  and  $50^\circ$  (refer Table 3.2). In more landward positions of the fold–thrust belt, the average inter-limb angles are between  $\approx 100^\circ$  and  $150^\circ$ , with the underlying south-eastwards dipping thrust faults having dips that range between  $\approx 40^\circ$  and  $60^\circ$  (refer Table 3.2). The average values of structural spacing of the fold-thrust belt in the southern segment decrease seaward from 8-15 km in more internal positions (8-12 km stratigraphic thickness) to about 4 - 12 km at the frontal wedge (4-6 km stratigraphic thickness) (refer Table 3.2; Figure 3.17). On whole, the folds and thrusts typically exhibit a general landward narrowing and steepening trend, on both southern and northern segments. However, the structural spacing of major thrusts decreases with shortening in a seawards direction in the southern segment, while in a landward direction in the northern segment.

Integrating field investigations and seismic data analysis, as presented, reveals that in general, the majority of the observed mode of tectonic compressional deformation onshore shows significant similarities in orientation with the deep-water fold and thrust deformation, striking NE-SW. This indicates that the main compressional stress that produced the structural style was from NW to SE. However, there are significant differences in geometrical aspect and structural style of each area, indicating that they formed by different mechanisms. The main structural styles of the internal imbricate structures of the allochthonous wedge show characteristics of tighter inter-limb angles ( $90^\circ$ - $150^\circ$ , with more than half being below  $140^\circ$ ), more closely spaced (1-4 km) and gentler dipping ( $10^\circ$ - $40^\circ$ ) thrusts than the deep-water-fold-thrust deformation (with distinct inter-limb angles ( $100^\circ$ - $170^\circ$ ), thrust spacing (4-15km), and thrust dips ( $20^\circ$ - $60^\circ$ )). The internal imbricates are geometrically comparable to the onshore deformation with tight inter-limb angles ( $30^\circ$ - $150^\circ$ ) and closely spaced thrusts (1-2km)). All of this indicates a compressional deformation with higher intensity than the deltaic compression, suggesting that the allochthon was tectonically controlled, similar to the onshore deformation, where shortening can be quite intense.

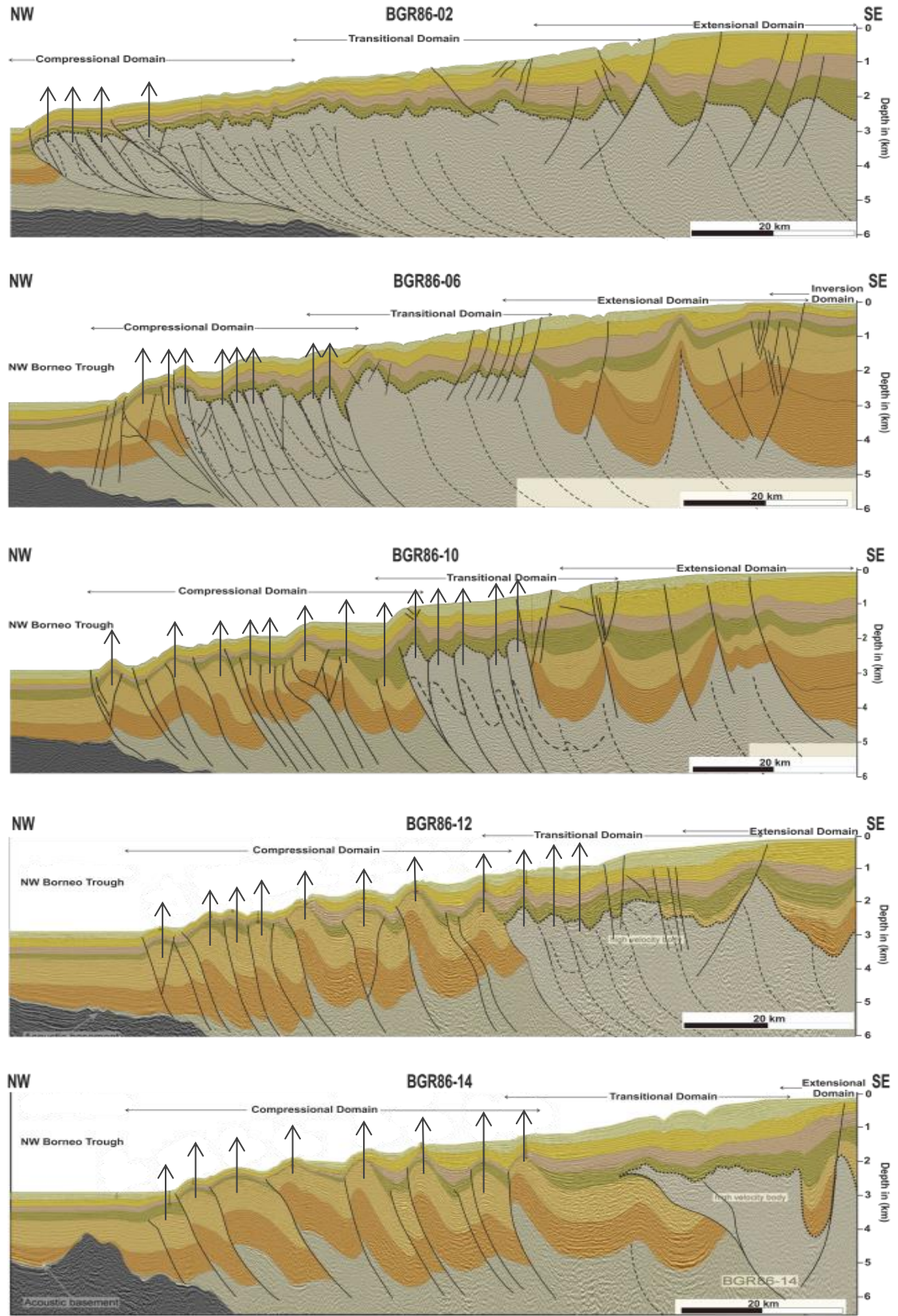


Figure 3.17. Continued.



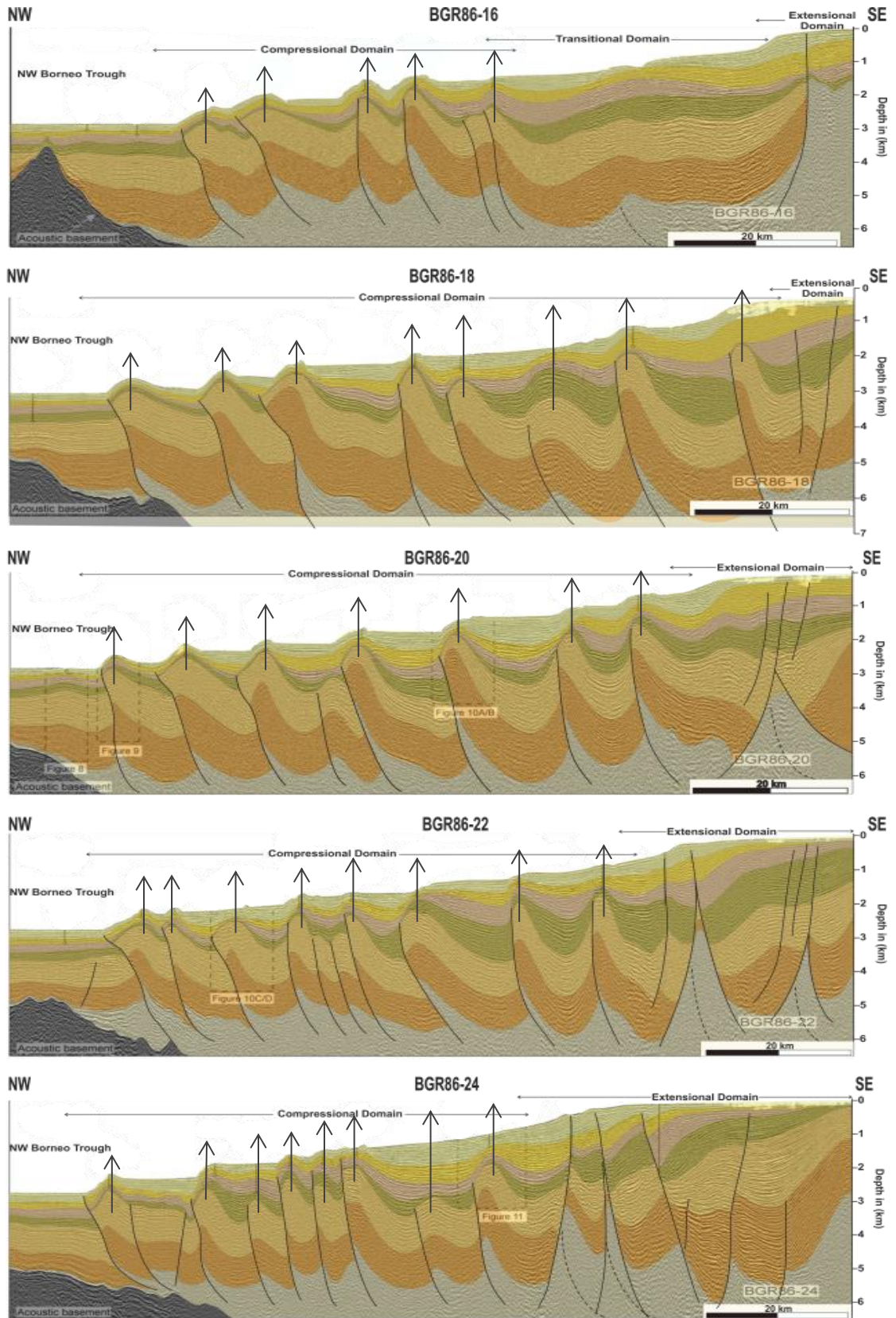


Figure 3. 17: Interpreted seismic profiles of the compressional domain used for fold analysis (from north to south; BGR86-02 to BGR86-24).

Table 3. 2 : Measurement of geometrical aspects of the fold and thrust in 2D depth converted seismic data: tightness of the fold (fold inter-limb angles), thrust spacing and dips (bold black, measurements of the deep-water fold thrust structures; italic black, measurements of the allochthon internal thrusting).

<b>Thrust Spacing (in Kilometres)</b>													
	<b>1</b>	<b>2</b>	<b>3</b>	<b>4</b>	<b>5</b>	<b>6</b>	<b>7</b>	<b>8</b>	<b>9</b>	<b>10</b>	<b>11</b>	<b>12</b>	<b>13</b>
<b>BGR24</b>		<b>4.5</b>	<b>9.2</b>	<b>7.0</b>	<b>5.0</b>	<b>4.5</b>	<b>4.6</b>	<b>9.8</b>	<b>8.3</b>				
<b>BGR22</b>		<b>5.2</b>	<b>7.7</b>	<b>8.3</b>	<b>3.8</b>	<b>3.1</b>	<b>3.0</b>	<b>7.6</b>	<b>14.2</b>	<b>10.7</b>			
<b>BGR20</b>		<b>8.6</b>	<b>9.6</b>	<b>8.6</b>	<b>5.0</b>	<b>12.3</b>	<b>13.8</b>	<b>10.1</b>					
<b>BGR18</b>		<b>11.9</b>	<b>9.1</b>	<b>14.5</b>	<b>7.1</b>	<b>9.1</b>	<b>12.5</b>	<b>15.0</b>					
<b>BGR16</b>		<b>10.2</b>	<b>12.1</b>	<b>7.9</b>	<b>10.4</b>	<b>4.5</b>							
<b>BGR14</b>		<b>4.2</b>	<b>4.2</b>	<b>9.0</b>	<b>7.1</b>	<b>8.2</b>	<b>7.8</b>	<b>3.7</b>					
<b>BGR12</b>		<b>5.8</b>	<b>3.6</b>	<b>2.6</b>	<b>2.4</b>	<b>3.4</b>	<b>6.6</b>	<b>6.3</b>	<b>7.9</b>	<b>5.3</b>	<i>2.8</i>	<i>3.1</i>	<i>3.5</i>
<b>BGR10</b>		<b>5.9</b>	<b>4.1</b>	<b>4.3</b>	<b>4.2</b>	<b>1.0</b>	<b>1.6</b>	<b>1.8</b>	<b>3.8</b>	<b>2.7</b>	<b>1.7</b>	<b>4.8</b>	<b>4.9</b>
	<b>14</b>	<b>15</b>	<b>16</b>	<b>17</b>									
	<i>1.2</i>	<i>3.9</i>	<i>4.3</i>	<i>2.6</i>									
<b>BGR06</b>		<b>1.0</b>	<b>1.5</b>	<b>3.0</b>	<b>4.0</b>	<b>1.1</b>	<i>1.40</i>	<i>2.9</i>	<i>2.9</i>	<i>1.9</i>	<i>2.1</i>	<i>4.8</i>	<i>1.5</i>
	<b>14</b>												

	3.0												
<b>BGR02</b>		4.5	2.9	2.0	4.5	1.0	2.0	2.9	3.6	3.0	2.0	2.7	2.9
<b>Thrust Dip (in degrees)</b>													
	1	2	3	4	5	6	7	8	9	10	11	12	13
<b>BGR24</b>	30.2	33.9	55.9	45.6	60.6	58.1	45.3	42.4	60.8				
<b>BGR22</b>	23.1	41.6	30.9	48.3	49.4	35.8	35.7	35.7	55.1	69.4			
<b>BGR20</b>	50.6	37.0	37.9	52.9	31.2	50.9	52.9	40.2					
<b>BGR18</b>	45.3	46.0	62.7	60.0	37.0	29.7	46.0	53.4					
<b>BGR16</b>	36.0	27.9	64.6	55.0	48.3	51.6							
<b>BGR14</b>	29.5	23.2	38.0	28.1	35.0	28.4	28.5	39.3					
<b>BGR12</b>	38.5	35.9	44.7	53.9	37.4	47.1	40.0	51.4	47.5	39.4	37.9	38.3	36.8
<b>BGR10</b>	26.0	23.0	37.5	37.9	26.0	32.0	31.0	26.0	20.0	21.8	64.0	38.0	28.0
	14	15	16	17									
	34.7	37.0	34.3	38.0									
<b>BGR06</b>	47.6	49.5	75.8	14.9	25.7	26.4	36.4	33.8	36.8	32.2	25.9	22.3	35.3
	14												
	33.0												

<b>BGR02</b>	10.5	13.2	18.4	20.0	11.3	13.1	29.8	22.3	16.9	25.5	26.4	25.9	24.7
<b>Inter-limb Angle of major thrust (fore-limb, back-limb, in degrees)</b>													
	<b>1</b>	<b>2</b>	<b>3</b>	<b>4</b>	<b>5</b>	<b>6</b>	<b>7</b>	<b>8</b>	<b>9</b>	<b>10</b>	<b>11</b>	<b>12</b>	<b>13</b>
<b>BGR24</b>	<b>150.1</b> (19.9, 10.0)	<b>173.3</b> (1.63, 5.19)	<b>136.8</b> (23.6, 19.8)	<b>154.1</b> (15.2, 10.6)	<b>119.3</b> (43.9, 17.4)	<b>135.2</b> (30.9, 13.9)	<b>151.2</b> (11.5, 17.3)	<b>133.6</b> (25.2, 21.2)					
<b>BGR22</b>	<b>153.3</b> (11.5, 15.2)	<b>150.5</b> (16.6, 12.9)	<b>145.4</b> (18.5, 16.1)	<b>123.5</b> (23.8, 32.7)	<b>138.3</b> (24.2, 17.5)	<b>141.6</b> (25.6, 12.8)	<b>112.1</b> (44.2, 23.7)	<b>103.1</b> (44.6, 32.3)					
<b>BGR20</b>	<b>153.9</b> (14.3, 11.8)	<b>157.3</b> (12.5, 10.2)	<b>138.8</b> (18.2, 23.0)	<b>133.5</b> (22.5, 24.0)	<b>129.4</b> (33.3, 17.3)	<b>125.6</b> (29.4, 25.0)	<b>134.9</b> (33.0, 12.1)						
<b>BGR18</b>	<b>161.6</b> (12.2, 6.2)	<b>150.3</b> (15.7, 14.0)	<b>149.5</b> (12.0, 18.5)	<b>129.0</b> (26.0, 25.0)	<b>139.4</b> (24.6, 16.0)	<b>154.0</b> (15.6, 10.4)	<b>131.8</b> (21.1, 27.1)	<b>108.3</b> (42.0, 29.7)					
<b>BGR16</b>	<b>157.1</b> (10.3, 12.6)	<b>165.2</b> (8.9, 5.6)	<b>133.7</b> (32.4, 13.9)	<b>135.7</b> (26.2, 18.1)	<b>134.7</b> (30.5, 14.8)								
<b>BGR14</b>	<b>170.7</b> (6.4,	<b>159.7</b> (14.4,	<b>162.4</b> (10.8,	<b>166.5</b> (7.8,	<b>136.1</b> (20.8,	<b>127.7</b> (30.2,	<b>148.4</b> (20.0,	<b>140.5</b> (23.0,					



	2.9)	5.9)	6.82)	5.7)	23.1)	22.1)	11.6)	16.5)					
<b>BGR12</b>	<b>158.8</b> (13.3, 7.9)	<b>153.2</b> (14.1, 12.7)	<b>139.0</b> (30.7, 10.3)	<b>152.5</b> (16.4, 11.1)	<b>146.3</b> (14.4, 19.3)	<b>138.5</b> (17.0, 24.5)	<b>140.5</b> (19.6, 19.9)	<b>135.1</b> (18.6, 26.3)	123.3 (27.4, 29.3)	137.2 (15.1, 27.7)	143.9 (9.0, 27.1)		
<b>BGR10</b>	<b>140.3</b> (20.0, 19.7)	<b>155.0</b> (15.2, 9.8)	<b>139.8</b> (12.2, 28.0)	<b>147.8</b> (19.6, 12.6)	<b>157.0</b> (15.5, 7.5)	<b>155.9</b> (15.3, 8.8)	<b>146.8</b> (16.6, 16.6)	<b>124.7</b> (32.0, 23.2)	122.5 (32.9, 24.6)	155.6 (16.1, 8.3)	148.8 (21.6, 9.6)	133.4 (19.1, 27.5)	144.4 (25.8, 9.8)
<b>BGR06</b>	<b>157.2</b> (18.3, 4.5)	<b>147.5</b> (10.6, 21.9)	147.6 (15.6, 16.8)	141.0 (20.4, 18.6)	132.5 (29.0, 18.5)	126.5 (26.9, 26.6)	124.4 (31.0, 24.6)	106.3 (43.4, 30.3)					
<b>BGR02</b>	138.7 (27.1, 14.2)	144.4 (19.8, 15.8)	96.6 (76.2, 7.2)	158.5 (9.8, 11.7)									

### 3.7 Discussion

Detailed correlation of the leading allochthonous over-thrust-front in the northern and southern segment reveals a seaward and north-westward younging direction, in displacements of the Late Miocene/Middle Miocene strata in the extensional/transitional domain in the south-eastern segment, while almost cutting the seafloor in the most distal part of the northern wedge (refer Figure 3.4 & 3.6). Hence, it is inferred that the allochthon wedge could be considered to represent the front of the NW Borneo accretionary wedge that must have been over-thrust from the original basin margin progressively seaward and north-west-wards along with seaward migration of basin-ward thinning Middle Miocene-Recent deltaic sediments, as well as seaward migration of the gravity-driven deformation system. This resulted in superimposition of gravity driven extensional and compressional structures on the pre-existing tectonic compressional structures. It is also anticipated that most of the allochthon internal imbricate thrusts were inactive during the second phase of shortening (gravity driven deltaic shortening), as evidenced by the internal imbricate fault traces being eroded and clearly truncated below the regional mappable angular unconformity boundary and the smoothly undulating roof of Middle Miocene to Recent deltaic sediments being geometrically compatible with a compaction drape rooted by a landward dipping imbricated thrust (refer Figure 3.6 & 3.7).

Previous workers have interpreted that the Brunei deep-water fold and thrust belt (southern part of NW Borneo), is underlain by a thick mobile shale unit with the associated mobile shale structures including shale ridges with crestal normal faults, shale pipes, shale expulsion, mini-basins, counter-regional growth faults, buckle folds and thrust shear fault propagation folds that involve a ductile substrate (Morley et al., 1998; Van Rensbergen et al., 1999; Morley, 2003; Van Rensberger & Morley, 2002; Morley et al., 2011; Gartrell et al. 2011). Moreover, numerical modelling of delta systems by McClay et al. (1998) has shown that ductile substrates such as over-pressured mobile shales are required to generate deformation features similar to those of the Baram Deltaic Province. In this study, observations on the occurrence of a thick zone of poor seismic data quality, which was termed the "allochthon", suggest that this unit is over-pressured and mobile. This is justified by the

chaotic and transparent seismic characteristic of the allochthon, associated with contrasting deformational styles varying from a progressive seaward and upward translation of a thick allochthon unit with internal imbricate thrusting and a compaction drape to discrete features of ductile structures including a low- to moderate-relief buckling roof and structural high (refer Figure 3.7 & 3.8). This observation is in agreement with King et al., (2009, 2010), who characterised the thick zone of poor seismic data quality in Sabah, as a thickened mobile shales region based on recent analysis of present-day maximum horizontal stress.

As for gravity driven deformation, most of its generated shortening structures did not branch out from the underlying pre-existing thrust faults (allochthonous internal imbricate thrusts). They formed new thrusts in the un-deformed area, forward of the pre-existing shortening structures as a result of progradation of the deltaic wedge (refer Figure 3.9). However, some newly formed shortening structures did utilize the trace of pre-existing faults to propagate upwards and towards the foreland, reactivating a pre-existing thrust. Based on the comparison between cross sections, it is relatively easy to identify the reactivated internal imbricate thrusts and inactive internal imbricate thrusts. The inactive thrusts are identifiable because their traces are clearly truncated by the unconformity boundary. In contrast, each reactivated thrust branches from an inactive internal imbricate thrust, propagates upwards and toward the foreland and penetrates through the unconformity and the upper sequences, carrying the inactive internal imbricate thrusts as part of the hanging wall (refer Figure 3.6).

At this stage, it is not possible to determine the potential processes that reactivated the internal imbricate thrusting of the wedge and translated the allochthonous wedge from the original basin margin progressively seaward and northwards. One possibility is that the wedge passively advanced seawards over time driven purely by the weight of the surrounding overburden or alternatively it was driven by compressional tectonics that were still active until at least the latest Pliocene. Based on GPS observations, Simons et al. (2007) suggest that subduction has continued until the Late Neogene or until the present-day. Hesse et al. (2009, 2010b) interpret that the offshore deformation is largely gravity-

driven but still suggest a contribution of regional compression on the offshore deformation in the northern Borneo and inferred that the imbalance between lengthening and shortening amount to indicate a role of tectonic stresses. Whereas, Hall (2013) suggests that most Neogene deformation (including the fold and thrust belt deformation) is a result of episodes of extension that caused subsidence and elevation in different places that was accompanied by magmatism (Mount Kinabalu) and mobility of the deeper crust, and topographically induced stresses can account for the deformation that continues at present. Structural analysis including restoration techniques need to be applied to the section to address this question and will be discussed in the following chapter.

### **3.8 Conclusion**

On the basis of detailed structural mapping of 2D multi-channel seismic profiles across the northern half of the NW Sabah margin (northern NW Borneo), and a selection of previously published depth-migrated seismic profiles from Hesse et al. (2010b), across the southern half of the NW Sabah margin (towards offshore Brunei), transecting the NW Borneo deep-water fold and thrust system, combined with sub-seismic scale outcrop investigations of onshore NW Sabah structural deformation, this chapter has presented detailed descriptions and interpretation of the general deformational style along the deltaic system and the allochthonous wedge in particular. This has led to an improved understanding of the regional-scale structural geometry along the NW Borneo margin and complements previous studies done in the region. In the following, results presented in this chapter are summarized.

Structural mapping of seismic data subdivided the deformation of the whole basin-ward thinning sedimentary wedge into four structural domains that are highlighted by the following examples of contrasting deformation; 1) The inversion domain is characterized by the inversion of most of the older extensional structures, both regional and counter-regional growth faults (on the inner shelf and onshore region); 2) The extensional domain is characterised by both gliding of regional growth faults and by spreading of counter-regional growth faults over a regional detachment; 3) The compressional domain varies from broad, well

developed imbricate zones of fault-related folds (~ 70 km), generally of similar size, and uniform-length thrusts with an average distance of 3-15 km between them in the southern deep-water-fold-thrust belt. This passes into regions of narrow imbricate zones (~ 40 km) of the northern deep-water-fold-thrust belt with a considerably more compressed style (1-9 km) with different sizes of thrusts that did not form sequentially from the hinterland to the foreland but in a rather irregular sequence, that sometimes included over-thrusts; 4) The transitional domain is typically wide in the northern segment and illustrates contrasting structures and geometries varying from a progressive culmination of the thick allochthon unit with internal thrusting, diminishing southward where the extensional domain is directly adjacent to the contractional domain.

Most of the gravity generated shortening structures formed new thrusts in the un-deformed area, forward of the pre-existing shortening structures as a result of progradation of the deltaic wedge. However, some newly formed shortening structures did utilize the trace of pre-existing faults to propagate upwards and towards the foreland, reactivating a pre-existing thrust. The absence of the over-thrusted allochthon in the southern segment deep-water fold-thrust-belt marks a notable difference in the geometrical characteristics of folding and the structural style. This implies that, in the northern segment, the allochthonous wedge could have acted as a moving body that induced deformation of the deltaic sequences in front of it at the time it translated. The allochthon can therefore be treated as a source of lateral structural variation.

The integration of field investigation and seismic data analysis shows that, although the observed mode of tectonic compressional deformation and deep-water fold and thrust deformation generally shows significant similarities in orientation (NE-SW), there are significant differences in geometrical aspect and structural style of each area, indicating that they formed by different mechanisms. The structural styles of the internal imbricate structures of the allochthon indicates a compressional deformation with higher intensity than the deltaic compression, suggesting that the allochthon was tectonically controlled, geometrically comparable to the onshore deformation, where shortening can be quite intense. Detailed correlation of the leading allochthonous over-thrust-

front in the northern and southern segment reveals that the allochthon wedge could be considered to represent the front of the NW Borneo accretionary wedge that must have been over-thrust from the original basin margin progressively seaward and north-west-wards along with seaward migration of the gravity-driven deformation system. Most of the allochthon's internal imbricate thrusts were inactive during the second phase of shortening, although recent activation of the imbricate thrusts does occur in local areas. Chaotic and transparent seismic characteristic of the allochthon, associated with contrasting deformational styles, varying from a progressive seaward and upward translation of a thick allochthon unit with internal imbricate thrusting and compaction drape to discrete features of ductile structures including low- to moderate-relief buckling roofs and structural highs, suggesting that the allochthon is over-pressured and mobile.



## **Chapter 4**

### **Tectonic and Gravity Driven Deformation; their Controls on the Geometry and Evolution of DWFTB.**

#### **4.1 Introduction**

Great efforts have been made to understand the basic geometries of deep-water fold and thrust belts (Schultz-Ela, 2001; Rowan et al., 2004; Bilotti and Shaw, 2005; Krueger and Gilbert, 2009; Morley et al., 2011). However, we still lack a detailed understanding of the interaction between gravity driven and tectonic driven deformation in passive margins and how they affect the style, timing, and location of deformation. One reason for the limited understanding is that linked systems can seldom be studied in other basins since the two mechanisms are commonly developed in isolation. An exception is the NW Borneo deep-water-fold-and-thrust belt where the Champion-Baram deltaic formation has pro-graded over the front of the accretionary wedge (NW Borneo accretionary wedge), causing the superimposition of gravity driven extensional and compressional structures on the pre-existing tectonic compressional structures, resulting in a complex tectonic setting. Therefore, the area is ideal to investigate the interaction between tectonic and gravity driven deformation and their controls on the geometry and evolution of a DWFTB.

In the previous chapter, the complex geometry of the NW Borneo fold-thrust-belt has been discussed using both seismic and field observations. In this chapter, we undertake a regional-scale structural analysis of the margin; 1) to constrain the relative timing of allochthon movement and the effect of the allochthon deformation on the geometry and kinematic development of fold and thrust belts, 2) to investigate the possible processes responsible for reactivation and translation of the allochthon from the original basin margin progressively seaward and northwards, and 3) to understand the interaction between tectonic and gravity driven deformation and their controls on the geometry and evolution of the DWFTB. With these aims in mind, two regional sections from the Sabah and the Brunei wedge are restored, compared and contrasted.

## 4.2 Data and Methodology

To better understand the structural evolution of the NW Borneo margin, two NW-SE-trending regional seismic profiles constrained by seismic structural and stratigraphic interpretations were used to reconstruct the history of the margin in detail. The location of line profiles is shown in figure 4.1. The regional seismic profile of the Sabah (BGR86-10) margin was constructed from seismic survey data acquired by Hess Corporation whereas the regional seismic profile of the Brunei (southern) margin was modified from previously published seismic profiles of Gartrell et al., (2011).

The restoration models constructed from NW-SE-trending regional cross-sections were imported into Midland Valley's 2D Move software. Restoration presented here involves taking the geometry of a deformed structure and restoring it to a horizontal or regional datum (Dahlstrom, 1990) and is achieved by using both kinematic and non-kinematic techniques, combining 'UNFOLD', 'MOVE ON FAULT' and 'DECOMPACTION' functions in 2D Move. Kinematic methods use geometric constraints to define material pathways for the purpose of restoring deformed prekinematic successions back to their predeformed state (e.g. Dahlstrom, 1990), whereas, non-kinematic restorations do not require geometric constraints (Mitra and Namson, 1989). The restoration algorithms used in this restoration are Flexural Slip (based on Kane et al., 1997) for 'UNFOLD' and Fault Parallel Flow (based on Egan et al., 1997; Kane et al., 1997) for 'MOVE ON FAULT'.

Fault parallel flow restoration process involves the creation of flow pathways that are aligned parallel to the geometry of the fault plane. The hanging wall block is then subsequently resorted by material flowing along the constructed flow paths. Flexural slip unfolding restores a folded layer to a horizontal or inclined datum by slip acting parallel to the folded layers. Thickness variations between beds and the line-length of passive beds are maintained throughout the restoration proses. Both fault parallel flow and flexural slip restoration algorithms are widely applied to contractional fold and thrust belts.

Seismic interpretation delivered five main stratigraphic units; Late Pliocene (HI), Early Pliocene (PLU), Late Miocene (SRU), Middle Miocene (DRU) and Early Miocene (TCU). Restoration of the model was undertaken by restoring each rock unit individually, starting with the youngest. Restoration of the regional cross-sections across the offshore NW Borneo margin in Figure 4.2 was accomplished by the following steps:

- i) The present day unit above horizon HI (Figure 4.4 & 4.5 (f)) was first removed using the 'DECOMPACTION' function and an isostatic correction sensu Burov & Diament (1992). De-compaction is a technique designed to remove the effects of volume loss (compaction) that occurs within a rock volume as it is progressively buried (Sclater and Christie, 1980).
- ii) As the horizon HI was cut by faults, the 'MOVE ON FAULT' function is used prior to 'UNFOLD'. The faulted segment of horizon HI was reconnected by restoring the hanging walls back to their original pre-deformed positions using the 'MOVE ON FAULT' function with the 'Fault Parallel Flow' algorithm.
- iii) The restored horizon was then unfolded to a datum using the 'UNFOLD' function with 'flexural slip' algorithm. The template bed (the bed which is actively chosen to be unfolded), the HI horizon, was unfolded around the pin. The pin was inserted through the anticlinal hinge line and underlying additional folded beds are unfolded passively during the restoration process until a representative pre-deformed state is achieved (Figure 4.4 & 4.5 (f)-(e)).
- iv) Restoration was carried out systematically starting at the deep-water deformation front moving in a progressively landward direction, from subsequent folding and thrusting in the delta toe to normal faulting in the delta top. A pin line was inserted in the undeformed area between the two domains.

- v) Complete fault-by-fault restoration and fold-by-fold unfolding of horizon HI (footwall and hanging wall cut-offs of each structure are joined and unfolded to their original pre-deformed state) was followed by a section-wide decompaction and isostatic correction.
- vi) Steps (ii)-(iii)-(iv)-(v) were repeated to restore the horizons PLU, SRU, DRU and TCU.

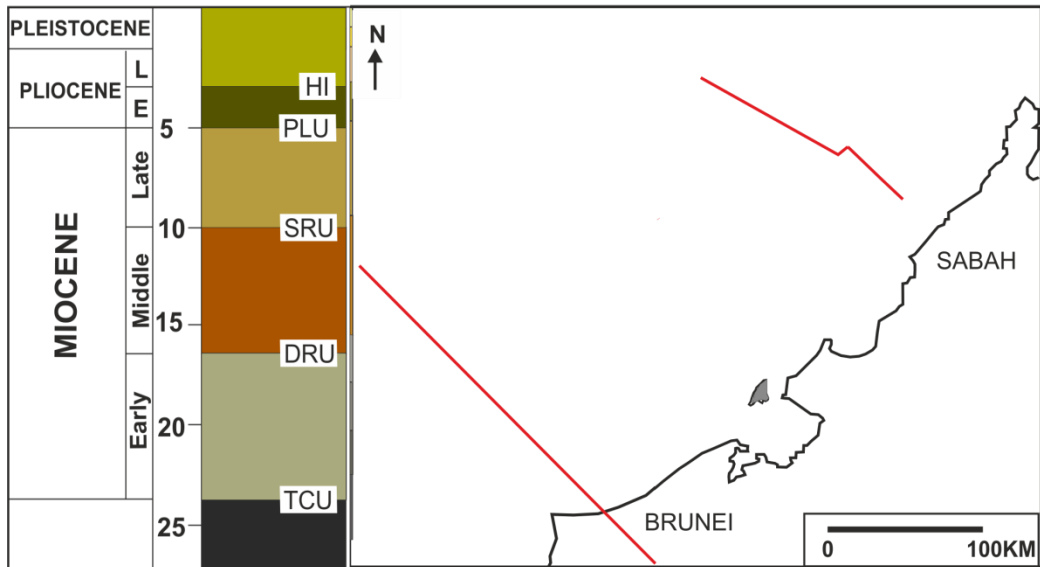


Figure 4. 1: The location of two selected NW-SE-trending regional seismic profiles representing the southern and northern segments that were used for restorations. The regional seismic profile of the Sabah (BGR86-10) margin was constructed from seismic survey data acquired by Hess Corporation whereas the regional seismic profile of the Brunei (southern) margin was modified from previously published seismic profiles of Gartrell et al., (2011).

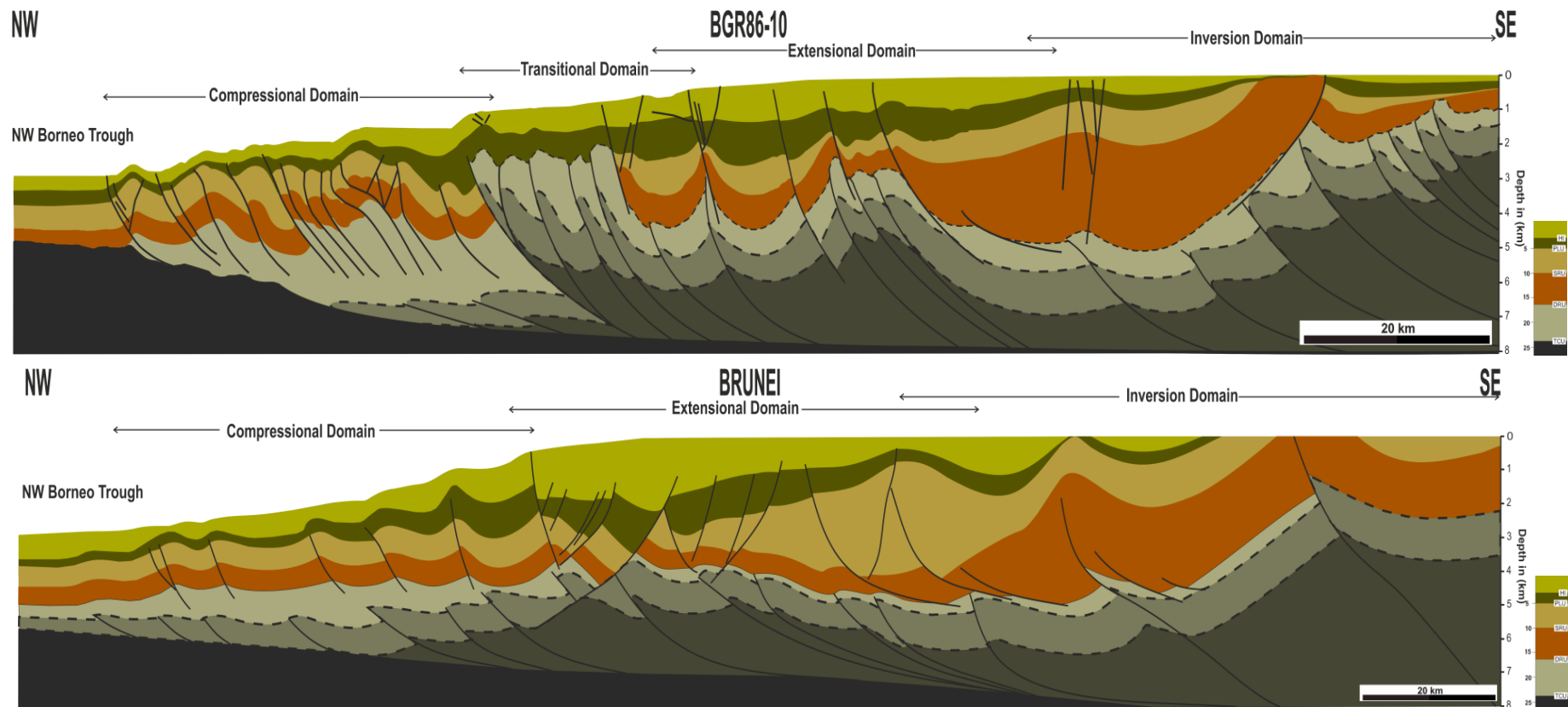


Figure 4. 2: Two selected NW-SE-trending regional seismic profiles of the offshore Sabah (BGR86-10) and Brunei margin highlighting the key features of contrasting margin deformation in the northern and southern segments respectively, and illustrating the deformation styles of the different structural domains. The offshore Sabah profile was constructed from seismic survey data acquired by Hess Corporation whereas the Brunei profile was modified from previously published seismic profiles of Gartrell et al., (2011).

## **4.3 Section Restoration: Synthesis of Margin Evolution**

### **4.3.1 Regional Cross Section Geometry**

In Figure 4.2, two NW-SE directed regional cross sections delineate the present key features of structural deformation in the different structural domains in the Sabah (northern) and Brunei (southern) margin respectively. This is highlighted by the following examples of contrasting deformation that have been discussed in the previous chapter (chapter 3):

- 1) The inversion domain is characterized by the inversion of most of the older extensional structures, both regional and counter-regional growth faults (on the inner shelf and onshore region).
- 2) The extensional domain is characterised by both gliding of regional growth faults and by spreading of counter-regional growth faults over a regional detachment.
- 3) The compressional domain varies from broad, well developed imbricate zones of fault-related folds (~ 70 km), generally of similar size, and uniform-length thrusts with an average distance of 3-15 km between them in the southern deep-water-fold-thrust belt. This passes into regions of narrow imbricate zones (~ 40 km) of the northern deep-water-fold-thrust belt with a considerably more compressed style (1-9 km) with different sizes of thrusts that did not form sequentially from the hinterland to the foreland but in a rather irregular sequence, that sometimes included over-thrusts.
- 4) The transitional domain is typically wide in the northern segment and illustrates contrasting structures and geometries varying from a progressive culmination of the thick allochthon unit with internal thrusting, diminishing southward where the extensional domain is directly adjacent to the contractional domain.



### **4.3.2 Section Restoration**

Seismic interpretation subdivided the Middle-Miocene to Pliocene seismic stratigraphy into six mappable stratal packages bounded by 5 sequence boundaries. These sequence boundaries represent horizons/ unconformities assigned as Late Pliocene (Late Pliocene Horizon, LPH), Early Pliocene (Pliocene Unconformity, PLU), Late Miocene (Shallow Regional Unconformity, SRU), Early Middle Miocene (Deep Regional Unconformity, DRU) and Oligocene-Late Early Miocene (Top Crocker Unconformity, TCU). Seismic facies were characterized using seismic reflection amplitude, continuity and internal reflection geometry whereas seismic unconformities or sequence boundaries are characterized by seismic top-lap, truncation and onlap. The age represented by each of the stratigraphic intervals cannot be determined precisely due to lack of well data. However the mapped seismic horizons are consistent with the accepted seismic stratigraphy (Levell, 1987; Hinz et al., 1989; Van Hattum et al., 2006; Franke et al., 2008; Hesse et al., 2009; Cullen et. al., 2010; Gartrell et al., 2011).

In describing the main aspects of the margin deformation in the study area, the shelf-edge trajectories (Helland-Hansen & Martinsen, 1996; Henriksen et al., 2009; Johannessen & Steel, 2005), were interpreted on a northwest-southeast trending depositional-dip-oriented seismic section across the Sabah margin (Figure 4.3), and tied with the regional section restorations (Figure 4.4 & 4.5), to illustrate the controls of structural deformation on the succession and vice versa. The paleo-shelf edge trajectories were determined using the first major basin-ward change in shelf gradient (Olariu & Steel, 2009). The vertical and horizontal changes of shelf-edge trajectories (aggradation-degradation, progradation-back-stepping) were determined and compared with the published shelf-edge trajectories analysis of the Brunei margin using available age control based on the work of Gartrell et al. (2011). Restoration of the regional section indicates three stages of basin evolution that will be presented below.

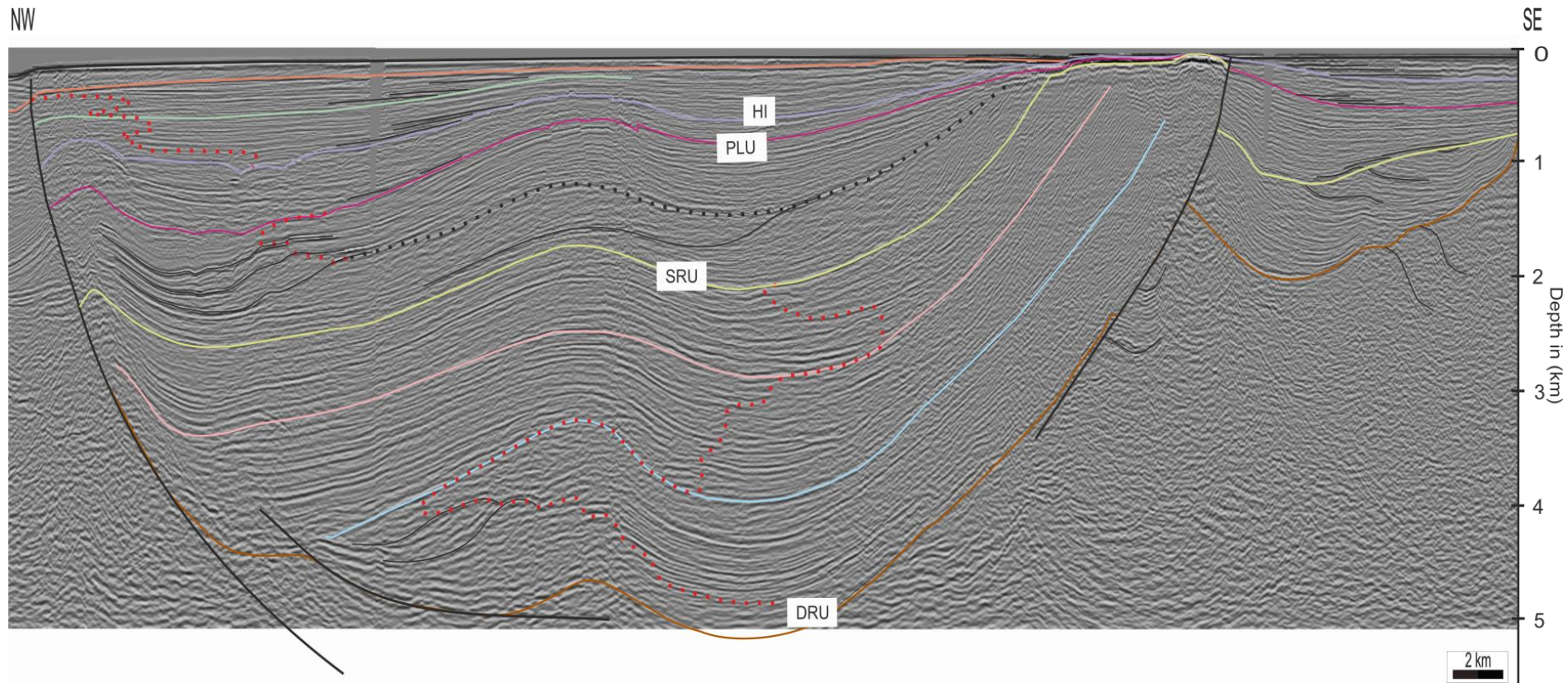


Figure 4. 3: Seismic section from the inboard area of the northern segment (Sabah) showing the shelf edge trajectories through time (illustrated by the red dots). The line profile shown is shown in figure 4.1.

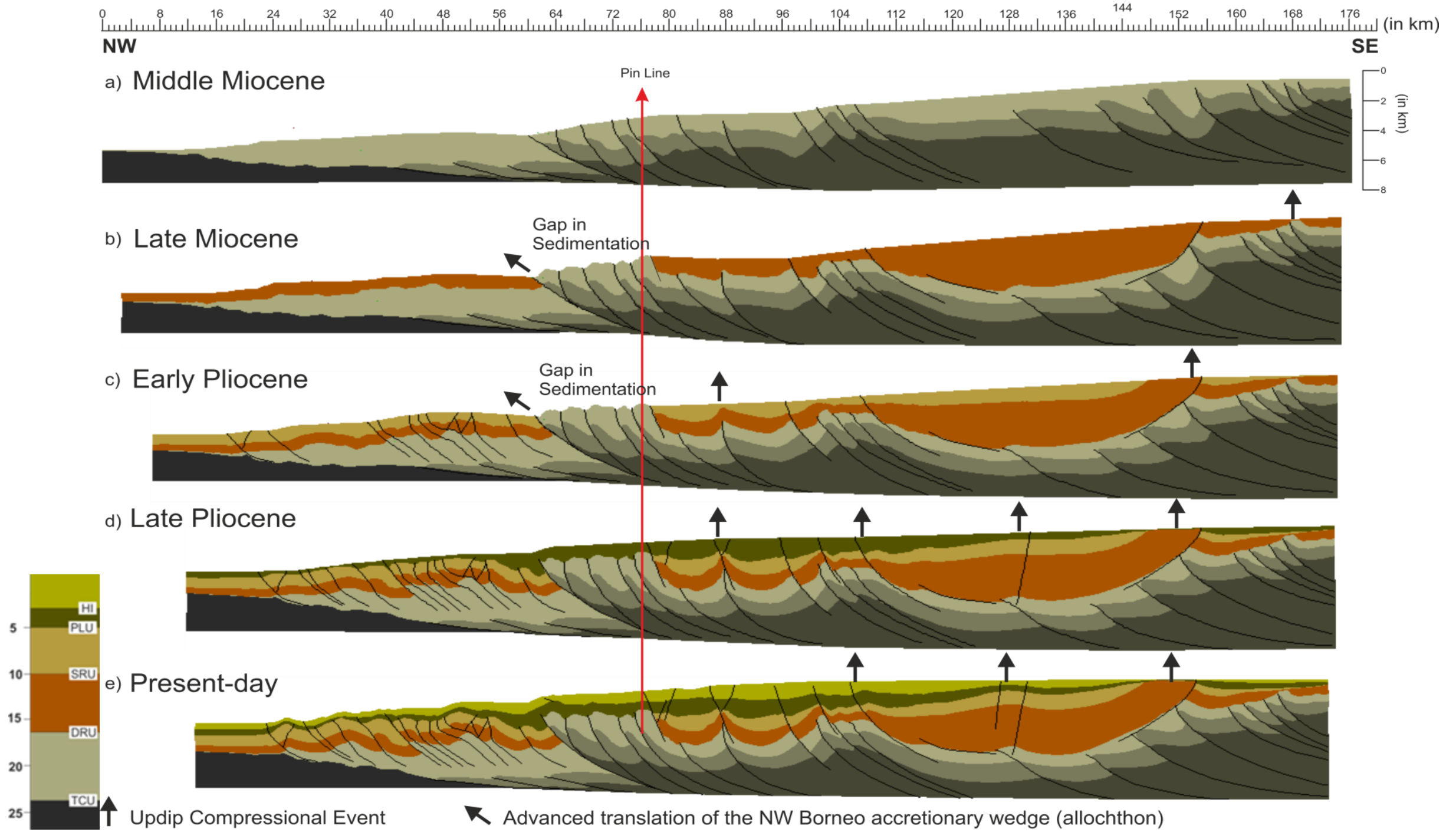


Figure 4. 4 : Structural restoration of the Sabah (northern) margin using Midland Valley 2D Move. The line profile shown was in depth (km) and the location of lines is shown in figure 4.1.

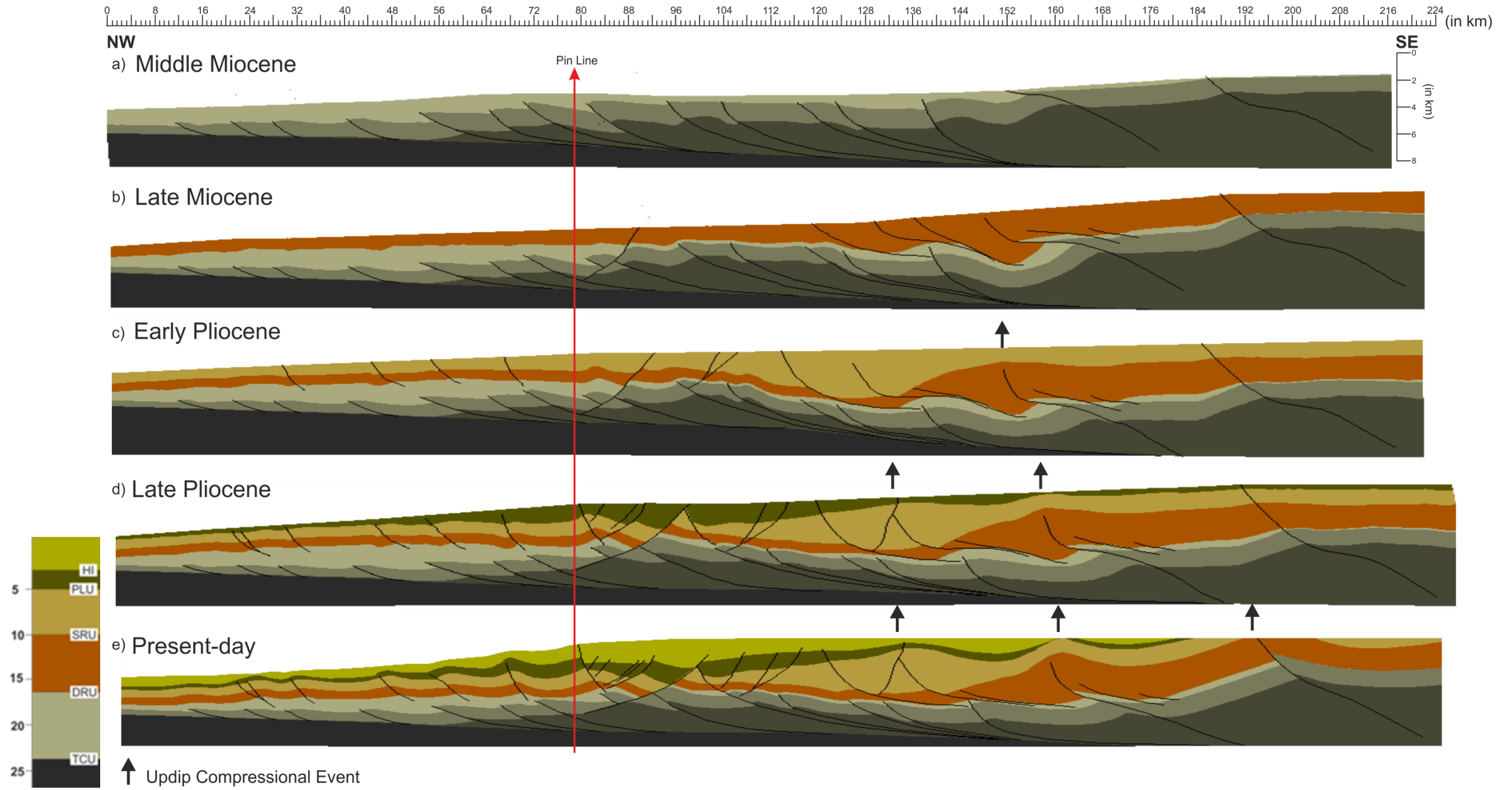


Figure 4. 5: Structural restoration of the Brunei margin using Midland Valley 2D Move. The line profile shown was in depth (km) and the location of lines is shown in figure 4.1.

## I) Early Miocene-Late Miocene

The end of the restoration process for both regional profiles implies that the allochthonous fold and thrust wedge underlies all the structural domains (Figure 4.4 & 4.5 (a)). An alternative interpretation is that the area was originally overlain by the allochthon, in this case the front of the NW Borneo accretionary wedge. The area was then dominated by deposition of marine shales known as the Setap Shale (Wilson and Moss, 1999), filling the piggyback basin of the accretionary wedge front during Early to Middle Miocene times. Restoration indicates that the movement of some of the thrust sheets continued and is marked by stratigraphic wedging in the piggyback basin (see Figure 4.4 & 4.5 (a)). Significant tectonic deformation occurred in the Middle Miocene, represented by the erosional boundary (Deep Regional Unconformity, DRU), succeeded by the deposition of thick Middle Miocene-Recent deltaic cover derived from the uplift and erosion of the hinterland (Figure 4.4 & 4.5 (b)). The timing of the erosional boundary (Deep Regional Unconformity, DRU) was linked to the end of south-south-eastward subduction below NW Borneo (Levell, 1987).

In the Brunei area, the early stage of deltaic progradation is characterized by a nearly flat shelf edge trajectory (progradational by more than 25 km) with almost no influence of growth faulting on the deltaic architecture (Gartrell et al., 2011). In Sabah on the other hand, the loading and progradation of the delta system was “captured” by a low angle counter-regional (landward dipping) growth fault very soon after the deltaic sedimentation, and is characterized by a progradational deltaic architecture over a distance of approximately ~15 km, with a minor component of aggradation occurring at the base of this progradational package (see Figure 4.3 & Figure 4.4 (b)).

During later stages of progradation, a major counter-regional growth fault with a large offset eventually began to develop in Brunei and increased the accommodation space (see Figure 4.5 (b)), resulting in the development of an extremely thick depocentre fill with aggradational stratal architecture parallel to the faults (Gartrell et al., 2011). Whereas in Sabah, the depositional systems retreat in a back stepping architecture (retro-gradational-degradational) resulting in an almost instantaneous landward shift of the shelf edge trajectory for almost ~18 km (see Figure 4.3).



Progradational systems later resumed in both areas and caused a significant basin-ward shift of facies for almost 15km in the Brunei area (Gartrell et al., 2011) and 6km in the Sabah area, until around the Shallow Regional Unconformity boundary (SRU) (see Figure 4.3). In Brunei, the lower part of this package corresponds to TB3.1 of Gartrell et al. (2011) and is coincident with a drop in eustatic sea level at 11.7 Ma (Haq et al., 1987). Whereas the erosional surface, the Shallow Regional Unconformity (or UC5 of Gartrell et al., 2011), at the top of this package may be explained as corresponding to a “local” tectonic pulse that interrupted the overall structural pattern in the extensional domain at about 10 Ma and which resulted in compressional doming (see Figure 4.4 & 4.5 (b) & (c)).

From Early-Middle to Late Miocene, as the front of the NW Borneo accretionary wedge (allochthon) was displaced sporadically by large gravity-driven extensional faults, the allochthon was eventually translated significantly upwards over the Middle-Late Miocene deltaic sequence by a series of reactivated thrusts that displaced and carried along the allochthon on their hanging wall (see Figure 4.4 & 4.5 (b)). Hence, although decollement surfaces connecting growth faults with the toe thrusts could not be recognized in the seismic data, this combination suggests an event which links the proximal extension and the allochthon advance.

In the Sabah area, this event has displaced and elevated the allochthon and its overburden over a distance of 1.63 km, higher than the equivalent stratigraphic position, by a leading over-thrust and a series of reactivated thrusts (see Figure 4.4 (b)). As the allochthon rested on the hanging wall of the leading over-thrust, was uplifted and eroded, it is proposed that the erosional material was transported down-dip and was deposited in the deep-water, hence leaving the piggyback basins of the elevated allochthon starved of sediment (see Figure 4.4 (b)). On both areas, major extensional movement on the upper-slope was accompanied by very subtle deformation in the un-deformed area in deep-water, foreland of the allochthon, where deformation was progressively absorbed in a broad zone of buckle folding (see Figure 4.4 & 4.5 (b)).

## II) Late Miocene-Early Pliocene

A significant compressional pulse during the Late Miocene-Early Pliocene has interrupted the overall deformation in the extensional domain, resulting in the development of local to semi-regional erosional unconformities accompanied by eventual locking and inversion of most of the older extensional structures and compressional doming (see Figure 4.4 & 4.5 (c)). The shallow regional unconformity (SRU) represented by an onlap surface is regionally mappable in offshore Sabah (see Figure 4.3). However, it is less pronounced in the north-eastern sector of offshore Brunei, and corresponds to conformable surfaces in the south-western sector of offshore Brunei Darussalam (Gartrell et al., 2011). Basin margin uplift and tilting during this time allowed the delta to prograde rapidly due to the reduction of accommodation space on the shelf.

In Sabah, the unconformable sequence boundary is overlain by a highly progradational package with topset deposition, and the extensional deformation had almost no influence on this package architecture (see Figure 4.3). There is a significant basin-ward shift of the shelf edge (approximately ~18 km), suggesting a major bypass of sediment supply into the deep water during this time (see Figure 4.3). In Brunei, the depositional geometry of this package becomes progressively pro-gradational up-sequence with prominent basinward shifts of the shelf edge trajectory of approximately 20-40 km (Saller & Blake, 2003), with a more aggradational component and a stationary shelf edge towards the north-eastern sector of offshore Brunei and in the fault-controlled depocenter (Gartrell et al., 2011).

In Brunei, the upper part of this progradational package corresponds to TB3.4 of Gartrell et al. (2011) and is coincident with a drop in eustatic sea level at 5.73 Ma (Haq et al., 1987). In both areas, the top of this package is an unconformable surface boundary with subtle onlap and subtle erosional features on the shelf (see Figure 4.3). The erosional surface boundary, the Pliocene Unconformity (or UC7 of Gartrell et al., 2011) at the top of this package corresponds to a "local" tectonic pulse that interrupted an overall structural deformation in the extensional domain at approximately 5 Ma.

Subsequent to the progradation and gravitational loading, the main depocenters shifted down-dip in the areas created by a new series of delta top extensional faults. In Sabah, the early phase of extensional faulting was succeeded by

landward-dipping counter-regional growth faults (see Figure 4.4 (c)). These faults (counter-regional growth faults) are observed to continue to traverse the entire deltaic sequence landward and downward into the deforming wedge as loading and progradation of the delta system was captured and trapped, restraining the volumes of sediment that could bypass across the shelf slope and deep-water. Concurrently, the front of the NW Borneo accretionary wedge (allochthon) was displaced and elevated for another 1.30 km by over-thrusts, that eventually creating a bathymetric escarpment (see Figure 4.4 (c)). We infer that this renewed translation event is a natural consequence of the ongoing thinning of the allochthon beneath the extensional domain, with thinner overburden in the deep-water area.

In contrast, in Brunei, the early phase of extensional faulting was succeeded by regional growth faults (basin-ward dipping) in the south-western sector of offshore Brunei Darussalam (Figure 4.5 (c)) and by counter-regional growth faults (land-ward dipping) in the north-eastern sector of offshore Brunei (Gartrell et al., 2011). The regional growth faults (basin-ward dipping) triggered an episode of extensional activity that further traversed the entire deltaic sequence seaward and downward into the deforming wedge as the delta-front propagated seaward, and this at the same time continued to supply significant volumes of sediment into deep-water. The progradation of condensed deltaic sediments into the deep-water area sealed the front of the NW Borneo accretionary wedge (allochthon), reduced its relief and restraining its advance (see Figure 4.5 (c)).

In the deep-water area, a number of newly formed toe-thrust anticlines began to develop, and expanded the contractional domain further seaward, coincident with major extensional movement and uplift on the upper-slope (see Figure 4.4 & 4.5 (c)).

### **III) Early Pliocene-Recent**

The margin is characterized by a further episode of uplift and inversion as demonstrated by the erosional truncation at the current seabed and significant thinning of the Pliocene-Recent sequences on top of most of the inverted anticline structures with thickening and ponding on both flanks (see Figure 4.3; Figure 4.4 & 4.5 (d & e)).

In Sabah, the shelf edge trajectory of this interval changed instantaneously from a highly progradational to minor component of back-stepping architecture (retrogradation of approximately ~2km) around the lower boundary of the package represented by the Pliocene Unconformity, marking the onset of inversion of extensional faults (see Figure 4.3). The shelf edge trajectory later evolved to a prograding architecture up-sequence (see Figure 4.3). In Brunei, the depositional geometry of the package overlying the erosional surface boundary was characterized by a highly progradational architecture with a minor aggradational component and dislocation of the shelf edge trajectory in the fault bounded depocentre (Gartrell et al., 2011). The progradational event in both areas could correspond to “local” tectonic pulses which reactivated and reinverted the already inverted structures during this time.

The later stage of progradation (Late Pliocene-Pleistocene-Recent) shows increasing complexity of the stratal architecture, yet with a consistent basinward shift in depocenters and shelf edge trajectory up-sequence; approximately 30-40 km in the Brunei area, with much thicker sedimentation (Saller & Blake, 2012), and by 12-15 km in the Sabah area with thinner sedimentation (see Figure 4.3). This event could correspond to the high-frequency of sea level fluctuations during this time (Gartrell et al., 2011), associated with superimposition of active tectonic and gravity driven deformation.

Slower deltaic progradation into deep-water in offshore Sabah caused the translational event of the front of the NW Borneo accretionary wedge (allochthon) by over-thrusts to continue much longer. Further translational events of the allochthon by over-thrusts have extended and elevated the allochthon and its overburden for another 1.14km during the Early Pliocene (see Figure 4.4 (d)). In the last stages of this evolution, the Late Pliocene-Pleistocene-Recent deltaic progradation seems to have capped and sealed the allochthon completely, thus restraining the advance of the allochthon seaward, leading to parallel bedded sediment deposition draping the underlying allochthon structures, both in Brunei and Sabah segments (see Figure 4.4 & 4.5 (e)).

Contractional deformation that formed forward of the allochthon continued to develop and expand further seaward, resulting in the formation of a series of seaward-migrating deep-water fold and thrust systems subsequent to the

continuous uplift and gravitational loading up-dip. The width of the compressional domain varies from broad, well developed imbricate zones (~ 70 km) in the Brunei deep-water-fold-thrust belt, passing into regions of narrow imbricate zones (~ 40 km) with a considerably contrasting style of thrust propagation and fold growth, from detached (buckle) folds and fault propagation folds in the Brunei margin to fault propagation folds with locally developed over-thrust folds towards the Sabah part of the margin (see Figure 4.4 & 4.5 (d) & (e)). This variation from buckled to more brittle structures can be interpreted to be a reflection of an increased frictional behaviour as a consequence of the influence of the underlying compressive structure (allochthon) on deep-water fold thrust belt deformation.

#### **4.4 Domain Interaction**

In the previous chapter, observations on the occurrence of the allochthon (the front of the NW Borneo accretionary wedge) that is characterized by a thick zone of poor seismic data quality, associated with contrasting deformational styles, varying from internal imbricate thrusting to discrete features of ductile deformation, suggested that this unit is over-pressured and mobile. This observation, is in agreement with King et al., (2009, 2010), who characterised the unit as thickened mobile shales region based on recent analysis of present-day maximum horizontal stress. The restorations presented in the previous sections have shown that the allochthon was sporadically translated and/or over-thrust upwards and downdip along with seaward migration of gravity-driven extensional structures updip, from latest Miocene onwards.

McClay et al. (1998) have shown through analogue modelling that severe thinning of the ductile shale layer beneath the extensional domain can force the ductile layer to flow outboard and downslope of the active delta-top system in response to the imposed differential load. This outboard and downslope flow of the ductile layer forms diapirs, pillows, ridges and contractional structures cored by the mobilized ductile layer in the outer domain where the shale section is clearly thickened (McClay et al., 1998). Mobile withdrawal or outboard flow of mobile shale may be indicated by recognition of the stratigraphic level in the syncline being grounded below the regional stratigraphic level (Van Rensbergen and Morley, 2003).



Therefore, it can be inferred that, there might be a link between the proximal extension updip and the allochthon (the front of the NW Borneo accretionary wedge) advance downdip. In other words, the over-pressured allochthon might have been displaced/flowed downdip and rose above its regional stratigraphic level as a function of domains interaction; due to the thinning of the allochthon beneath the extensional domain updip by deltaic sediments that sink below their regional level. On this basis, it is inferred that variation in the magnitude of the allochthon involved in the NW Borneo deep-water-fold-thrust belt spatially and laterally resulted from the variation in the amount of extension that fed translation into deep water.

Applying the same conceptual basis for calculation of salt (Hudec and Jackson, 2004), the cross-sectional area of the allochthon displaced upward/seaward above its regional stratigraphic level should; 1) be compensated by an equivalent area (or less) of deltaic sediments in their piggyback basin that sink below their regional level in the absence of basement shortening, and 2) exceed the area of deltaic sediments in their piggyback basin that sink below their regional level if basement shortening is involved (Figure 4.6). A regional line was defined as a line connecting the elevations of the top of allochthon on either side of the basin (Hudec and Jackson, 2004). To test this, a regional line was then drawn on the two regional cross sections (Brunei segment and Sabah segment) that have been restored in previous section, connecting the elevations of the top allochthon on either side of the basin (see Figure 4.1 for line location). The total cross-sectional area of allochthon above their regional level and deltaic sediment below their regional level was measured for four configurations (the Late Miocene, Early Pliocene, Late Pliocene and Present day) and is achieved by using 'POLYGON AREA' function under 'ANALYSIS' tab in Midland Valley's 2D Move software. The results are shown in Table 4.1, Figure 4.7 and Figure 4.8.

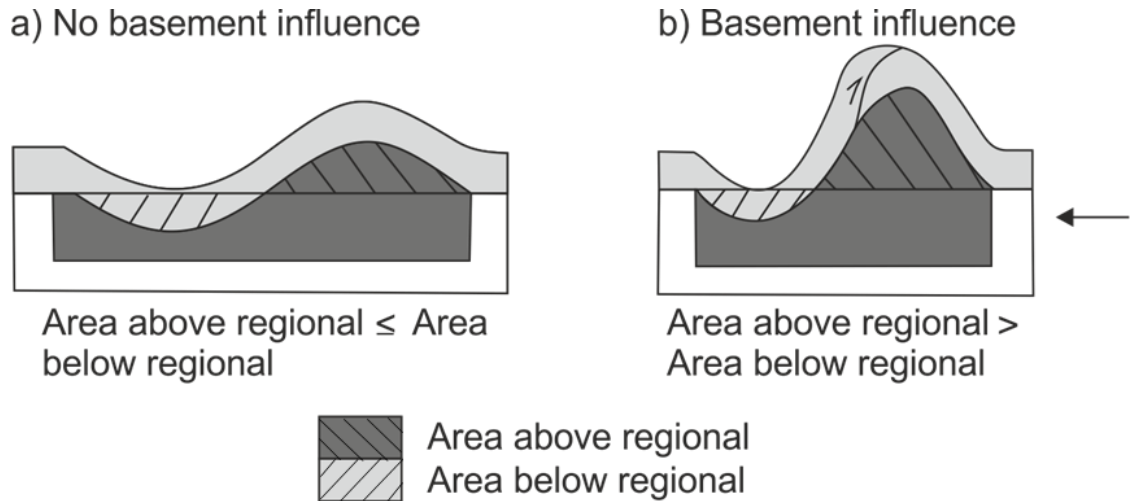


Figure 4. 6: Schematic diagram showing conceptual basis for allochthon above regional calculations (modified from Hudec and Jackson, 2004). (a) In the absence of basement shortening, the cross-sectional area of allochthon displaced upward/seaward above their regional level should be compensated by an equivalent (or lesser) area of deltaic sediments in their piggyback basin that sink below their regional level. (b) If basement is shortened, the cross-sectional area of allochthon displaced upward/seaward above their regional level may exceed the area of deltaic sediments in their piggyback basin that sink below their regional level.

Table 4. 1: Total cross-sectional area of allochthon above their regional level and total cross-sectional area of deltaic sediments that sink below their regional level.

		<b>Allochthon above regional</b>	<b>Sediment below regional</b>
<b>Sabah (North)</b>	Present-day	24.24 km <sup>2</sup>	110.54 km <sup>2</sup>
	Late Pliocene	24.62 km <sup>2</sup>	129.16 km <sup>2</sup>
	Early Pliocene	26.03 km <sup>2</sup>	107.21 km <sup>2</sup>
	Late Miocene	17.84 km <sup>2</sup>	101.88 km <sup>2</sup>
<b>Brunei (South)</b>	Present-day	17.90 km <sup>2</sup>	107.43 km <sup>2</sup>
	Late Pliocene	34.93 km <sup>2</sup>	80.67 km <sup>2</sup>
	Early Pliocene	43.76 km <sup>2</sup>	95.47 km <sup>2</sup>
	Late Miocene	7.42 km <sup>2</sup>	107.58 km <sup>2</sup>

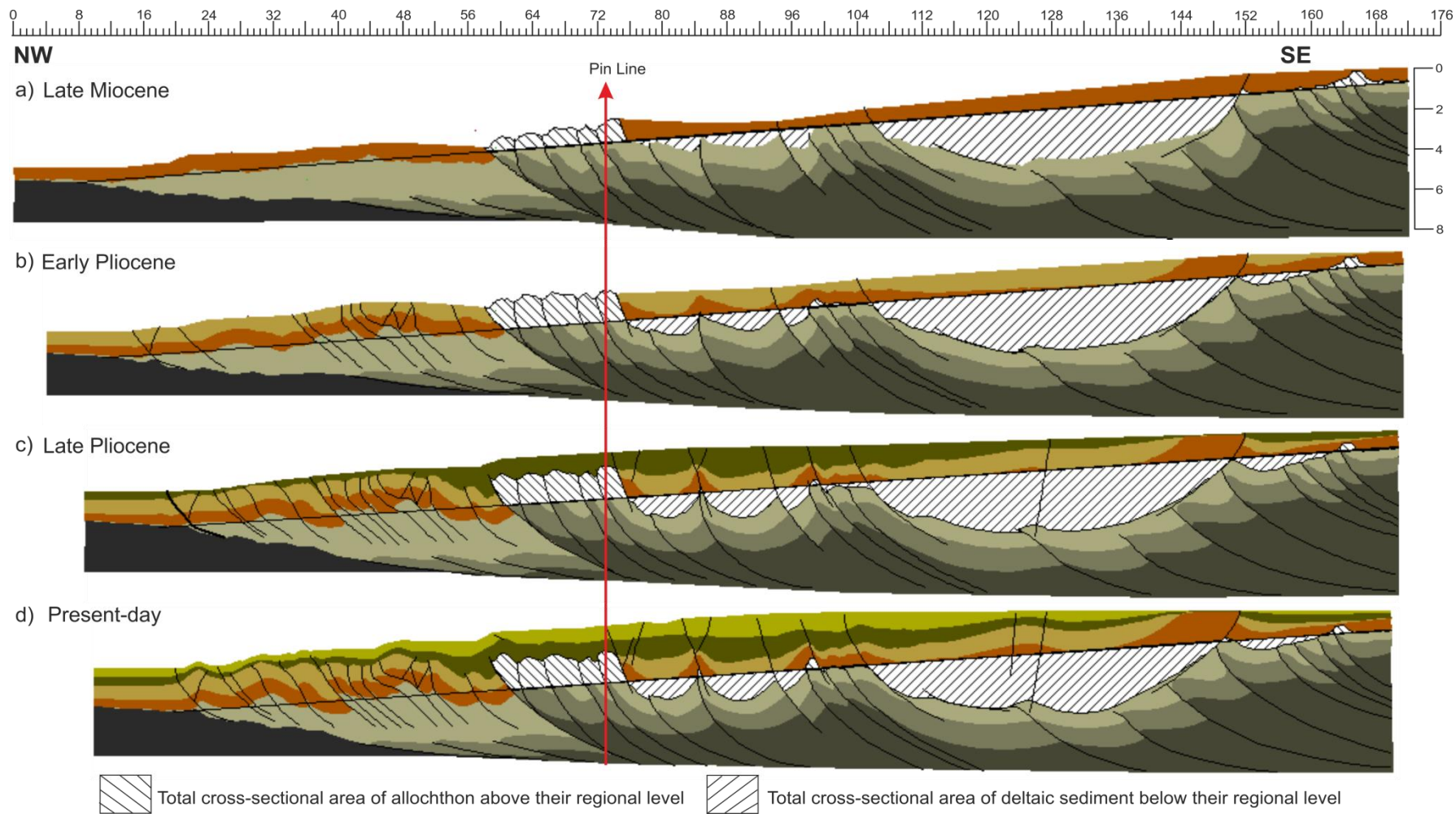


Figure 4. 7: Regional profile across the northern segment of the NW Borneo margin (Sabah) used to measure the present-day total cross-sectional area of allochthon above regional and the deltaic sediments in their piggyback basin that sinks below regional.

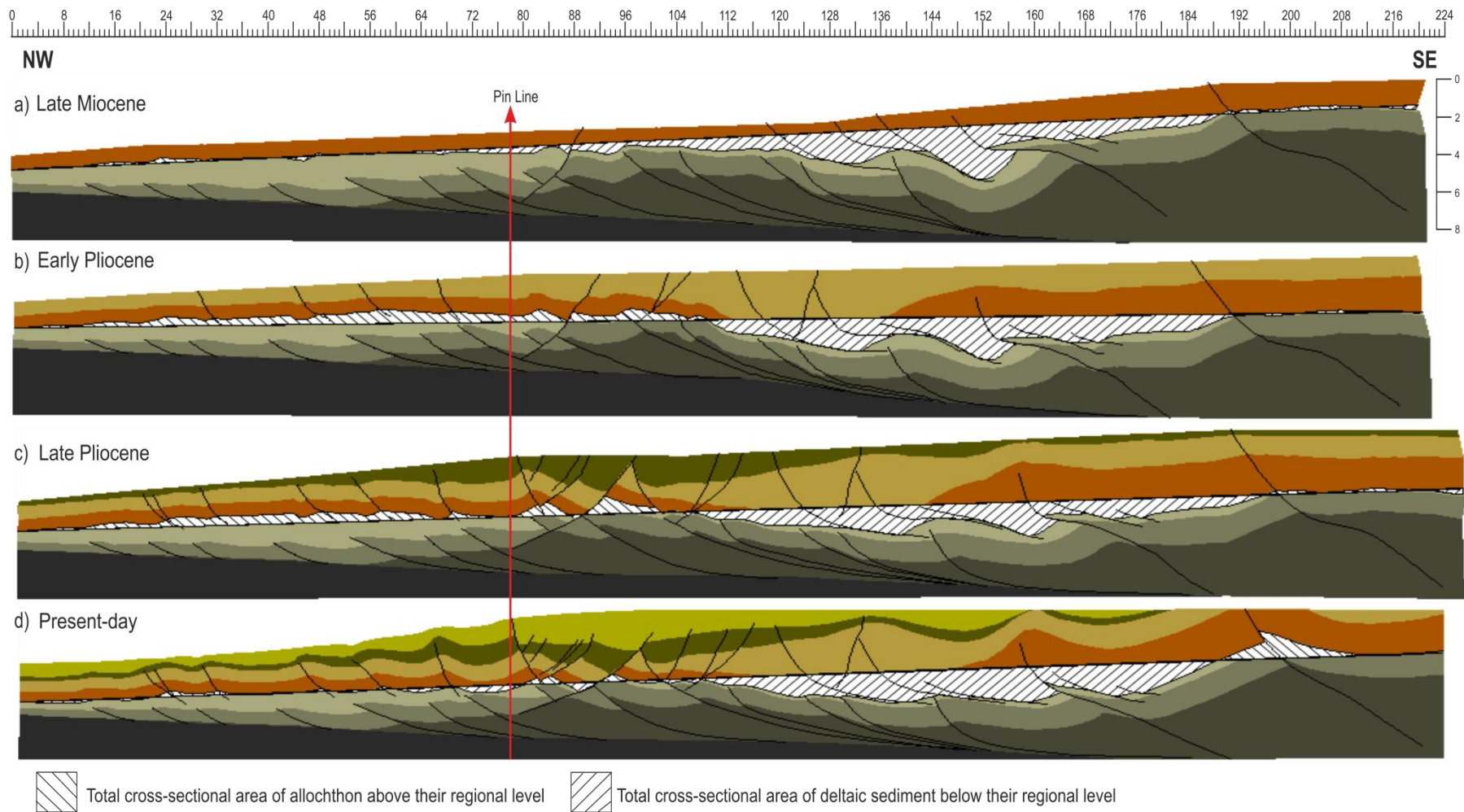


Figure 4. 8: Regional profile across the southern segment of the NW Borneo margin (Brunei) used to measure the present-day total cross-sectional area of allochthon above regional and the deltaic sediments in their piggyback basin that sinks below regional.

#### **4.4.1 Translation magnitudes**

##### **I) Late Miocene Translation**

The results presented in Table 4. 1 show that during the Late Miocene, the total cross-sectional area of the allochthon above their regional level in the northern segment is 17.84 km<sup>2</sup> compared with 101.88 km<sup>2</sup> of deltaic sediments in their piggyback basin that sink below their regional level (Figure 4.7 (a)). Whereas in the southern segment, the total cross-sectional area of the allochthon above their regional level is 7.42 km<sup>2</sup> compared with 107.58 km<sup>2</sup> of deltaic sediments that sink below their regional level (Table 4.1; Figure 4.8 (a)). On both segments, the large volume of deltaic sediment that sinks below regional at this stage is created by the Middle Miocene-Late Miocene depocentre that accumulated more than 3.5 km of sediments (see Figure 4.7 & 4.8 (a)). This thinning of the mobile layer beneath the depocentre is an early mobility feature that developed syn-depositionally to localize sedimentation, which may have driven the later stage of deformation in the outer fold thrust belt.

The mechanism of shale deformation would have mainly been as a result of over-pressuring that reduced the internal shear strength of rock in the shale-rich sequence (Weimer and Slatt, 2004). Overpressures develop in sediments primarily due to rapid burial of low-permeability units that will lead to entrapment of high fluid pressure, and secondarily due to hydrocarbon maturation that will result in a significant increase in fluid volume and hence pressure (Morley and Guerin, 1996; Weiner et al., 2010). Overpressure may also develop secondarily due to superposed tectonic stresses either by a gravitational movement in a linked system (delta toe compression-delta top extension) and/or superposed plate tectonic stresses in an active margin (Weiner et al., 2010). In NW Borneo, the weak mobile shales that forms a weak ductile substrate for the deltaic succession is the Early to Middle Miocene marine prodelta shale known as the Setap Formation, (Morley, 2003; Van Rensbergen et al., 1999; Morley et al., 2011). Where deeply buried, this marine shale is typically over-pressured, under-compacted and mobile; and is the source of shale diapirs offshore (Morley et al., 1998).

At this stage, the overpressure is anticipated to have been generated from disequilibrium compaction/differential loading of the under-compacted shale



layer associated with superposed stresses of the gravity driven extensional and compressional structures onto the previously active thrust margin (front of the NW Borneo accretionary wedge). Moreover, the weak mechanical behavior of the shale-rich sequence is not confined to a specific stratigraphic unit in either time or space (Morley, 2003; Morley and Guerin, 1996) and can occur at multiple stratigraphic levels depending on the migration of pore fluids pressure (Weiner et al., 2010). The pore fluids of under-compacted mobile shales can migrate and induce overpressure to a degree where the stratified shales within the country rock become mobile (Van Rensbergen et al., 1999; Morley and Guerin, 1996), and lithified blocks are incorporated within the shale mass (Van Rensbergen et al., 1999). In this case, migration of pore fluid pressure of the over-pressured, under-compacted Setap shale generated by disequilibrium compaction associated with superposed stresses is believed to have induced overpressure within the allochthon to a degree where it became mobilized. Increase of overpressure reduces acoustic velocity differences between stratified sand and shale, hence causing the dimming of seismic reflections due to a lack of impedance contrast (Maucione & Surdam, 1997).

## **II) Early Pliocene Translation**

The Early Pliocene time was a phase of significant outboard spreading of the ductile allochthon layer in the outer domain where it's clearly thickened. The total cross-sectional area of the allochthon above their regional level in the Early Pliocene increases significantly to 26.03 km<sup>2</sup> in the northern segment and to 43.76 km<sup>2</sup> in the southern segment (Table 4. 1; Figure 4.7 & 4.8 (b)). In the northern segment, the deltaic sediment in the extensional domain continues to sink below their regional level. The total cross-sectional areas of the deltaic sediments that sink below their regional level increase to 107.21 km<sup>2</sup> (see Figure 4.7 (b)). In the southern segment, on the other hand, the amount of deltaic sediments that sink below their regional level decrease to 97.47 km<sup>2</sup> (see Table 4. 1). It can be inferred that the phase of basin inversion in this segment was quite significant to reduce the amount of deltaic sediments that sink below their regional level, as evidenced by thinning and curving of growth strata towards the crest of a compressional anticline (see Figure 4.8 (b)). This phase of compressional pulse that caused uplift of the inner margin and

inversion of the growth fault up slope is believed to also have favoured the downslope translation of the allochthon, and hence caused a significant increase in the total cross-sectional area of the allochthon above their regional level in the southern segment (see Figure 4.8 (b)).

Moreover, the thickness variation of the overburden (decreasing abruptly seaward to about 1.0 to 1.5 km) is believed to cause a high seaward pressure gradient in the mobile shale that would have aided outward flows of the shale mass from the base of the rapidly accumulating depocentre (more than 3.5 km thick), leading it to bulge and rise above its regional stratigraphic level (see Figure 4.7 & 4.8 (b)). Besides that, over-pressured shale provides a weak detachment layer, hence the stress transmitted to the down-dip end of the linked system (extensional-compressional domain) due to the thinning of the mobile layer beneath a rapidly accumulating depocentre (more than 3.5 km thick in the extensional domain) is believed to have reactivated the pre-existing thrusts (within the allochthon), and translated the allochthon significantly upwards above its regional stratigraphic level. The reactivation of any pre-existing thrust could have caused extensive lateral spreading of overpressure as it carried along the over-pressured allochthon in its hanging wall.

Gas generation in Brunei is interpreted to occur at 3.5km to 4.5-4.5 km deep (Sandal, 1996). During this time, the top of the Early Miocene-Middle Miocene layer (Setap shale) and the base of the deltaic sediments (in the extensional domain) were within the gas window (see Figure 4.7 & 4.8 (b)). Hence, the overpressure within the mobile layer is interpreted to have been reactivated by secondary over-pressure generation, in particular gas generation, to increase the pore fluid pressure, during this time.

### **III) Late Pliocene and Present Time Translation**

Later in the Late Pliocene and towards the present, the total cross-sectional areas of the allochthon above their regional level started to decrease. In Sabah, the total cross-sectional areas of allochthon above their regional level start to decrease to 24.62 km<sup>2</sup> in Late Pliocene and slightly to 24.24 km<sup>2</sup> at present time (Table 4.1; Figure 4.7 (c) & (d)). In Brunei, the total cross-sectional areas of allochthon above their regional level start to decrease to 34.93 km<sup>2</sup> in the Late

Pliocene and significantly to 17.90 km<sup>2</sup> at present time (Table 4.1; Figure 4.8 (c) & (d)). This condition can be linked to significant erosion of the inner domain due to continuous uplift, that provided significant volumes of sediment for progradation and deposition across the shelf slope and deep-water area, with approximately 30-40 km of progradational event in offshore Brunei and 12-15 km in offshore Sabah (refer section 4.32; Figure 4.3) . Significant progradation and deposition has capped the allochthon wedge, thus hindering its advance.

The deltaic sediments in the extensional domain in the northern segment continued to sink below regional until reaching 129.16 km<sup>2</sup> in the Late Pliocene before decreasing to 110.54 km<sup>2</sup> at present time (see Table 4.1; Figure 4.7 (c) & (d)). Whereas in the southern segment, the amount of deltaic sediments that sink below regional continued to decrease to 80.67 km<sup>2</sup> in the Late Pliocene before an increase to 107.43 km<sup>2</sup> at present time (see Table 4.1; Figure 4.8 (c) & (d)). This variation is inferred to correlate with the variations in sedimentation rate and uplift rate in the extensional domain.

On the whole, the results presented demonstrate that, even with continuous uplift of the inner margin, the observed up-dip deltaic extensional structures accommodating basin-ward translation are capable by themselves of generating enough Late Miocene-Recent translation to account for seaward and upwards translation of the allochthon in the outer domain. In recent times, the observed accommodation by up-dip deltaic extensional structures allowing basin-ward translation exceeds the total cross-sectional area of allochthon above regional by 86.30 km<sup>2</sup> and 89.53 km<sup>2</sup> in the northern and southern segment respectively.

#### **4.5 Stratigraphic Thickness Variation: How does it affect the Critical Wedge Geometry and Deformation Styles of the Area?**

The results reported have shown that the evolution of the NW Borneo margin results from the combination of gravity and tectonic deformation, but they were not the only factors. In NW Borneo, it has been documented that the accumulation of the Miocene-Recent shallow marine deltaic section along the NW Borneo margin is focused on the southern segment where deltaic sedimentation and progradational episodes have deposited large volumes of sediment, while the northern margin has experienced lower and much smaller

sediment supply and hence has a thinner sedimentary column (~10–12 km thick towards Brunei, vs. ~6 km in Sabah; Morley et al., 2003).

It is expected that variation in sedimentary supply and stratigraphic thickness in the study area affects the critical taper wedge angle of the deforming wedge. Variation in the critical taper wedge angle of the deforming wedge leads to profound effects in the location and pattern of structural deformation within the wedge (e.g., Liu et al., 1992; Dahlen et al., 1984). The critical wedge taper angle is measured by the bathymetric slope angles ( $\alpha$ ) and basal detachment dip ( $\beta$ ) (Dahlen, 1984). In the study area, critical taper wedge angle of the deforming wedge have been measured on four selected lines, BGR02, BGR10, BGR20 and BGR24. The BGR02 and BGR10 profiles (located in the northern segment) were acquired by Hess Corporation whereas the BGR20 and BGR24 profiles (located in the southern segment) were modified from previously published seismic profiles of Hesse et al. (2010)). The average taper angle measured for BGR02, BGR10, BGR20 and BGR24 (from north to south) varies from,  $\alpha+\beta=1.8^\circ+0.9^\circ$ ,  $\alpha+\beta=2.4^\circ+3.9^\circ$ ,  $\alpha+\beta=1.3^\circ+5.2^\circ$  and  $\alpha+\beta=1.7^\circ+4.4^\circ$  respectively, while the stratigraphic thickness varies from ~6-7 km in the north to ~10–12 km in the south (Table 4.2; Figure 4.9).

Table 4. 2: Critical taper wedge angle of the deforming wedge measured across the study area.

	<b>Surface slope (<math>\alpha</math>)</b>	<b>Basal décollement dip (<math>\beta</math>)</b>	<b>Wedge taper</b>
<b>BGR86- 02</b>	1.8°	1.0°	2.7°
<b>BGR86- 10</b>	2.4 °	3.9°	6.3°
<b>BGR86- 20</b>	1.5°	5.2°	6.5°
<b>BGR86- 24</b>	1.7°	4.4°	6.1°

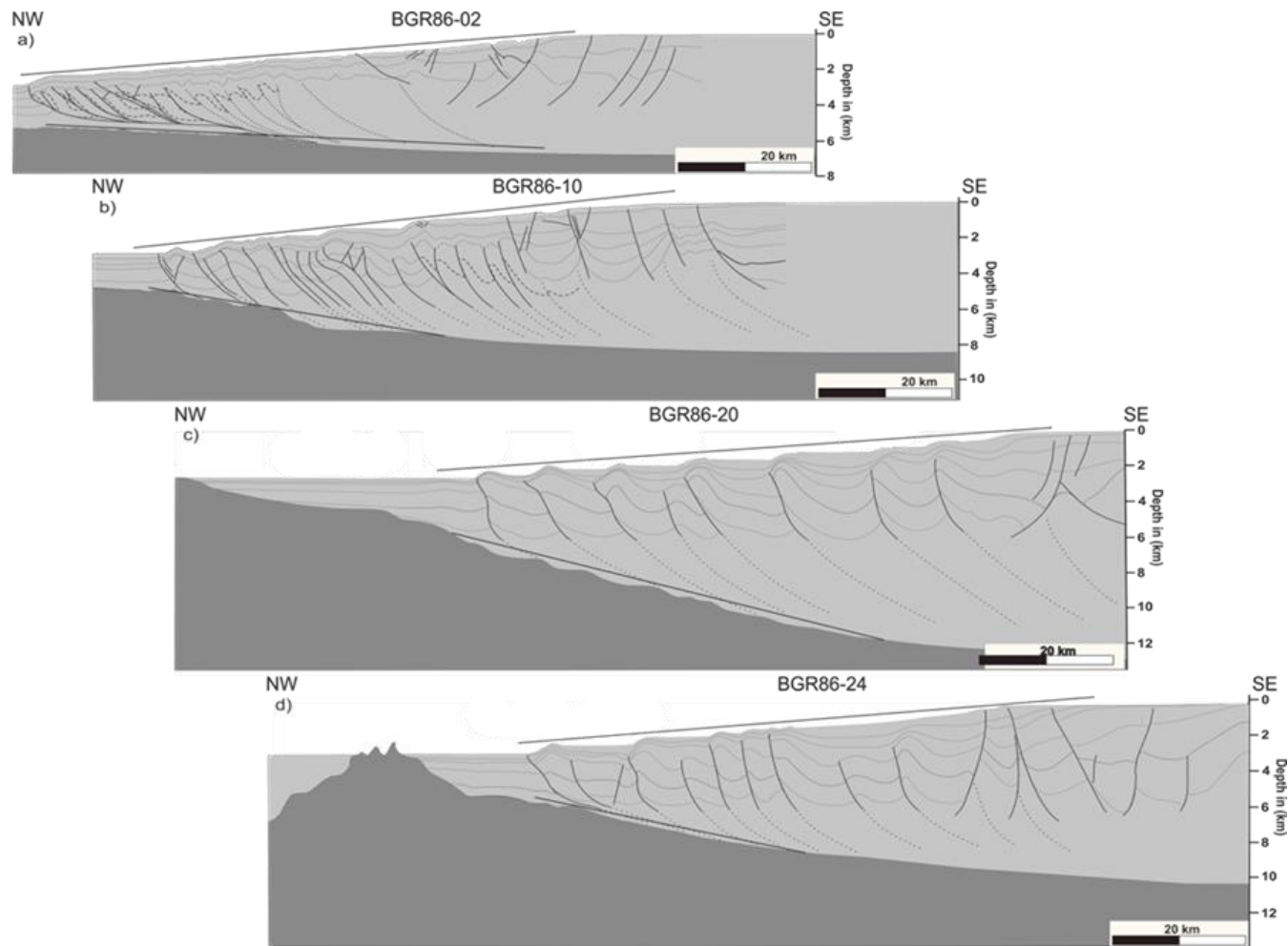


Figure 4. 9: The wedge surface slope ( $\alpha$  = angle of the wedge surface to the horizontal) and the dip of the basal décollement ( $\beta$  = angle of decollement to the horizontal) measured across the study area. Note that lateral thickness variation from north (a) to south (d) is consistent with variation in the deformational style.



Lower sediment supply in the northern deep-water segment (BGR86-02, BGR86-10) can inhibit the building of surface slope and critical taper. This condition (wedge is less steep than the ideal angle) forces the deforming wedge to deform internally until the critical taper is achieved (Nieuwland et al., 2000). Therefore, more thrusts or out-of-sequence thrusts are required to uplift the wedge either by reactivation of existing faults, or by the generation of new thrusts, or both, to attain the topography that satisfies the critical angle within the deforming wedge (Nieuwland et al., 2000; Figure 4.10). In the northern segment of NW Sabah, the deformation under the condition mentioned above results in a less extensive compressional domain with a considerably more compressed style, out-of-sequence thrusting and the emergence of the deep-water fold crests at the seafloor (see Figure 4.9 (b)). This condition (wedge is less steep than the ideal angle) at the same time favours the allochthon wedge to fail by faulting and to be thrust-over progressively into shallower levels, in an attempt for the deforming wedge to gain the taper angle (critical taper), thus explaining why the allochthon has advanced significantly in the northern segment. Accordingly, assuming that the current taper is the critical taper, the bathymetry of the current seafloor dips quite steeply seaward ( $2.4^\circ$ ), even with lower basal detachment dips ( $0.9^\circ$ - $3.9^\circ$ ) and lower stratigraphic thickness (~6-8 km) (see Table 4.2; Figure 4.9 (a) & (b)).

In the southern deep-water segment, high and persistent sedimentary accumulation on the shelf and upper slope tends to increase the slope dips, aiding the building of taper and further destabilizing the margin. This condition (wedge is steeper than the ideal angle) requires deformation to decrease the bathymetric slope angles, to reduce the destabilizing effects. In other words, the deforming wedge will respond to these unstable supercritical states (wedge is steeper than the ideal angle) by propagating forward or/and lengthening the wedge, which promotes significant forward movement of the deformation front that consequently will broaden the slope and reduce the taper back to critical (Nieuwland et al., 2000; Billotti and Shaw, 2005; see Figure 4.10). In the southern segment of NW Sabah, the deformation under the condition mentioned above results in a well-developed, extensive compressional domain and wider spacing of structures with fewer seafloor expressions of fault-propagation folds (see Table 4.2; Figure 4.9 (c) & (d)). Accordingly, assuming that the current taper is the critical taper, the bathymetry of the current seafloor dips in the southern segment by  $1.3^\circ$ - $1.7^\circ$ , almost equivalent with the northern segment, even with higher basal detachment dips ( $4.4^\circ$ - $5.2^\circ$ ) and higher stratigraphic thickness (~10-12 km) (see Table 4.2; Figure 4.9 (c) & (d)). Furthermore, condensed sediment supply will simultaneously capped and buried the allochthon wedge, leading to parallel bedded sediment draping the

underlying allochthon structures, reducing its relief and restraining its advance in the southern segment. This outcome is possible since increase in the proportion of the overlying deltaic deposit will restrain reactivation of the underlying pre-existing structures and the effects of pre-existing structures on the development of fold-thrust systems during the second shortening phase.

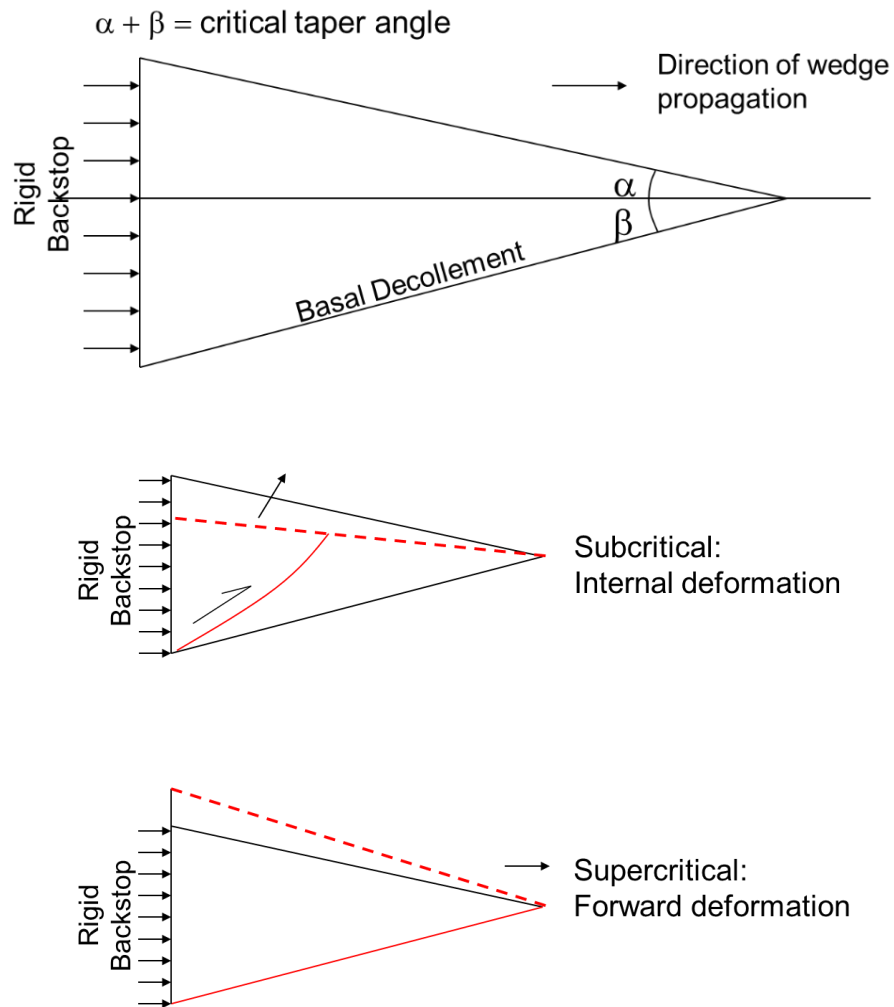


Figure 4. 10: Basic diagram of a critically tapered wedge. Wedge taper is defined as the wedge surface slope ( $\alpha$  = angle of the wedge surface to the horizontal) plus the dip of the basal décollement ( $\beta$  = angle of décollement to the horizontal). The wedge will respond to unstable states by attempting to obtain the critical taper angle, either by deforming internally and uplifting the wedge, or by propagating forward and lengthening the wedge.

The relationship plot between pore-fluid pressure ratio ( $\lambda$ ), surface slope ( $\alpha$ ), and basal detachment dip ( $\beta$ ) for NW Sabah fold-and thrust belt at critical taper indicate that the ratio of pore fluid pressure to lithostatic pressure at the base of the wedge ( $\lambda$ ) appear to be nearer to the lithostatic pressure toward the SE ( $0.91 < \lambda < 0.97$  from BGR10 to BGR24) (Figure 4.11). This trend continues toward the offshore Brunei fold-and thrust belt (located SE of offshore NW Sabah) with the ratio of pore fluid pressure to lithostatic pressure at the base of the wedge ( $\lambda$ )  $\approx 1.0$  ( $> 0.97$ ) (Morley, 2007) (see Figure 4.11). This observation agrees with evidence for high pore-fluid pressures both on the shelf and in the deep-water area of Brunei (Morley, 2007) and considerably contrasting style of deformation from detached (buckle) folds and fault propagation folds in the Brunei margin (Gartrell et al., 2011) to fault propagation folds with wider spacing and less well developed out-of-sequence thrusting in the southern NW Sabah (BGR22 & BGR 24) to more compressed style of fault propagation folds with out-of-sequence thrusting and the emergence of the deep-water fold crests at the seafloor in the northern NW Sabah (BGR10) (from buckled to more brittle structures; see Figure 4.9).

In the northern end of the study area, the critical taper wedge measured is  $2.7^\circ$  (BGR02), very low compared to the other part of the study area (see Table 4.2; Figure 4.9 (a)). Low taper is typical of low-permeability, clay dominated prisms (Saffer and Bekins, 2002). In other words, the wedge geometry is consistent with it overlying a very weak décollement with low friction and/or high fluid pressure. That prediction agrees with the relationship plot between pore-fluid pressure ratio ( $\lambda$ ), surface slope ( $\alpha$ ), and basal detachment dip ( $\beta$ ) that indicate a high pore fluid pressure to lithostatic pressure ratio at the base of the wedge ( $\lambda > 0.97$ ; see Figure 4.11). Deep-seated lateral expulsion of fluids ocean-ward from beneath the shelf (Van Rensbergen and Morley, 2003) due to an ocean-ward lateral decrease in lithostatic pressure gradient (Tingay et al., 2005) have been advocated as the possible mechanism for sustaining high basal pore-fluid pressures in NW Borneo (Morley, 2007).

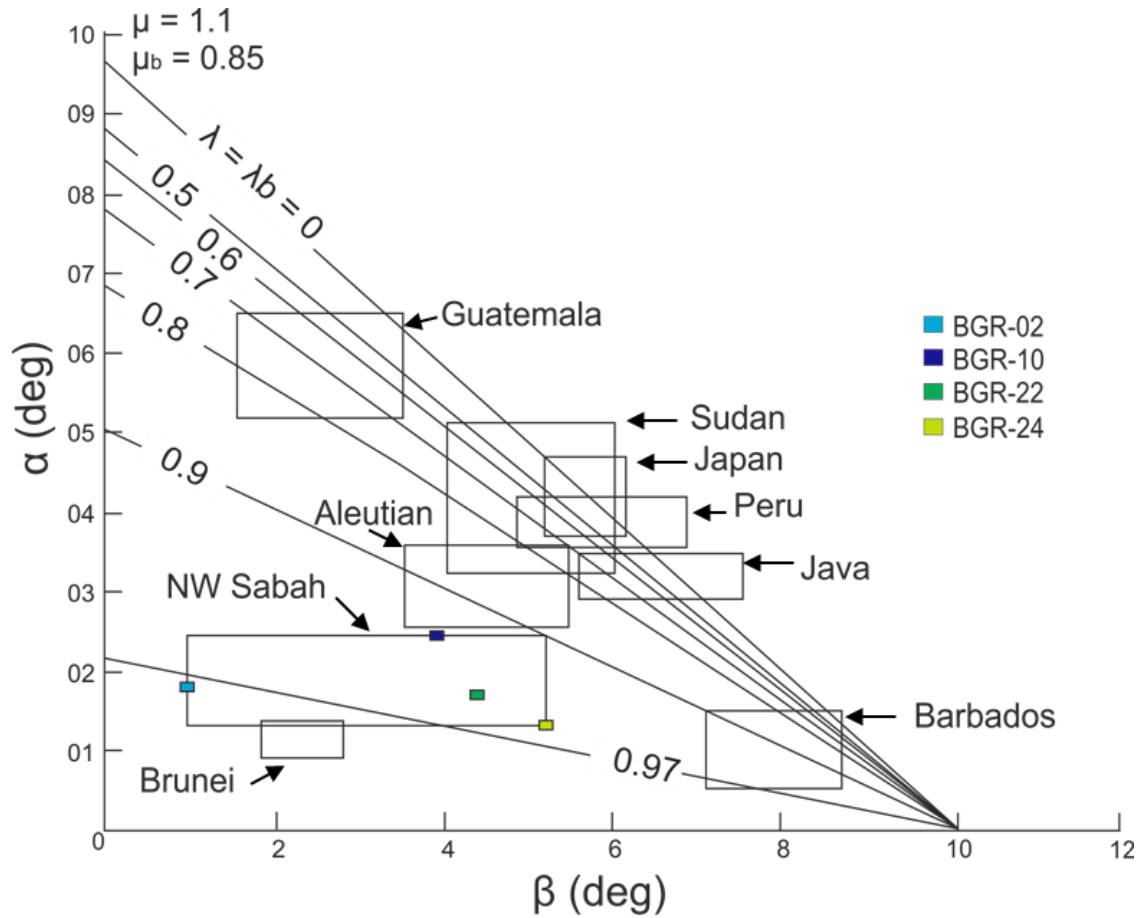


Figure 4. 11: Relationship between pore-fluid pressure ratio ( $\lambda$ ), surface slope ( $\alpha$ ), and basal detachment dip ( $\beta$ ) for a submarine fold-and thrust belt at critical taper, assuming Coulomb material behaviour (Dahlen, 1984; Morley, 2007). Critical wedge geometry and taper angle of offshore NW Sabah are based on seismic reflection data acquired by Hess Corporation (BGR02 and BGR10) and previously published seismic profiles of Hesse et al. (2010; BGR20 and BGR24).  $\mu$ - internal coefficient friction for the wedge;  $\mu_b$  - internal coefficient friction at the base of the wedge;  $\lambda_b$ - ratio of pore fluid pressure to lithostatic pressure at the base of the wedge.

## **4.6 Discussion: Model of Evolution and How This Fits With Current Understanding of the Area**

In NW Borneo, the deep-water fold and thrust belt shows a lot in common with gravity-driven deep-water fold and thrust belts such as the Niger Delta, where deformation is driven by linked up-dip extensional and down-dip contractional systems due to deltaic sedimentary loading above a weak mobile shale that forms an underlying substrate for the system (Morley, 2003; Corredor et al., 2005; Weiner et al., 2010; Morley et al., 2011). However, in NW Borneo, progradation of the large Baram-Champion deltaic formation over the front of the NW Borneo accretionary wedge has caused the superimposition of gravity driven extensional and compressional deformation on the pre-existing tectonic compressional deformation.

The model of structural deformation interpreted in this study consists of a sedimentary wedge prograded over and grew above a former fold and thrust front (Figure 4.12 (a)). Initial progradation of the delta associated with rapid deltaic accumulation caused substantial upper-slope subsidence where the first counter-regional or paired regional and counter-regional growth faults started to develop in the extensional domain. This occurred by the end of the Middle Miocene (Figure 4.12 (b)). The normal fault was initiated in the sedimentary wedge on top of the early fold where surfaces of weakness were present, instigated by the accumulation of the delta front sediments. As sediment load increased, the fault grew and soled down into the mobile substrate and trapped a significant volume of sediment. As loading and progradation of the deltaic system continued, the delta-front continued to move and initiate a second counter-regional growth fault on top of the early fold, forward of the earlier counter-regional growth fault. The main depocenter would have shifted seaward, as allowed by expansion of new counter-regional growth fault; whereas the earlier counter-regional growth fault was inverted by the tectonic compressional pulse (Figure 4.12 (c) & (d)).

This model of gravity-driven deformation (counter-regional growth fault) controlled by the emplacement of the delta-front, initiated on the top of the early folds, is in many ways similar to the ideas of Morley and Guerin (1996), Saller and Blake (2003), Gartrell et al. (2011) and Sapin et al. (2012). In this study, the model was reproduced and improvised to show the interaction between the



gravity and tectonic deformation, particularly the formation and evolution of the gravity driven proximal extension and distal fold-thrust structures and their relationship with the underlying tectonic compressional structures, the mobile allochthon, as will be discussed below.

The cycle of faulting and sedimentation in the extensional domain that lead to overpressure generation caused a feedback mechanism that generate toe thrusting in the deep-water. The up-dip extension is interpreted to be linked at depth with the down-dip contraction through detachment surfaces, that can be at various levels and positions, where deformation is transferred (Bilotti and Shaw, 2005; Corredor et al., 2005; Weiner et al., 2010; Morley et al, 2011). In general, interpretations locate the decollement surface where the listric toe thrusts become sub-horizontal. In contrast, Dean et al. (2015) from discrete element simulations show that deformation with thin mobile shales or on a smooth basement may form a thin decollement surface linking the extensional and compressional domains, whereas, deformation with a thicker mobile shale or over a rough basement surface may form a region of distributed strain throughout the mobile shale layer, that propagated ocean-ward over time without a discrete decollement surface.

In NW Borneo, the mobile shale layer is known to be thick and a connection between the thrust roots and the detachment level as well as decollement surfaces connecting the extensional faults with the toe thrusts could not be recognized in seismic data. Nonetheless, previous workers have proposed the decollement surfaces to be on top of or within the mobile substrate, the Setap shale due to the listric geometry of most of the faults (Hesse et al, 2010). In this study, it is inferred that the stress from loading and progradation of the delta system associated with large gravity-driven extensional faults superimposed on the accretionary wedge (allochthon), was transmitted down-dip over time as a diffuse region of distributed strain within the thick, overpressured, mobile allochthon. This diffuse zone of shear that transmitted down-dip over time caused a feedback mechanism translating the allochthon sporadically upwards above its regional stratigraphic level, by reactivating the pre-existing thrusts, then progressing seaward to generate toe thrusting in the deep-water area, without a discrete decollement surface (Figure 4.12).

Subsequently, as the cycle of sedimentary loading and delta front prograding continues, the deformation was succeeding by outer shelf growth faulting; counter regional growth faults dominate the northern segment (Figure 4.12 (e)) and regional growth faults dominate the southern segment (Figure 4.12 (f)). Sapin et al., (2012) suggest that the absence of early folds in the southern segment restrained the development of counter regional growth faults. We infer that the absence of early folds in the southern segment, that would provide planes of weakness to initiate the counter regional growth faults in the southern segment, is due to high and persistent sediment supply associated with thicker stratigraphic thicknesses (~10-12 km) that buried and restrained the advance of the allochthon to a shallower level. In contrast, lower sediment supply with thinner stratigraphic thicknesses (~6-8 km) in the northern segment resulted in the emergence of the allochthon into shallower levels by out-of-sequence thrusting, in an attempt for the northern wedge to achieve taper. This condition favours the formation of a gravity-driven counter regional growth fault on the top of the early folds of the emergent allochthon.

The translational event of the allochthon slowed down/stopped as Late Pliocene-Pleistocene deltaic progradation capped and sealed the allochthon completely, thus restraining the advance of the allochthon outward, leading to parallel bedded sediment deposition draping the underlying allochthon structures (see Figure 4.12 (e) & (f)). The weight of the surrounding overburden is capable alone of generating enough Late Miocene-Recent translation to account for seaward translation of the allochthon in the outer domain and the reactivation of the internal imbricate thrusting. Nevertheless, compressional tectonics were still active until at least the latest Pliocene, evidenced by continuous uplift of the inner margin and inversion of the earlier counter regional growth fault up slope. In the deep-water, immediately in front of the allochthon wedge, deformation was dominated by a series of younger seaward, in-sequence thrust folds, with a more compressed style towards the northern segment.

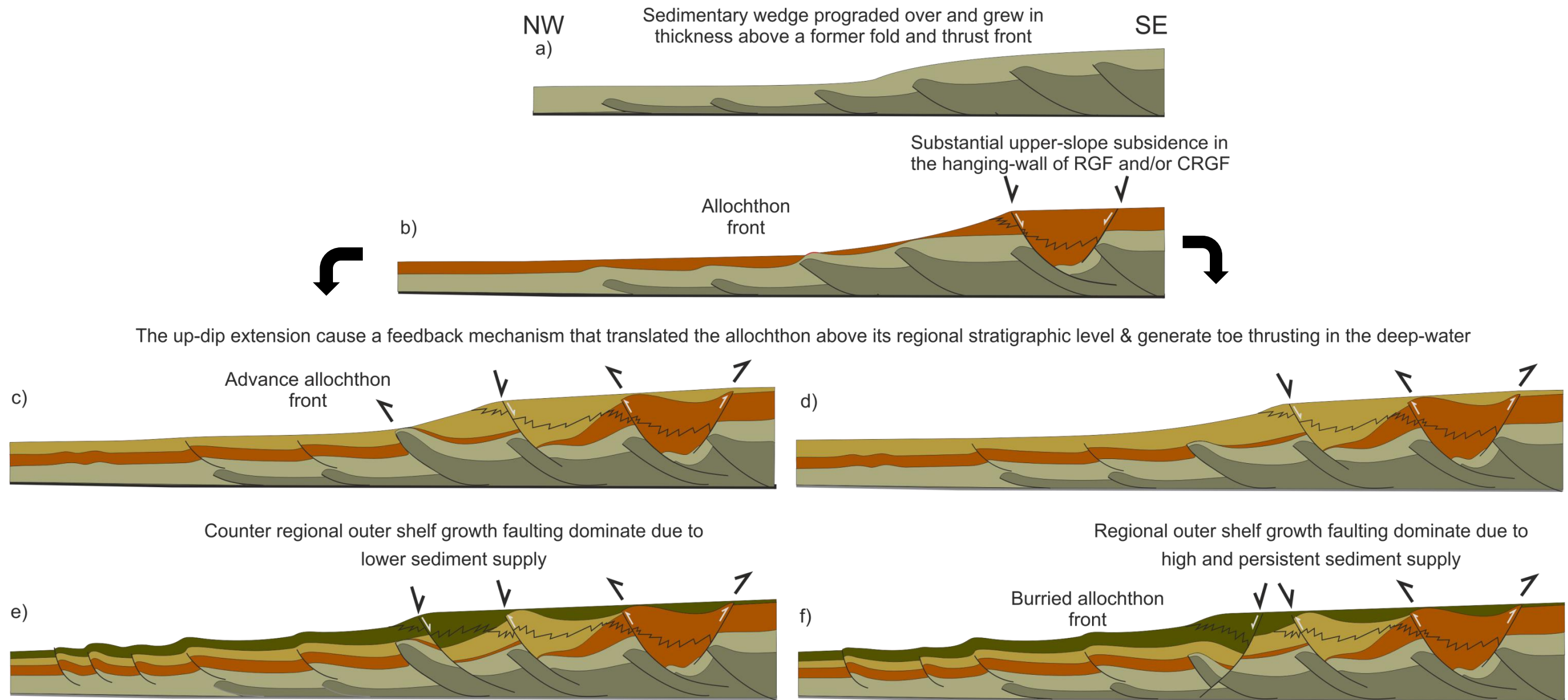


Figure 4. 12: **(a)** Model of structural deformation consisting of a sedimentary wedge which prograded over and grew in thickness above a former fold and thrust front; **(b)** Initial pro-gradation of the delta caused substantial upper-slope subsidence in the hanging-wall of a regional growth fault (RGF) and/or counter-regional growth faults (CRGF); **(c) & (d)** The delta-front continues to prograde and initiate a second CRGF on top of the early folds, forward of the earlier CRGF, while the earlier fault was inverted by tectonic compressional pulse. The up-dip extension linked at depth with the down-dip contraction through a diffuse region of distributed strain within the mobile allochthon, that transmitted down-dip overtime, causing a feedback mechanism that translated the allochthon sporadically basinwards and upwards above its regional stratigraphic level, by reactivating the pre-existing thrusts, then progressing seaward to generate toe thrusting in the deep-water area, without a discrete decollement surface; **(e) & (f)** Tectonic compressional pulses continue to invert the earlier CRGF up slope whereas the extensional deformation was succeed by outer shelf growth faulting, as the cycle of sedimentary loading and delta front prograding continues. Due to variation in sediment supply and stratigraphic thickness in the study area, RGF dominate the southern segment while CRGF dominate the northern segment. Moving down-dip, the translational event of the allochthon slowed down as the deltaic progradation capped and sealed the allochthon, thus restraining the outward advance of the allochthon. In the deepwater, contractional deformation that formed forward of the allochthon continued to develop and expand further seaward, resulting in the formation of a series of seaward-migrating deep-water fold and thrust systems subsequent to the continuous uplift and gravitational loading up-dip, with a considerably more compressed style towards the northern segment.

## 4.7 Conclusion

This chapter has presented a regional-scale structural analysis of the NW Borneo margin including restoration of two regional sections from the northern and the southern parts of the deltaic wedge. Quantitative measurements combined with seismic interpretation have led to improved insights relating to the nature of the allochthon and the interaction between tectonic and gravity driven deformation as well as controls on the geometry and evolution of the DWFTB, complementing previous studies done in the region.

The results reported here have shown that the structural deformation of the NW Borneo deep-water folds and thrust belt consists of a deltaic sedimentary wedge which prograded over and grew above a former fold and thrust front (the NW Borneo accretionary wedge). The Baram-Champion deltaic formation shows an overall basin-ward prograding deltaic system (with a minor component of aggradation and dislocation of the shelf edge trajectory in the fault bounded depocentre, and a back stepping architecture corresponding to a "local" tectonic pulse), along with basin-ward migration of linked extensional-compressional deformation.

The allochthon has been displaced/flowed sporadically downdip and rose above its regional stratigraphic level from latest Miocene onwards in conjunction with seaward migration of gravity-driven extensional structures updip; as a function of domain interactions; a natural consequence of the ongoing thinning of the allochthon beneath the extensional domain in response to the imposed differential load. Severe thinning of the allochthon layer beneath a depocentre is an early mobility feature that developed syn-depositionally to localize sedimentation, caused a feedback mechanism that drove the outward and upward flow of the mobile allochthon layer. This formed an elevated/advanced allochthon front.

Besides that, even with continuous uplift of the inner margin and inversion of the earlier counter regional growth fault up slope, the weight of the surrounding overburden (thinning of the allochthon beneath the extensional domain) is capable alone of generating enough Late Miocene-Recent translation to account for seaward translation of the allochthon in the outer domain. Nevertheless, compressional tectonics were still active as evidenced by

continuous uplift of the inner margin and inversion of the earlier counter regional growth fault up slope.

However, the magnitude of the allochthon involved in the deep-water-fold-and-thrust belt did not solely result from the variation in the amount of extension that fed translation into deep water. Variation in sedimentary supply and stratigraphic thickness in the study area (which varies from ~6-7 km in the north to ~10-12 km in the south) led to profound effects in the location and pattern of structural deformation within the wedge. In the south, high and persistent sediment supply with an associated thicker stratigraphic thickness buried and restrained the advance of the allochthon. In the north, lower sediment supply with thinner stratigraphic thickness and slower deltaic progradation into deep-water favoured the advance of the allochthon.

The variation in sedimentary supply and stratigraphic thickness in the study area also led to contrasting styles of deep-water deformation, with well-developed, extensive imbricate zones (~ 70 km) in the Brunei deep-water-fold-thrust belt, passing into regions of narrow imbricate zones (~ 40 km) with a considerably more compressed style towards the northern segment. Moreover, the style of thrust propagation and fold growth, varies from detached (buckle) folds and fault propagation folds in the Brunei margin to fault propagation folds with locally developed over-thrust folds towards the Sabah part of the margin, implying a northward increasingly frictional behaviour, that can be interpreted to be a reflection of the influence of the underlying compressive structure (allochthon) on deep-water fold thrust belt deformation.



## **Chapter 5**

### **Regional restorations of 2D profiles across NW Borneo, quantifying the amount of extension vs compression.**

#### **5.1 Introduction**

The northern Borneo offshore fold and thrust belt remains the subject of disagreement and discussion. Several key mechanisms have been discussed as the main controlling factors for deep-water compressional deformation. Some authors suggest that subduction has continued until the Late Neogene or present-day and that the NW Borneo deep-water fold belt and trough represent an accretionary complex and an active subduction trench respectively (Tongkul, 1991, Simons et al., 2007, Sapin et al., 2011). Others interpret that the offshore deformation is the result of regional compressional events with thrusting resulting in a foreland fold and thrust belt (Bol and van Hoorn, 1980; Hinz et al., 1989; Cullen, 2010). Several authors interpret that the offshore deformation as largely gravity-driven but still suggest a contribution of regional compression on the offshore deformation (Tan and Lamy, 1990; Morley, 2007; Hesse et al., 2009, 2010b; King et al., 2010; Gartrell et al., 2011), and inferred that variation in shortening magnitudes, stress orientations and GPS observations (Simons et al., 2007) to indicate tectonic stresses.

Other authors proposed that the offshore deformation is mainly the result of crustal shortening with a small contribution from gravity-related delta tectonics (Ingram et al., 2004, Franke et al. 2008). In contrast, the fold and thrust belt has been interpreted as solely developed in response to gravitational delta tectonics (e.g. Hazebroek and Tan, 1993, Hall, 2013) analogous to the deep-water fold and thrust belt of the Niger Delta. Moreover, Hall (2013) suggests there is no plate convergence in the NW Borneo– Palawan region and that most Neogene deformation is a result of episodes of extension, not compression as there is no shortage of tectonic events that could cause inversion in the sedimentary basins of northern Borneo during the Miocene–Recent.

Therefore, to answer the above question, an emphasis is placed here to; 1) evaluate the amount of extension and compression of the margin and describe along-strike variations in shortening and lengthening deformation through time, 2) verify what are the principle driving forces responsible for seaward and northwards translation of the allochthon from the original basin margin, and deep-water fold and thrust belt deformation particularly, 3) discuss how the excess of shortening (if present) might be accommodated and how it's influence the structural development.

With these aims in mind, a selection of previously published seismic profiles from Hesse et al. (2010b) transecting the southern half of NW Borneo deep-water fold thrust belt (BGR86-24 to BGR86-12) was combined with the available seismic data acquired by Hess Corporation transecting the northern half of NW Borneo deep-water fold thrust belt (BGR86-10 to BGR86-02). The location of the seismic profiles is shown in figure 5.1. For the structural restoration presented in this study, the regional scale of the seismic data allows extending the analyses to another 100 km northwards along the northern Sabah fold and thrust belt, from previous studies of Hesse et al. (2010b).

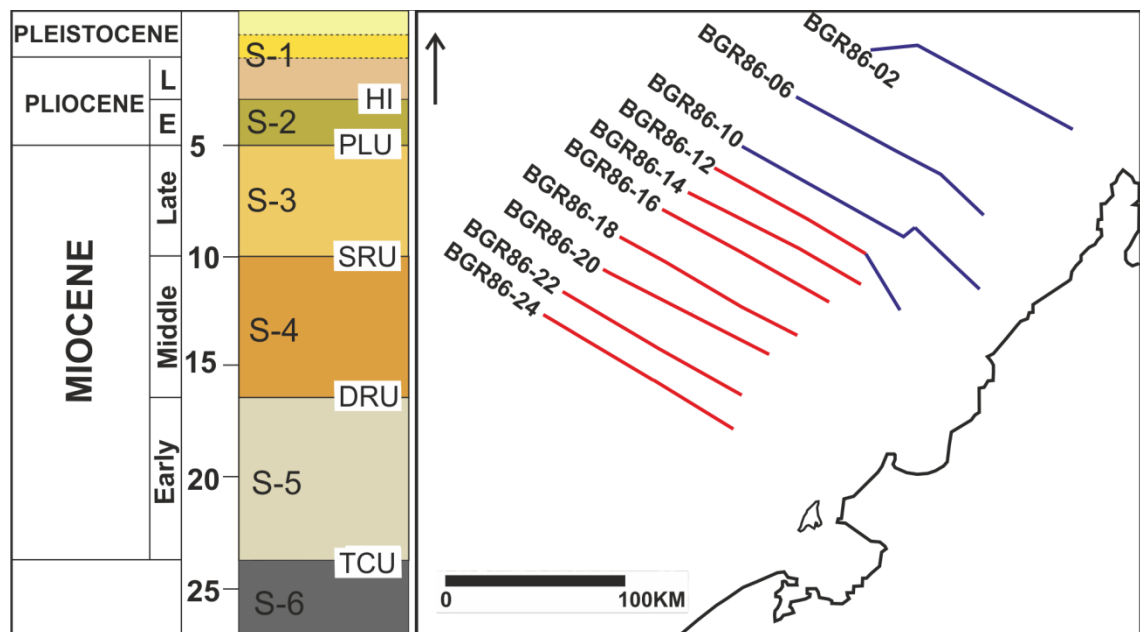


Figure 5. 1: The location of the selected seismic profiles from the available seismic survey data acquired by Hess Corporation (blue) and the previously published seismic profiles from Hesse et al. (2010b) (red).

## 5.2 Structural Reconstruction

Section balancing was performed using Midland Valley's 2D Move software. Restoration presented here involves taking the geometry of a deformed structure and restoring it to a horizontal or regional datum (Dahlstrom, 1990) and is achieved by combining 'UNFOLD', 'MOVE ON FAULT' and 'DECOMPACTION' functions in 2D Move. The restoration algorithms used in this restoration are Flexural Slip (based on Kane et al., 1997) for 'UNFOLD' and Fault Parallel Flow (based on Egan et al., 1997; Kane et al., 1997) for 'MOVE ON FAULT'. Seismic interpretation delivered five main stratigraphic units; Late Pliocene (HI), Early Pliocene (PLU), Late Miocene (SRU), Middle Miocene (DRU) and Early Miocene (TCU). A pin line was inserted in the un-deformed area between the compressional domain and the extensional domain. Restoration was undertaken by restoring each rock unit individually, starting with the youngest.

Restoration of nine selected cross-sections across the offshore NW Borneo margin in Figure 5.1 was accomplished by the following steps:

- i) The present day unit above horizon HI (Figure 5.2 (a)) was first removed using the 'DECOMPACTION' function and an isostatic correction sensu Burov & Diament (1992). De-compaction is a technique designed to remove the effects of volume loss (compaction) that occurs within a rock volume as it is progressively buried and the rock volume is allowed to vertically expand (Sclater and Christie, 1980).
- ii) As the horizon HI was cut by faults, the 'MOVE ON FAULT' function is used prior to 'UNFOLD'. The faulted segment of horizon HI was reconnected by restoring the hanging walls back to their original pre-deformed positions using the 'MOVE ON FAULT' function with the 'Fault Parallel Flow' algorithm.
- iii) The restored horizon was then unfolded to a fixed datum using the 'UNFOLD' function with 'flexural slip' algorithm. The template bed (the bed which is actively chosen to be unfolded), the HI horizon, was unfolded around the pin. The pin was inserted through the anticlinal hinge line and underlying additional folded beds are unfolded passively

during the restoration process until a representative pre-deformed state is achieved (Figure 5.2 (a)-(b)).

- iv) Restoration was carried out systematically starting at the deep-water deformation front moving in a progressively landward direction, from subsequent folding and thrusting in the delta toe to normal faulting in the delta top (A pin line was inserted in the un-deformed area between the two domains).
- v) Complete fault-by-fault restoration and fold-by-fold unfolding of horizon HI (footwall and hangingwall cut-offs of each structure are joined and unfolded to their original pre-deformed state), the length of restored section is measured based on age assignments for assessing the horizontal shortening and lengthening amounts from each reconstructed regional section (Table 5.1).
- vi) The reconstructed section was then followed by a section-wide decompaction and isostatic correction (Figure 5.2 (b)).
- vii) Steps (ii)-(iii)-(iv)-(v) were repeated to restore the horizons PLU, SRU, DRU and TCU.

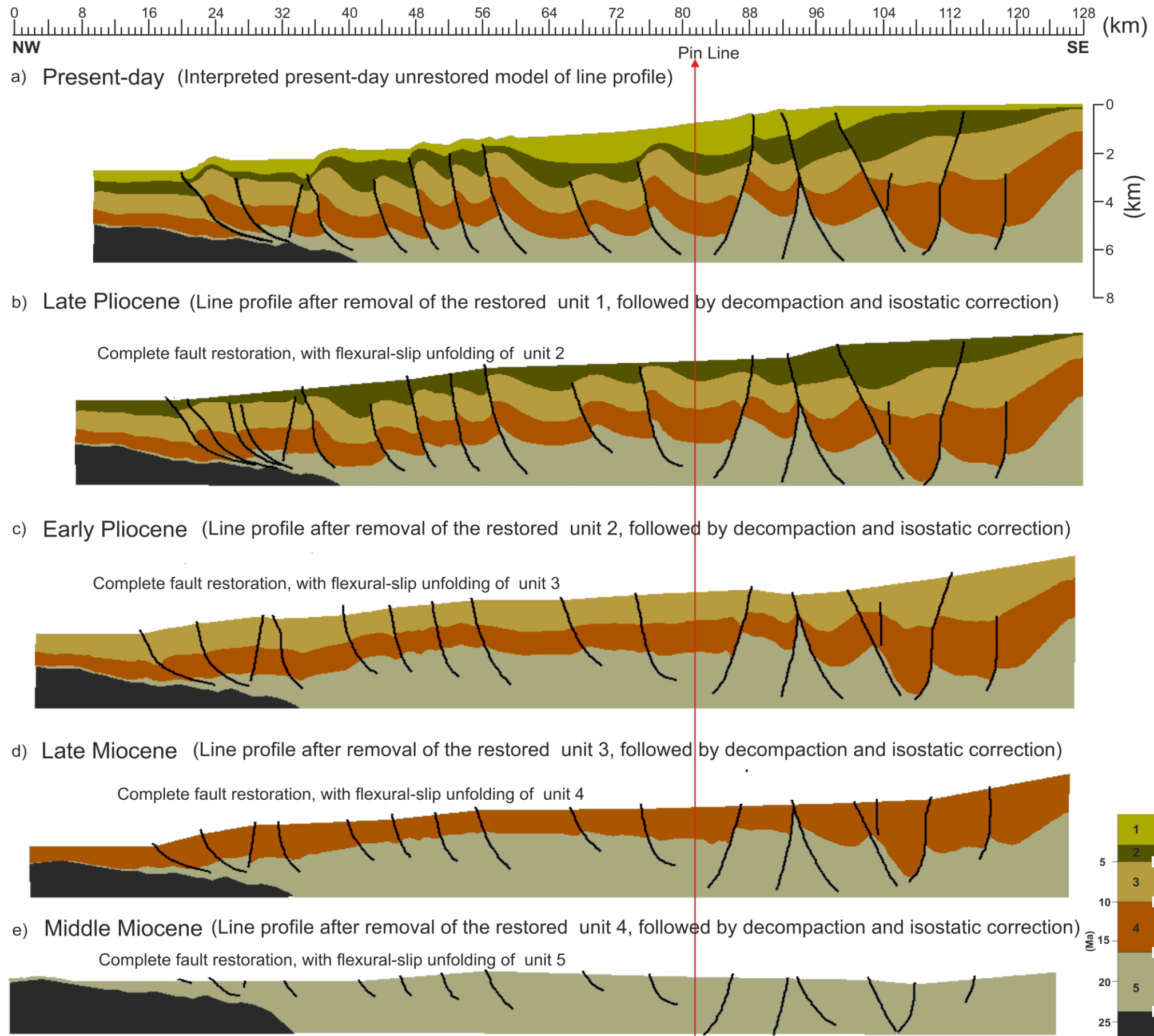


Figure 5. 2: Structural restoration of BGR86-24 using Midland Valley 2D Move. The location of line profile is shown in Figure 5.1.



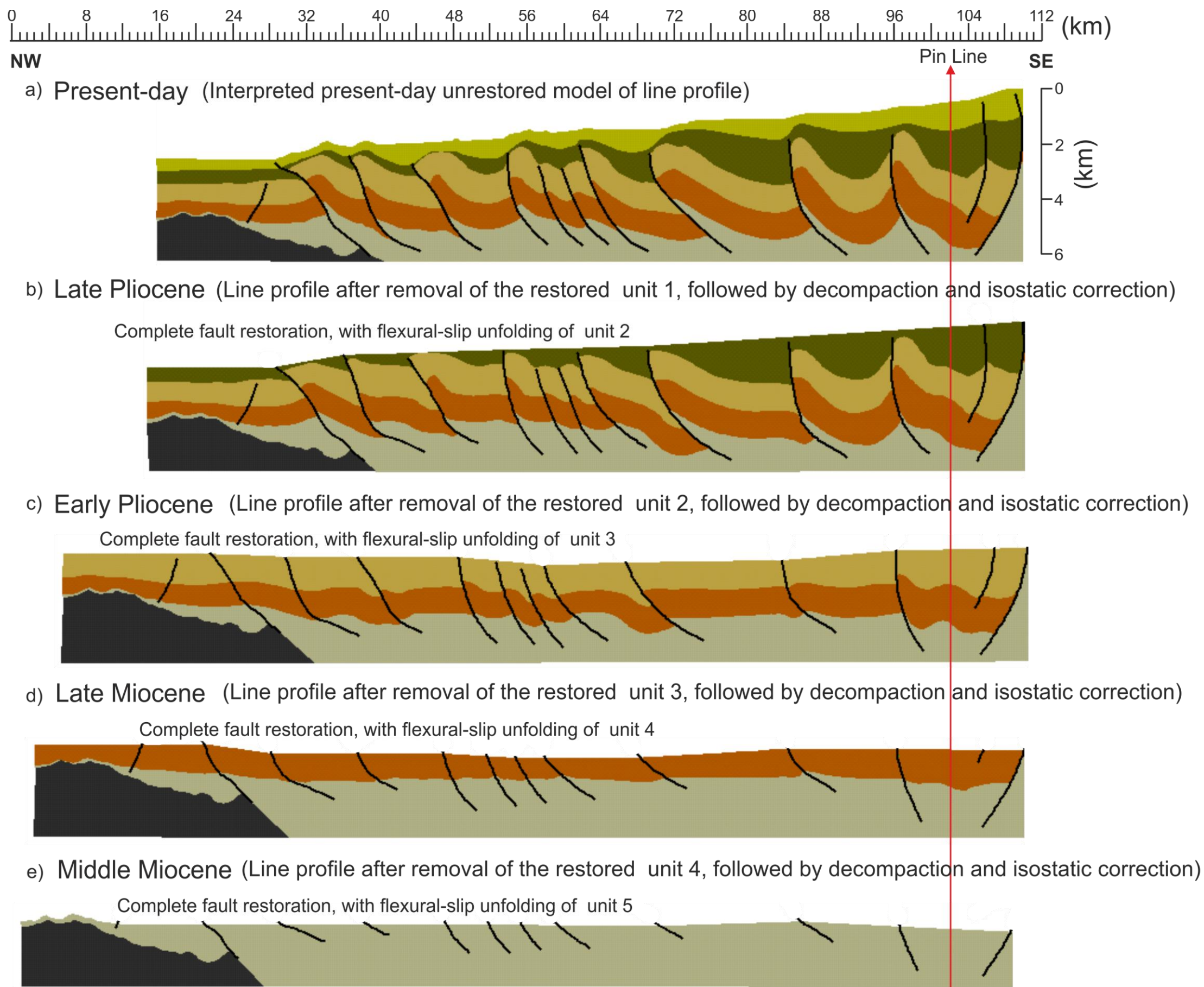


Figure 5. 3: Structural restoration of BGR86-22 using Midland Valley 2D Move. The location of line profile is shown in Figure 5.1.

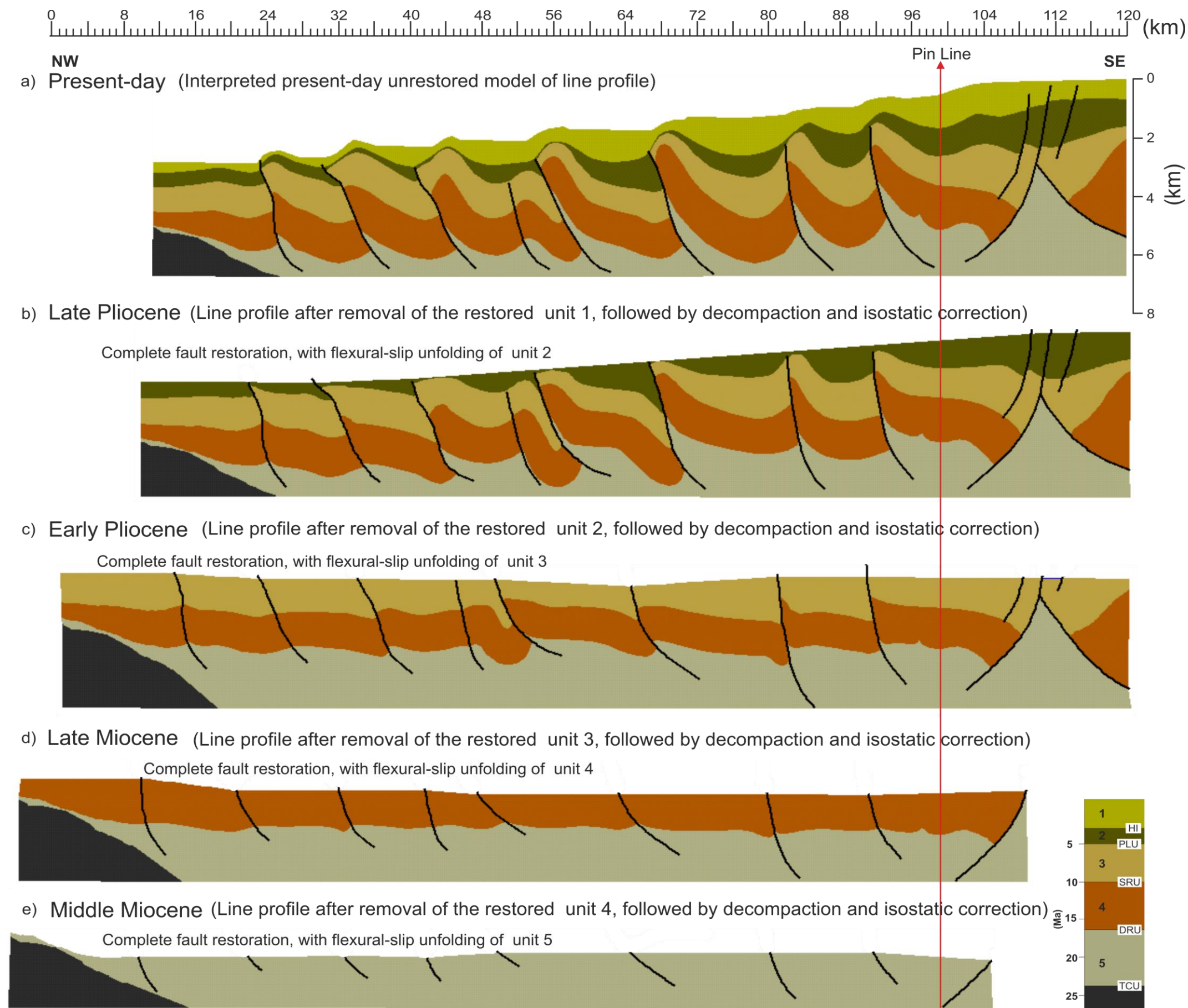


Figure 5. 4: Structural restoration of BGR86-20 using Midland Valley 2D Move. The location of line profile is shown in Figure 5.1.



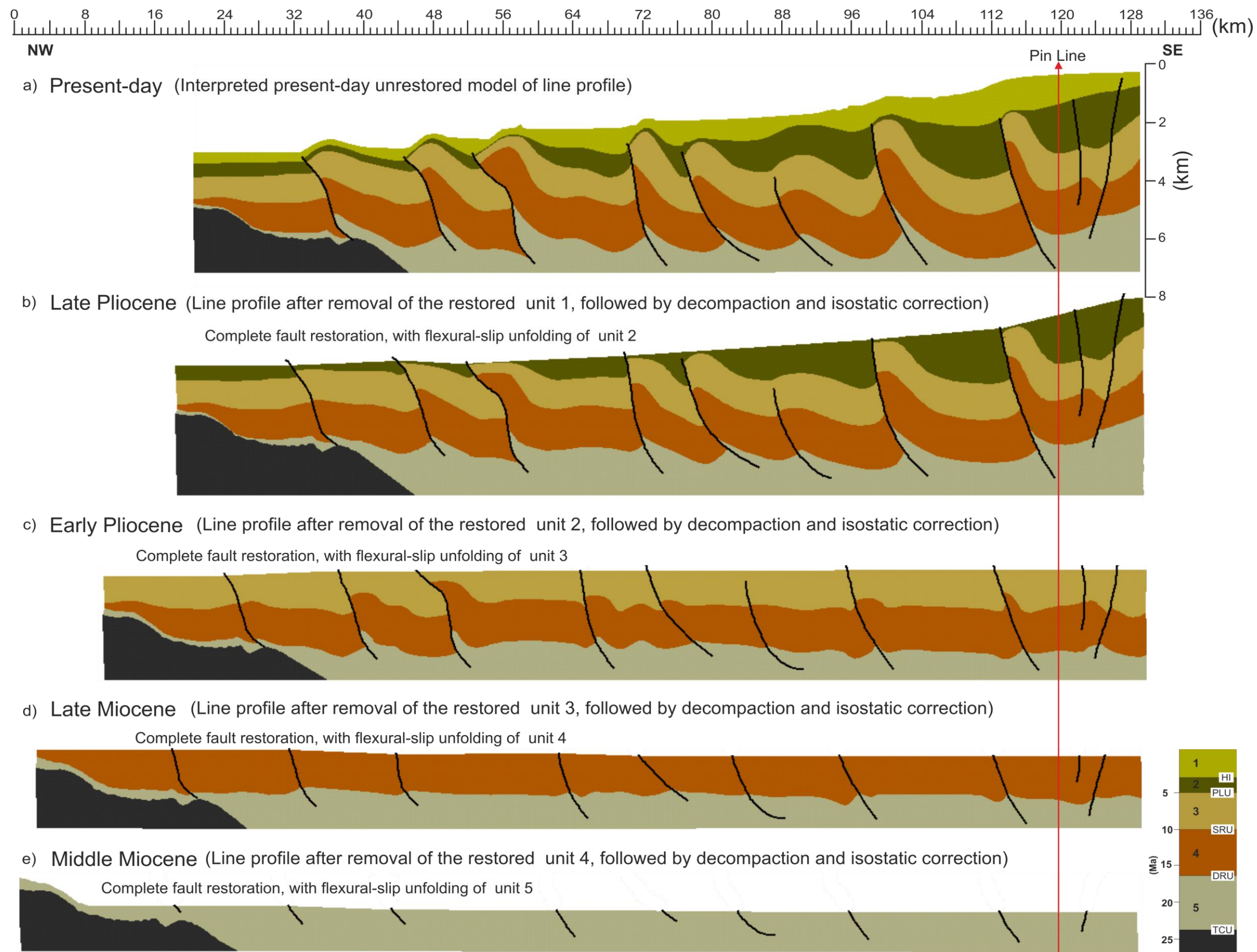


Figure 5. 5: Structural restoration of BGR86-18 using Midland Valley 2D Move. The location of line profile is shown in Figure 5.1.

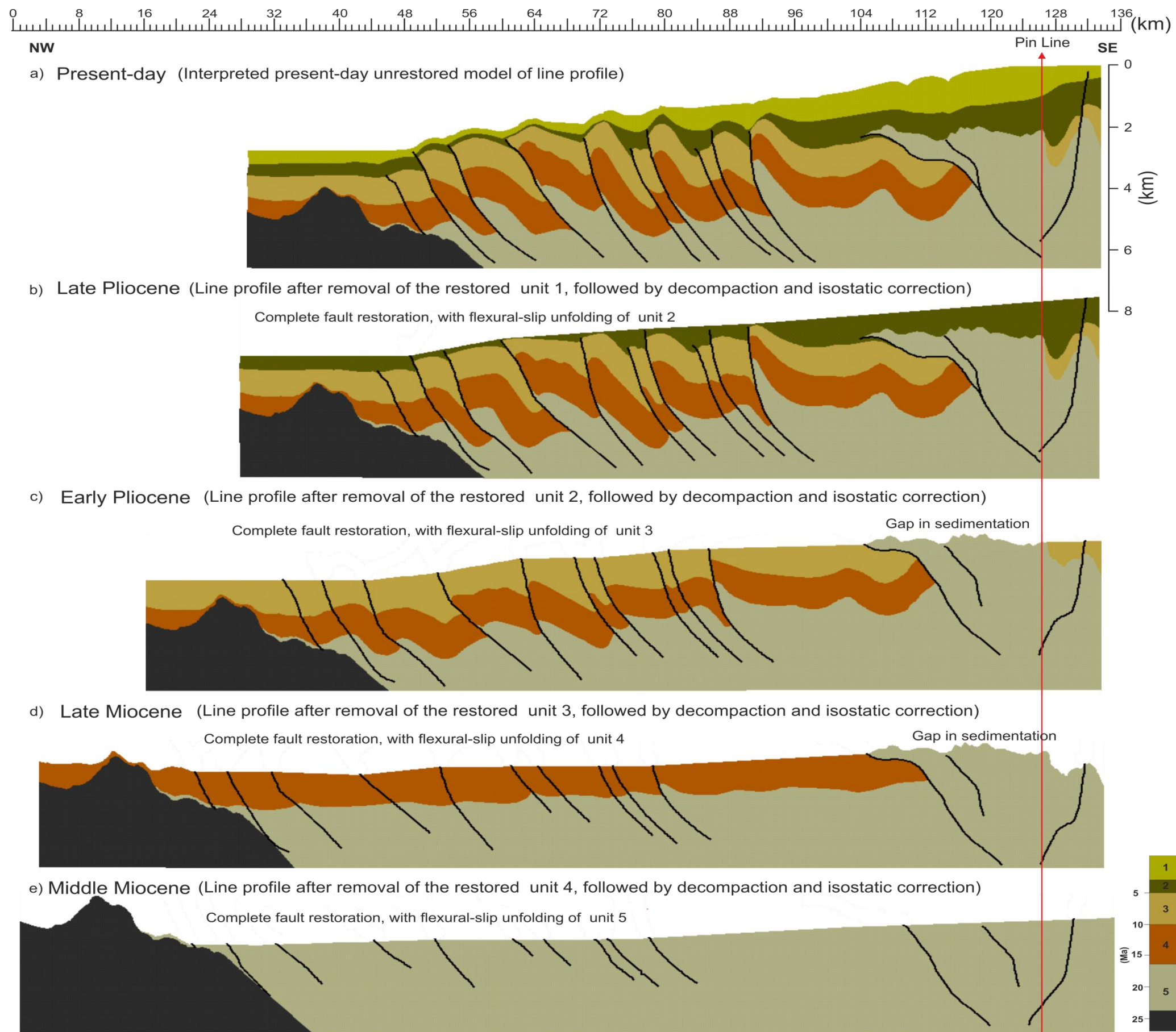


Figure 5. 6: Structural restoration of BGR86-14 using Midland Valley 2D Move. The location of line profile is shown in Figure 5.1.



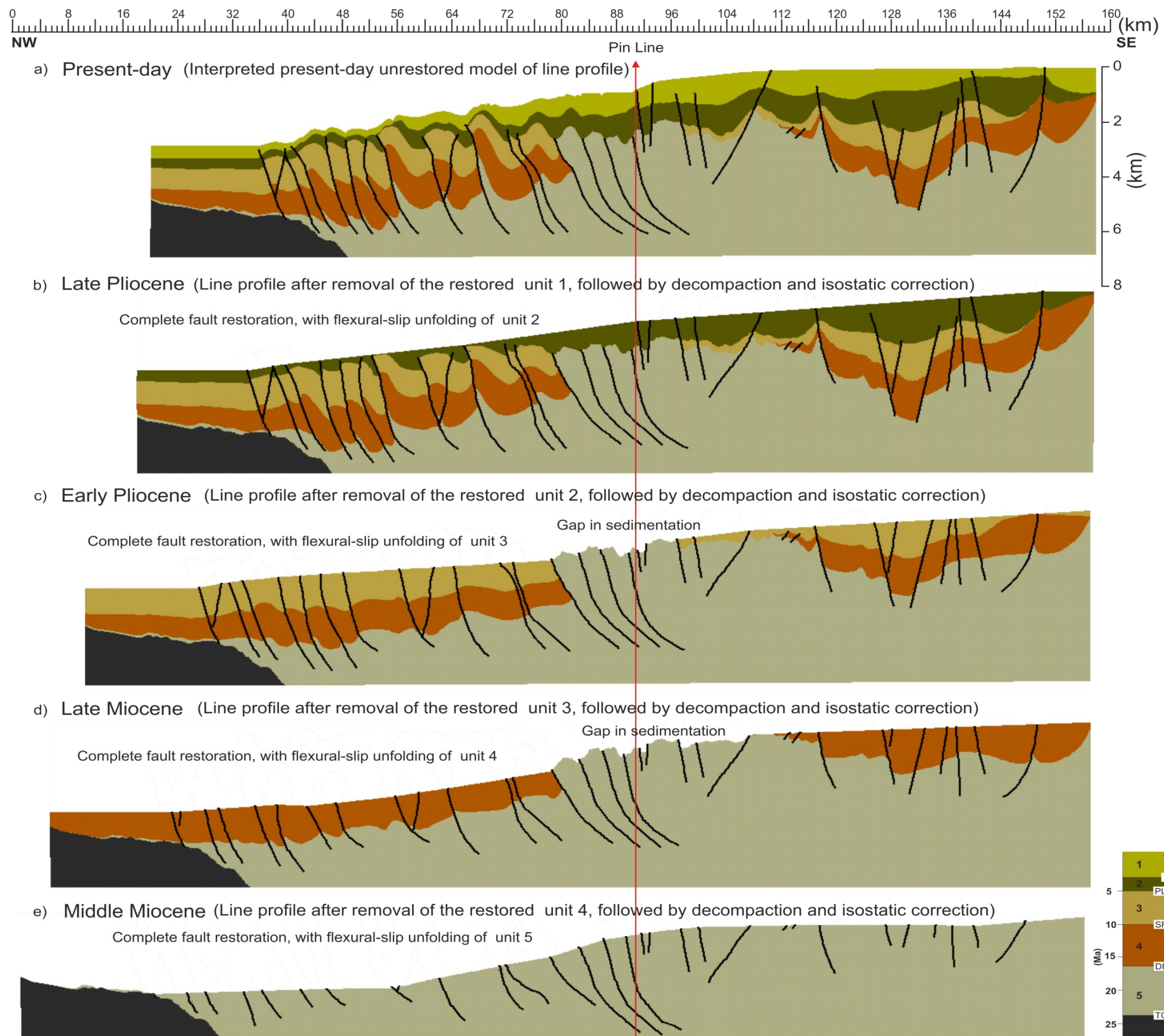


Figure 5. 7: Structural restoration of BGR86-12 using Midland Valley 2D Move. The location of line profile is shown in Figure 5.1.



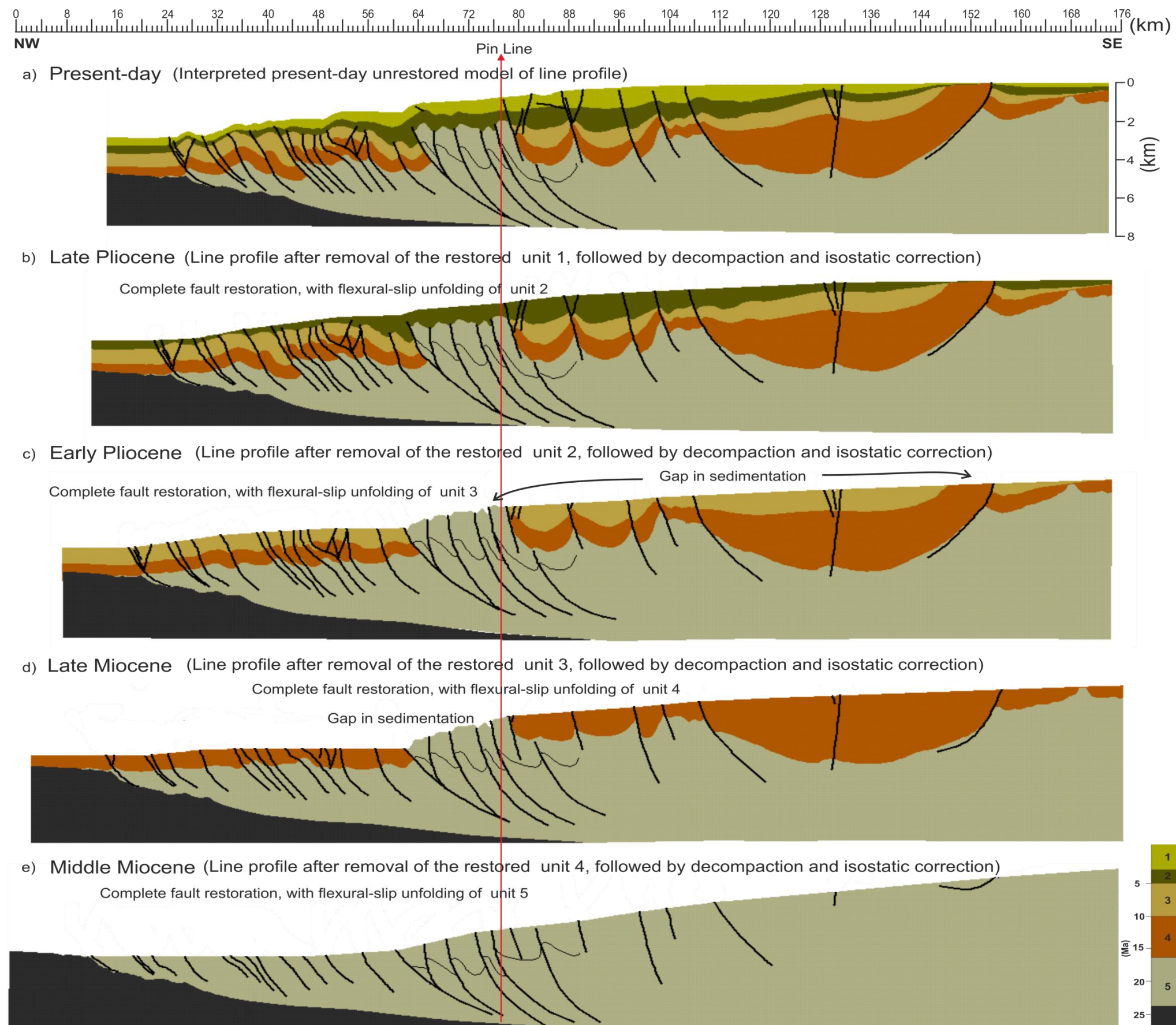


Figure 5. 8: Structural restoration of BGR86-10 using Midland Valley 2D Move. The location of line profile is shown in Figure 5.1.



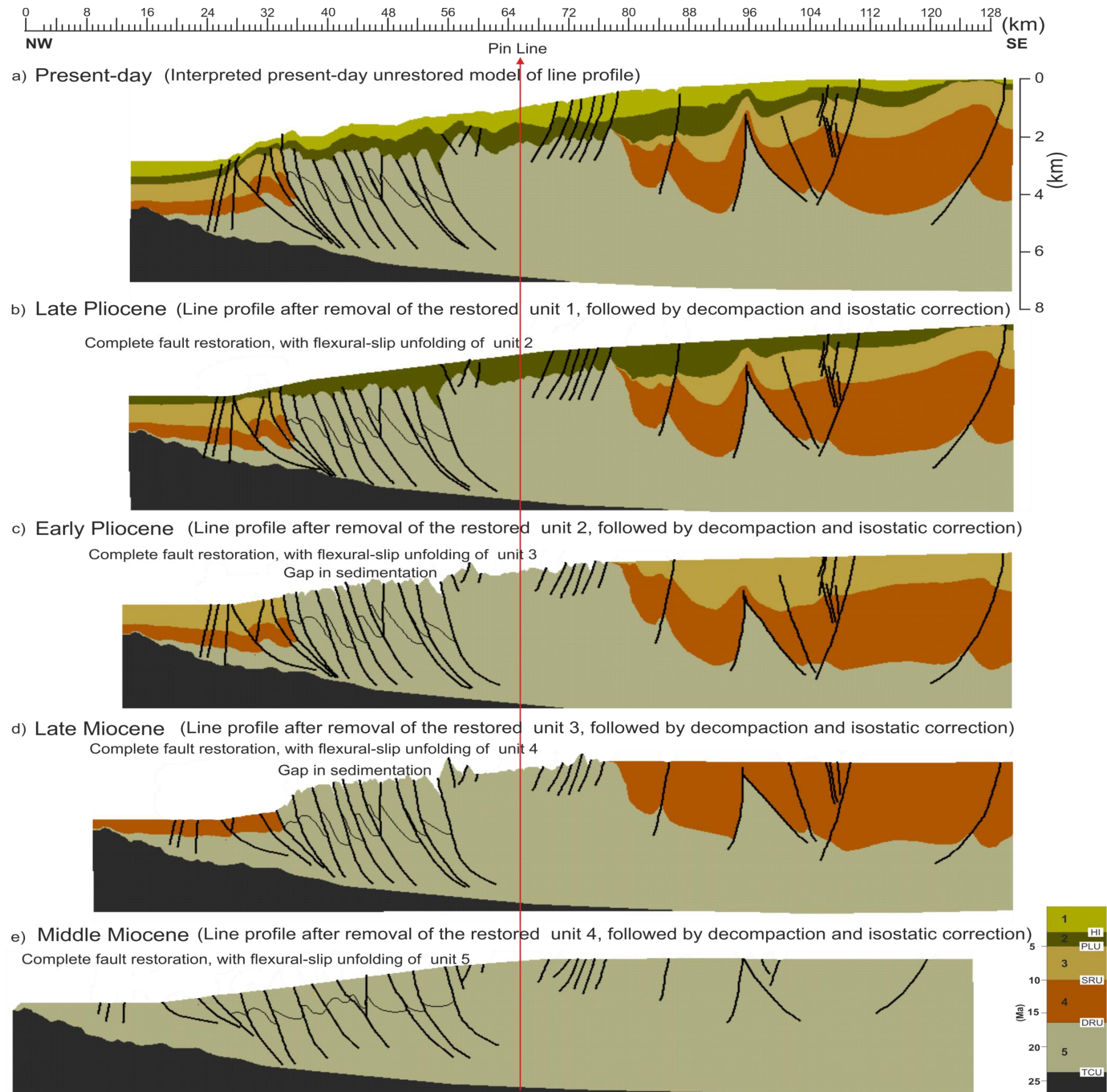


Figure 5. 9: Structural restoration of BGR86-06 using Midland Valley 2D Move. The location of line profile is shown in Figure 5.1.



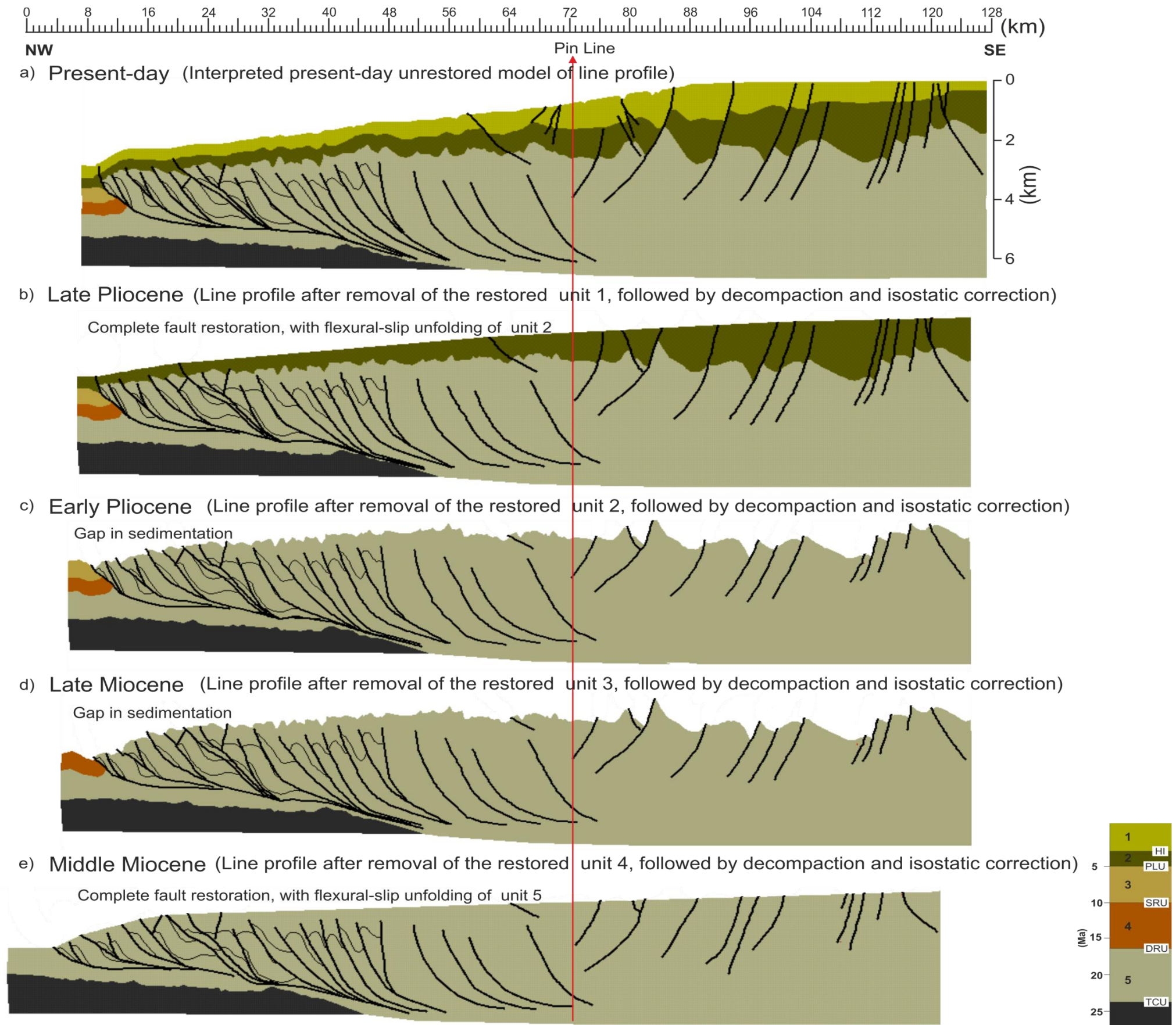


Figure 5. 10: Structural restoration of BGR86-02 using Midland Valley 2D Move. The location of line profile is shown in Figure 5.1.

### 5.3 Miocene-Recent Shortening

The restoration results measured on nine NW-SE-trending seismic profiles, that transecting generally perpendicular to structural trends of deep-water deformation, demonstrated a significant variation in incremental shortening amount through time (Figure 5.2 to Figure 5.10; Table 5.1). To quantify the amount of incremental deep-water shortening values based on age division, the measurement is given by the subtraction of the selected line length (based on age) from the current line length. For example, the amount of Late Pliocene deep-water shortening is given by the subtraction of the Late Pliocene line length (compressional domain) from the present-day line length (compressional domain). The results shown in Figure 5.14 demonstrated that, the imbalance between the Early Pliocene-Recent shallow-water shelfal extension and deep-water compression (excess in shortening value) increased gradually from a minimum value of 0.2 km at line BGR86-24 in the south-west and 0.4 km at line BGR86-06 in the north-east, to a maximum value of 10.2 km at line BGR86-14 in the central part of the study area. Whereas, the amount of Early Pliocene-Recent shallow-water shelfal extension is balanced against the amount of Early Pliocene-Recent deep-water compression, at line BR 1 until line BR 4, in the south-western ends of the study area (see Figure 5.14). The amount of Middle Miocene shortening measured across the study area increasing towards the north-east, from a minimum value of 2.0 km at line BGR86-24, to a maximum value of 10.4 km at line BGR86-06 (Table 5.1; Figure 5.11). In the Late Miocene, the restoration results show that, the amount of Late Miocene shortening, measured across the study area increases gradually from a minimum value of 0.8 km at line BGR86-02 in the north-east and at line BR86-24 in the south-west, to a maximum value of 13.2 km at line BGR86-14, in the central part of the study area (see Table 5.1; Figure 5.11).

Later in the Early Pliocene, the amount of shortening increases south-west wards from a minimum value of 0.8 km at line BGR86-06 in the north-east, to a maximum value of 11.2 km at line BGR86-14, and then fluctuates moderately until line BGR86-24 in the south-west, ranging between 5.2 km to 9.2km (see Table 5.1; Figure 5.11). In the Late Pliocene, the amount of shortening varies non-uniformly, from a minimum value of 0.4 km at line BGR86-02 in the north-east, to a maximum value of 2.4 km at line BGR8-10, and then fluctuates

moderately until line BGR86-24 in the south-west, ranging between 1.2 km and 2.0 km (see Table 5.1; Figure 5.11).

The overall results reported here have shown that shortening values, measured on all selected seismic profiles, increased through time, from the Middle Miocene to Early Pliocene, except for BGR86-06 and BGR86-02, where their highest shortening deformation occurred in the Middle Miocene (see Table 5.1; Figure 5.11). When analysed from north to south, the amount of Middle Miocene-Recent shortening increased from a minimum value of 10 km at line BGR86-02 in the north-east, and line BR86-24 in the south-west, to a maximum value of 27.6 km at line BGR86-14, in the central part of the study area, giving an overall arcuate geometry (see Table 5.1; Figure 5.11).

Table 5. 1: Incremental deep-water shortening values based on age division (Middle Miocene to Recent), measured by structural restoration of nine NW-SE-trending seismic profiles, across the study area (see Figure 5.2 to Figure 5.10). The location of line profiles is shown in Figure 5.1.

<b>Survey Line (South to North)</b>		<b>Present- day</b>	<b>Late Pliocene</b>	<b>Early Pliocene</b>	<b>Late Miocene</b>	<b>Early M. Miocene</b>	<b>Total Shortening</b>
<b>BGR 24</b>	Line Length (km)	72.0	74.0	79.2	80.0	82.0	<b>10.0 km</b>
	Shortening (km)	0	2	5.2	0.8	2.0	
<b>BGR 22</b>	Line Length (km)	86.4	87.6	96.8	99.6	101.2	<b>14.8 km</b>
	Shortening (km)	0	1.2	9.2	2.8	1.6	
<b>BGR 20</b>	Line Length (km)	88.0	89.2	98.0	102.8	104.0	<b>16.0 km</b>
	Shortening (km)	0	1.2	8.8	4.8	1.2	
<b>BGR 18</b>	Line Length (km)	99.2	101.2	109.6	117.2	119.2	<b>20.0 km</b>
	Shortening (km)	0	2	8.4	7.6	2.0	
<b>BGR 14</b>	Line Length (km)	97.6	98.8	110.0	123.2	125.2	<b>27.6 km</b>
	Shortening (km)	0	1.2	11.2	13.2	2.0	
<b>BGR 12</b>	Line Length (km)	70.8	72.8	80.4	85.6	89.6	<b>18.8 km</b>
	Shortening (km)	0	2.0	7.6	5.2	4.0	
<b>BGR 10</b>	Line Length (km)	62.8	65.2	70.0	75.2	78.4	<b>15.6 km</b>
	Shortening (km)	0	2.4	4.8	5.2	3.2	
<b>BGR 06</b>	Line Length (km)	51.6	52.0	52.8	56.8	67.2	<b>15.6 km</b>
	Shortening (km)	0	0.4	0.8	4.0	10.4	
<b>BGR 02</b>	Line Length (km)	65.2	65.6	67.2	68.0	75.2	<b>10.0 km</b>
	Shortening (km)	0	0.4	1.6	0.8	7.2	



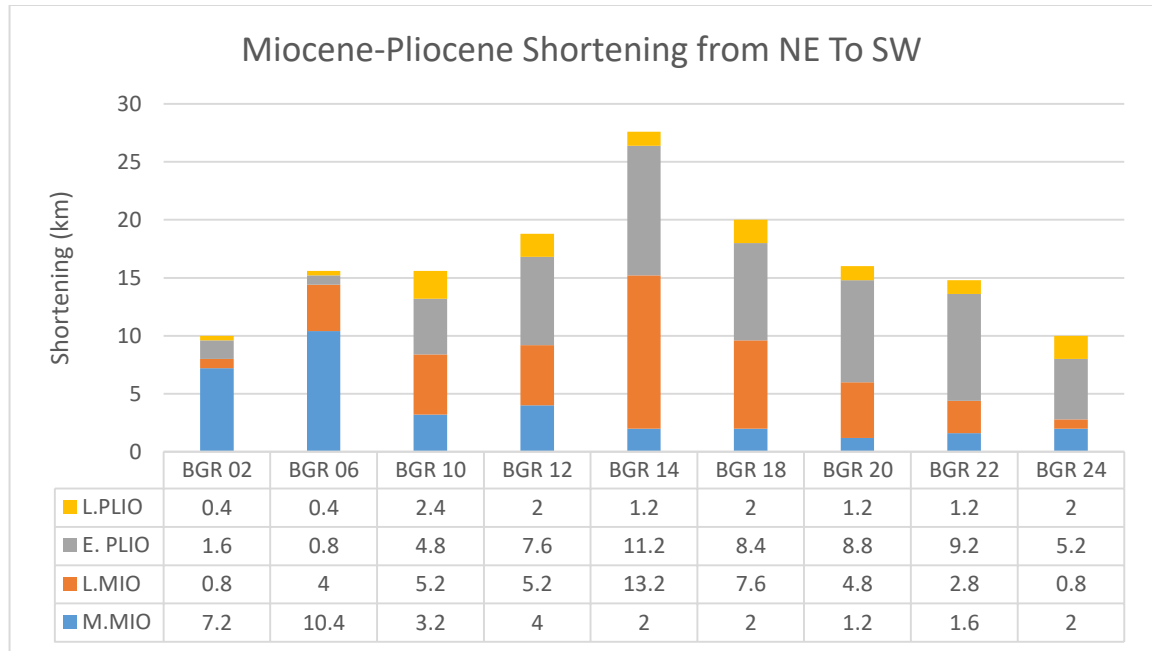


Figure 5. 11: Incremental value of Middle Miocene-Recent deep-water shortening measured by structural restoration of nine selected seismic profiles, across the study area (see Figure 5.2 to Figure 5.10). The location of line profiles is shown in Figure 5.1.

## 5.4 Lengthening Vs Shortening

### 5.4.1 Early Pliocene-Recent

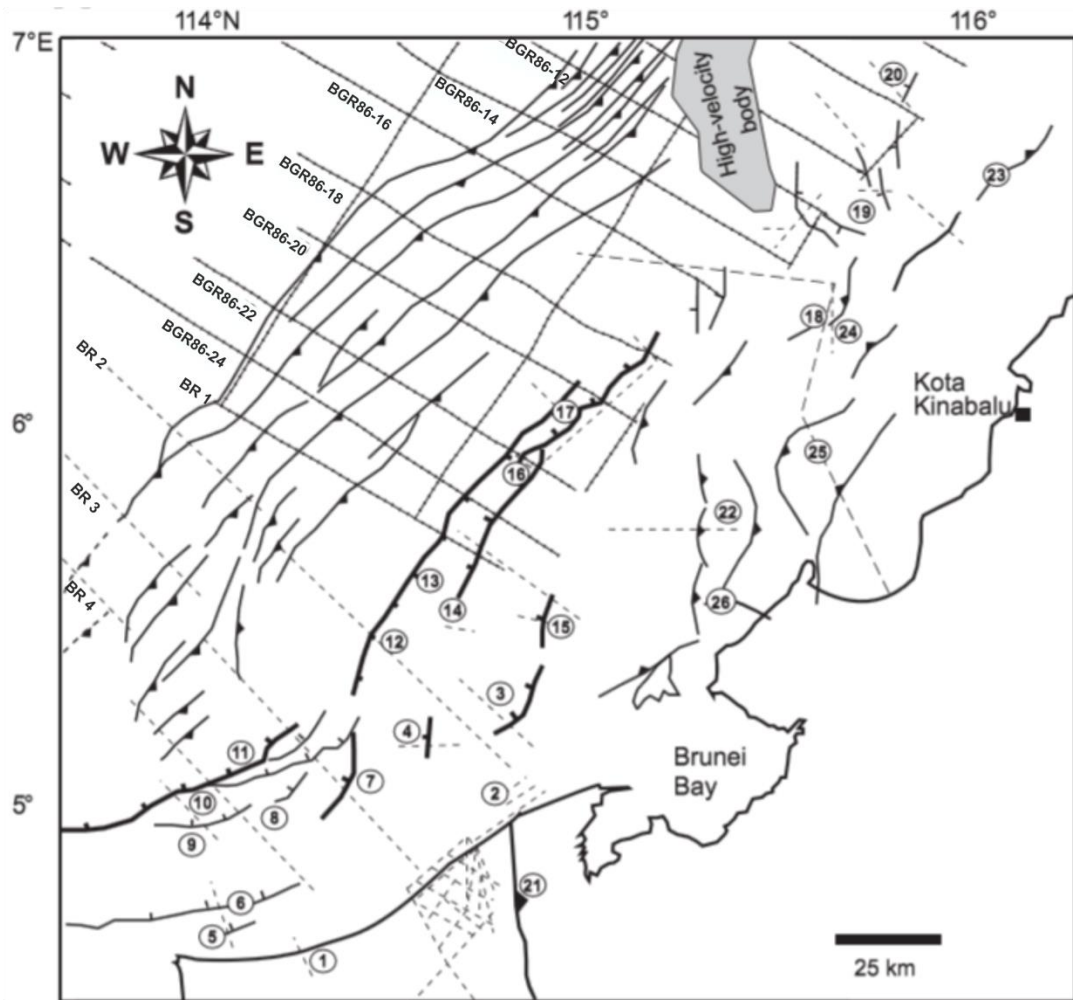
In this study, the selected seismic profiles from the previously published seismic data of Hesse et al. (2010b), didn't fully capture the deformation in the extensional domain, hence prohibits a completed paired system of extension and contraction to be examined. Therefore, to fully quantify the amount of shortening versus lengthening across the study area, the structural restoration result of Early Pliocene to Recent shortening and lengthening, measured on nine selected seismic profiles (see Figure 5.2 to Figure 5.10), are linked with previous studies by Hesse et al.(2010b) and the references therein (Figure 5.12; Table 5.2).

The results demonstrate that the total amount of Early Pliocene-Recent shortening and lengthening generally increase southward. The amount of Early Pliocene-Recent shortening increases significantly from a minimum value of 0.8 km at line BGR86-06 in the north-east, gradually from a value of 4.0 km at line

BR-4 in the south-west, to a maximum value of 11.2 km at line BGR86-14 in the central part of the study area (Table 5.2; Figure 5.13). The amount of Early Pliocene-Recent lengthening, on the other hand, increases gradually south-west-ward, from a minimum value of 0.4km at line BGR86-02 in the north-east, to a maximum value of 6.0 km at line BR-1 in the south-west (see Table 5.2; Figure 5.13).

Table 5. 2: The amount of Early Pliocene-Recent shortening and lengthening measured by structural restoration of nine selected seismic profiles across the study area (see Figure 5.2 to Figure 5.10) linked with previous studies of Hesse et al.(2010b) and the references therein (Bold italic letters: Early Pliocene-Recent shortening and lengthening values from Hesse et al.(2010b) and the references therein).

Survey Line	E. Pliocene Compression	E. Pliocene Extension	Compression Vs Extension
<b><i>BR4</i></b>	<b>4 km</b>	<b>4 km</b>	<b>balance</b>
<b><i>BR3</i></b>	<b>5 km</b>	<b>5 km</b>	<b>balance</b>
<b><i>BR2</i></b>	<b>6 km</b>	<b>6 km</b>	<b>balance</b>
<b><i>BR1</i></b>	<b>6 km</b>	<b>6 km</b>	<b>balance</b>
BGR 24	5.2 km	<b>5 km</b>	0.2 km
BGR 22	9.2 km	<b>4 km</b>	5.2 km
BGR 20	8.8 km	<b>2.5 km</b>	6.3 km
BGR 18	8.4 km	<b>2 km</b>	6.4 km
BGR 14	11.2 km	<b>1 km</b>	10.2 km
BGR 12	7.6 km	0.4 km	6.8 km
BGR 10	4.8 km	0.4 km	4 km
BGR 06	0.8 km	0.4 km	0.4 km
BGR 02	1.6 km	0.4 km	1.2 km



Extension (Upper Miocene/Pliocene to recent):

① Seria: > 0.5 km (Sandal, 1996; Watters et al., 1999)	⑪ Outer Shelf GF: ~ 4 km (Van Rensbergen and Morley, 2000)
② Jerudong: ~ 1 km (Back et al., 2008)	⑫ Frigate GF (south): ~ 4 km (Saller and Blake, 2003)
③ Champion: > 1 km (Imber et al., 2003)	⑬ Frigate GF (center): ~ 3 km (Van Rensbergen and Morley, 2000)
④ Iron Duke: > 1 km (Sandal, 1996)	⑭ Kinabalu: ~ 1 km (Petronas, 1999)
⑤ SW Ampa: < 0.5 km (Sandal, 1996)	⑮ Glayzer: ~ 2 km (Petronas, 1999)
⑥ Ampa: < 0.5 km (Morley et al., 2003)	⑯ Nosong-Tapir (south): > 2 km (Hesse et al., 2010)
⑦ Magpie: > 1 km (Sandal, 1996)	⑰ Nosong-Tapir (north): > 1 km (Hesse et al., 2010)
⑧ Egret: > 0.5 km (Sandal, 1996)	⑱ Erb West: < 1 km (Petronas, 1999)
⑨ Fairley: > 0.5 km (Saller and Blake, 2003)	⑲ Tembungo: > 0.5 km (Petronas, 1999)
⑩ Gannet: > 0.5 km (Sandal, 1996)	⑳ Gaya Hitam: > 0.5 km (Petronas, 1999)

Shortening (Upper Miocene/Pliocene to recent):

⑳ Jerudong: 0.6 km (Back et al., 2008)
㉑ Sabah Ridges: ~ 3 km (Bol and van Hoorn, 1980)
㉒ St. Joseph: ~ 2 km (Bol and van Hoorn, 1980)
㉓ Magalum: ~ 3 km (Levell, 1987)
㉔ Kunau-Kimanis: ~ 3 km (Petronas, 1999)
㉕ Gordon-Klias: ~ 2 km (Hazebroek and Tan, 1993)

Figure 5. 12: Early Pliocene-Recent shelfal extension and deep-water compression from Hesse et al. (2010b) and the references therein.

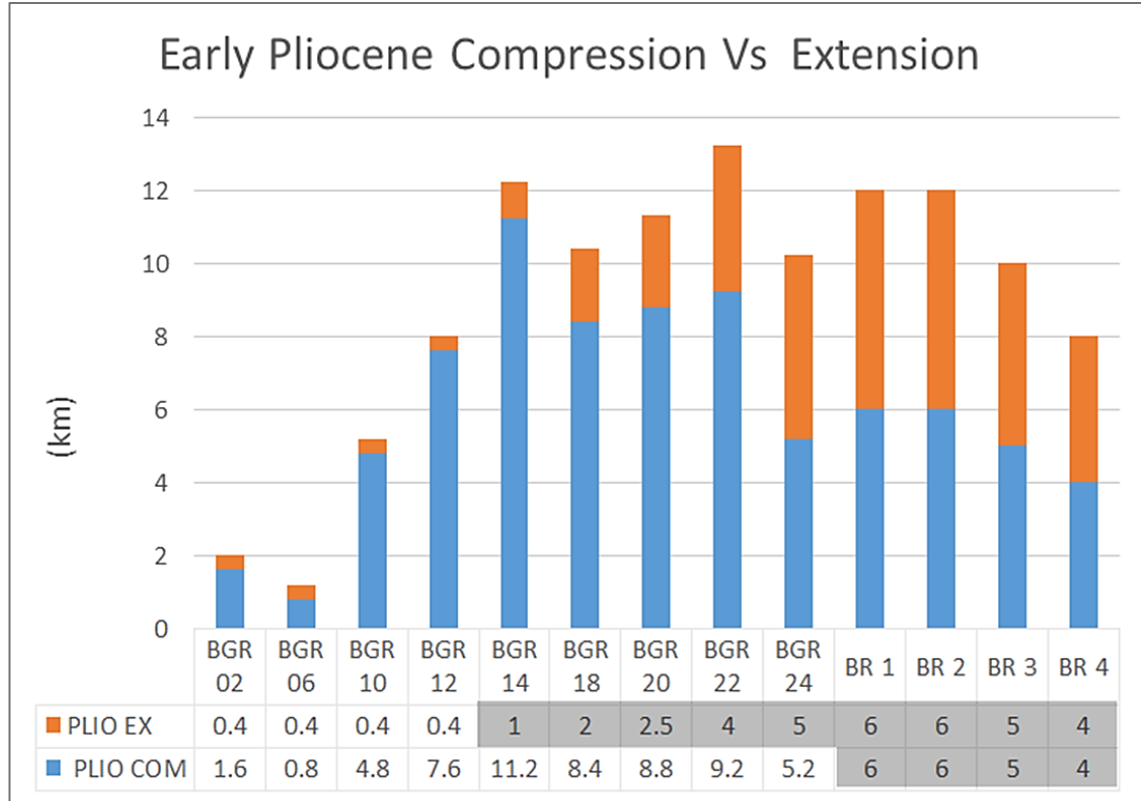


Figure 5. 13: Early Pliocene-Recent shelfal extension and deep-water compression measured by structural restoration of nine selected seismic profiles across the study area (see Figure 5.2 to Figure 5.10) linked with previous studies of Hesse et al.(2010b) and the references therein (Grey shaded data).

To quantify the Early Pliocene-Recent restoration balance and imbalance, the measurement is given by the subtraction of the Early Pliocene-Recent shelfal extension values from the Early Pliocene-Recent deep-water shortening values. The results shown in Figure 5.14 demonstrated that, the imbalance between the Early Pliocene-Recent shallow-water shelfal extension and deep-water compression (excess in shortening value) increased gradually from a minimum value of 0.2 km at line BGR86-24 in the south-west and 0.4 km at line BGR86-06 in the north-east, to a maximum value of 10.2 km at line BGR86-14 in the central part of the study area. Whereas, the amount of Early Pliocene-Recent shallow-water shelfal extension is balanced against the amount of Early Pliocene-Recent deep-water compression, at line BR 1 until line BR 4, in the south-western ends of the study area (see Figure 5.14).

As a summary, the overall results documented that, from north to south, there is no amount of Early Pliocene-Recent shelfal extension appears to exceed the amount of Early Pliocene-Recent deep-water compression, in the study area. The total amount of Early Pliocene-Recent deep-water compression measured across the study area (78.6 km) exceeds the total amount of Early Pliocene-Recent shelfal extension (37.1 km), by 41.5 km (see Table 5.2). Therefore, there is an excessive amount of Early Pliocene-Recent shortening (41.5 km), accommodated by the delta toe, is not driven by the gravity related delta tectonics. Moreover, high excess of the Early Pliocene-Recent shortenings, measured between line BGR86-10 and line BGR86-22 (see Figure 5.14), can be interpreted as indicating of an increase in basement-driven shortening towards this area. In contrast, balance between the Early Pliocene-Recent shelfal extension and deep-water compression between line BR 1 and line BR 4, in the south-western ends of the study area (Brunei margin), indicating a purely gravity driven deformation (see Figure 5.14).

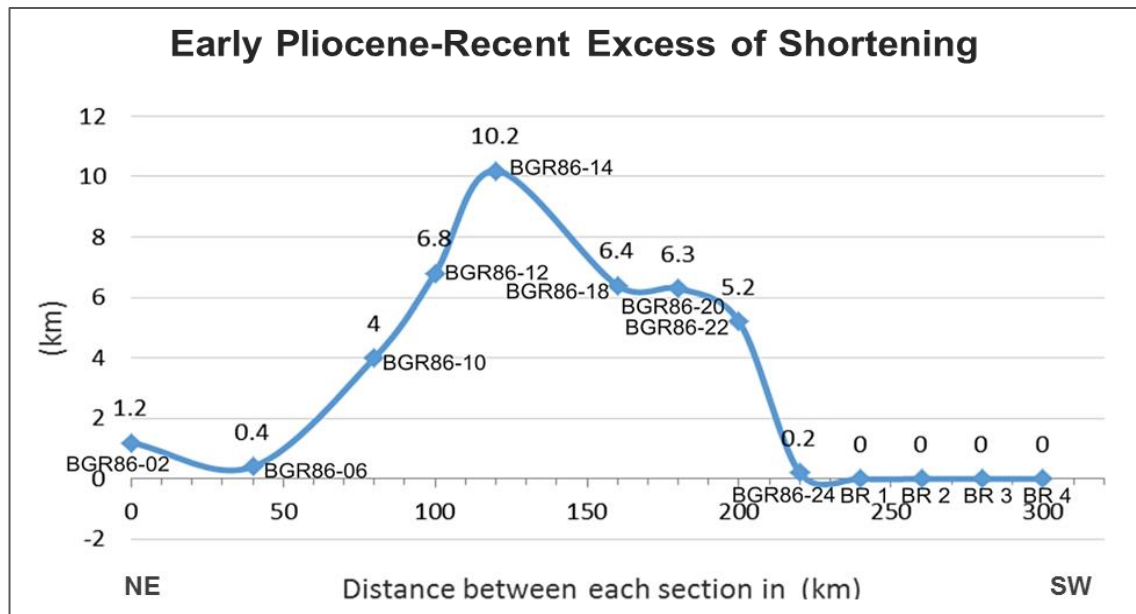


Figure 5. 14: Early Pliocene-Recent excess of shortening (given by the subtraction of the Early Pliocene-Recent shelfal extension from the Early Pliocene-Recent deep-water shortening) measured by structural restoration of nine selected seismic profiles across the study area (see Figure 5.2 to Figure 5.10) linked with previous studies of Hesse et al.(2010b) and the references therein. High excess of Early Pliocene-Recent shortening between line BGR86-10 and line BGR86-22 can be interpreted as indicating of an increase in basement-driven shortening in the central part of the study area.



### 5.4.2 Miocene-Recent

Due to limited data available, the amount of Middle Miocene-Recent shortening and lengthening can only be measured on 3 seismic profiles (BGR86-10, BGR86-06 and BGR86-02), located on the northern segment of the study area (Table 5.3; Figure 5.15; see Figure 5.1 for line location). The restoration results indicate that, the highest shortening and lengthening deformation occurred in the Middle Miocene except for BGR86-10 (see Table 5.3; Figure 5.15). The total Middle Miocene-Recent shelfal extension decreases south-ward, from a maximum value of 4.4 km at line BGR86-02 and 4.8 km at line BGR86-06, to a minimum value of 0.8 km at line BGR86-10 (Table 5.3; Figure 5.16). In contrast, the total Middle Miocene-Recent deep-water compression decreases northward, from 13.2 km at line BGR86-10 and 15.2 km at line BGR86-06, to a minimum value of 9.6 km at line BGR86-02 (see Table 5.3; Figure 5.16). The amount of Middle Miocene-Recent deep-water compression measured on BGR86-10, BGR86-06 and BGR86-02, appears to exceed the amount of Early Pliocene-Recent shelfal extension (see Table 5.3; Figure 5.16). The overall results presented here shown that, the Middle Miocene-Recent shortening and lengthening measured on BGR86-10, BGR86-06 and BGR86-02, show similar pattern with the measured Early Pliocene-Recent shortening and lengthening; with increasing imbalance (excess of shortening value) towards BGR86-10 (towards the central part of the study area)(see Figure 5.14 & 5.16).

Table 5. 3: Total and incremental Middle Miocene-Recent shortening and lengthening measured by structural restoration of three selected seismic profiles (BGR86-10, BGR86-06 and BGR86-02).

Survey Line		Early Pliocene	Late Miocene	Mid. Miocene	Compression Vs Extension
<b>BGR 10</b>	Com (km)	4.8	5.2	3.2	13.2>0.8 km
	Ex (km)	0.4	0	0.4	
<b>BGR 06</b>	Com (km)	0.8	4.0	10.4	15.2>4.8 km
	Ex (km)	0.4	0	4.4	
<b>BGR 02</b>	Com (km)	1.6	0.8	7.2	9.6>4.4km
	Ex (km)	0.4	0	4	

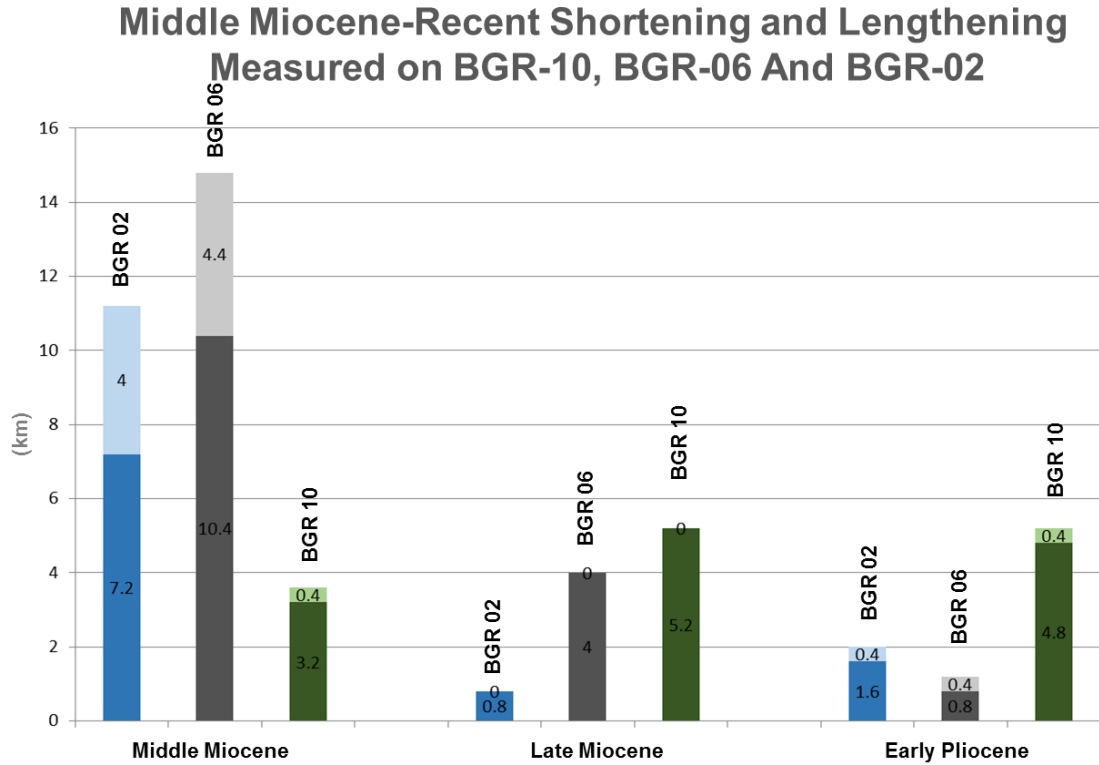


Figure 5. 15: Middle Miocene, Late Miocene and Early Pliocene shelfal extension and deep-water compression measured by structural restoration of three selected seismic profiles (BGR86-10, BGR86-06 and BGR86-02).

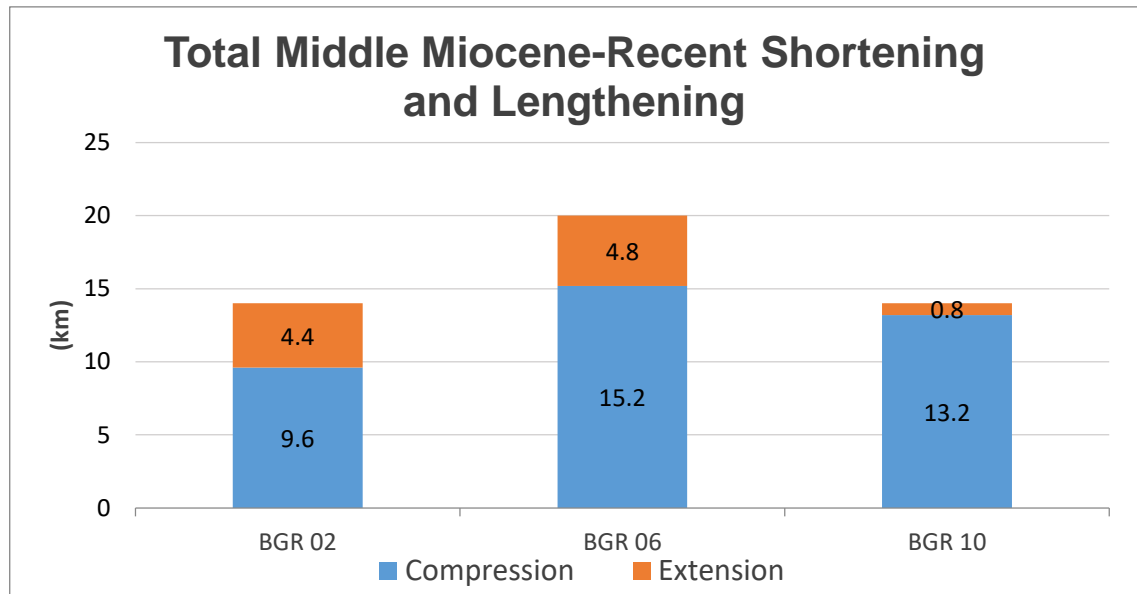


Figure 5. 16: Total Middle Miocene-Recent shelfal extension and deep-water compression measured by structural restoration of three selected seismic profiles (BGR86-10, BGR86-06 and BGR86-02). The location of line profiles is shown in figure 5.1.

## 5.5 Discussion

### 5.5.1 Spatial and Lateral Variation in Deep-Water Shortening; How Does This Link with the Formation and Translational event of the allochthon.

The restoration results presented have revealed that the incremental shortening, measured on all selected seismic profiles, increased through time, from the Middle Miocene to Early Pliocene, except for BGR86-06 and BGR86-02, located in the northern segment of the study area (refer Table 5.1; Figure 5.11). The incremental deep-water shortening measured on BGR86-02 and BGR86-06, shows a decreasing amount of shortening through time, from Middle Miocene until Recent. The highest shortening occurred in the Middle Miocene (refer Table 5.3; Figure 5.15). Moreover, the Middle Miocene-Recent shortening and lengthening measured on BGR86-06 and BGR86-02, have shown that the highest imbalance between the shelfal extension and the deep-water compression also occurred during the Middle Miocene, with 6 km (BGR86-06) and 3.2 km (BGR86-02) excess of shortening respectively (refer Table 5.3; Figure 5.16).

Combining quantitative measurements from the restored sections, the observed mode of deep-water shortening through time suggest that the deep-water deformation occurred mainly on the Latest Miocene-Pliocene onwards except for BGR86-02 and BGR86-06. Therefore, it is inferred that, the Middle Miocene shortening event in the northern end of the study area (BGR86-02 and BGR86-06), marks the time of the initial deformation and translation of the allochthon seaward and northward, before the area was dominated by the deposition of thick Middle Miocene-Recent deltaic cover.

This outcome is possible since from seismic interpretation (see details in Chapter 3), the allochthon compressive wedge is seen to be underlying a regional map-able erosional unconformity, the Top Crocker Unconformity (TCU of Van Hattum et al., 2006) or often called the Base Miocene Unconformity (BMU) by oil companies (e.g. Gartrell et al., 2011). Besides that, the allochthon compressive wedge is seen to be sealing by another regional map-able erosional unconformity dated in offshore Palawan wells as Middle Miocene (Aurelio et al., 2014), which can be correlated to the Deep Regional Unconformity (DRU) by Levell (1987), in the NW Borneo. The Deep Regional

Unconformity (DRU) by Levell (1987) is a collision-related unconformity (Levell, 1987; Cliff et al., 2008) dated approximately 16–15 Ma (Hutchison, 2005; Gartrell et al., 2011).

It is commonly accepted that complete subduction of the proto-South China Sea oceanic crust beneath the northern Borneo-Cagayan Arc active margin was followed by under-thrusting and collision of the extended South China Sea continental crust namely the Dangerous Grounds/Reed Bank/North Palawan block with the NE-SW oriented northern Borneo-Cagayan Arc active margin (e.g., Levell 1987; Hazebroek & Tan 1993; Hutchison 1996, 2000; Hall 1996; Milsom et al. 1997; Rangin et al., 1990; Morley, 2002). The South China Sea extension is interpreted to have been driven by slab pull of the proto-South China Sea that subducted beneath north Borneo (Hall, 1996). The pull forces exerted by the subducted oceanic slab could maintain under-thrusting of the thinned continental crust for a period after the beginning of the continent-continent collision in the Early Miocene (Hutchison et al. 2000; Hall, 2013). This pull force is interpreted to continue to cause a major shortening event and uplift throughout the Early Middle until Late Miocene, as expressed by the elevation of the Crocker-Rajang mountainous terrain inland Borneo, uplift and exhumation of the Mount Kinabalu granite during the Middle and Late Miocene (Levell, 1987; Hutchison, 1996b; Hutchison et al., 2000).

This pulses of proximal uplift from Early Middle Miocene onwards is interpreted to have affected the margin deformation by increasing the overall slope elevation that further destabilize the margin (critical wedge model of Davis et al. 1983), which at the same time increased the driving force for gravity spreading. Meaning that, there is a requirement for the NW Borneo accretionary wedge (allochthon) to respond to the unstable state (the wedge is steeper than the ideal angle) by faulting, which promotes significant forward deformation front in a form of large thrust sheets. This event will allow the front of the NW Borneo accretionary wedge (allochthon) to propagate seaward, away from the uplifted margin, to its present position. Hence, the thinning of the Tertiary Basement unit abruptly towards the allochthon thrust wedge as expressed by decreasing Moho depths gradually between 33 km and 26 km from northwest to southeast (towards the allochthon thrust sheet) (Sidek et. al., 2016) would have been typical behaviour of continental crust thinning due to the loading and prograding of the allochthon thrust wedge offshore.

Therefore, as discussed above, most of the internal imbricate thrust faulting and folding of the allochthon wedge, along with its translational event from the original basin margin progressively seaward and north-east-wards, must have taken place between the Early Miocene to Middle Miocene times. Moreover, the wedge must have been over-thrusted into shallower level and exposed to erosion (Deep Regional Unconformity) before the overlying Middle Miocene-Recent Champion-Baram deltaic sequence being deposited and grew above the allochthon, and caused the superimposition of gravity driven extensional and compressional deformation on the pre-existing tectonic compressional deformation. If this hypothesis is correct, this event marks a major shortening along the northern segment during the Middle Miocene times.

### **5.5.2 Gravity-Tectonics Imbalance**

In the previous chapter, we discussed the interaction between the cross-sectional area of allochthon above their regional level and thinning of allochthon beneath the extensional domain by deltaic sediments that sink below their regional level. The results presented demonstrate that, the observed up-dip deltaic extensional structures accommodating basin-ward translation are capable by themselves of generating enough Late Miocene-Recent translation to account for seaward translation of the allochthon in the outer domain. However, during the Middle Miocene, we infer that the shortening event in the northern end of the study area (BGR86-02 and BGR86-06), that marks the time for the initial deformation and translation of the allochthon from the original basin margin progressively seaward and north-east-wards (before the deposition of the deltaic sequence) must have been driven by compressional tectonics that were still active.

Regional structural restoration and shelf edge trajectories analysis (see details in Chapter 4) have shown that the Middle Miocene-Recent Baram-Champion deltaic formation shows an overall basin-ward prograding deltaic system (with a minor component of aggradation and dislocation of the shelf edge trajectory in the fault bounded depocentre, and a back stepping architecture corresponding to a "local" tectonic pulse), along with basin-ward migration of linked gravity driven extensional-compressional deformation. Therefore, all the unambiguously extensional structures (inverted extensional structure) up-dip of



the deltaic wedge can be examined as previously potential extensional structures to accommodate deep-water shortening before they were inverted by pulses of proximal uplift from Middle Miocene onwards, yet restoring it might have contributed to the shortening component. Accordingly, the imbalance between shallow-water shelf extension and deep-water compression in the study area could be due to incomplete balancing of up-dip gravity driven extensional structure (inverted extensional structure).

In that case, we infer that extension driven by delta tectonics is transferred downslope, serving as primary control for the deep-water compressional deformation. In other words, the fold and thrust belt deformation is interpreted to develop primarily due to gravitational delta tectonics. Meaning that, the deep-water compressional deformation is not an accretionary prism and is not developed as a result of collision that continues until today, although some authors suggest that subduction has continued until the Late Neogene or present-day and the NW Borneo deep-water fold thrust belt and trough represent an accretionary complex and an active subduction trench respectively (e.g., Tongkul, 1991, Simons et al., 2007, Sapin et al., 2011). However, there is no significant volcanic activity and no seismicity below or landward of the trough that can be associated with a subducting slab (Hall, 2013).

Nevertheless, the deformation events along the NW Borneo margin have been superposed in a way that cannot be explained solely by progradation of the delta. The basin deformation appears to have been influenced by compressional tectonics that was still active until at least the latest Pliocene, but restricted to the inner margin and onshore region, as evidenced by continuous uplift of the inner margin, and inversion of the earlier growth fault up slope. By extending our regional scale analysis to another 100 km northwards from the previous studies of Hesse et al., (2010), the results revealed that high excess of the Early Pliocene-Recent shortening between lines BGR86-10 and BGR86-22, can be interpreted as indicating of an increased in tectonic-driven shortening towards the central segment of the study area (refer Table 5.2; Figure 5.13 & Figure 5.14).

The controlling mechanism for the continuous Late Neogene-Recent uplift remains the subject of disagreement and discussion. The contributions of the regional compressional stress onto the Borneo Island have been discussed as

one of the possible mechanism that caused the Late Neogene-Recent uplift, as the island is surrounded by an actively deforming region. These include; 1) Australia-SE Asia collision that caused counter-clockwise rotation the of Borneo, around 25 and 10 Ma (Hall 1996; Hall and Nichols, 2002); 2) recent GPS strain measurement proposes a southwest-directed movement of NW Borneo up to 8 mm/yr. with respect to the Sundaland block (Simon et al., 2007). In contrast, Hall (2013) suggested that most of the Neogene deformation is a result of episodes of extension, not compression as there is no shortage of tectonic events that could cause inversion in the sedimentary basins during the Miocene–Recent. Accelerated erosion of Borneo and increased loading of areas close to Borneo contributed to the rates of uplift of Borneo by flexural effects (Hall and Nichols, 2002; Hall, 2013).

## **5.6 Conclusion**

This chapter presented a section balancing of nine selected NW-SE-trending seismic profiles across the NW Borneo margin to fully quantify the deformation amount across the study area, and to verify the balancing of upslope and downslope deformation over time. The selected seismic profiles allow extending the analysis to another 100 km northwards from previous studies. This has led to an improved understanding of the regional-scale structural deformation along the NW Borneo margin, complementing previous studies in the region.

The restoration results revealed a significant variation in both total and incremental shortening amounts through time. Combining quantitative measurements from the restored sections, the observed mode of deep-water shortening through time suggest that the deep-water deformation occurred mainly on the Latest Miocene-Pliocene onwards except for BGR86-02 and BGR86-06. A major Middle Miocene shortening event in the northern end of the study area (BGR86-02 and BGR86-06), is interpreted to mark the time for the initial deformation and translation of the allochthon seaward and northward from the original basin margin (before the area was dominated by the deposition of thick Middle Miocene-Recent deltaic cover) by compressional tectonics that were still active. Progradation of the Champion-Baram Delta onto the allochothon caused the superimposition of gravity driven extensional and

compressional deformation on the pre-existing tectonic compressional deformation.

The fold and thrust belt deformation and Late Miocene-Recent translation of the allochthon is interpreted to develop primarily due to gravitational delta tectonics. Meaning that, the deep-water compressional deformation is not an accretionary prism and is not developed as a result of collision that continues until today. The imbalance between shallow-water shelf extension and deep-water compression in the study area could be due to incomplete balancing of all the unambiguously extensional structures up-dip (inverted extensional structures), that were inverted by pulses of proximal uplift from Latest Miocene onwards. The basin deformation appears to have been influenced by compressional tectonics that was still active until at least the latest Pliocene, restricted to the inner margin and onshore region.

## **Chapter 6**

### **Discussion and Conclusion**

Chapters 3, 4, and 5 where research results are detailed also included discussion sections. This chapter aims to summarise all the findings and perspectives, and outline the implications.

#### **6.1 Contrasting Deformation of Different Structural Domains.**

The analyses of Chapter 3 have subdivided the deltaic deformation into four structural domains that are highlighted by the following examples of contrasting deformation; 1) The inversion domain characterized by the inversion of most of the older extensional structures, both regional and counter-regional growth faults (on the inner shelf and onshore region); 2) The extensional domain that is characterised by both gliding of regional growth faults and by spreading of counter-regional growth faults over a regional detachment; 3) The compressional domain, varying from broad, well developed imbricate zones of fault-related folds (~ 70 km), generally of similar size, and uniform-length thrusts with an average distance of 3-15 km between them in the southern deep-water-fold-thrust belt, passing into regions of narrow imbricate zones (~ 40 km) of the northern deep-water-fold-thrust belt with a considerably more compressed style (1-9 km) with different sizes of thrusts that did not form sequentially from the hinterland to the foreland but in a rather more irregular sequence, that sometimes included over-thrusts; 4) The transitional domain, typically wide in the northern segment and illustrates contrasting structures and geometries varying from a progressive culmination of the thick allochthon unit with internal thrusting, diminishing southward where the extensional domain is directly adjacent to the contractional domain

The integration of field investigation and seismic data analysis shows that, although the observed mode of tectonic compressional deformation and deep-water fold and thrust deformation generally shows significant similarities in orientation (NE-SW), there are significant differences in geometrical aspect and structural style of each area, indicating that they formed by different mechanisms. The structural styles of the internal imbricate structures of the

allochthon indicate a compressional deformation with higher intensity than the deltaic compression, suggesting that the allochthon was tectonically controlled, geometrically comparable to the onshore deformation, where shortening can be quite intense. Detailed correlation of the leading allochthonous over-thrust-front in the northern and southern segment reveals that the allochthon wedge could be considered to represent the front of the NW Borneo accretionary wedge, that must have been over-thrust from the original basin margin progressively seaward and north-west-wards along with seaward migration of the gravity-driven deformation system, and most of the allochthon's internal imbricate thrusts were inactive during the second phase of shortening, although recent activation of the imbricate thrusts do occur in local areas. Chaotic and transparent seismic characteristics of the allochthon, associated with contrasting deformational styles, varying from a progressive seaward and upward translation of a thick allochthon unit with internal imbricate thrusting and compaction drape to discrete features of ductile structures including low- to moderate-relief buckling roofs and structural highs, suggest that the allochthon is over-pressured and mobile.

## **6.2 Succession of Significant Events and Their Implication for NW Borneo Evolution**

Together, Chapters 3, 4 and 5 have improved understanding of the margin structure and evolution, with significant implications for the evolution of the NW Borneo and particularly the DWFTB. In the following, the succession of significant events and their implication for NW Borneo evolution are summarized.

In the Oligocene, part of the proto-South China Sea oceanic crust was subducted beneath the Northern Borneo (Hamilton 1979). It is commonly accepted that complete subduction of the proto- South China Sea oceanic crust beneath the northern Borneo-Cagayan Arc active margin was followed by under-thrusting and collision of the extended South China Sea continental crust namely the Dangerous Grounds/Reed Bank/North Palawan block with the NE–SW oriented northern Borneo-Cagayan Arc active margin (e.g., Levell 1987; Hazebroek & Tan 1993; Hutchison 1996, 2000; Hall 1996; Milsom et al. 1997; Rangin et al., 1990; Morley, 2002). Under-thrusting and collision later locked the



subduction zone, caused folding and thrusting in northern Borneo in the Early Miocene, (e.g., Hutchison 1996, 2000; Hall 1996; Milsom et al. 1997; Rangin et al., 1990; Morley, 2002). The South China Sea extension is interpreted to have been driven by slab pull of the proto-South China Sea that subducted beneath north Borneo (Hall, 1996). The pull forces exerted by the subducted oceanic slab could maintain under-thrusting of the thinned continental crust for a period after the beginning of the continent-continent collision (Hutchison et al. 2000; Hall, 2013). This pull force is interpreted to continue to cause a major shortening event and uplift throughout the Early, Middle until Late Miocene, as expressed by the elevation of the Crocker–Rajang mountainous terrain inland Borneo, uplift and exhumation of the Mount Kinabalu granite during the Middle and Late Miocene (Levell, 1987; Hutchison, 1996b; Hutchison et al., 2000).

The pulses of proximal uplift from Early Middle Miocene onwards is interpreted to have affected the margin deformation by increasing the overall slope elevation that further destabilize the margin (critical wedge model of Davis et al. 1983), which at the same time increased the driving force for gravity spreading. Meaning that, there is a requirement for the NW Borneo accretionary wedge (allochthon) to respond to the unstable state (the wedge is steeper than the ideal angle) by faulting, which promotes significant forward deformation front in a form of large thrust sheets. This event will allow the front of the NW Borneo accretionary wedge (allochthon) to propagate seaward, away from the uplifted margin, to its present position. Therefore, it is inferred that, the Middle Miocene shortening event in the northern end of the study area (BGR86-02 and BGR86-06), marks the time of the initial deformation and translation of the allochthon seaward and northward from the original basin margin (before the area was dominated by the deposition of thick Middle Miocene-Recent deltaic cover) by compressional tectonics that were still active. Hence, the thinning of the Tertiary Basement unit abruptly towards the allochthon thrust wedge as expressed by decreasing Moho depths gradually between 33 km and 26 km from northwest to southeast (towards the allochthon thrust sheet) (Sidek et. al., 2016) would have been typical behaviour of continental crust thinning due to the loading and prograding of the allochthon thrust wedge offshore.

This outcome is possible since the allochthon compressive wedge is seen to be underlying a regional map-able Early Miocene erosional unconformity, the Top Crocker Unconformity (TCU of Van Hattum et al., 2006) and is sealing by

another regional map-able erosional unconformity dated in offshore Palawan wells as Middle Miocene (Aurelio et al., 2014), which can be correlated to the Deep Regional Unconformity (DRU) by Levell (1987), in the NW Borneo. In other words, most of the internal imbricate thrust faulting and folding of the allochthon wedge, along with its translational event from the original basin margin progressively seaward and north-east-wards, must have took place between the Early Miocene to Middle Miocene times and the wedge must have been over-thrusted into shallower level and exposed to erosion (Deep Regional Unconformity) before the overlying Middle Miocene-Recent Champion-Baram deltaic sequence being deposited and grew above the allochthon.

Progradation of the Middle Miocene-Recent Champion-Baram Delta derived from the uplifted inner margin onto the allochothon caused the superimposition of gravity driven extensional and compressional deformation on the pre-existing tectonic compressional deformation. The cycle of loading and prograding of the delta system, associated with deltaic driven extensional faulting, leads to overpressure generation within the Early Miocene-Middle Miocene prodelta Setap shale that forms a weak ductile substrate for the deltaic system. Overpressure generation within the Setap shale by disequilibrium compaction/differential loading and superposed stresses of the gravity driven extensional onto the previously active thrust margin (allochthon), caused a feedback mechanism that generated toe thrusting in the deep-water and induced overpressure within the allochthon. Severe thinning of the allochthon layer beneath the extensional domain is an early mobility feature that developed syn-depositionally to localize sedimentation, forced outward and upward flow of the mobile allochthon layer. This outward and upward flow formed an elevated/advanced of allochthon front that rose above its regional stratigraphic level from latest Miocene onwards.

In the deep-water, compressional deformation developed mainly in the Latest Miocene-Pliocene onwards, formed newly thrusts concentrated in the undeformed area in deep-water, foreland of the first shortening phase (allochthon wedge/tectonic wedge) as a result of progradation of the deltaic system. However, some newly formed shortening structures did utilize the trace of pre-existing faults to propagate upwards and towards the foreland, reactivating a pre-existing thrust. The deep-water fold and thrust belt deformation is interpreted to develop primarily due to gravitational delta

tectonics. Meaning that, the deep-water compressional deformation is not an accretionary prism and is not developed as a result of collision that continues until today. Some authors suggest that subduction has continued until the Late Neogene or present-day and the NW Borneo deep-water fold thrust belt and trough represent an accretionary complex and an active subduction trench respectively (e.g., Tongkul, 1991, Simons et al., 2007, Sapin et al., 2011). However, there is no significant volcanic activity and no seismicity below or landward of the trough that can be associated with a subducting slab (Hall, 2013).

Nevertheless, the deformation events along the NW Borneo margin have been superposed in a way that cannot be explained solely by progradation of the delta. The basin deformation appears to have been influenced by compressional tectonics that was still active until at least the latest Pliocene, restricted to the inner margin and onshore region as evidenced by continuous uplift of the inner margin, and inversion of the earlier counter regional growth fault up slope. The imbalance between shallow-water shelf extension and deep-water compression in the study area could be due to incomplete balancing of all the unambiguously extensional structure up-dip (inverted extensional structure), that are examined as previously potential extensional structures to accommodate deep-water shortening before it have been inverted by pulses of proximal uplift from latest Miocene onwards. Restoration results revealed that high excess of the Early Pliocene-Recent shortening between lines BGR86-10 and BGR86-22, can be interpreted as indicating of an increased in tectonic-driven shortening towards the central segment of the study area.

The controlling mechanism for the continuous Late Neogene-Recent uplift remains the subject of disagreement and discussion. The contributions of the regional compressional stress onto the Borneo Island have been discussed as one of the possible mechanism that caused the Late Neogene-Recent uplift, as the island is surrounded by an actively deforming region. These include; 1) Australia-SE Asia collision that caused counter-clockwise rotation the of Borneo, around 25 and 10 Ma (Hall 1996; Hall and Nichols, 2002); 2) recent GPS strain measurement proposes a southwest-directed movement of NW Borneo up to 8 mm/yr. with respect to the Sundaland block (Simon et al., 2007). In contrast, Hall (2013) suggested that most of the Neogene deformation is a result of episodes of extension, not compression as there is no shortage of

tectonic events that could cause inversion in the sedimentary basins during the Miocene-Recent. Accelerated erosion of Borneo and increased loading of areas close to Borneo contributed to the rates of uplift of Borneo by flexural effects (Hall and Nichols, 2002; Hall, 2013).

### **6.3 Parameters Controlling Deformation**

The basin deformation appears to have been influenced by: (1) proximal uplift. (2) progradation of the deltaic sediment (i.e. stratigraphic thickness) ; and (3) pre-existing structure.

#### **6.3.1 Proximal Uplift**

Continuous pulses of Middle Miocene to recent proximal uplift started in the eastern, now onshore part of NW Borneo and play an important role in increasing the overall slope elevation and sediment supply to the basin. As a result shortening has been produced in response to gravity spreading of the uplifted continental interior; serving as primary control for seaward translation of the thrust wedge (allochthon) from the original basin margin progressively seaward and northwards during Middle Miocene.

Additionally, continuous uplift of the inner margin and inversion of earlier growth fault up slope from the Middle Miocene onwards caused imbalance between shallow-water shelf extension and deep-water compression (with an excessive amount of shortening) in the study area especially between lines BGR86-10 and BGR86-22. This is due to incomplete balancing of all the unambiguously extensional structures up-dip (inverted extensional structures), that are examined as previously potential extensional structures to accommodate deep-water shortening before they were inverted.

#### **6.3.2 Stratigraphic Thickness**

Sedimentation and progradational episodes of the deltaic succession have deposited large volumes of sediment in the southern segment with thicker

sedimentary column, and much lower and smaller sediment supply towards the northern segment, which therefore has a thinner sedimentary column (~10-12 km thick towards Brunei, vs. ~6 km in Sabah; Morley et al., 2003). Variation in sedimentary supply and stratigraphic thickness in the study area affects the critical taper angle of the deforming wedge and leads to profound effects in the location and pattern of structural deformation within the wedge and the magnitude of the allochthon involved in the deep-water-fold-and-thrust belt.

High and persistent sediment supply with an associated thicker stratigraphic thickness requires deformation to decrease the bathymetric slope angles by propagating forward or/and lengthening the wedge, which promotes significant forward movement of the deformation front that consequently will broaden the slope and reduce the taper. This condition buried and restrained the advance of the allochthon, and results in a well-developed, extensive compressional domain (~ 70-80 km) and wider spacing of structures with fewer seafloor expressions of fault-propagation folds.

In contrast, lower sediment supply with thinner stratigraphic thickness and slower deltaic progradation into deep-water, requires more thrusts or out-of-sequence thrusts to uplift the wedge either by reactivation of existing faults, or by the generation of new thrusts, or both, to attain the topography that satisfies the critical angle within the deforming wedge. This condition favours the advance of the allochthon into shallower level, and results in a less extensive compressional domain (~ 40-50 km) with a considerably more compressed style, with out-of-sequence thrusting and the emergence of the deep-water fold.

### **6.3.3 Pre-existing Compressional Structure**

The structural deformation in this margin consists of a sedimentary wedge that prograded over and growing above a former folds and thrust front. The initiation of normal faulting, especially the counter-regional growth faulting was controlled by the presence of the early folds where surfaces of weakness were present. High and persistent sediment supply in the southern segment restrained the advance of the allochthon and buried the early folds that would provide planes of weakness, to initiate the counter regional growth faults. The emergence of the allochthon into shallower levels by out-of-sequence thrusting



in the northern segment due lower sediment supply, favours the formation of an outer shelf counter regional growth fault on the top of the early folds of the emergent allochthon.

The absence of the over-thrusted allochthon in the southern deep-water fold-thrust-belt marks a notable difference in the geometrical characteristics of folding and the structural style. The style of thrust propagation and fold growth, varies from detached (buckle) folds and fault propagation folds in the Brunei margin to fault propagation folds with locally developed over-thrust folds towards the Sabah part of the margin, implying a northward increasingly frictional behaviour, that can be interpreted to be a reflection of the influence of the underlying compressive structure (allochthon) on deep-water fold thrust belt deformation.

#### **6.4 Summary and Future Work**

As a summary, combining outcrop-scale to seismic-scale, quantitative measurements with a seismic interpretation of the deep-water fold thrust belt have provided detailed descriptions and interpretations of the general appearance of different deformational styles (deltaic system and the tectonic wedge (allochthon)) related to different deformation mechanism, identifying the interaction between tectonic and gravity driven deformation and how it affects the style, timing, and location of deformation. Additionally, the margin evolution and their impact on NW Borneo evolution have also been evaluated. This study has properly answered the previously raised unanswered questions.

In the future, work on NW Borneo could focus on:

- I) Incorporation of well data with seismic velocities and biostratigraphic data and sediment cores through the succession of the Baram Delta will enable the lithological types, facies to be determined and evaluated more accurately.
  
- II) Access to denser spaced of 2D and/or 3D seismic coverage throughout the southern and northern segment of the NW Borneo margin would

significantly reduce the uncertainty and therefore the error that was introduced when interpreting.

- III) A regional investigation on the Neogene extensional tectonics of NW Borneo would add further information on the margin evolution.
- IV) An integrated study from NW Borneo including Brunei and offshore southwest Palawan would help to better understand relationships of tectonic events that affected the fold-thrust belt offshore Northwest Borneo and that formed offshore southwest Palawan.

## List of Reference

- Ajakaiye, D. E., and A. W. Bally, 2002, Course Manual and Atlas of Structural Styles on Reflection Profiles from the Niger Delta. Continuing Education Course Note Series. v. 41, AAPG, Tulsa. Axen.
- Aurelio, M. A., Forbes, M. T., Taguibao, K. J. L., Savella, R. B., Bacud, J. A., Franke, D., Pubellier, M., Savva, D., Meresse, F., Steuer, S., and Carranza, C. D., 2014, Middle to Late Cenozoic tectonic events in south and central Palawan (Philippines) and their implications to the evolution of the southeastern margin of South China Sea: Evidence from onshore structural and offshore seismic data: *Marine and Petroleum Geology*, v. 58, p. 658-673.
- Balaguru, A., and Lukie, T., 2012, Tectono-stratigraphy and development of the Miocene delta systems on an active margin of Northwest Borneo, Malaysia: Petroleum Geoscience Conference & Exhibition Delivering Value: Realising Exploration & Development Potential Kuala Lumpur, Malaysia, 23-24 April 2012.
- Balaguru, A., and Nichols, G.J., 2004, Tertiary stratigraphy and basin evolution, southern Sabah (Malaysian Borneo): *Journal of Asian Earth Sciences*, v. 23, p. 537–5554.
- Barckhausen, U., and Roeser, H.A., 2004, Seafloor spreading anomalies in the South China Sea revisited, In: Clift, P., Wang, P., Kuhnt, W., Hayes, D.E.

(Eds.), *Continent–Ocean Interactions within the East Asian Marginal Seas*, American Geophysical Union Geophysical Monograph, v. 149, p. 121–125.

Billotti, F., and Shaw, J.H., 2005, Deep-water Niger Delta fold and thrust belt modeled as a critical-taper wedge: The influence of elevated basal fluid pressure on structural styles: *AAPG Bulletin*, v.89, no.11, p. 1475-1491.

Bol, A.J., and van Hoorn, B., 1980, Structural style in western Sabah offshore: *Bulletin of the Geological Society of Malaysia*, v.12, p. 1–16.

Bowen, J.M., and Wright, J.A., 1957, Geology of the Crocker Range and adjoining areas, In: P. Liechti (ed), *Geology of Sarawak, Brunei and Northwest Sabah*. Brit. Terr. Borneo Geol. Survey.

Briais, A., Patriat, P., and Tapponnier, P., 1993, Updated interpretation of magnetic anomalies and sea floor spreading stages in the South China Sea: implications for the Tertiary tectonics of Southeast Asia: *Journal of Geophysical Research*, v. 98, p. 6299–6328.

Burov, E.B., and Diament, M., 1992, Flexure of the continental lithosphere with multilayered rheology: *Geophysical Journal International*, v. 109, p. 449-468.

Clift, P., Lee, G. H., Duc, N. A., Barckhausen, U., Van Long, H., and Zhen, S., 2008, Seismic reflection evidence for a Dangerous Grounds Miniplate: no extrusion origin for the South China Sea: *Tectonics*. v. 27, p. 1-16.

- Corredor, F., J. H. Shaw, and F. Bilotti, 2005, Structural styles in the deep-water fold and thrust belts of the Niger Delta: AAPG Bulletin, v. 89, p. 753-780.
- Crevello, P.D., 2001, The Great Crocker Submarine Fan: a world class foredeep turbidite system: Indonesia Petroleum Association, 28th Annual Convention, Jakarta, Indonesia.
- Cullen, A. B., 2010, Transverse segmentation of the Baram-Balabac Basin, NW Borneo: refining the model of Borneo's tectonic evolution: Petroleum Geoscience, v. 16, p. 3-29.
- Dahlen, F. A., J. Suppe, D. M. Davis, 1984, Mechanics of fold-and-thrust belts and accretionary wedges: cohesive Coulomb theory: Journal of Geophysical Research, v. 89, p. 10,087- 10,101.
- Dahlstrom, C. D. A., 1990, Geometric constraints derived from the law of conservation of volume and applied to evolutionary models for detachment folding: American Association of Petroleum Geologists Bulletin, v. 74, no. 3, p. 336-344.
- Davis, D., Suppe, J., and Dahlen, F.A., 1983, Mechanics of fold-and-thrust belts and accretionary wedges: Journal of Geophysical Research, v. 88; no. 2, p. 1153-1172.
- Dean, S., Morgan, J., and Brandenburg, J. P., 2015, Influence of mobile shale on thrust faults: Insights from discrete element simulations: American Association of Petroleum Geologists Bulletin, v. 99, no. 3, p. 403-432.



- Egan, S. S., Buddin, T. S., Kane, S. J., and Williams, G. D., 1997, Three dimensional modelling and visualisation in structural geology: New techniques for the restoration and balancing of volumes: Proceedings of GIG conference on Geological Visualisation - the Intelligent Picture?, British Geological Survey, October 1996, v. 1, no. 7, p. 67-82.
- Franke, D., Barckhausen, U., Heyde, I., Tingay, M., and Ramli, N., 2008, Seismic images of a collision zone offshore NWSabah/Borneo: Marine and Petroleum Geology, v. 25, p. 606–624.
- Gartrell, A., Torres, J., and Hoggmascall, N., 2011, A regional approach to understanding basin evolution and play systematic in Brunei – unearthing new opportunities in a mature basin, In: International Petroleum Technology Conference, Bangkok, Thailand, p. IPTC 1571, 1–5.
- Hall, R., 1996, Reconstructing Cenozoic SE Asia, In: Hall, R., Blundell, D.J. (Eds.), Tectonic Evolution of Southeast Asia, Geological Society of London Special Publication, v. 106, p. 153–184.
- Hall, R., 1997, Cenozoic plate reconstructions of SE Asia, In: Hall, R. & Blundell, D.J. (eds) Tectonic Evolution of Southeast Asia, Geological Society, London, Special Publications, v. 106, p. 153–184.
- Hall, R., 2002, Cenozoic geological and plate tectonic evolution of SE Asia and the SW Pacific: computer-based reconstructions, model and animations: Journal of Asian Earth Science, v. 20, p. 353–434.

- Hall, R., and Nichols, G., 2002. Cenozoic sedimentation and tectonics in Borneo: climatic influences on orogenesis: Geological Society, London, Special Publications, v. 191, p. 5-22.
- Hall, R., 2013, Contraction and extension in northern Borneo driven by subduction roll back: *Journal of Asian Earth Sciences*, v. 76, p. 399–411.
- Hamilton, W., 1979, Tectonics of the Indonesian region: *Geol. Soc. Malaysia, Bulletin 6*, July 1973; p. 3-10.
- Haq, B.U., Hardenbol, J., Vail, P.R., 1987. Chronology of Fluctuating Sea Levels Since The Triassic. *Science*, v. 235, p. 1156-1167.
- Hazebrook, H. P., and Tan, D. N. K., 1993, Tertiary Tectonic Evolution of NW Sabah Continental Margin. In: Teh, G. H., ed., *Proceedings of the Symposium of Tectonic Framework and Energy Resources of Western Margin of Pacific Basin*. *Bulletin of Geology Society of Malaysia*, v. 33, p. 195-210.
- Henriksen, S., Hampson, G.J., Helland-Hansen, W., Johannessen, E.P., Steel, R.J., 2009. Shelf Edge and Shoreline Trajectories, a Dynamic Approach to Stratigraphic Analysis. *Basin Research*, v. 21, p. 445-453.
- Helland-Hansen, W., Martinsen, O.J., 1996. Shoreline Trajectories And Sequences; Description Of Variable Depositional-Dip Scenarios. *J. Sediment. Research*, v. 66, no. 4, p. 670-688.

- Hesse, S., Back, S., and Franke, D., 2009, The deep-water fold-and-thrust belt offshore NW Borneo: Gravity-driven versus basement-driven shortening: Geological Society of America Bulletin, v.121, no. 5-6, p. 939-953.
- Hesse, S., Back, S., and Franke, D., 2010a. The structural evolution of folds in a deepwater fold and thrust belt – a case study from the Sabah continental margin offshore NW Borneo, SE Asia: Marine and Petroleum Geology, v. 27, p. 442– 454.
- Hesse, S., Back, S., and Franke, D., 2010b. Deepwater folding and thrusting offshore NW Borneo, SE Asia: Geological Society, London, Special Publications, v. 248, p. 169-185.
- Hinz, K., and Schlüter, H. U., 1985, Geology of the Dangerous Grounds, South China Sea and the Continental Margin off Southwest Palawan: Results of SONNE cruises SO-23 and SO-27: Energy, v. 10, p. 297-315.
- Hinz, K., Frisch, J., and Kempter, E.H.K., et al. 1989, Thrust tectonics along the continental margin of Sabah, Northwest Borneo: Geologische Rundschau, v. 78, p. 705–730.
- Hiscott, R.N., 2001, Depositional sequences controlled by high rates of sediment supply, sea-level variations, and growth faulting: the Quaternary Baram Delta of northwestern Borneo: Marine Geology, v. 175, p. 67–102.
- Hudec, M. R., and Jackson M. P. A., 2004, Regional restoration across the Kwanza Basin, Angola: Salt tectonics triggered by repeated uplift of a metastable passive margin: AAPG Bulletin, v. 88, no. 7 (July 2004), p. 971–990

- Hutchison, C.H., 1996, The 'Rajang accretionary prism' and 'Lupar Line' problem of Borneo. In: Hall, R., Blundell, D. (Eds.), Tectonic Evolution of Southeast Asia: Geol. Soc. of London Special Publication, v. 106, p. 247–261.
- Hutchison, C., Bergman, S. C., Swauger, D. A., and Graves, J. E., 2000, A miocene collisional belt in north Borneo: uplift mechanism and isostatic adjustment quantified by thermochronology: Journal of Geological Society, London, v. 157, p. 783-793.
- Hutchison, C.S., 2004, Marginal basin evolution: the southern South China Sea. Marine and Petroleum Geology, v. 21, p. 1129–1148.
- Hutchison, C.S., 2005, Geology of North-West Borneo. Elsevier.
- Hutchison, C., and Vijayan, S., 2010, What are the Spartlys Island?: Journal of Asian Earth Sciences. v. 39: p. 371-38
- Ingram, G.M., Chisholm, T.J., Grant, C.J., Hedlund, C.A., Stuart-Smith, P., and Teasdale, J., 2004, Deepwater North West Borneo: Hydrocarbon accumulations in an active fold and thrust belt: Marine and Petroleum Geology, v. 21, p. 879–887.
- Johannessen, E.P., Steel, R.J., 2005. Shelf-margin clinoforms and prediction of deepwater sands. Basin Research, v. 17, p. 521-550.
- Kane, S. J., Williams, G. D., Buddin, T. S., Egan, S. S., and Hodgetts, D., 1997, Flexural-slip based restoration in 3D, a new approach: AAPG Annual Convention Official Program A, v. 58.

- King, R., Hillis, R., Tingay, M., and Morley, C. K., 2009, Present-day stress and neotectonic provinces of the Baram Delta and deep-water fold-thrust belt: *Journal of the Geological Society, London*, v. 166, p. 197-200.
- King, R., Backe, G., Morley, C. K., Hillis, R., and Tingay, M., 2010, Balancing deformation in NW Borneo: Quantifying plate-scale vs. gravitational tectonics in a delta and deepwater fold-thrust belt system, v. 27, p. 238-246.
- Krueger, A.C.V.A., and Gilbert, E., 2009, Deepwater Fold-Thrust Belts: Not All the Beasts Are Equal: AAPG Search and Discovery Article, AAPG International Conference and Exhibition, Cape Town, South Africa, October, 26-29.
- Lambiase, J.J., Tzong, T.Y., William, A.G., and Cullen, A.B., 2008, The West Crocker Formation of northwest Borneo: A Paleogene accretionary prism, In: Draut, A.E., et al., eds., *Formation and applications of the sedimentary record in arc collision zones: Geological Society of America Special Paper*, v. 436, p. 171–184.
- Leloup, P.H., Arnaud, N., and Lacassin, R., et al. 2001, New constraints on the structure, thermochronology and timing of the Ailao Shan–Red River shear zone, SE Asia: *Journal of Geophysical Research*, v. 66, p. 6083–6732.
- Levell, B.K., 1987, The nature and significance of regional unconformities in the hydrocarbon-bearing Neogene sequences offshore West Sabah: *Geological Society of Malaysia Bulletin*, v. 21, p. 55–90.

- Liu, H., McClay, K.R., and Powell, D., 1992, Physical models of thrust wedges, In: McClay, K.R., (Ed.), Thrust Tectonics, Chapman and Hall, London, p. 71–81.
- Loncke, L., Gaullier, V., Mascle, J., Vendeville, B., Camera, L. 2006. The Nile deep-sea fan: An example of interacting sedimentation, salt tectonics, and inherited subsalt paleotopographic features. *Marine and Petroleum Geology*, 23, 297-315.
- Maltman, A. J., and A. Bolton, 2003, How sediments become mobilized. In: Subsurface Sediment Mobilization (Ed. by P. V. Rensbergen, R. R. Hillis, A. J. Maltman, and C. K. Morley) Geological Society, London, Special Publications, v. 216, p. 9-20.
- McClay, K. R., T. Dooley, and G. Lewis, 1998, Analog modeling of progradational delta systems: *Geology*, v. 26, p. 771-774.
- Milsom, J., Holt, R., Ayub, D.B., and Smail, R., 1997, Gravity anomalies and deep structural controls at the Sabah–Palawan margin, South China Sea, In: Fraser, A.J., Matthews, S.J., Murphy, R.W. (Eds.), *Petroleum Geology of SE Asia*, Geological Society of London Special Publication, v. 126, p. 417–427.
- Mitra, S., and J. Namson, 1989, Equal-area balancing: *American Journal of Science*, v. 289, p. 563-599
- Morley, C.K., and Guerin, G., 1996, Comparison of gravity-driven deformation styles and behaviour associated with mobile shales and salt: *Tectonics*, v. 15, p. 1154–1170.



- Morley, C. K., P. Crevello, and Z. H. Ahmad, 1998, Shale tectonics and deformation associated with active diapirism: The Jerudong anticline, Brunei Darussalam: *Journal of the Geological Society (London)*, v. 155, p. 475–490.
- Morley, C.K., 2002, A tectonic model for the Tertiary evolution of strike-slip faults and rift basins in SE Asia. *Tectonophysics*, 347, 189–215.
- Morley, C. K., 2003, Mobile shale related deformation in large deltas developed on passive and active margins: Geological Society, London, Special Publication, v. 216, p. 335-357.
- Morley, C. K., Back, S., Rensbergen, V., Crevello, P., and Lambiase, J. J., 2003. Characteristics of repeated, detached, Miocene–Pliocene tectonic inversion events, in a large delta province on an active margin, Brunei Darussalam, Borneo: *Journal of Structural Geology*, v. 25, p. 1147-1169.
- Morley, C.K., 2007, Interaction between critical wedge geometry and sediment supply in a deepwater fold belt, NW Borneo: *Geology*, v. 35, p. 139–142.
- Morley, C. K., Tingay, M., Hillis, R., and King, R., 2008, Relationship between structural style, overpressures, and modern stress, Baram Delta Province, northwest Borneo: *Journal of Geophysical Research*, v. 113, p. 1-23.
- Morley, C.K., 2009, Growth of folds in a deep-water setting: *Geosphere*, v. 5, p. 59–89.

- Morley, C. K., King, R., Hillis, R., Tingay, M., and Backe, G., 2011, Deepwater fold and thrust belt classification, tectonics, structure and hydrocarbon prospectivity: A review, *Earth- Science Reviews*, v. 104, p. 41–91.
- Nieuwland, D.A., Leutscher, J.H., and Gast, J., 2000, Wedge equilibrium in fold-and-thrust belts: prediction of out-of-sequence thrusting based on sandbox experiments and natural examples: *Geologie en Mijnbouw / Netherlands Journal of Geosciences*, v. 79, p. 81-91.
- Olariu, C., and Steel, R.J., 2009, Influence of point-source sediment-supply on modern shelf-slope morphology; implications for interpretation of ancient shelf margins: *Basin Research*, v. 21, p. 484-501.
- Osborne, M. J., and R. E. Swarbrick, 1997, Mechanisms for generating overpressure in sedimentary basins; a reevaluation: *AAPG Bulletin*, v. 81, p. 1023-1041.
- Paton, D. A., Van der Spuy, D., Di Primio, R., and Horsfield, B., 2008, Tectonically induced adjustment of passive margin accommodation space; influence on the hydrocarbon potential of the Orange Basin, South Africa: *AAPG Bulletin*, p. 589-609.
- Platt, J. P., Dynamics of orogenic wedges and the uplift of high-pressure metamorphic rocks. *Geological Society of America Bulletin*. 97, 1037-1053.
- Rangin, C., Bellon, H., Benard, F., Letouzey, J., Müller, C., and Tahir, S., 1990, Neogene arccontinent collision in Sabah, N. Borneo (Malaysia). *Tectonophysics* 183, 305–319. 410.

- Rowan, M.G., Peel, F.J., and Vendeville, B.C., 2004, Gravity-driven fold belts on passive margins: in McClay, K.R., ed., Thrust tectonics and hydrocarbon systems: AAPG Memoir, v. 82, p. 157–182.
- Saffer, D. M., Bekins, B. A., 2002, Hydrologic controls on the morphology and mechanics of accretionary wedges: *Geology*, v. 30, no. 3, p. 271-274.
- Sapin, F., Pubellier, M., Lahfid, A., Janots, D., Aubourg, C., and Ringenbach, J. C., 2011, Onshore record of the subduction of a crustal salient: example of the NW Borneo Wedge, *Terra Nova*, v. 23, p. 232–240.
- Sapin, F., Ringenbach, J. C., Rives, T., and Pubellier, M., 2012, Counter-regional normal faults in shale-dominated deltas: Origin, mechanism and evolution: *Marine and Petroleum Geology*, v. 37, p. 121–128.
- Sapin, F., Hermawan, I., Pubellier, M., Vigny, C., Ringenbach, J. C., 2013, The recent convergence on the NW Borneo Wedge—a crustal-scale gravity gliding evidenced from GPS: *Geophysical Journal International*, v. 193 (2), p. 549-556.
- Schultz-Ela, D. D., 2001, Excursus on gravity gliding and gravity spreading: *Journal of structural Geology*, v. 23, p. 725-731
- Sclater, J. G., and Christie, P. A. F., 1980, Continental stretching: an explanation of the post-Mid-Cretaceous subsidence of the Central North Sea Basin: *Journal of Geophysical Research*, v. 85, p. 3711–3739.
- Saller, A. and Blake, G., 2003. Sequence Stratigraphy and syn-depositional tectonics of Upper Miocene and Pliocene deltaic sediments, offshore

- Brunei Darussalam. In: Tropical Deltas of Southeast Asia. Sedimentology, Stratigraphy, and Petroleum Geology (Ed. by F.Hasan Sidi, D.Nummedal, P. Imbert, H. Darman & H.W. Posamentier), SEPM, Special Publication 76, p. 219-234.
- Sidek, A., Hamzah, U., Samsudin, A. R., Arifin, M. H., and Junin, R., 2016, Deep crustal profile across NW Sabah Basin: Integrated Potential Field Data and Seismic Reflection: Journal of Engineering and Applied Sciences v. 11, no. 3, p. 1401-1411.
- Simons, W., Socquet, A., Vigny, C., Ambrosius, B., Haji Abu, S., Promthong, C., Subarya, C., Sarsito, D.A., Matheussen, S., Morgan, P., and Spakman, W., 2007, A decade of GPS in Southeast Asia: resolving Sundaland motion and boundaries: Journal of Geophysical Research, 112.
- Steuer, S., Franke, D., Meresse, F., Savva, D., Pubellier, M., Auxietre, J.-L., and Aurelio, M., 2013, Time constraints on the evolution of the southern Palawan Island, Philippines from onshore and offshore correlation of Miocene limestones: Journal of Asian Earth Science, v. 76, p. 412–427.
- Steuera, S., Franke, D., Meresse, F., Savva, D., Pubellier, M., and Auxietre, J. L., 2014, Oligocene-Miocene carbonates and their role for constraining the rifting and collision history of the Dangerous Grounds, South China Sea: Marine and Petroleum Geology, v. 58, p. 644-657.
- Tan, D. N. K., and Lamy, J. M., 1990, Tectonic Evolution of the NW Sabah Continental Margin since the Late Eocene: Bulletin Geological Society of Malaysia, v. 27, p. 241-260.

- Taylor, B., and Hayes, D. E., 1983, Origin and history of the South China Sea Basin: The Tectonic and Geologic Evolution of Southeast Asian Seas and Islands, edited by D. E. Hayes, p. 23-56.
- Tingay, M. R. P., Hillis, R. R., Morley, C. K., Swarbrick, R. E and Drake, S. J., 2005, "Prograding" tectonics in Brunei: Regional implications for fault sealing: ARMA/USRMS, 05-785, 14 p.
- Tingay, M., Hillis, R., Swarbrick, R. E., Morley, C. K., and Damit, A. R., 2009, Origin of overpressure and pore-pressure prediction in the Baram Province, Brunei: AAPG Bulletin, v. 93, p. 51-74.
- Tongkul, F., 1987, The sedimentology and structure of the Crocker Formation in the Kota Kinabalu area, Sabah: Unpublished PhD thesis, University of London.
- Tongkul, F., 1990, Structural Styles and Tectonics of Western and Northern Sabah: Bulletin Geological Society of Malaysia, v. 27, p. 227-240.
- Tongkul, F., 1991, Tectonic evolution of Sabah, Malaysia: Journal of Southeast Asian Earth Sciences, v. 6, p. 395–406.
- Tongkul, F., 2003, Stratigraphic architecture of a deep-water deposit in Northwest Borneo: AAPG Search and Discovery Article, AAPG Annual Meeting, May 11-14, Salt Lake City, Utah.
- Van Hattum, M.W.A., Hall, R., Pickard, A.L., and Nichols, G.J., 2006, SE Asian sediments not from Asia: provenance and geochronology of North Borneo sandstones: Geology, v. 34, p. 589–592.

- Van Rensbergen, P., and C. K. Morley, 2000, 3D Seismic study of a shale expulsion syncline at the base of the Champion delta, offshore Brunei and its implications for the early structural evolution of large delta systems: *Marine and Petroleum Geology*, v. 17, p. 861-872.
- Van Rensbergen, P., and Morley, C., 2003, Re-evaluation of mobile shale occurrences on seismic sections of the Champion and Baram deltas, offshore Brunei, In: Van Rensbergen, P., Hillis, R.R., Maltman, A.J., Morley, C.K. (Eds.), *Subsurface sediment mobilization*. Geological Society [London] Special Publication, v. 216, p. 395–409.
- Vendeville, B. V., and M. P. A. Jackson, 1992, The fall of diapirs during thin-skinned extension: *Marine and Petroleum Geology*, v. 9, p. 354–371.
- Vinnels, J.S., Butler, R.W.H., Paton, D.A, and McAffrey, W.D., 2010, Depositional processes across the Sinú Accretionary Prism, offshore Colombia: *Marine and Petroleum Geology*, v. 27, p. 794-809.
- Weiner, R. W., M. G. Mann, M. T. Angelich, and J. B. Molyneux, 2010, Mobile shale in the Niger Delta: Characteristics, structure, and evolution, in L. Wood, ed., *Shale tectonics: AAPG Memoir*, v. 93, p. 145-161.
- Weimer P, Slatt RM (2004) *Petroleum systems of deepwater settings, distinguished instructor series, No. 7*, Society of Exploration Geophysicists and European Association of Geoscientists and Engineers, p. 1-1 to 9-75.
- Williams, H. H., 1997, Play concepts northwest Palawan, Philippines, *J. Asian Earth Science*, v. 15, p. 251-273.



Wilson, R.A.M., 1964, The geology and mineral resource of the Labuan and Padas Valley area, Sabah: Malaysia Geological. Survey, Memior, 17.

Wilson, M.E.J., and Moss, S.J., 1999, Cenozoic paleogeographic evolution of Sulawesi and Borneo: Palaeogeography, Palaeoclimatology, Palaeoecology, v. 145, p. 303-337.